

**Development of a Grey Box Thermal Dynamic Model without Building Construction  
Knowledge**

by

Elizabeth LeRiche

B.Sc. in Mechanical Engineering, Queen's University, 2016

A thesis

presented to Ryerson University

in partial fulfillment of the

requirements for the degree of

Master of Applied Science

in the program of

Building Science

Toronto, Ontario, Canada, 2019

© Elizabeth LeRiche, 2019

## AUTHOR'S DECLARATION FOR ELECTRONIC SUBMISSION OF A THESIS

I hereby declare that I am the sole author of this thesis. This is a true copy of the thesis, including any required final revisions, as accepted by my examiners.

I authorize Ryerson University to lend this thesis to other institutions or individuals for the purpose of scholarly research.

I further authorize Ryerson University to reproduce this thesis by photocopying or by other means, in total or in part, at the request of other institutions or individuals for the purpose of scholarly research.

I understand that my thesis may be made electronically available to the public.

Development of a Grey Box Thermal Dynamic Model without Building Construction  
Knowledge

Master of Applied Science 2019, Elizabeth LeRiche

Building Science, Department of Architectural Science, Ryerson University

ABSTRACT

Model Predictive Controllers (MPC) in building Heating Ventilation and Air Conditioning (HVAC) systems have demonstrated significant energy savings when compared to typical on/off controllers. MPCs require information about the building's thermal dynamics which is challenging to model, especially for older structures without buildings specifications. This research investigates the ability to develop a grey box thermal dynamic model that can determine the net thermal dynamics, without any building construction information. Sensors were installed within a test cell to monitor the building automation system (BAS) points, and collect building element surface temperature data. The simulation program *Simulink* was used to develop and test iterations of grey box models. The final model, that relies solely on BAS points, is able to predict the ambient temperature for a 3-hour Prediction Window to within 1.7% accuracy. This model demonstrates the potential for more buildings to implement HVAC MPC systems with grey box thermal dynamic modeling.

## ACKNOWLEDGMENTS

I would like to send a special thank you to my supervisor, Jenn McArthur, who has been incredibly supportive throughout this research. I learnt a lot from working with Jenn over the past year and I am grateful for her guidance throughout this project. I thank Zaiyi Liao for sharing his knowledge of *Simulink* and providing feedback throughout this year. I thank Alan Fung for accepting to be third reader, and the entire defense committee for providing their knowledge and feedback on this work. I would also like to thank Greg Labbe, who was instrumental in acquiring the calibration equipment and rooftop weather data for this research, as well as for being a confidant throughout the past year.

Finally, I thank my parents for their love and support, along with the wonderfully supportive network of friends and family who encouraged me during the completion of my masters.

## Table of Contents

<b>1</b>	<b>INTRODUCTION.....</b>	<b>18</b>
<b>1.1</b>	<b>Research Objective .....</b>	<b>20</b>
<b>1.2</b>	<b>Research Questions .....</b>	<b>20</b>
<b>2</b>	<b>BACKGROUND.....</b>	<b>21</b>
<b>2.1</b>	<b>Model Predictive Control.....</b>	<b>21</b>
2.1.1	Economic Model Predictive Control .....	22
2.1.2	Thermal Dynamic Modeling .....	23
<b>2.2</b>	<b>Use of Test Cells in Predictive Control Development .....</b>	<b>23</b>
2.2.1	Use of Temperature Sensors .....	24
2.2.2	Internal Load.....	24
2.2.3	HVAC Systems.....	25
2.2.4	Occupancy Modeling .....	25
2.2.5	Modeling of External Conditions .....	26
<b>2.3</b>	<b>White Box Model.....</b>	<b>26</b>
<b>2.4</b>	<b>Black Box Model .....</b>	<b>27</b>
2.4.1	Linear Models .....	28
2.4.2	Neural Networks.....	28
2.4.3	Black Box Models vs Grey Box Model.....	31
2.4.4	Challenges of Black box Models .....	32
<b>2.5</b>	<b>Grey Box Models .....</b>	<b>32</b>
2.5.1	RC-Network Structure .....	34
2.5.2	RC Network Structure Optimisation .....	37
<b>2.6</b>	<b>Building Parameter Estimation .....</b>	<b>40</b>
<b>2.7</b>	<b>Subtractive Linear Regression.....</b>	<b>41</b>
<b>2.8</b>	<b>Validation and Error Analysis.....</b>	<b>42</b>

<b>2.9</b>	<b>Lessons from Literature Review used within this Thesis .....</b>	<b>43</b>
<b>3</b>	<b>METHODOLOGY.....</b>	<b>46</b>
<b>3.1</b>	<b>Test Cell Apparatus.....</b>	<b>47</b>
<b>3.2</b>	<b>Sensor Description.....</b>	<b>47</b>
<b>3.3</b>	<b>Sensor Installation .....</b>	<b>51</b>
<b>3.4</b>	<b>Sensor Modifications .....</b>	<b>54</b>
<b>3.5</b>	<b>Data Analytics to Overcome Data Gaps .....</b>	<b>55</b>
<b>3.6</b>	<b>Data Collection .....</b>	<b>57</b>
<b>4</b>	<b>WHITE BOX MODEL DEVELOPMENT .....</b>	<b>58</b>
<b>4.1</b>	<b>Calculation of Internal Heat Loads .....</b>	<b>61</b>
4.1.1	Occupancy .....	62
4.1.2	Interior Lighting .....	62
4.1.3	Ventilation .....	62
4.1.4	Heater.....	63
4.1.5	Thermal Storage .....	63
4.1.6	Calculation of External Heat Loads.....	64
<b>4.2</b>	<b>White Box Model Implementation in Matlab .....</b>	<b>67</b>
<b>5</b>	<b>GREY BOX MODEL CREATION.....</b>	<b>69</b>
<b>5.1</b>	<b>First Generation, First Iteration Grey box Model (G1v1) .....</b>	<b>70</b>
<b>5.2</b>	<b>First Generation, Second Iteration Grey box Model (G1v2).....</b>	<b>70</b>
<b>5.3</b>	<b>First Generation, Third Iteration Grey box Model (G1v3).....</b>	<b>70</b>
<b>5.4</b>	<b>Second Generation (G2) Model.....</b>	<b>72</b>
<b>5.5</b>	<b>Third Generation (G3) Model.....</b>	<b>74</b>

<b>5.6</b>	<b>Final Model</b> .....	<b>75</b>
<b>5.7</b>	<b>Sensitivity Analysis</b> .....	<b>75</b>
<b>5.8</b>	<b>Error Analysis</b> .....	<b>76</b>
<b>6</b>	<b>GREY BOX MODEL RESULTS</b> .....	<b>78</b>
<b>6.1</b>	<b>G1 Model</b> .....	<b>79</b>
6.1.1	Nighttime Simulation.....	79
6.1.2	Daytime Unoccupied Simulations.....	82
6.1.3	Daytime Occupied Simulations.....	85
6.1.4	Summary of G1v1 model Performance .....	91
<b>6.2</b>	<b>G1v2 model I: Heater Convective Heat Load</b> .....	<b>92</b>
<b>6.3</b>	<b>G1v3 Model: Cp Parameter Optimization</b> .....	<b>95</b>
<b>6.4</b>	<b>Summary of G1 model</b> .....	<b>101</b>
<b>6.5</b>	<b>G2 model: Regression Analysis</b> .....	<b>102</b>
6.5.1	Exterior Wall .....	103
6.5.2	Ceiling .....	105
6.5.3	Floor.....	106
6.5.4	Spandrel.....	109
6.5.5	Window .....	111
6.5.6	Interior Wall.....	113
6.5.7	Summary of G2 model.....	115
<b>6.6</b>	<b>G3 Model: Neural Network Analysis</b> .....	<b>116</b>
<b>6.7</b>	<b>Final Model</b> .....	<b>117</b>
<b>6.8</b>	<b>Summary of Final Model Results</b> .....	<b>139</b>
<b>6.9</b>	<b>Overall Summary of Results</b> .....	<b>141</b>
6.9.1	Findings from Model Comparison .....	148
<b>6.10</b>	<b>Sensitivity Analysis</b> .....	<b>149</b>

6.10.1	Heat Capacity with Final Model .....	149
6.10.2	Training Period.....	150
6.10.3	Seasonal Sensitivity.....	152
<b>6.11</b>	<b>Error Analysis .....</b>	<b>154</b>
6.11.1	Plug Load Error Analysis.....	154
6.11.2	Point Measurement Error Analysis .....	156
<b>6.12</b>	<b>Latent Heat Error Analysis.....</b>	<b>157</b>
<b>7</b>	<b>DISCUSSION .....</b>	<b>158</b>
<b>8</b>	<b>CONCLUSIONS.....</b>	<b>162</b>
	REFERENCES .....	163
	APPENDIX A SOLAR RADIATION CALCULATIONS.....	170
	APPENDIX B ARDUINO CODE.....	175
	APPENDIX C CALIBRATION .....	186
	APPENDIX D U-VALUE CALCULATIONS .....	190
	APPENDIX E MATLAB CODE.....	192
	APPENDIX F SIMULINK IMAGES.....	195

## List of Figures

Figure 1 Artificial Neural Network Structure showing Relationship between Inputs and Outputs using Neurons [30].....	29
Figure 2 Hidden Layer of Neural Network [30] .....	29
Figure 3 R2C Network Structure with (left) and without (right) window component .....	34
Figure 4 R-C Network Representing the Mixed-mode Energy Building [16].....	35
Figure 5 R-C Network Representing a Solar Decathlon House [23].....	36
Figure 6: 1st-5th Order Grey Box Models used within the study [21] .....	37
Figure 7 R6C3 Model used to Represent an Office Building [11] .....	38
Figure 8 4R3C Model Representing an Office Space [12] .....	38
Figure 9 4R4C Structure Representing a House [17] .....	39
Figure 10 Arduino Circuit Diagram for Test Cell .....	51
Figure 11: Test Cell Sensor Layout .....	52
Figure 12 Balometer used for Calibration of Airflow sensor .....	54
Figure 13: Occupancy and Plug Load Correlation .....	56
Figure 14 Example of Data Collected from the Test Cell Sensors during November.....	57
Figure 15 RC-network of Test Cell .....	58
Figure 16 Simulink Implementation of Differential Temperature Equations.....	67
Figure 17 Grey Box Model Subsystem Structure .....	68
Figure 18 November 17, 2017 Actual vs Predicted Temperatures for each Prediction Window.	80
Figure 19 November 29, 2017 Actual vs Predicted Temperatures for each Prediction Window.	81
Figure 20 January 6 <sup>th</sup> , 2018 Actual vs Predicted Temperatures for each Prediction Window .....	82
Figure 21 December 31 <sup>st</sup> , 2017 Actual vs Predicted Temperatures for each Prediction Window	83
Figure 22 January 13 <sup>th</sup> , 2018 Actual vs Predicted Temperatures for each Prediction Window ...	84
Figure 23 January 2 <sup>nd</sup> , 2018 Actual vs Predicted Temperatures for each Prediction Window ...	85
Figure 24 February 12 <sup>th</sup> , 2018 Actual vs Predicted Temperatures for each Prediction Window .	87
Figure 25 January 8 <sup>th</sup> , 2018 Actual vs Predicted Temperatures for each Prediction Window .....	88
Figure 26 February 7 <sup>th</sup> , 2018 Actual vs Predicted Temperatures for each Prediction Window ...	89
Figure 27 December 8 <sup>th</sup> , 2017 Actual vs Predicted Temperatures for each Prediction Window .	90
Figure 28 December 5 <sup>th</sup> , 2017 Actual vs Predicted Temperatures for each Prediction Window .	91

Figure 29 Ambient Temperature Prediction Error for February 7th, 2018 when using Turbulent and Natural Convection to Represent the Heater Unit.....	93
Figure 30 Ambient Temperature Prediction Error for January 8th, 2018 when using Turbulent and Natural Convection to Represent the Heater Unit .....	94
Figure 31 Ambient Temperature Prediction Error for December 8th, 2017 when using Turbulent and Natural Convection to Represent the Heater Unit.....	94
Figure 32 Ambient Temperature Prediction for November 17th, 2017 comparing the use of the Initial and Optimized Internal Heat Capacity Values .....	97
Figure 33 Ambient Temperature Prediction for November 29th, 2017 comparing the use of the Initial and Optimized Internal Heat Capacity Values .....	97
Figure 34 Ambient Temperature Prediction for January 6th, 2018 comparing the use of the Initial and Optimized Internal Heat Capacity Values.....	98
Figure 35 Ambient Temperature Prediction for December 31st, 2017 comparing the use of the Initial and Optimized Internal Heat Capacity Values .....	98
Figure 36 Ambient Temperature Prediction for January 13 <sup>th</sup> , 2018 comparing the use of the Initial and Optimized Internal Heat Capacity Values.....	99
Figure 37 Ambient Temperature Prediction for January 2 <sup>nd</sup> , 2018 comparing the use of the Initial and Optimized Internal Heat Capacity Values.....	99
Figure 38 Ambient Temperature Prediction for February 12 <sup>th</sup> , 2018 comparing the use of the Initial and Optimized Internal Heat Capacity Values.....	100
Figure 39 Ambient Temperature Prediction for January 8 <sup>th</sup> , 2018 comparing the use of the Initial and Optimized Internal Heat Capacity Values.....	100
Figure 40 Ambient Temperature Prediction for February 7 <sup>th</sup> , 2018 comparing the use of the Initial and Optimized Internal Heat Capacity Values.....	100
Figure 41 Ambient Temperature Prediction for December 8 <sup>th</sup> , 2017 comparing the use of the Initial and Optimized Internal Heat Capacity Values.....	101
Figure 42 Ambient Temperature Prediction for December 5 <sup>th</sup> , 2017 comparing the use of the Initial and Optimized Internal Heat Capacity Values.....	101
Figure 43 November 17, 2017 Prediction Error for all Building Elements along with Ambient Temperature .....	118
Figure 44 November 17 <sup>th</sup> , 2017 Predicted vs Actual Ambient Temperature .....	119

Figure 45 November 29, 2017 Prediction Error for all Building Elements along with Ambient Temperature .....	120
Figure 46 November 29th, 2017 Predicted vs Actual Surface Temperature of the Window and Spandrel Panel .....	121
Figure 47 November 29 <sup>th</sup> , 2017 Predicted vs Actual Ambient Temperature .....	121
Figure 48 January 6 <sup>th</sup> , 2018 Prediction Error for all Building Elements along with Ambient Temperature .....	122
Figure 49 January 6th, 2018 Predicted vs Actual Surface Temperature of the Window and Spandrel Panel.....	123
Figure 50 January 6 <sup>th</sup> , 2018 Predicted vs Actual Ambient Temperature.....	123
Figure 51 December 31 <sup>st</sup> , 2017 Prediction Error for all Building Elements along with Ambient Temperature .....	124
Figure 52 December 31 <sup>st</sup> , 2017 Predicted vs Actual Surface Temperature for the Window and Spandrel Panel .....	125
Figure 53 December 31 <sup>st</sup> , 2017 Predicted vs Actual Ambient Temperature .....	125
Figure 54 January 13 <sup>th</sup> , 2018 Prediction Error for all Building Elements along with Ambient Temperature .....	126
Figure 55 January 13th, 2018 Predicted vs Actual Surface Temperature for the Window and Spandrel Panel .....	127
Figure 56 January 13th, 2018 Predicted vs Actual Ambient Temperature.....	127
Figure 57 January 2 <sup>nd</sup> , 2018 Prediction Error for all Building Elements along with Ambient Temperature .....	129
Figure 58 January 2nd, 2018 Predicted vs Actual Surface Temperature of the Window and Spandrel Panel .....	129
Figure 59 January 2 <sup>nd</sup> , 2018 Predicted vs Actual Ambient Temperature .....	129
Figure 60 February 12 <sup>th</sup> , 2018 Prediction Error for all Building Elements along with Ambient Temperature .....	130
Figure 61 February 12th, 2018 Predicted vs Actual Surface Temperature for the Window and Spandrel Panel. ....	131
Figure 62 February 12 <sup>th</sup> , 2018 Predicted vs Actual Ambient Temperature.....	131

Figure 63 January 8 <sup>th</sup> , 2018 Prediction Error for all Building Elements along with Ambient Temperature .....	132
Figure 64 January 8 <sup>th</sup> , 2018 Predicted vs Actual Surface Temperature for the Window, Spandrel Panel, and Interior Wall .....	133
Figure 65 January 8 <sup>th</sup> , 2018 Predicted vs Actual Ambient Temperature .....	133
Figure 66 February 7 <sup>th</sup> , 2018 Prediction Error for all Building Elements along with Ambient Temperature .....	134
Figure 67 February 7 <sup>th</sup> , 2018 Predicted vs Actual Surface Temperature of the Exterior Wall .	135
Figure 68 February 7 <sup>th</sup> , 2018 Predicted vs Actual Ambient Temperature .....	135
Figure 69 December 8 <sup>th</sup> , 2017 Prediction Error for all Building Elements along with Ambient Temperature .....	136
Figure 70 December 8 <sup>th</sup> , 2017 Predicted vs Actual Surface Temperature for the Window, Spandrel Panel, and Interior Wall .....	137
Figure 71 December 8 <sup>th</sup> , 2017 Predicted vs Actual Ambient Temperature .....	137
Figure 72 December 5 <sup>th</sup> , 2017 Prediction Error for all Building Elements along with Ambient Temperature .....	138
Figure 73 December 5 <sup>th</sup> , 2017 Predicted vs Actual Surface Temperature for the Window and Spandrel Panel .....	139
Figure 74 December 5 <sup>th</sup> , 2017 Predicted vs Actual Ambient Temperature .....	139
Figure 75 Comparison of Ambient Temperature Prediction Performance for the G1v1, G1v3, and Final Model at the Three-Hour Prediction Window. ....	141
Figure 76 Comparison of the G1v1, G1v3, and the Final Model Performance for the Simulation day of November 17 <sup>th</sup> , 2017 .....	142
Figure 77 Comparison of the G1v1, G1v3, and the Final Model Performance for the Simulation day of November 29 <sup>th</sup> , 2017 .....	142
Figure 78 Comparison of the G1v1, G1v3, and the Final Model Performance for the Simulation day of January 6 <sup>th</sup> , 2018 .....	143
Figure 79 Comparison of the G1v1, G1v3, and the Final Model Performance for the Simulation day of December 31, 2017 .....	144
Figure 80 Comparison of the G1v1, G1v3, and the Final Model Performance for the Simulation day of January 13, 2018 .....	144

Figure 81 Comparison of the G1v1, G1v3, and the Final Model Performance for the Simulation day of January 2, 2018 .....	145
Figure 82 Comparison of the G1v1, G1v3, and the Final Model Performance for the Simulation day of February 12, 2018 .....	146
Figure 83 Comparison of the G1v1, G1v3, and the Final Model Performance for the Simulation day of January 8, 2018 .....	146
Figure 84 Comparison of the G1v1, G1v3, and the Final Model Performance for the Simulation day of February 7, 2018 .....	147
Figure 85 Comparison of the G1v1, G1v3, and the Final Model Performance for the Simulation day of December 8, 2017 .....	147
Figure 86 Comparison of the G1v1, G1v3, and the Final Model Performance for the Simulation day of December 5, 2017 .....	148
Figure 87 April 4 <sup>th</sup> , 2017 Prediction Error for all Building Elements along with Ambient Temperature .....	153
Figure 88 April 4 <sup>th</sup> , 2017 Predicted vs Actual Surface Temperature for the Window and Spandrel Panel.....	154
Figure 89 April 4 <sup>th</sup> , 2017 Predicted vs Actual Ambient Temperature .....	154

## List of Tables

Table 1 Summary of Sensors and Data Collection .....	48
Table 2 Legend for Arduino Circuit Diagram .....	50
Table 3: Heat Capacity of Elements within the Test Cell.....	60
Table 4: Building Element Differential Equations .....	61
Table 5: U-value for Elements of the Test Cell .....	66
Table 6 Internal Heat Capacity Optimisation using G1v3 Model .....	71
Table 7 Regression Model Training Period Analysis using the Final Model.....	76
Table 8 Summary of Simulation Periods used for Model Testing.....	78
Table 9 Prediction Error for Temperatures of Simulated Elements as a Function of Prediction Window Duration for November 17, 2017 ( $T_{out} = 0.93^{\circ}\text{C}$ , wind speed = 0.5 to 1.5 m/s) .....	80
Table 10 Prediction Error for Temperatures of Simulated Elements as a Function of Prediction Window Duration for November 29, 2017 ( $T_{out} = 4.7^{\circ}\text{C}$ , wind speed = 0.5 to 1.5 m/s).....	81
Table 11 Prediction Error for Temperatures of Simulated Elements as a Function of Prediction Window Duration for January 6, 2018 ( $T_{out}=-19.19^{\circ}\text{C}$ , wind speed ranging from 0.5 to 1.5 m/s) .....	82
Table 12 Prediction Error for Temperatures of Simulated Elements as a Function of Prediction Window Duration for December 31, 2017 ( $T_{out}=-16.04^{\circ}\text{C}$ , wind speed ranging from 0.5 to 1.5m/s) .....	83
Table 13 Prediction Error for Temperatures of Simulated Elements as a Function of Prediction Window Duration for January 13, 2018 ( $T_{out}=-13.04^{\circ}\text{C}$ , wind speed ranging from 0 m/s, and solar radiation $400\text{W}/\text{m}^2$ ).....	84
Table 14 Prediction Error for Temperatures of Simulated Elements as a Function of Prediction Window Duration for January 2, 2018 ( $T_{out}=-10.02^{\circ}\text{C}$ , wind speed ranging from 2-4 m/s, and solar radiation $50\text{W}/\text{m}^2$ ).....	85
Table 15 Prediction Error for Temperatures of Simulated Elements as a Function of Prediction Window Duration for February 12, 2018 ( $T_{out}=-2.51^{\circ}\text{C}$ , wind speed ranging from 0.5-2 m/s, and solar radiation $120\text{W}/\text{m}^2$ ).....	86
Table 16 Prediction Error for Temperatures of Simulated Elements as a Function of Prediction Window Duration for January 8, 2018 ( $T_{out}=0.5^{\circ}\text{C}$ , wind speed ranging from 1-2.5 m/s, and solar radiation $50\text{W}/\text{m}^2$ ).....	88

Table 17 Prediction Error for Temperatures of Simulated Elements as a Function of Prediction Window Duration for February 7, 2018 ( $T_{out}=-3.57^{\circ}\text{C}$ , wind speed ranging from 0.5-1.5 m/s, and solar radiation $50\text{W}/\text{m}^2$ ).....	89
Table 18 Prediction Error for Temperatures of Simulated Elements as a Function of Prediction Window Duration for December 8, 2017 ( $T_{out}=1.04^{\circ}\text{C}$ , wind speed ranging from 2.5-3.5m/s, and solar radiation $50\text{W}/\text{m}^2$ ).....	90
Table 19 Prediction Error for Temperatures of Simulated Elements as a Function of Prediction Window Duration for December 5, 2017 ( $T_{out}=10.93^{\circ}\text{C}$ , wind speed ranging from 2-4m/s, and solar radiation $50\text{W}/\text{m}^2$ ).....	91
Table 20 Prediction Error for G1v2 Model on February 7 <sup>th</sup> , 2018 using Turbulent and Natural Convection when Representing the Heater Unit.....	92
Table 21 Prediction Error for G1v2 Model on January 8 <sup>th</sup> , 2018 using Turbulent and Natural Convection when Representing the Heater Unit.....	92
Table 22 Prediction Error for G1v2 Model on December 8 <sup>th</sup> , 2017 using Turbulent and Natural Convection when Representing the Heater Unit.....	93
Table 23 Internal Mass Heat Capacity found using the Parameter Estimation Tool.....	95
Table 24 Internal heat capacity performance.....	96
Table 25 Results of the general regression model and the split regression model for each building element with RMSE, MAE and WAPE performance measurements.....	102
Table 26 Summary of p-value confidence intervals .....	103
Table 27 Performance of the Exterior Wall Occupied Regression Model .....	104
Table 28 Student t-test P-values and t-values for Occupied Exterior Wall Regression Model..	104
Table 29 Student t-test P-values and t-values for Unoccupied Exterior Wall Regression Model .....	105
Table 30 Performance of the General Ceiling Regression Model .....	106
Table 31 Student t-test P-values and t-values for Ceiling General Regression Model.....	106
Table 32 Performance of the Occupied and Unoccupied Floor Regression Models.....	107
Table 33 Student t-test P-values and t-values for Occupied Floor Regression Model .....	108
Table 34 Student t-test P-values and t-values for Unoccupied Floor Regression Model .....	108
Table 35 Performance of the Occupied and Unoccupied Spandrel Regression Models .....	109
Table 36 Significance of the Variables within the Occupied Spandrel Regression Model .....	110

Table 37 Student t-test P-values and t-values for Unoccupied Spandrel Regression Model.....	111
Table 38 Performance of the Occupied and Unoccupied Window Regression Models.....	112
Table 39 Student t-test P-values and t-values for Occupied Window Model.....	112
Table 40 Student t-test P-values and t-values for Unoccupied Window Model.....	113
Table 41 Performance of the Occupied and Unoccupied Interior Wall Regression Models.....	114
Table 42 Student t-test P-values and t-values for Occupied Interior Wall Model.....	114
Table 43 Student t-test P-values and t-values for Unoccupied Interior Wall Model.....	115
Table 44 Hidden Layer Optimisation for each Neural Network.....	116
Table 45 Comparison of the Split Regression Models and the Neural Network Models for the Exterior Wall, Spandrel Panel and Window .....	117
Table 46 Prediction Error for Temperatures of Simulated Elements as a Function of Prediction Window Duration for November 17, 2017 ( $T_{out}=0.93^{\circ}\text{C}$ , wind speed ranging from 0.5 to 1.5 m/s) .....	118
Table 47 Prediction Error for Temperatures of Simulated Elements as a Function of Prediction Window Duration for November 29, 2017 ( $T_{out}=0.93^{\circ}\text{C}$ , wind speed ranging from 0.5 to 1.5 m/s) .....	120
Table 48 Prediction Error for Temperatures of Simulated Elements as a Function of Prediction Window Duration for January 6, 2018 ( $T_{out}=-19.19^{\circ}\text{C}$ , wind speed ranging from 0.5 to 1.5 m/s) .....	122
Table 49 Prediction Error for Temperatures of Simulated Elements as a Function of Prediction Window Duration for December 31, 2017 ( $T_{out}=-16.04^{\circ}\text{C}$ , wind speed ranging from 0.5 to 1.5 m/s, and solar radiation $400\text{W}/\text{m}^2$ ) .....	124
Table 50 Prediction Error for Temperatures of Simulated Elements as a Function of Prediction Window Duration for January 13, 2018 ( $T_{out}=-13.04^{\circ}\text{C}$ , wind speed ranging from 0 m/s, and solar radiation $400\text{W}/\text{m}^2$ ).....	126
Table 51 Prediction Error for Temperatures of Simulated Elements as a Function of Prediction Window Duration for January 2, 2018 ( $T_{out}=-10.02^{\circ}\text{C}$ , wind speed ranging from 2-4 m/s, and solar radiation $50\text{W}/\text{m}^2$ ).....	128
Table 52 Prediction Error for Temperatures of Simulated Elements as a Function of Prediction Window Duration for February 12, 2018 ( $T_{out}=-2.51^{\circ}\text{C}$ , wind speed ranging from 0.5-2 m/s, and solar radiation $120\text{W}/\text{m}^2$ ).....	130

Table 53 Prediction Error for Temperatures of Simulated Elements as a Function of Prediction Window Duration for January 8, 2018 ( $T_{out}=0.5^{\circ}\text{C}$ , wind speed ranging from 1-2.5 m/s, and solar radiation $50\text{W}/\text{m}^2$ ).....	132
Table 54 Prediction Error for Temperatures of Simulated Elements as a Function of Prediction Window Duration for February 7, 2018 ( $T_{out}=-3.57^{\circ}\text{C}$ , wind speed ranging from 0.5-1.5m/s, and solar radiation $50\text{W}/\text{m}^2$ ).....	134
Table 55 Prediction Error for Temperatures of Simulated Elements as a Function of Prediction Window Duration for December 8, 2017 ( $T_{out}=1.04^{\circ}\text{C}$ , wind speed ranging from 2.5-3.5m/s, and solar radiation $50\text{W}/\text{m}^2$ ).....	136
Table 56 Prediction Error for Temperatures of Simulated Elements as a Function of Prediction Window Duration for December 5, 2017 ( $T_{out}=10.93^{\circ}\text{C}$ , wind speed ranging from 2-4m/s, and solar radiation $50\text{W}/\text{m}^2$ ).....	138
Table 57 Heat Capacity Values found for the Final Grey Box Model in Comparison to those found previously in the G1 Model. ....	150
Table 58 Performance of the Final Model when Trained with 1 week, 2 weeks, and 4 weeks of data.....	151
Table 59 Internal heat capacity values found from the parameter estimation tool for the 1 week, 2 week and one-month models .....	152
Table 60 April 9th, 2018 Simulation Conditions.....	152
Table 61 Prediction Error for Temperatures of Simulated Elements as a Function of Prediction Window Duration for April 4 <sup>th</sup> , 2017 ( $T_{out}=5.27^{\circ}\text{C}$ , wind speed ranging from 1.5 to 4 m/s, and solar radiation $600\text{W}/\text{m}^2$ ).....	153
Table 62 Final Model and G1v1 Model results when using true plug load data compared to calculated plug load data.....	155
Table 63 Overall comparison results for the G1 grey box model and final grey box model.....	155
Table 64 Final Model and G1v1 model when considering latent heat and when omitting latent heat .....	157

## 1 Introduction

Climate change is one of the greatest challenges of our generation. This issue is caused by an increase in greenhouse gas (GHG) emissions caused by human activity [1]. The Intergovernmental Panel on Climate Change (IPCC) reports that buildings are responsible for 32% of total global energy use and 19% of energy-related GHG emissions [2]. This energy consumption is only expected to increase in the coming years due to growing population, and lifestyle changes. It is estimated that by 2035, energy consumption in the building sector will increase by 28% [3]. Therefore, as our society moves forward, it is crucial for our buildings to be constructed to higher standards so that we can reduce the GHG emissions from the building sector and help mitigate global climate issues.

The energy breakdown for the building sector demonstrates space heating accounting for between 32 and 34% of the overall energy consumption in both residential and commercial buildings [2]. New building regulations encourage the use of high-performance equipment however, it has been shown that most modern heating systems are not properly used and are not adjusted to the thermal demands of the building [4]. A study released by the National Renewable Energy Laboratory (NREL) [5] identified the principal challenge in achieving energy efficient buildings is the “lack of innovative controls and monitoring systems”. Therefore, research interest in more advanced control systems has started to increase. Model predictive control (MPC) for building control systems is one type of “smart” control system that has been widely reported as a promising alternative to current HVAC control strategies [4]. This can be seen in the study by Carrascal *et al.* [6], where the implementation of MPC in the HVAC system of a municipal housing building resulted in 15% energy savings compared to using typical PID controllers.

Model predictive control systems utilize predictions of disturbance effects such as weather, solar radiation, and occupancy, along with, knowledge of the building’s thermal dynamics to determine the necessary HVAC output. The greatest advantage of this system compared to other HVAC control systems is information on the building’s thermal behaviour [7]. The building dynamics however, can be difficult to model as the thermal dynamics increase in complexity with the number of modeling zones and are subject to uncertain disturbances such

as occupancy and weather [4]. For MPC, three modeling types are used to represent the thermal dynamics: white box models, black box models, and grey box models.

White box models are detailed physical representations of the building and are typically simulated using software such as EnergyPlus [8,9]. These models are very accurate representations of the thermal behavior as they have extensive knowledge of the properties and parameters of the building [8]. However, white box models are not widely used for thermal dynamic modeling within MPC systems due to their high computational time and the considerable expense involved in creating the model [8].

Black box models stand in contrast with white box models as they have no physical knowledge of the building, but are instead completely data-driven, using linear or non-linear mathematical functions [9]. It is common to see artificial neural network (ANN) black box models as MPC thermal dynamic models due to their ability to handle multivariable and nonlinear modelling issues, such as building thermal dynamics [7]. The prediction accuracy of this type of model however, is limited to the data it is presented; this leads to large forecasting errors when the model is introduced to data outside the training domain space. Therefore, to train black box models to the level of accuracy required for MPC, large data sets covering all seasons are required.

Grey box models integrate the physical representation of white box models with the data analytics properties of black box models. These models use the physical information of the space to create the model structure and data measurements to solve for unknown parameters. This reduces the challenges associated with both model types, lowering the computation costs and time needed to create the models and reducing the size of the training data sets. Grey box models commonly represent the physical structure using resistor-capacitance (RC) networks. RC networks represents the thermal dynamics as an electrical circuit with lumped representative resistors and capacitors [7]. The resistors represent the building's thermal resistance, and the capacitors represent the building's thermal capacitance. These values are commonly found from building construction drawings and specifications. One of the greatest challenges with creating grey box thermal dynamic models is determining these values when the building no longer has the construction specifications. Previous research has solved this issue by using parameter estimation techniques to determine the resistance and capacitance

values [5,6,8, 10,11,12,13,14,15,16,17]. The parameter estimation techniques used within these studies include *Matlab* Optimization Toolbox using hill climbing algorithm [10], *Matlab* Optimization Toolbox using interior point algorithm [11], *Matlab* greyest function [12], and linear fitting using least squares method [13]. The study conducted by Berthou *et al.* [11] used an interior point algorithm to solve for the RC parameters in the grey box model, resulting in an ambient temperature prediction error of less than 2% for both heating and cooling seasons. The use of parameter estimation tools to solve for unknown building property values allows for the creation of grey box thermal dynamic models for older structures. This in turn expands the number of buildings that can use MPCs with grey box thermal dynamic modeling in their HVAC system.

Parameter estimation tools are one solution for the issue surrounding thermal dynamic modeling for older structures. This research aims to explore the potential of a different modeling technique. This thesis investigates the ability to create a grey box model without building information where the model is able to determine the net thermal dynamics using only building automation system (BAS) points. This is the first observed study attempting to eliminate the resistance and capacitance values within grey box thermal dynamic models.

### 1.1 Research Objective

The objective of this study is to create of a grey box thermal dynamic model that has no building parameter information, relying solely on building automation system points to determine the net thermal dynamics. This research also determines the suitability of this model type for use within MPC HVAC systems. The final model is analyzed for its ability to predict the test cell's indoor ambient temperature, and the generalisation ability of the model in terms of required training period and performance in other seasons.

### 1.2 Research Questions

1. Can a grey box thermal dynamic model be developed with the ability to accurately determine the net thermal dynamics without any building construction information, relying solely on the Building Automation System (BAS) points?
2. Does a model of this type have the generalisation ability to predict temperatures with reasonable accuracy in new conditions?

## 2 Background

### 2.1 Model Predictive Control

HVAC systems are one of the largest contributors to the overall energy consumption of commercial building's [2]. The implementation of advanced and predictive control systems has significant potential in reducing energy consumption, with energy savings as high as 25% [13]. Despite the research dedicated to developing more advanced HVAC controls, the most common HVAC control systems installed within commercial buildings remains a combination of proportional-integral derivative (PID) control and on/off control [19]. These systems control actuators within the HVAC system based on the current and previous ambient temperature. It has been stated that HVAC systems controlled with PID/on-off controllers often result in over-heating or over-cooling of a building due the fact that their control algorithm does not consider thermal dynamics, delaying their response to the indoor temperature [19]. This results in a building with poor thermal comfort and excess energy consumption.

In recent years, Model Predictive Control (MPC) has been the subject of increasing research interest. MPC systems demonstrate the potential to improve the efficiency of HVAC system performance by considering both available passive gains and time-of-use electricity rates [21]. MPC systems use inputs of: the current conditions of the space, along with, relevant disturbance effects such as weather, solar radiation, and occupancy [19]. For each sampling interval of the model a finite-horizon optimal control problem is formulated using the prediction data to create a heating / cooling plan that satisfies both the dynamics and the building constraints [20]. The success of MPC is due to its simplicity and its ability to handle complex systems with hard control constraints and many inputs and outputs [22]. The improvement of MPC controllers over typical PID controllers can be witnessed in many research studies including the work conducted by Dong and Lam [23], who achieved 30% heating energy and 17.8% cooling energy savings in a solar decathlon house with the implementation of Nonlinear MPC instead of setpoint control. In a similar study of 1960's social housing, researchers compared the use of MPC HVAC controller to a traditional PID controller [6]. Switching the HVAC control to MPC, without any other form of building upgrades, resulted in energy savings between 10-15% [6]. Similarly, research for a newly constructed building comparing the performance of MPC HVAC system to a typical PID controller demonstrated 12.7% savings in the summer months

and 2% savings in the winter when using the MPC HVAC system [24]. Finally, a summary written by Afram *et al.* [25] comparing classical on/off PID control and MPC systems concluded that MPC had the greatest energy and cost savings, more robustness to dynamic disturbances, and better peak load shifting ability. The findings from these comparative studies clearly demonstrate the superior energy saving performance of MPC over other HVAC control systems.

### 2.1.1 Economic Model Predictive Control

Economic MPC controllers' function in the same manner as MPC controllers and have the same input information, with the addition of electricity pricing input, allowing the system to optimize both the HVAC system performance and energy costs. The optimization function for this MPC system uses information about on-peak and off-peak electricity hours along with the building's active thermal storage properties to condition the building at off-peak times. In a study investigating the use of an MPC system in a test cell residential home, the model demonstrated savings of 50% in operating costs during the summer when compared to an on/off controller with fixed set point set at 24°C [26]. Similarly, a single room test bed study conducted by Soudari *et al.* [13] investigated the use of personalized energy management systems for HVAC control based on economic MPC in residential buildings. Their research concluded energy savings between 9.7% and 25% and cost savings between 8.2% and 18.2% can be achieved using this system, depending on the occupant behavior and external conditions [13]. Economic MPC systems have also been researched within commercial buildings, as shown in the study of a single storey commercial building in Chicago Illinois by Ma *et al.* [27]. The results from this study demonstrated the building used 25% less energy and saved 28% in energy related costs when using economic MPC in comparison to the baseline control system; the baseline system involved a temperature setpoint in the lower bound of the comfort region when the building was occupied and turning off the HVAC system when the building was unoccupied [27]. Unlike the studies mentioned previously, which used test cell measurements, this study was based entirely on simulated results from *EnergyPlus* (with connection to *Matlab* for HVAC control simulation). Although the studies above demonstrated strong performance results, the success and degree of cost savings for an economic MPC scheme is dependent on the buildings construction. Buildings constructed with lightweight materials do not have the necessary

thermal storage capacity to be as successful using this control system. As seen in the study conducted by Alhaj *et al.*[5], the savings from the Economic MPC were less obvious when compared to a PID controller due to the low thermal inertia qualities of the building. This is demonstrated again in the study by Široký *et al.* [20] when comparing the performance of economic MPC on insulated and uninsulated blocks of a building. The insulated blocks demonstrated energy savings of up to 29% while the uninsulated sections had energy savings of up to 17% [20] .

### 2.1.2 Thermal Dynamic Modeling

The thermal dynamic model in MPC systems give information on the thermal behavior of the space, determining the future ambient temperature based on the model inputs. The most challenging component of MPC implementation is modeling the thermal dynamics of the building [19]. The thermal dynamics are complex and vary greatly from building to building, as well as, increase in complexity with the number of zones in the building [4]. Some of the difficulties include having several uncertain disturbances such as weather and occupancy which, require the prediction of non-Gaussian distributed loads such as ambient temperature and occupancy load [19]. Further, the internal space of a building is divided into several zones that are conditioned by individual air handling units creating a multiple-input, multiple-output system [19]. The thermal dynamic model used within MPCs must therefore be able to describe the relations between the input and output variables. Additionally, the thermal dynamic model used within MPCs must have the ability to predict conditions when short term disturbances and long term accumulated changes in building temperature are known. For control purposes, it has been stated that models need to be simple enough that they can be solved in an adequate amount of time, while also having enough complexity to accurately model the thermal dynamics of the space [7]. To undertake the problem of modeling thermal dynamics for use in MPC three models can be used: physical white box models, statistical black box models, or grey box models.

## 2.2 Use of Test Cells in Predictive Control Development

The use of test cells for collecting site data, either for input (grey box or black box models) or validation (any model type), is widespread in the field of predictive control. Most studies will

either install sensors within a test cell [12], or use an existing building monitoring system (BMS) [16,29], building automation system (BAS) [20], or data acquisition system (DAQ) [23] to gather this data. On the rare occasion, such as in the study by Berthou *et al.* [11], the grey box model is trained using synthetic learning data to avoid noise and measurement uncertainties. Another method is using data from a simulation model, as conducted in the study by Gyalistras *et al.* [29] and in the study by Alhaj *et al.* [5]. Variables collected for the creation of grey box and black box models include the ambient and surface temperatures, HVAC system heat load, occupancy, weather, and solar conditions.

### 2.2.1 Use of Temperature Sensors

Both black box and grey box models require measurements of ambient temperature for model training, and validation. The indoor ambient temperature measurements are collected using ambient measurement devices, installed either at varying heights [23] or at an average room height [8].

In addition to the ambient temperature measurements, grey box models also collect surface temperature measurements for parameter estimation or tuning purposes [13,18]. This is seen in the work of Terés-Zubiaga *et al.* [18] where the surface temperature measurements are used to adjust parameters in the grey box model to achieve more accurate surface temperature results. The sensors were installed with conductive paste for good surface contact and reflective tape to protect against solar radiation. Additionally, heat flux plates were installed on the walls of the building in this study to measure the value of the heat flux through the facades, floor, and ceiling elements.

### 2.2.2 Internal Load

Internal heat energy is included within predictive control models to account for the generation of sensible heat within the space. Lighting and plug load are often estimated using heat load values from ASHRAE 90.1 [10]. For studies that use simulation models to gather data, the internal load values are defined in the simulation program [14,27]. Some models choose to ignore these loads as negligible compared to the other heat loads, and thus leave them out of the thermal dynamic model [7,8]. Still other models install energy meters for monitoring plug load data [18,23,31].

### 2.2.3 HVAC Systems

HVAC systems vary greatly between buildings depending on the climate and building type. Therefore, how they are modeled within thermal dynamic models and MPC systems vary. In order to effectively represent HVAC systems, data is collected to calculate the energy loads of the system. Sometimes the temperature and relative humidity of the supply air along with supply airflow rate is measured to calculate the ventilation heat loads, as seen in [7,10,31]. Other models collect data at the equipment level with sensors measuring the return and supply water temperature along with the water flow rate [7, 12,16,20]. To monitor test cells with electric heating electrical load data is collected [17,18]. In contrast, Hydronic heating systems are typically monitored with the supply and return water temperature sensors [20].

### 2.2.4 Occupancy Modeling

Occupancy is one of the more challenging data points to capture for thermal dynamic models due to the sporadic behavior of occupants. Many models simplify the occupancy load as a set profile based on historic data [10,11,16]. An example of this can be seen in the study [10] where the occupancy load in the thermal dynamic model was assumed to be 85 people from 8am to 10pm, Monday to Friday. The heat load of the occupants was found using ASHRAE 90.1-2005 standards [10]. More complex occupancy data collection can be seen in [13] with limit switches measuring door-firings, along with, retro-reflective sensors and door-mat sensors measuring occupant movement to infer room occupancy. In other studies, carbon dioxide sensors were used to determine the occupancy based on the carbon dioxide ppm concentrations within the room [23,31,32]. The work conducted by Mustafaraj *et al.* [32], demonstrates the importance of including occupancy load within thermal dynamic models as their results demonstrate improved prediction performance of the black box model when incorporating occupant count from carbon dioxide data. Their conclusion was that future research should consider the full heat and humidity effects of occupants in thermal dynamic models for MPC [32].

### 2.2.5 Modeling of External Conditions

Solar radiation affects the exterior of the modeling space, warming the façade, and the interior of the modeling space, with the radiation entering through the window. Most thermal dynamic models incorporate solar radiation and weather effects with significant variety in how these elements are considered. One method of determining the solar radiation value is using energy modeling simulation programs such as *EnergyPlus* to calculate the solar heat load and extracting the data [10]. *Energyplus* considers variables such as the direct and diffuse solar radiation from the sun, ground, and sky reflectance; building geometry and orientation; any potential building shading; the window transmittance along with the time of year; latitude; and weather conditions [10]. Another solar radiation method is using solar radiation algorithm with inputs of cloud cover and building information pertaining to orientation, location, solar protection, and glazing to calculate the direct and indirect solar heat loads, as seen in the study [11]. The most commonly seen method however, is the use of local weather stations to gather overall solar radiation measurements [12,13,16,17,18,20]. In a rare case, where the building was programmed with external shading devices, the solar load was omitted from the internal heat load calculation for the thermal dynamic model due to the sun being blocked during daytime hours [7].

Similar to how solar radiation is measured, exterior weather conditions are commonly found using the closest weather station to the simulation building [12,18,33,31]. Other studies gathered data from online databases [30] ; or when simulating within energy modeling software used weather files [8,10,11,29]. Some research installed exterior sensors to gather the outdoor temperature and relative humidity conditions [7,23].

### 2.3 White Box Model

White box models are created using detailed physics-based equations. These are used to model the building components, sub-systems, and systems to predict the building behavior [35]. The input parameters – including weather conditions, building structure, building systems, and building equipment – need to be obtained from building design plans, site measurements or manufacturer catalogs [35]. White box models are commonly run on simulation software such as *EnergyPlus* [14,15] or *TRNSYS* [36]. Due to their level of detail and representation of

underlying physical mechanisms, they have the potential to represent the thermal dynamics of the building very well [35].

A significant drawback of using white box models for use in MPC's is the complexity associated with their creation and solution [35]. The models require detailed information on the building construction and system parameters that are usually difficult to obtain, if they are available at all. These models are therefore very time consuming to create and computationally slow to solve [35]. Another challenge when using white box models in MPC systems is connecting the white box model simulation output to the MPC control system input. Energy modeling simulation programs cannot be stopped once the simulation has started, therefore the results from the model simulation cannot be sent to the HVAC control system and the HVAC control parameters cannot be sent to the simulation. To solve this problem, a building control virtual test bed (BCVTB) was created by Lawrence Berkley national laboratories [24] and is used in many MPC studies as a communication software between energy modeling software such as *EnergyPlus* [24,27,29] and *TRNSYS* [37] and HVAC control models.

It has been shown that the level of detail within white box models is not truly necessary for determining thermal dynamic behavior [23]. Within the study [23], researchers compared a white box model made in Modelica to a simplified, linear white box model. The Modelica model, named the 'complex model', used the simulation program's physical acausal modeling approach, which uses a resistance and capacitance network to represent the thermal zones. By reducing the number of zones corresponding to the hydraulic system, a simplified form of the Modelica model was created. This 'simplified model' was created based on energy balances, similarly to what is done with grey box models. The study found that compared to the complex model, the simplified version had temperature prediction deviation of less than 0.07 kelvin. Therefore, it can be extended from this study that simplified models, such as grey box models, can accurately predict the ambient temperature without the level of detail required for a white box model.

## 2.4 Black Box Model

Black box models by definition are based purely on data relationships, and do not incorporate any knowledge of the building's physical structure [8]. Statistical models are applied to determine correlations between the operational data, and energy consumption [35]. Black box

models use data measurements from the building to train the model, such that it is able to predict the building operations. The black box model simplicity is beneficial as it is computational efficient and easy to create [35].

#### 2.4.1 Linear Models

Black box thermal dynamic models can be linear or nonlinear models. One type of statistical linear black box model, seen in research [32], is an Autoregressive with exogenous input (ARX) model. ARX models are time series linear models that use past building load information to determine future building loads [38]. The study conducted by Powell *et al.* [38] compared the linear ARX model to a neural network based Nonlinear Autoregressive network with Exogenous inputs (NNARX). NNARX models are similar to ARX models that use previous load data to forecast future building loads, however, this model uses neural networks to solve for the future loads [38]. The study determined that the NNARX model predicted the temperature and relative humidity more accurately, due to the non-linear design of neural network models. As temperature and relative humidity are governed by nonlinear diffusion equations, nonlinear models demonstrate a stronger ability to predict future conditions [32]. Another study by [7], discusses the same issue with linear models stating they have an inability to capture the non-linear thermal dynamic effects, potentially resulting in larger errors when strong nonlinear variables are present in the system.

#### 2.4.2 Neural Networks

Recently, there has been a shift towards the use of Artificial Neural Networks (ANN) models for building simulation and control. Studies demonstrate these models as being superior for modeling nonlinear HVAC systems compared to other modeling methods [7,19,38]. Neural network models mimic the human neuron system, developing learning ability using historical data, weighted networks, and learning rules [7]. The parameters of neural networks are the number of neurons and the weights connected to the input variables [7]. Neural network models gain the ability to learn from historical data by adjusting the weights of the connections between the various nodes (“neurons”) [7]. An ANN structure has three layers, as illustrated conceptually in Figure 1.

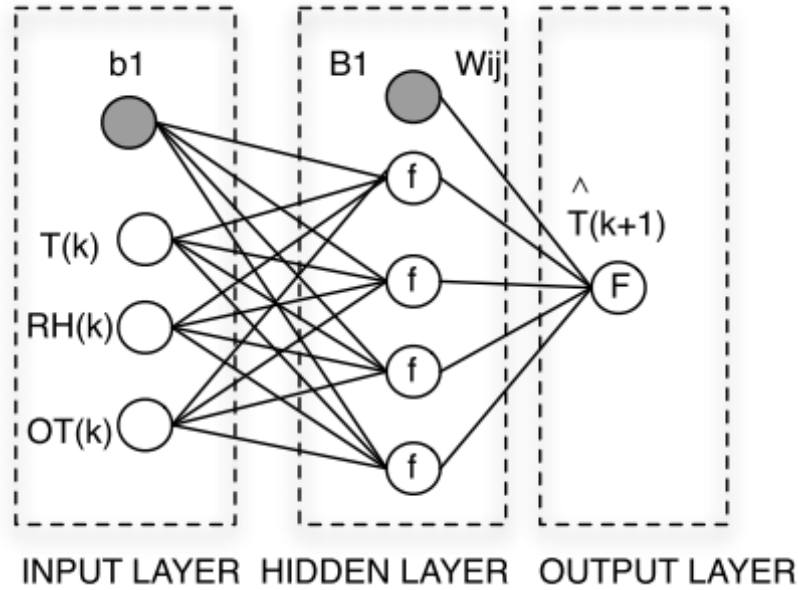


*Figure 1 Artificial Neural Network Structure showing Relationship between Inputs and Outputs using Neurons [30]*

The first layer of an ANN consists of sensory units that are fed data from the input variables [7]. The inputs to the first layer are multiplied by their respective weights, summed, and added to the bias before being sent to the second layer. This second layer consists of one or more hidden layers designed with a set number of neurons and with each neuron having its own activation function, logical sigmoid function, and a sum operator to perform nonlinear transformations on the input data [7], as seen in Figure 2.

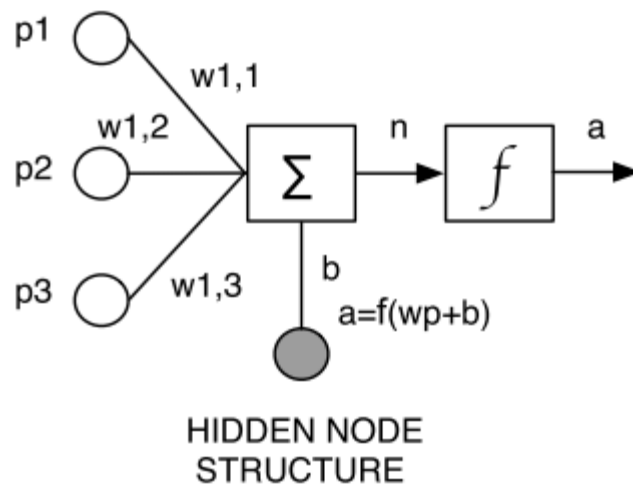


*Figure 2 Hidden Layer of Neural Network [30]*

The number of neurons within the second hidden layer of the neural network is chosen by the designer, and varies with every neural network. For example, the network model in [12] optimized the number of neurons for the NARX model by investigating models with hidden layer size ranging from 0 to 10. Using cross validation methods, the model that demonstrated the most accurate results had a hidden layer size of 1 [12]. Comparatively, within the research [13], the hidden layer size was optimized using a trial and error approach, determining that eight hidden layers was the best balance of accuracy and computational time. Each of the neurons performs nonlinear transformation using a sum operator and an activation function, shown below [7].

$$f(x) = \frac{1}{1 + e^{-x}} \quad (1)$$

Neural networks are trained using input and output data along with an optimization algorithm. Based on the input and output data, the algorithm determines the neural network parameter that best represents the training data set. The optimization algorithms used in neural net training varies; the most commonly seen method is the Levenberg-Marquardt (LM) approach [12,30,32]. This algorithm minimizes the mean square error between the predicted and the actual output value. LM is considered a faster optimization algorithm compared to other algorithms, but with the disadvantage of being more computationally expensive [12]. Other studies, such as [7], use Bayesian regularisation as the parameter training method stating that it improves the generalisation of the ANN model to prevent over fitting but at the cost of a slower convergence speed.

When creating a neural net, the network is trained and tested using different sets of data. This is to ensure that the testing results from the neural network are based on data it has never seen before. The data also needs to be normalized before being input into the model to ensure data with larger values do not overpower data with lower values, which might be equally influential. The study [7], describes the training method for the neural network with 70 percent of the data being used for training, 15 percent of the data being used for validation, and 15 percent of the data being used for testing. The data used within the model was normalized on a scale of 1 to -1 to avoid dominant effects of select variables. This is reversed at the output of the network so that the output is the real system value.

There are two types of neural network architecture: feedforward, and feedback [39]. In a feedforward network the data moves in one direction only while feedback neural networks have additional feedback from the previous layer. Feedback models are commonly used for adaptive control applications [39]. An example of a feedback neural network thermal dynamic model is in [30] where the researchers investigated the use of multi-input multi-output (MIMO) network structures instead of the more typically used multi-input single-output (MISO). This research looked into the implications of using neighboring zone temperatures as neural network inputs and the result of thermal zone coupling on prediction accuracy. Their findings demonstrated that the feedback neural network had better prediction results when considering the neighboring zone temperature and both interior and exterior zones could be predicted accurately based on outdoor temperature [30]. This structure is seen again in a later study conducted by Huang *et al.* [7] where a feedback nonlinear autoregressive model with exogenous input (NARX) model is used to represent the thermal system for an airport in southern Australia [7]. This study, similar to the previous research, investigated the implications when considering neighboring HVAC zone conditions in an open concept space. The two modeling methods compared include a MIMO neural network model representing all five HVAC zones and five MISO neural network models representing each individual HVAC zone. The study found the multi-zone model had better performance than the single zone network model, due to the fact that the model considered thermal coupling between zones [7]. The research concluded that the MIMO model is a good solution for modeling of commercial buildings that are often built with large open areas conditioned by multiple HVAC systems [7].

#### **2.4.3 Black Box Models vs Grey Box Model**

Grey box models, as briefly described in Section 2.1, are combinations of both white box and black box models, incorporating both physical representations of the space and training data. A study was conducted to compare the thermal dynamic modeling accuracy of black box and grey box models [12]. The black box models compared within the study were linear ARX and nonlinear NARX models while the grey box models were variations of RC networks, with the most complex being a 4R3C structure (see Section 2.5.1). The models were tested for a winter simulation period, resulting in the NARX model having 14% lower RMSE than the ARX model, and 21% lower RMSE than the 4R3C grey box model [12]. However, this study did not

simulate the models in different seasons which, is the weakness of black box models. Black box models are constrained to the building operation conditions within their training domain space; this often leads to large forecasting errors when the simulation is run during conditions that the model has never seen before [35]. Therefore, although the study above demonstrated the black box models having the best performance for the winter season, there is a likelihood that it would not perform as well when simulated for other seasons as it was specifically trained for the winter season.

#### *2.4.4 Challenges of Black box Models*

A considerable disadvantage for black box models is the fact that the quality of the data used to train the models directly determines their predictive performance. To create a robust model, measurements from all seasons of the year are needed to assure that the model is not skewed to one period. In the research conducted in [7] the training data included both the historical maximum values as well as the minimum values to increase the generalisation of the model. This study also used a sliding window method to make the neural networks more adaptive to change. This method stores the training data in a sliding window, so new data collected from the site will replace the older data and the model can be re-trained periodically [7].

A second concern when using a neural network black box model is overfitting the network. This occurs when the number of data points is similar to the number of parameters. This permits the network to memorize the training examples, making the model unable to perform well in new situations [40]. This can be avoided by using cross-validation to artificially expand the number of data points when training the black box models [12]. Initially this value along with the training error decreases during the first number of iterations but, when the network begins overfitting the validation error increases. The *Matlab* neural network app monitors this and stops training the network if the validation error is observed to continually increase for a set number of iterations [40].

## **2.5 Grey Box Models**

Grey box models are created using a combination of physical white box models and statistical black box models. This type of model uses physical relationships to define the model's structure and its state equations, while data measurements are used for the identification process to

determine model parameters [8]. Compared to black box models they have better generalization ability [25] and compared to white box models they are less time consuming and expensive to construct [35].

The white box component, the physical representation of the space, is created using an equivalent electrical (RC) network. The model represents different building components through resistances (R) and capacities (C) analogous to an electrical network [8]. These building components are lumped together with the heating loads of the space to create the lumped RC network model. The RC network models the heat transfer relationship within the space in an equivalent electrical circuit – a simplified representation of the thermal dynamics. Typical simplifying assumptions that are used when creating RC network models include: one-dimensional heat transfer, uniform surface temperature, fully mixed ambient temperature, and constant density value of the interior air [24].

RC networks are used to derive the differential equation for each of the temperature nodes. The differential equations are derived from physical laws defining the dynamics of the building [21]. Grey box models are made up of a set of these differential equations formulated in a state space form. A state space model represents the dynamics of a  $N^{\text{th}}$  order system as a first order differential equation in an N-vector [41]. An example of a standard linear state-space is illustrated in equation (2) and (3) below.

$$\dot{x}(t) = Ax(t) + Bu(t) + Ed(t) \quad (2)$$

$$y(t) = Cx(t) \quad (3)$$

Within these state space equations  $x$  represents the walls and zone temperature vector,  $\dot{x}$  is the differentiation with respect to time,  $y$  is the output vector of the simulated zone temperature,  $u$  is a vector representing the controlled HVAC inputs to the space, and  $d$  is the vector of disturbances to the space including exterior conditions and heat gains [4]. When integrating these models into control processes it is preferred for the models to have a simpler structure, as it has been concluded that second order state space is sufficient to describe the thermal dynamics [5]. The order of the state space describes the order of the differential equation that can represent the system, so a second order system is represented by a second order differential equation. This type of model, a second order system, can be seen in the work [5] where after

parameter estimation the grey box model was successfully installed within an MPC control system achieving 25% energy savings [5].

### 2.5.1 RC-Network Structure

The structure of the RC network varies for every study depending on the space being represented and the amount of detail added by the designer. One consistency amongst these models is the use of a 3R2C model ( Figure 3, right) for representing the exterior wall [6,8,10,16,24]. This model structure is commonly paired with a parallel resistor to represent a window unit in the wall [6,10], as illustrated in Figure 3 (left) .The meaning of the subscripts in Figure 3 are, ‘in’ representing interior, ‘out’ representing exterior, ‘a’ representing ambient properties, ‘e’ representing the equivalent resistivity value, and ‘e,win’ representing the resistivity value for the window. The three resistors in the model represent the resistivity of the interior air film, the elements being modeled, and the exterior air film. The two capacities represent the heat storage of the interior and exterior sides of the wall.

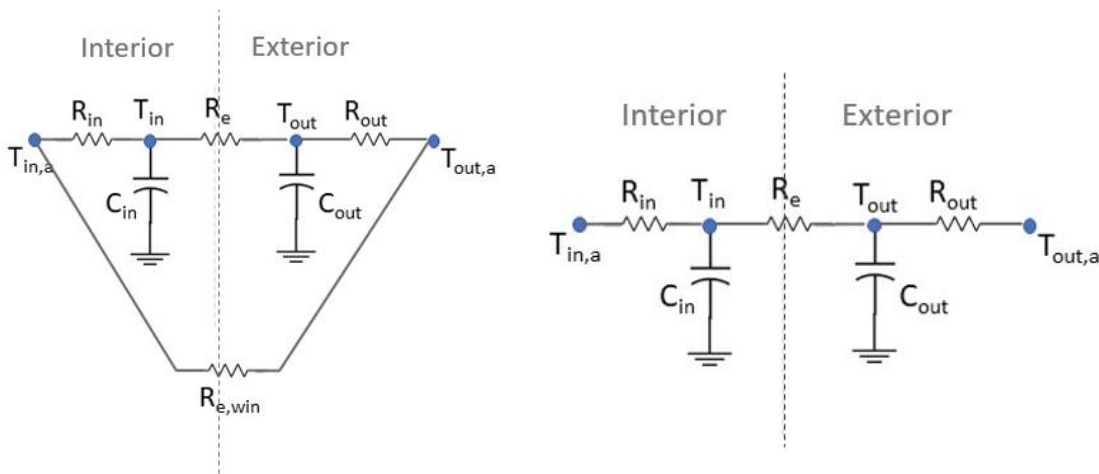


*Figure 3 R2C Network Structure with (left) and without (right) window component*

Elements with low heat storage capacity are represented with an equivalent resistance, as seen with the window in Figure 3. For curtain wall or window wall assemblies, the window is a single resistor represented on a separate branch of the RC network not attached parallel to any other RC network branches. For elements where conductive heat transfer is not modeled but the surface temperature affects the ambient temperature, the component is modeled with a 1R1C structure, as seen in [8] and [17] with the interior walls represented as 1R1C systems.

The arrangement of an RC network depends on the structure of the space and the resistance/capacitance values depend on the materials and dimensions [4]. An example of an RC network representing a mixed-mode building is illustrated in Figure 4 [16]. This study represents the roof and the exterior wall as separate 3R2C network branches, the window unit as a single resistance branch, and the internal mass as a 2R2C branch.

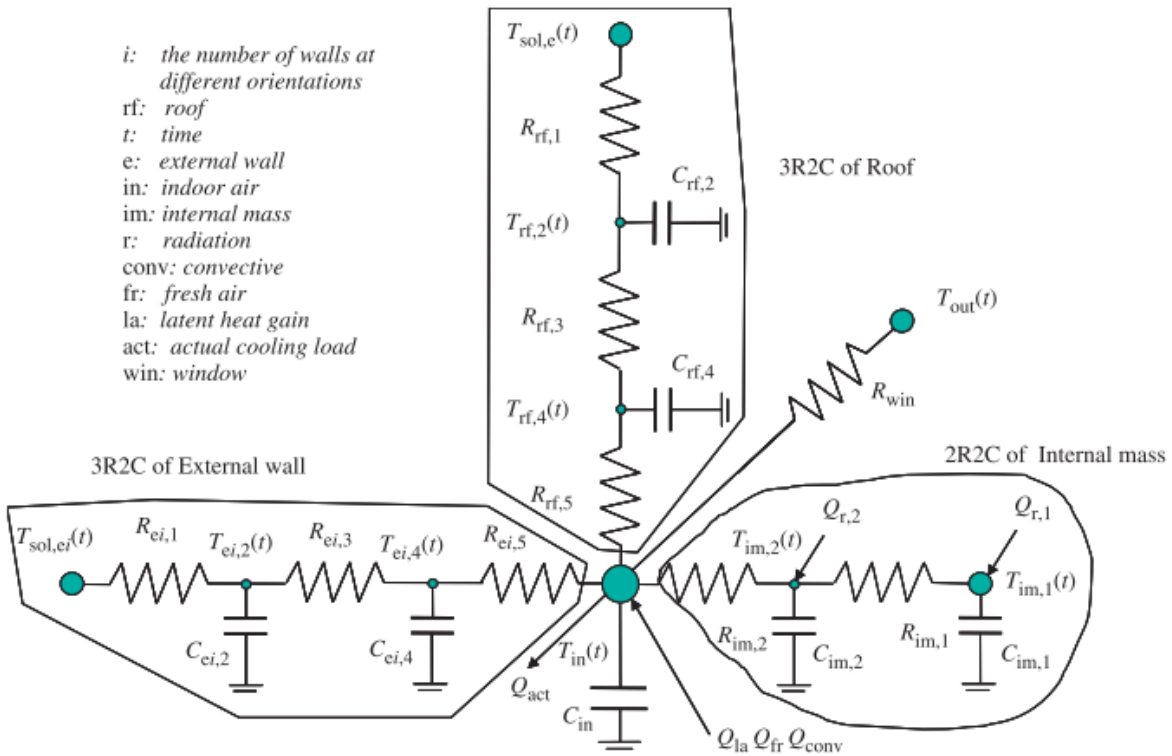


Figure 4 R-C Network Representing the Mixed-mode Energy Building [16]

This RC network models the buildings relationship with the exterior conditions and the internal heat loads. This structure is unique in its creation with the use of a 2R2C representative internal mass branch. Other grey box models combine the internal mass heat capacity with the ambient air capacity [6,7,8,11,16].

One of the more complex RC networks observed represents two HVAC conditioning zones within a solar decathlon house [23], as shown in Figure 5.

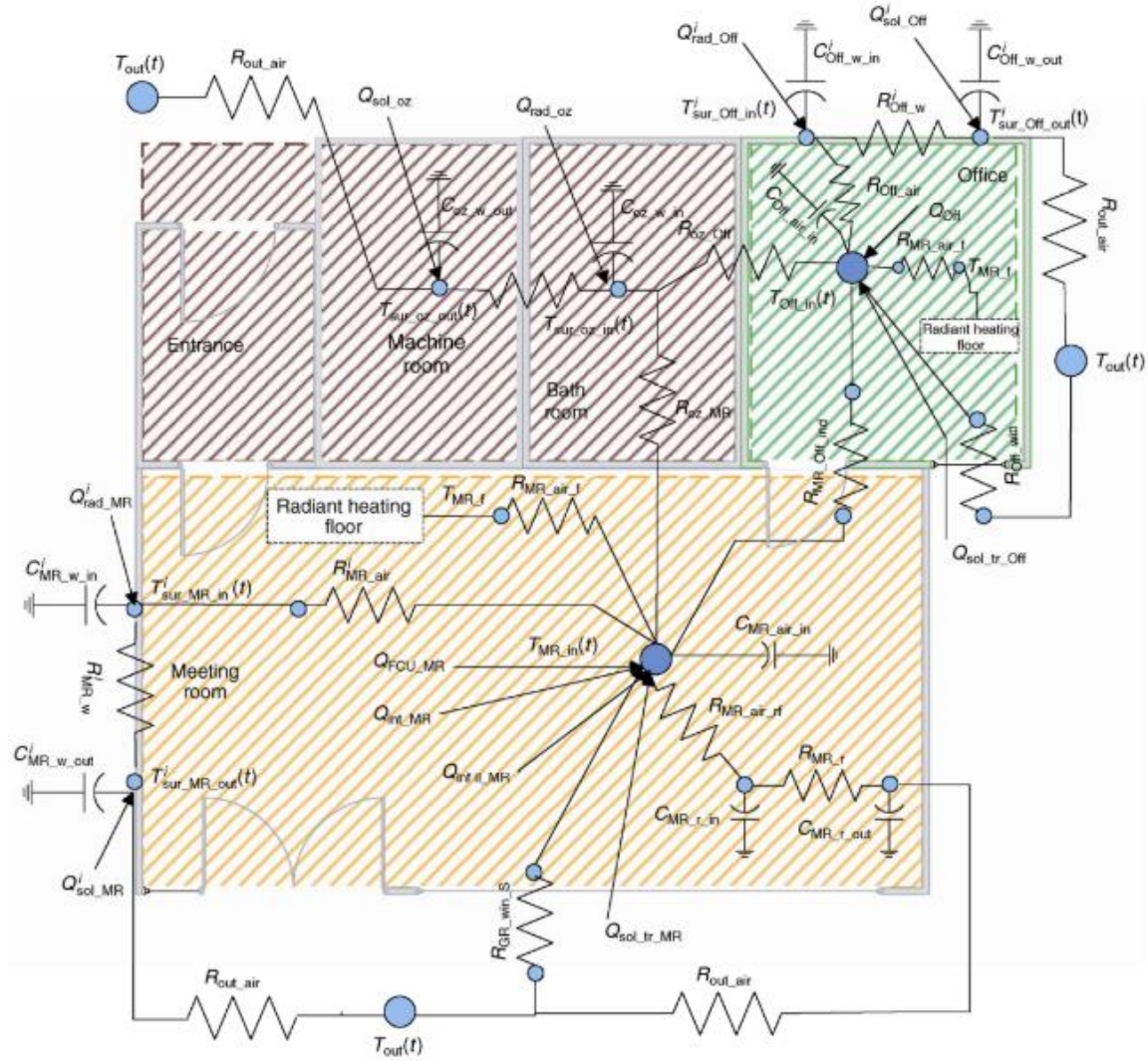


Figure 5 R-C Network Representing a Solar Decathlon House [23]

Using this grey box model within the MPC system was able to reduce the heating load of the solar decathlon house by 30% and the cooling load by 18% when compared to an on/off control HVAC system [42]. This research demonstrates the complexity of RC networks and the challenge associated in creating them, especially as the building becomes larger and involves more zone interactions. In the study conducted on a 25-zone building, the RC network was made of 494 resistors and 341 capacitors with every wall represented as a 3R2C structure [4]. In this 25-zone model, as well as in the model within the study [6], the RC network models were reduced to a simpler state space model for implementation within an MPC system.

## 2.5.2 RC Network Structure Optimisation

It has been stated that for control design, such as MPC, more simplified grey box models are preferred to larger scale RC networks [4]. Many researchers have conducted studies optimizing the RC networks to balance simplicity of the network design with accuracy of the ambient temperature prediction [11,12,17]. In a study conducted by Reynders *et al.* [21] the researchers compared the performance of five grey box models ranging in complexity from 1<sup>st</sup> order to 5<sup>th</sup> order models, demonstrated in Figure 6.

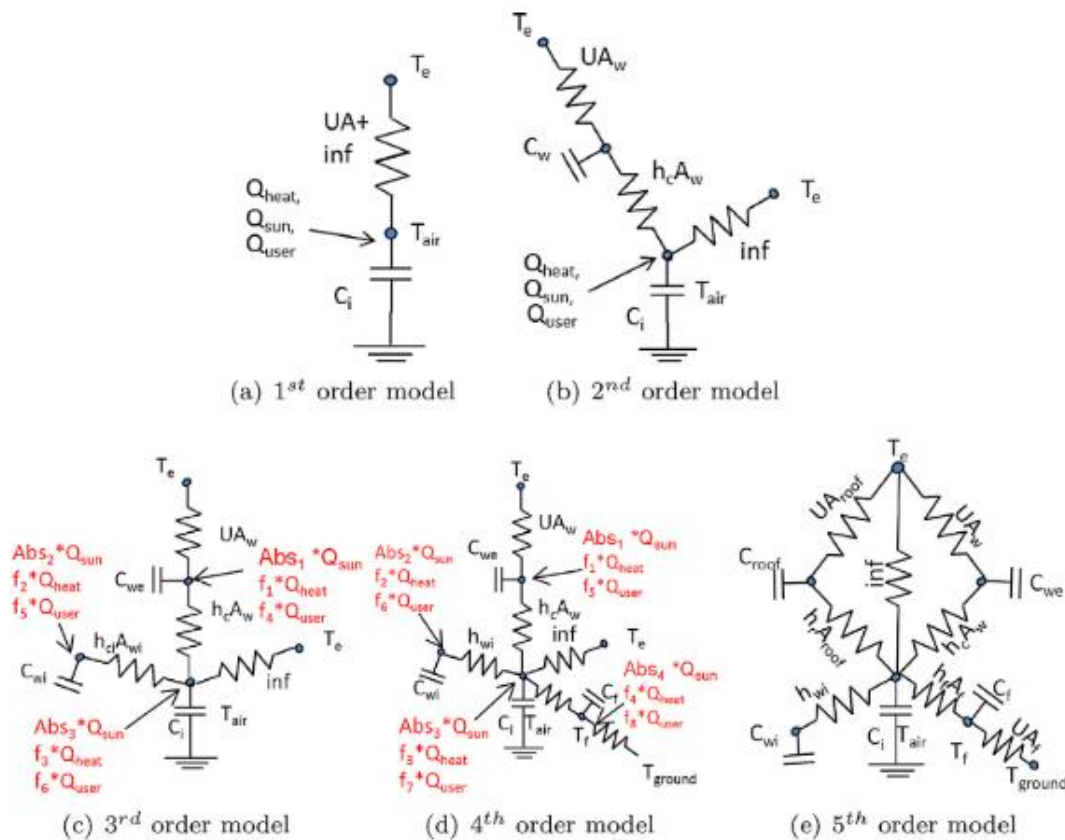


Figure 6: 1st-5th Order Grey Box Models used within the study [21]

The results from this study demonstrated that the fourth order model best represented the uninsulated building and the fifth order model best fit the insulated building [21]. The models were selected based on their root mean squared error, residuals, and model performance for day-ahead prediction [21]. A comparison of these models to their equivalent white box models demonstrated strong agreement in interior temperature results especially during the winter simulations [21]. Other studies who have similarly investigated the optimisation of RC

networks found varying results in the optimal degree of complexity for the RC network. In the research [11] three models were simulated in *TRNSYS*, the results demonstrate the 6R2C model (Figure 7) had the most accurate prediction results with a model error of less than 2%. The research summarized that the simplest model that can accurately represent a building's thermal dynamic behavior is a second order model [11]. The optimized structure in this research is unique as it includes an equivalent resistance for mechanical ventilation of the room, as illustrated in Figure 7. Typically, the mechanical ventilation heat load is added to the total interior heat load, which is connected to the ambient temperature node [6,7,8,11,16].

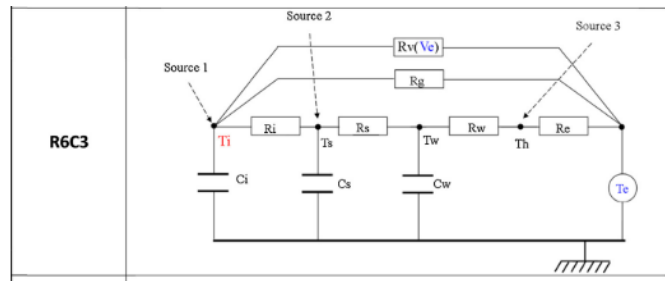


Figure 7 R6C3 Model used to Represent an Office Building [11]

In an analogous study comparing first order, second order, and third order grey box models concluded that the third order model, with 4R3C structure (Figure 8), had the most accurate ambient temperature prediction results [12]. This model uses the 1R1C structure for modeling the interior walls but differs from most models by representing the exterior wall with a 2R1C structure.

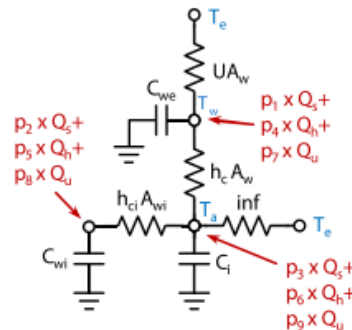


Figure 8 4R3C Model Representing an Office Space [12]

Likewise, in the study by Peder *et al.* [17] the RC network (Figure 9) uses a 2R1C structure to represent the envelope of the building and a 1R1C structure for the interior wall, designated as

‘sensor’. This 4R4C structure most accurately predicted the ambient temperature compared to five other RC network iterations.

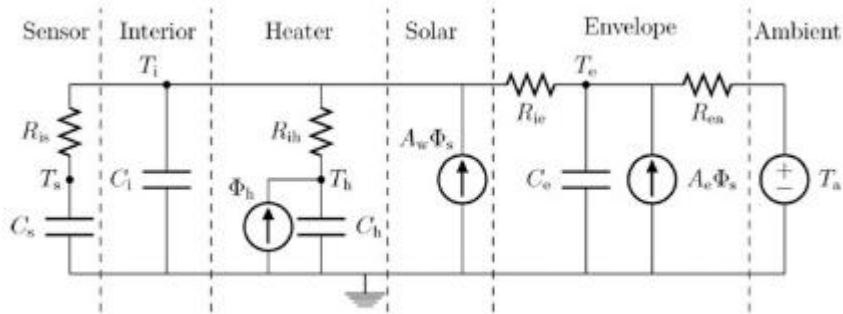


Figure 9 4R4C Structure Representing a House [17]

### RC Network Heat Loads

All of the RC networks discussed in the previous section model the heat loads due to exterior temperature, solar radiation, and internal heat sources. The majority of models represent the internal heat loads of the occupancy, interior lighting, and HVAC conditioning as one internal heat load connected to the ambient temperature [6,7,8,11,16]. Not all of the studies, however, include the HVAC load with the internal heat load calculation, as seen within [11]. Another exception includes the study [11] that models radiant in floor heating. In this system the heating load is connected to the floor temperature node, instead of the ambient temperature node. Another modeling method seen in study [17] represents the heater with its own temperature node and connects it to the ambient temperature through an internal air film resistor, instead of being incorporated within the internal load.

For the solar representation within RC networks, many studies model the solar radiation impacting both the interior and exterior of the room [6,18,23,34]. The solar radiation affects the interior by entering through the window and impacts the exterior wall by warming the facade. The solar radiation entering the space has been shown in previous studies to be connected to the interior temperature node, representing the solar radiation absorbed by the internal mass [23,34]. Other studies, such as the one discussed within the paper by J.Wen [43], connected the solar radiation to the floor node. Researchers for this study observed the floor element to be directly in the sunlight, absorbing the radiation, and then transferring the heat load to the ambient air through convective heat transfer. For larger buildings, as seen in [4], the

researchers combined the model disturbances of the RC network. With the solar radiation affecting all of spaces of the same orientation and occupancy impacting building spaces of similar purpose, patterns common to multiple estimated disturbance states were extracted by Principal Component Analysis (PCA) [4].

## 2.6 Building Parameter Estimation

Building parameter estimation is used when grey box model parameters, resistance and capacitance values, are unknown, or when solving for the weights of a steady state equation. Optimization algorithms, similar to those used in black box models, are used to solve for the parameters using input and output data. The internal heat capacity is a common parameter within grey box models that is solved for using parameter estimation [10,11,12,17,34]. As seen in [6,10,12,17,18,20,44], this value frequently encompasses heat capacities from multiple sources, making it hard to calculate. The study [11] defines this value as the “internal air and light furniture capacitance”. The internal heat capacity was solved for in [16], when the building construction drawings were available for the creation of the RC network but the resistivity and capacitance values of the representative 2R2C internal mass branch were unknown. The study was able to determine the values using a genetic algorithm and root mean square error optimisation. The resulting energy model had a relative error of 8% when predicting the cooling energy consumption in the summer and a relative error of 10% when predicting the cooling energy consumption in the winter [16]. In another study, the researchers chose not to solve for the internal mass using parameter estimation but instead used the assumption that the ambient air heat capacity increases by a factor of 5 when incorporating miscellaneous internal heat sinks [21]. One unique study, conducting RC network optimisation, demonstrated that the best performing model had no internal heat capacity value at all [8].

In addition to solving for the internal mass, studies have also used parameter estimation to determine the material property values for RC networks, and the variables for state space models [5,6,8,10,11,12,16,17,18,19,20]. In the study conducted by McKinley and Alleyne [10], hill climbing optimisation procedures were used with the model’s ambient and HVAC supply air data to solve for the zone mass, four thermal resistances, and two thermal capacitances. The hill climbing function in this study was run using the *Matlab 7.1 Optimization Toolbox* with results from the parameter estimation demonstrating parameter accuracy and repeatability

below 1% [10]. Similarly, the study by Soudari *et al.* [13], solved for the parameters within the state space model using the least squares method. This research, along with the previous study [10], used data collected from test sites to solve for the grey box model parameters. Comparatively, in [11], data generated from the TRNSYS building model was used within the parameter estimation interior point algorithm. This study concluded the parameter fit is good when the thermal needs are high and low during shoulder seasons when the thermal need is low [11]. Although these studies demonstrate accurate grey box model results when using parameter estimation tools, a study found that models of at least fourth order (see Figure 6) should be used when conducting parameter estimation for models representing well insulated buildings [21].

No consistent algorithm is observed to be used within research that conducts parameter estimation. One study used the *greyest* function within *Matlab* to assure good results as this function uses Gauss-Newton direction, Levenburg-Marquardt, and steepest descent gradient search [12]. Another study concluded that swarm optimisation is the best option for models with high dimensionality and low levels of input excitation [4]. It is stated that this algorithm is robust against the problem of convergence at a local minimum [4].

## 2.7 Subtractive Linear Regression

Linear regression models are the preliminary black box model components added to the grey box model in this thesis, replacing building element physical representations. As no other study to date has created this kind of thermal dynamic model there are no previous studies for reference. The regression models were created using a subtractive linear regression approach. This method determines the linear relationship of the output value, in this case the building element surface temperature, based on the input values and the monitored data from the test cell. In a subtractive approach, all of the monitored values from the test cell are included within the first iteration of the regression model and then the input values are gradually reduced to the key input values. The elimination of data points from the regression model is determined based on their p-value and the adjusted  $R^2$  value of the regression model. The p-value of the variable indicates the statistical significance, where the lower the p-value the more significant the variable is to the regression model. The  $R^2$  value is often referred to as the ‘goodness of fit’ of the regression model [45]. This value tells us that the proportion of variability in the dependent

variable is accounted for by the independent variables; if the predicted values closely resemble the actual values, the  $R^2$  value will be close to 1 [45]. The  $R^2$  value however, tends to increase and decrease with the addition or subtraction of input terms in the regression model [45]. As a subtractive regression approach is used in this analysis, involving the number of variables changing with every iteration, an adjusted  $R^2$  value is used as the performance criteria of the regression model. Therefore, if the adjusted  $R^2$  value decreases when a parameter (with the lowest p-value) is removed from the regression model, then the best fit model is previous model iteration.

## 2.8 Validation and Error Analysis

For MPC systems to be able to program the future HVAC conditioning requirements, they require accurate prediction of the ambient temperature from the thermal dynamic model. In previous research, when analyzing the prediction performance of a thermal dynamic model, predicted the ambient temperature for different lengths of time. One study stated that MPCs require the thermal dynamic model to predict the conditions of the room three hours in advance [12]. Comparatively, another study stated shorter prediction periods of between 15 and 30 minutes are adequate for thermal dynamic models [32].

To evaluate the thermal dynamic model's ability to predict ambient temperature, the error between the predicted and actual temperatures is calculated. The error calculations used in previous research include root mean square error (RMSE) [8,11,12,19,21,34], mean average error (MAE) [9,10,23,32], and mean average percent error (MAPE) [13,25]. The RMSE calculation is based on the sum of squared errors - a function of the average error, the distribution of the error magnitudes, and the sample size to the power of a half [46]. The MAE is found by summing the magnitudes of the errors to determine the total error and then dividing the total error by the sample size [46]. The MAPE value is the same calculation as the MAE but represents the error as a percentage. Although previous research did not calculate the weighted average percent error (WAPE), this value will be considered in our error analysis. The WAPE value differs from the MAPE value by accounting for each value's proportional weight to the total error [47]. The equation for each of these calculations is shown below, where  $n$  is the sample size,  $y^*$  is the actual value, and  $y$  is the predicted value.

$$RMSE = \sqrt{\frac{1}{n} \sum_{i=1}^n (y_i^* - y_i)^2} \quad (4)$$

$$MAE = \frac{1}{n} \sum_{i=1}^n |y_i^* - y_i| \quad (5)$$

$$MAPE = \frac{1}{n} \sum_{i=1}^n \frac{|y_i^* - y_i|}{y_i^*} \quad (6)$$

$$WAPE = \frac{\sum_{i=1}^n |y_i^* - y_i|}{\sum_{i=1}^n y_i^*} \quad (7)$$

The most commonly seen error calculations are RMSE [8,11,12,19,21,34], MAE [7,26,31,32], or a combination of both values [9,10,23,32]. Studies have been conducted to analyze which error calculation is the most accurate [42,46]. The research [46] suggests MAE is the most natural measurement of average error magnitude and recommends using MAE over RMSE [46]. In comparison, the study [42] found that RMSE is more appropriate than MAE when the model errors follow normal distribution [42]. It concludes that MAE might be affected by large quantities of error values within the range of the average error and will be unable to reflect instances of large error deviation [42]. In comparison, RMSE would perform better in such a situation by giving higher weights to unfavorable conditions, better revealing differences in model performance [42]. Studies also calculate the mean average percent error (MAPE) to analyze model performance [13,25]. MAPE calculations however, are biased towards forecast values that are below the actual value, resulting in model performance penalization when underprediction occurs [47]. A way to avoid this is by calculating the weighted average percent error (WAPE), where each simulation error is proportionally weighted to the total [47].

## 2.9 Lessons from Literature Review used within this Thesis

This thesis created grey box models based on the methods outlined in the studies discussed above. Similar to previous work, data was gathered using a test cell rather than being collected from a simulation program. This test cell installed surface temperature sensors using thermal conductive paste, similar to the study [18]. For monitoring the HVAC system, the ventilation air temperature and airflow rate were collected, as in [7,10,31]. The heater activity was determined using a surface temperature sensor that was installed on the hot water pipe, as it

was not possible to monitor the hot water temperature like in the study [20]. As commonly conducted by previous studies [18,23,31], the internal heat gains from equipment within the space was gathered using a watt meter. For occupancy the test cell used a manual sign in sensor system to measure the occupancy within the cell and a limit switch on the door (indicating position) to provide complementary data for validation. This thesis also followed the most popular and convenient method for exterior weather data collection, using the building rooftop weather station to measure exterior temperature and wind speed measurements [12,13,16,17,18,20]. The solar radiation data was also gathered from this station, with direct and indirect solar radiation calculated using a similar method to the study conducted by Berthou *et al.* [11].

For the creation of the grey box RC network this thesis follows the findings from previous studies [6,8,10,16,24]. It uses a 3R2C circuit to represent the exterior wall, parallel resistors to represent the window and spandrel panel, and 1R1C circuits to represent the ceiling and floor slabs. The model within our research however, is not optimised and uses a circuit slightly more complicated than the optimized models in [11,12,17,21] shown in Section 2.5.2 above. This work however, did use parameter estimation technique to solve for the internal heat capacity value similar to previous studies [10,11,12,17,34]. For representing the heat loads of the test cell, the mechanical ventilation is modeled using the same method as [6,7,8,11,16]. The ventilation heat load is added to the total interior heat load value and connected to the ambient temperature node. Similarly, the heat load from the heater is added to the total sensible heat load value of the test cell and connected to the ambient temperature node. The solar radiation heat load was represented in the model using the same method as described in [43], connecting the radiative heat load to the floor temperature node.

The grey box model gradually introduces black box models into its structure; starting with linear black box models. Due to the findings of [7] and [38], demonstrating neural network models predicting the thermal dynamics better than linear models, neural network models are also investigated within this thesis. The neural network fitting method described in [7], using 70% of the data as training data, 15% as validation data, and 15% as testing data was used in this thesis. This was the only observed study to describe the training process

and other research does not give any indications of contradicting this method. The *Matlab* neural network fitting app was used in this study with LM algorithm, similar to the studies [12,30,32]. This *Matlab* app minimizes the potential for overfitting by monitoring the validation error throughout the training process [36].

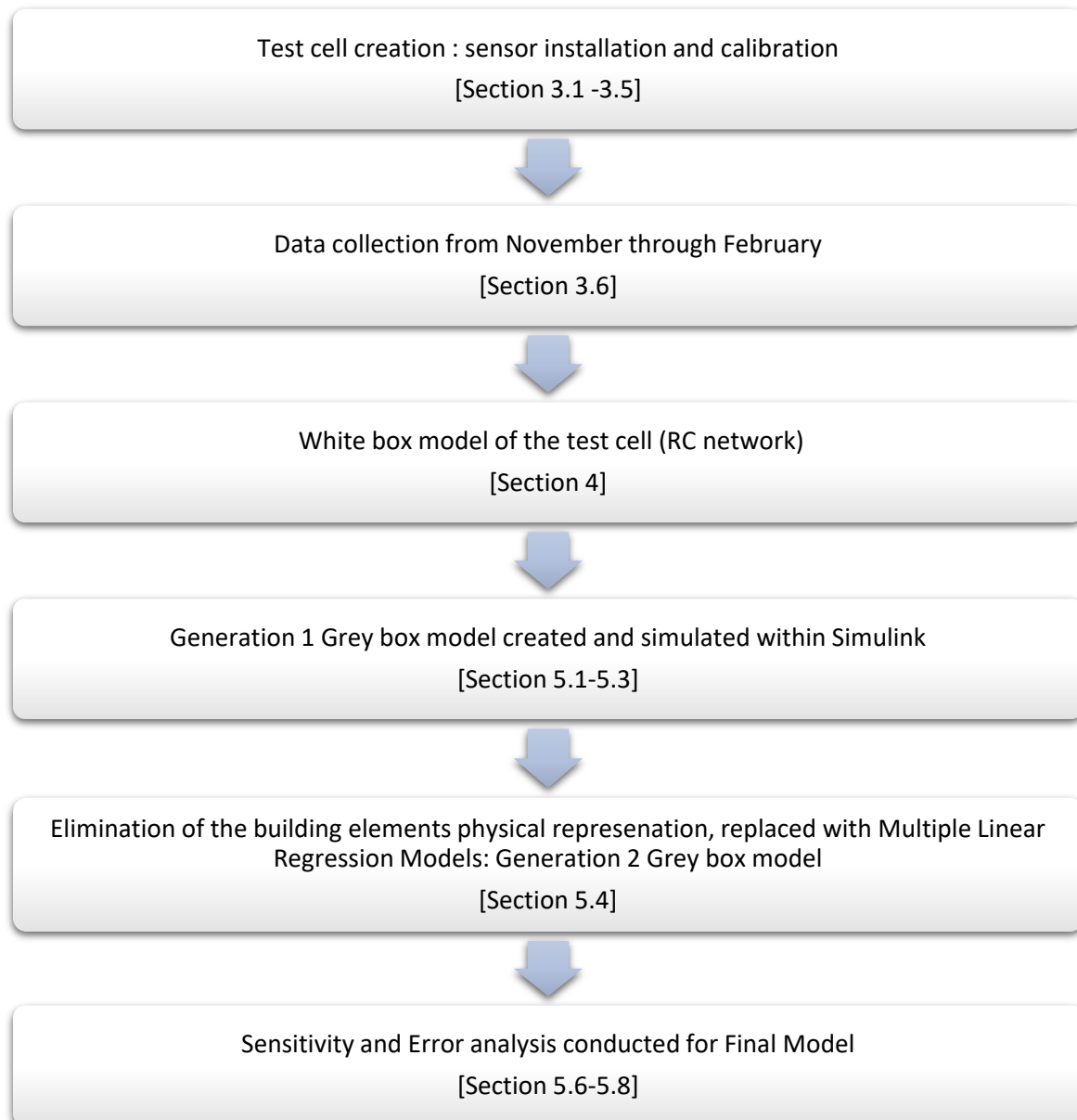
Based on the mandatory Prediction Window described in [12] for MPC systems, the grey box models created in this thesis are evaluated based on their prediction performance at 15, 30, 45, 60, 120, and 180 Prediction Windows. The model performance is often analyzed based on the prediction error.

$$Prediction\ Error(\%) = \frac{T_{predicted} - T_{actual}}{T_{actual}} * 100 \quad (8)$$

The results are analyzed using a combination of RMSE, MAE, and WAPE values. It is noted that although the results from this thesis are mainly discussed for MPC system use, it is also applicable for economic MPC systems. The test cell is within a heavy thermal mass structure, predominantly constructed of thick concrete slabs, making it a strong candidate for economic MPC systems, as shown in [20].

### 3 Methodology

The major steps taken to create the final grey box model include: test cell sensor installation and data collection, white box model creation, grey box model creation, and analysis of grey box model. These steps are outlined below with the respective sections where they are fully described.



### 3.1 Test Cell Apparatus

This research uses an office space within a 1970-era university building (concrete construction; Brutalist architectural style) as the test cell. The test cell is located in Toronto, Ontario, at 43.66 latitude and -79.38 longitude. The cell is approximately 90 ft<sup>2</sup>, featuring one external eastern facing wall with three window panes and one spandrel panel. Most building elements including the floor/ceilings and exterior siding are made from thick concrete slabs. The other elements include double pane-aluminum framed windows, a spandrel panel made of steel sheet metal sandwiching fiberglass insulation, and internal walls constructed of steel framing at 16 inches on centre with drywall on either side. The test cell is connected on the North and South side to office spaces that make up the same HVAC conditioning zone. There are office spaces both above and below the test cell. Overall, the test cell experiences little direct sunlight due to the test cell's orientation and the orientation of surrounding buildings.

The test cell is an office space that features one desktop computer. The schedule of the space during the study period is relatively sporadic due to change in academic terms and schedules along with the winter holidays. Generally speaking, the hours of occupation stay within standard working hours of 9am-5pm Monday to Friday. The heating, ventilation, and air conditioning systems for the space include an air source heat pump and radiant heater. The air source heat pump receives preconditioned air from an air handling unit. The air handling unit splits its output to both the heat pump and a direct line to the test cell through the left duct. The conditioned air from the air source heat pump is delivered to the test cell through the right ventilation duct. The ventilation system has no return duct, the room is balanced by the air circulating to the hallway. The floor mounted radiative heater in the room runs hot water through the pipe when the weather falls below 15°C which, is for the majority of the heating season considered in this research.

### 3.2 Sensor Description

The sensors installed within the test cell are monitoring eight major room characteristics: surface temperatures, ambient temperatures, solar radiation, ventilation input, plug load, occupancy, interior lighting, and door position. An overview of sensors installed within the test cell with their make, model, and description is shown in Table 1.

Table 1 Summary of Sensors and Data Collection

Data collected	Sensor (make and model)	Description
Surface Temperature	MadgeTech OctTemp with Type T Thermocouples	Temperature (0.05°C resolution, ±0.5 accuracy) [48] of each surface within the test space
Indoor Ambient Temperature	<i>OmniSense S-10</i> Ambient Sensors	Temperature (+/- 0.4°C accuracy) [49] and relative humidity (+/- 3.5%) [49] of ambient air at four locations around the test space.
Exterior Conditions	HBO Weather Station	Weather station collecting, exterior ambient temperature, wind speed, and solar radiation
Ventilation Input	Modern Devices Wind Sensor Rev P AM2302 Temperature-humidity Sensor	The unit reads the temperature and flow rate of the incoming air from the ventilation ducts and transmits the data to the <i>Arduino Mega</i> .  The sensor is installed within the ducts leading to the test cell reading the temperature (±0.5 °C) and relative humidity (±2-5%) of the incoming air
Electrical Watts	Watts up? PRO	A Wattmeter measures power consumption at the power bar serving the computer and other electrical equipment.
Occupancy	Toggle switch	Manual toggle switches are used by people entering the test cell to record occupancy data on the <i>Arduino Mega</i> .
Interior Lighting	Toggle switch	A manual toggle switch next to the light switches of the lab sends ON/OFF status to the <i>Arduino Mega</i> .
Door Position	Reed switch	A reed switch is set up on the door of the office to record its OPEN/CLOSED position on the <i>Arduino Mega</i> .

Surface temperature measurements are collected from eight key elements of the test cell: the exterior concrete wall, the middle window, the spandrel panel, the floor slab, the ceiling slab, the supply pipe of the radiant heater, the interior side of the adjacent hallway wall, and the exterior side of the adjacent hallway wall. The thermocouple sensors are type *T* cables (copper and constantan) wired to the *Madgetech OctTemp Data Logger*. The system has an accuracy of ±0.5°C and resolution of 0.1 °C. The system was set up to take measurements at one-minute time intervals. The *Madgetech* logger software was installed on the office’s desktop computer to communicate with the logging unit, and download the data in the logger memory.

The ambient temperature is collected using *OmniSense* wireless temperature/RH sensors and gateway. The sensors have an accuracy of ± 0.4°C with a resolution of 0.1°C and data collection

frequency of 5-6 minutes. The data is logged to the *Omnisense* website through internet connection.

Initially the test cell was set up with a PV panel facing outward on one of the windows within the test cell. The panel was able to detect brightness however it was discovered that it could not distinguish between direct and diffuse solar radiation which was needed in this study. Therefore, the direct and diffuse solar radiation data used in this research was found using data from the rooftop weather station, along with solar calculation method described in the research conducted by Finch [50]. These calculations determine the direct and diffuse solar radiation values for vertical surfaces using data collected from horizontal solar collectors. An example of the calculations can be seen in Appendix A Solar Radiation Calculations.

The sensors installed within the ventilation ducts are *WindSensor Rev P* data loggers. The sensors detect the temperature (°C) and velocity (MPH) of the incoming air and send the data to the *Arduino Mega*. The sensors are produced by an independent vendor that does not provide accuracy ratings for the sensors. The sensors include an *Arduino* conversion code to calculate the temperature and velocity values based on the received input voltage from the sensors. These values are then recorded onto the SD card attached to the *Arduino*.

The plug load in the test cell is monitored using a *WattsUp Pro* meter. An extension cord was installed within the cell to power the desktop computer, and data logging equipment. The extension cord is plugged into the *WattsUp* meter where it receives power, and the meter records the watts being used. The data logger is set to collect data at intervals of 3 minutes and can store the data for up to two weeks. The data is collected from the meter using a USB outlet and the *WattsUp* logging software.

The occupancy and interior lighting are monitored for the test cell using toggle switches, read by the *Arduino Mega* unit. The light status records the UP position of the lighting toggle switch as “ON” and the down position as “OFF”. The occupancy is recorded using a sequence of toggle switches that are associated with a dedicated occupancy count. The first switch in the sequence is read as one occupant, the second switch is read as two occupants, and so on. The occupancy system is accompanied with LED visual confirmation to confirm the number of LEDs turned on matches the occupancy count. The door position for the cell is recorded using a Reed switch. The Reed switch opens and closes a circuit based on the presence of a magnetic

field. A magnet was placed on the door to the test cell with the Reed switch installed on the door frame. When the door is closed the *Arduino* unit reads 1, when the door is open the unit reads 0.

The *Arduino* unit is set up with a Real Time Clock, SD Card reader, and Bluetooth serial output. When the data logging code is uploaded to the *Arduino Mega*, the Real Time Clock records the date and time from the computer. The program incrementally increases the time over each sampling period and prints the date and time stamp with the *Arduino* data. The data and time stamp is printed to the SD Card in a .csv file, and the .csv file is retrieved from the card weekly. The Bluetooth serial output was used when calibrating the sensors in the cell by streaming the incoming *Arduino* data on a laptop remotely. The *Arduino* network is shown in Figure 11, with the diagram legend shown in Table 2.

*Table 2 Legend for Arduino Circuit Diagram*

Occupancy Toggle Switches	1-4
Occupancy LED lights	5-8
Lighting Toggle Switch	9
Door Reed Switch	10
Real Time Clock	11
Bluetooth board	12
AM3203 Temperature and Relative Humidity Sensors	13-14
WindSensor Rev P airflow and temperature sensors	15-16



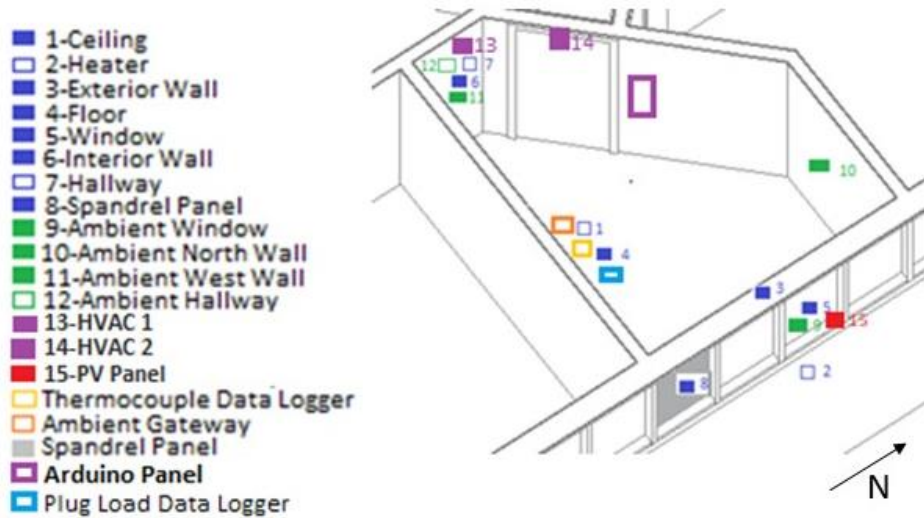


Figure 11: Test Cell Sensor Layout

The thermocouple wires are connected to their respective surfaces using conductive paste to assure good connection. The wires are connected back to the *OctTemp* datalogger, which is positioned centrally within the cell to minimize resistance loss discrepancies in the data.

Four ambient sensors were placed in the test cell at the east end of the room next to the window, the middle of the room, the wall adjacent to the hallway, and in the hallway, as shown in Figure 11. The sensors were installed by placing the units in their respective places and assuring that the antenna was directed upwards. The gateway (data logger) was positioned in the centre of the room where it is recording the data collected from the sensors wirelessly, and logging them on the *Omnisense* website through its Ethernet connection.

The plug meter was installed within the test cell in close proximity to the wall outlet, and plug load extension cord. The extension cord is plugged into the meter, and the meter to the wall.

The *Wind Sensor Rev P* units were installed in the middle of both duct openings on the outward side of the grate (inside the test cell). The sensors are wired to the Analog input connection points of the *Arduino* Mega unit where the input signals are read, and converted into their respective temperature and velocity measurements using the data logging *Arduino* code.

Similarly, the *AM2302* temperature/RH sensors are installed inside the middle of both ducts behind the grate. These sensors also connect back to the *Arduino* through the Analog input

ports, where the voltage signals are read, and converted into temperature and relative humidity values using the data logging *Arduino* code.

An *Arduino Mega* unit installed within the entrance of the test cell serves as the data logger for the occupancy, interior lighting, door position, *Wind Sensor Rev P*, and *AM2302* temperature/RH sensors. This location, close to the light toggle switch, door reed switch, and ventilation sensors, allows for shorter wiring and less disruption in the sensor signals. The *Arduino* code used for data collection is shown in Appendix B *Arduino Code*.

The type-T thermocouples, *WindSensor Rev P* temperature/airflow sensors, along with the *AM2302* temperature/RH sensors were calibrated upon installation. The other sensors were not calibrated because they are either logic signal switches, or, in the case of the *Omnisense* ambient temperature sensors, have manufacturer guaranteed lifetime calibration.

The type-T thermocouple surface temperature sensors within the test cell were calibrated using the High-Low calibration method. Each thermocouple was submerged in 100°C boiling water, and 0°C ice water alongside a thermometer with resolution of  $\pm 0.1^\circ\text{C}$ . The measurement readings from the *Madgetech* logging software were compared to the thermometer readings. The offset from both the high and low measurements were input into the *Madgetech* software calibration settings where the software used the offset values to calibrate each temperature sensor.

The *WindSensor Rev P* and *AM2302* sensors were calibrated for temperature measurements, and for the *AM2302* calibrated for RH readings, using a point temperature measurement sensor (resolution of  $0.01^\circ\text{C}$  and accuracy  $\pm 2^\circ\text{C}$ ). The calibration was conducted by taking temperature and RH measurements at the sensor location. A laptop with Bluetooth capabilities was installed next to the measurement station, live streaming the *Arduino* sensor readings. The timestamp from the *Arduino* live stream was recorded at the time of each calibration sensor reading. The *WindSensor Rev P* and *AM2302* sensor readings, found on the *Arduino* SD card, at the time stamps recorded were compared to the calibration instrument readings. The *WindSensor Rev P* airflow measurements were also calibrated using a balometer (resolution 1 CFM) shown in Figure 12. The balometer determines the overall airflow of the duct by equalizing the pressure of the chamber shown in Figure 12, when the device is held up against the opening of the duct. Similar to the previous calibration, the live streaming capabilities of the *Arduino* was used to

record the timestamp on the *Arduino* when the calibration measurements were taken. The measurements collected from balometer recordings were compared to the *Wind Sensor* readings. The calibration results for both devices is shown in Appendix C Calibration.



*Figure 12 Balometer used for Calibration of Airflow sensor*

### 3.4 Sensor Modifications

While initially it was assumed that relative humidity could be determined from the base building system monitoring, in fact, this data was found to be both uncontrolled and inconsistent in a review of the building data. As a result, this information was lacking for the heating season data. To resolve this moving forward, *AM3202* Temperature/RH sensors were installed in the test cell in March 2018, after the heating season cut-off for this study. It was attempted, using linear regression and machine learning techniques, to determine a relationship between the ventilation RH and other measured values including the ventilation temperature (from the *WindSensor Rev P*), outdoor temperature, and outdoor relative humidity. Unfortunately, as a correlation did not appear no relationship was found and the relative humidity of the ventilation air could not be back calculated using the data measurements taken during the research study period. This study, therefore, only considers the sensible heat load

from the ventilation system. The *AM3202* Temperature/RH sensors are currently installed and collecting data for future research.

### 3.5 Data Analytics to Overcome Data Gaps

The *WattsUp Pro* sensor is an older watt meter manufactured by a company that has since dissolved. Unfortunately, the first installed watt meter of this type malfunctioned in the month of November and no steady data was collected until December 6<sup>th</sup>. During the end of January, the collection laptop crashed, losing all data logging software. The challenge in finding the *WattsUp* data logging software resulted in the loss of data for between the time when the laptop crashed at the end of January until mid-February. Due to the large gaps in data, the plug load values used throughout this study were determined from the occupancy patterns of the cell. These values were used for all simulation periods, even periods when the watt meter was working, to maintain consistency throughout the research and in the results. A sensitivity study, Section 6.11.1, was conducted to analyze the impact of this simplification on the model results.

A strong correlation between occupancy and plug load readings can be seen in Figure 13. When the occupant was not in the test cell an average reading of 45W can be observed. Therefore, for this study the plug load is calculated by assuming a value of 45W when the test cell is unoccupied and a plug load value of 77W when it is occupied. The 77W value is based on the observed trend in the data collected from the watt meter and the recommended heat gain value from ASHRAE [51] for desktop computers with 3.0 GHz and 2 GB RAM.

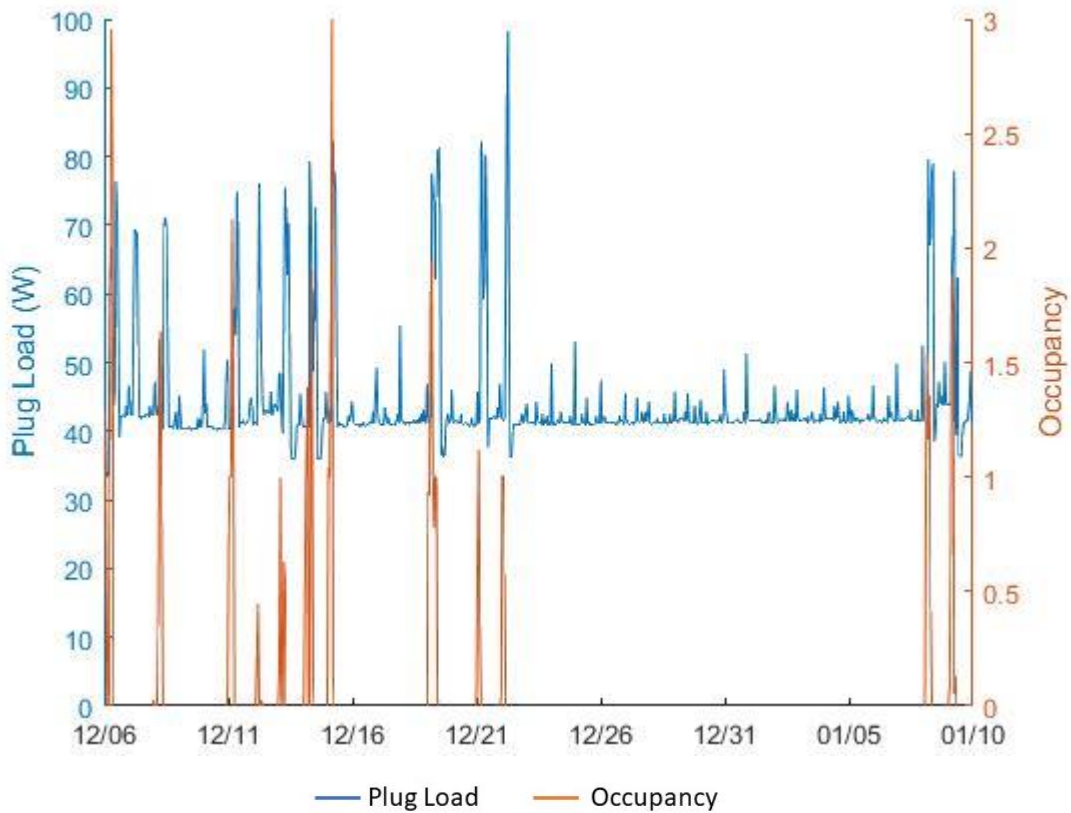


*Figure 13: Occupancy and Plug Load Correlation*

A second issue arising in the data collection was the loss of the data signal from the door sensor for one month. As the loss occurred during December, the impact of the data loss was minimized as the test cell was unoccupied for the last 2 weeks of the month. The missing door position status was calculated using the occupant count and lighting status from the test cell; when it was observed that an occupant entered the room and the lights went on, the door was changed from closed to open. When the occupant count went to zero and the lights were off, the door returned to a closed position.

### 3.6 Data Collection

Full data collection of all sensors within the test cell began at the beginning of November 2017. Figure 14 illustrates the sensor readings on a typical weekday in November. The graph in the upper left-hand corner demonstrates the surface and ambient temperature readings. The graph in the upper right-hand corner demonstrates the outdoor air temperature readings. The graph in the bottom left-hand corner demonstrates the data collected from the *Arduino* unit including the occupancy, lighting, and initial PV solar sensors. The graph in the lower right-hand side shows the supply air velocity and temperature for both the ventilation ducts. The *Arduino* data collection code can be seen in Appendix B Arduino Code.

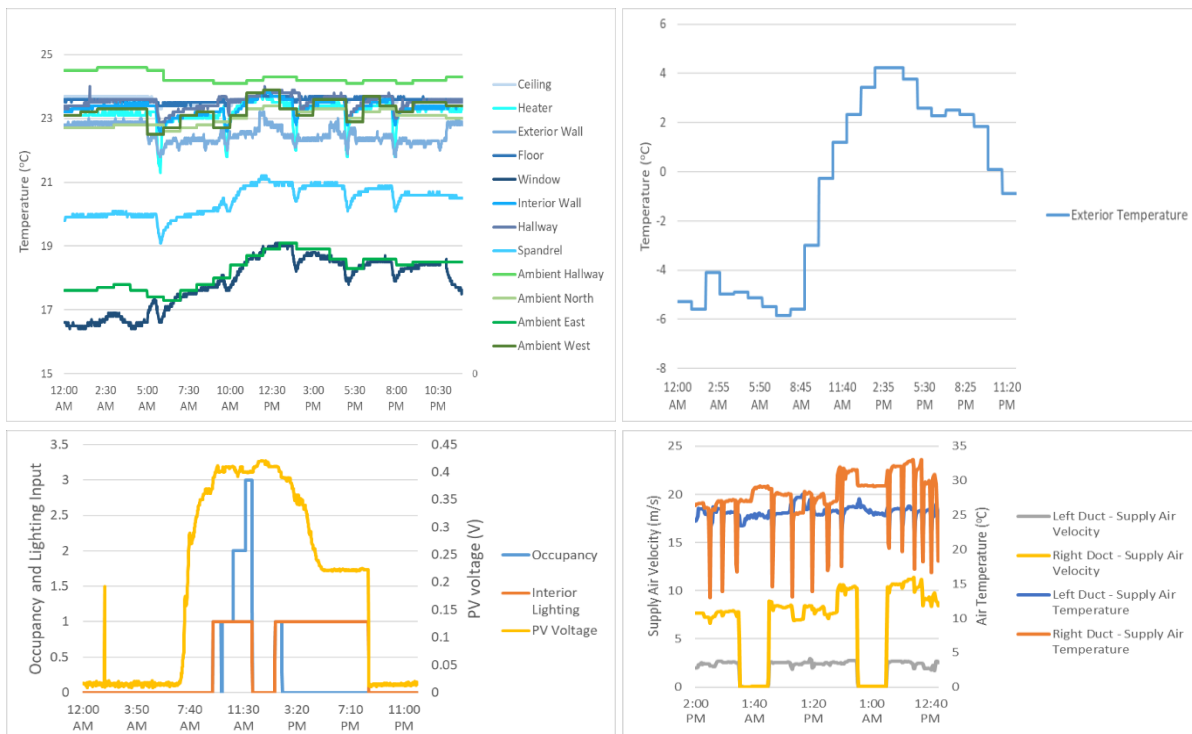


Figure 14 Example of Data Collected from the Test Cell Sensors during November

## 4 White Box Model Development

The simplified energy balance of the test cell was used to create the RC Network physical white box model, as illustrated in Figure 15. This model can be split into four major sections: (1) heat transfer from the hallway, (2) heat storage in the ceiling and floor, (3) the internal sensible heat gains, and (4) the heat transfer through the exterior wall.

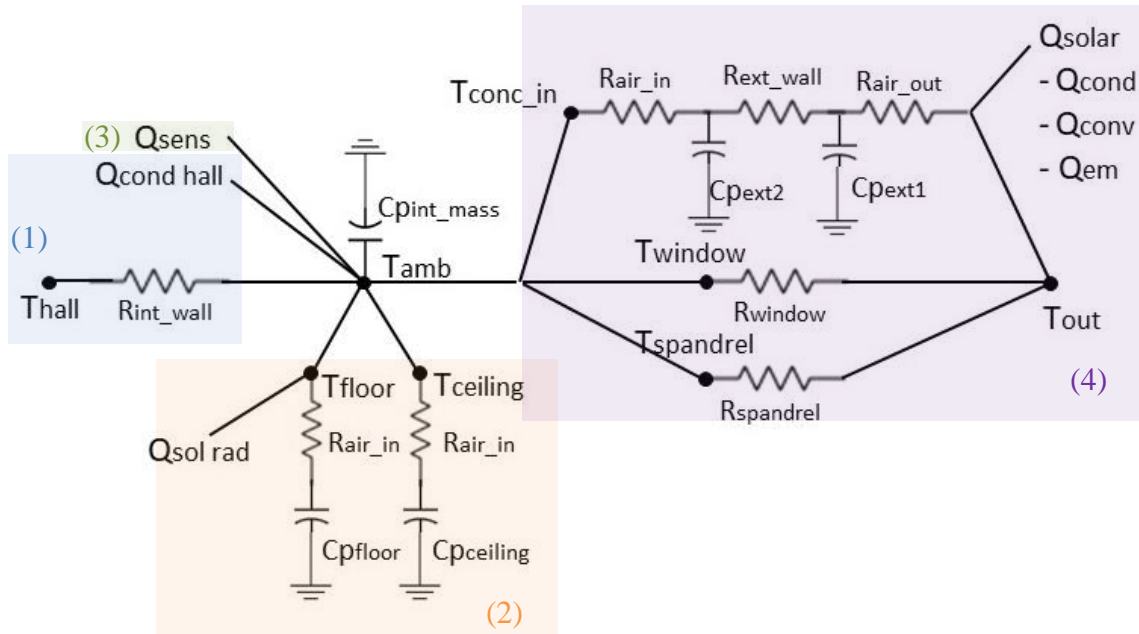


Figure 15 RC-network of Test Cell

Several simplifying assumptions were made:

1. All heat transfer was assumed to be 1-dimensional only.
2. The interior walls of the test cell were assumed adiabatic. The offices on either side of the test cell are conditioned by the same HVAC system, resulting in minimal temperature gradient between the offices.
3. The only radiant heat contribution considered was solar radiation entering through the window. Although there is a percentage of radiant heat emitted by the occupants and the interior lighting, they are found to be insignificant heat contributions compared to the other heat loads affecting the space and are therefore ignored.

4. Exterior infiltration and exfiltration are assumed to be negligible. The ventilation system for the test cell is designed with two supply ducts and no return duct. This creates a positively pressurized space where all air leakage is exfiltrated from the test cell. The model therefore does not consider infiltration loads as there are none when the ventilation system is on and minimal loads when it is off. The pressure within the test cell forces the air out three ways: through the exterior façade, through the interior walls/floor/ceiling, and through the doorway into the hallway. A study of air tightness levels from 400 different commercial buildings within the United States found on average an air leakage rate of  $16.7 \text{ m}^3/\text{h}\cdot\text{m}^2$  for commercial buildings ranging in construction type and age [44] . Using this rate, the airflow for the exterior wall and interior elements of the test cell respectively are  $162\text{m}^3/\text{h}$  and  $809.95 \text{ m}^3/\text{h}$ . In comparison, the airflow rate of the conditioned air entering the space from the ventilation system is  $41,611.4 \text{ m}^3/\text{h}$ . The air leaving the test cell through exterior and interior wall exfiltration is therefore equivalent to only 2.34% of the air entering the room. This suggests that the other 97.66% of the air is leaving the room through the doorway. For simplicity within the model it is therefore assumed that all air leaving the test cell is through the doorway, and that the flowrate of the air entering the room from the ventilation system is the same flowrate as the air leaving the room.
5. A single ambient temperature was used to represent the overall cell temperature. This simplifies the reality, as the cell has sensors monitoring ambient temperature in three locations and their data demonstrates the variance in ambient temperatures when in proximity to the window and the ventilation ducts. Vertical stratification was also ignored in this study.
6. The internal walls, window, and spandrel panel heat capacity was ignored. Table 3 compares the total heat capacity of each element and demonstrates that the window, spandrel panel, and the interior wall have significantly less storage than the concrete elements.
7. The solar radiation entering through the eastern windows hit the northern wall and floor of the test cell. As the interior walls are not being considered for heat storage within this model, the northern wall is not modeled in the radiant heat contribution of the room. The solar radiation heat contribution to the test cell is therefore modeled using only the floor heat gain.

8. The floor and ceiling of the test cell are surrounded above and below by conditioned space and are also assumed adiabatic. Due to the minimal temperature difference experienced by the components along with their heat storage properties they are modeled as 1R1C systems. This model represents them as on only heat storage elements ignoring conductive heat transfer. The resistivity component of this model represents the interior air film between their surfaces and the ambient air.

*Table 3: Heat Capacity of Elements within the Test Cell*

	Specific Heat (kJ/kgK)	Volume (m <sup>3</sup> )	Density (kg/m <sup>3</sup> )	Storage Value (kJ/K)
<b>Floor/Ceiling</b>				
Concrete	0.90	2.92	2400.00	6306.62
<b>Element Total</b>				<b>6306.62</b>
<b>North Internal Wall</b>				
Gypsum board (x2)	1.15	0.12	640.00	84.65
Air (20°C)	1.00	0.52	1.23	0.64
Steel	0.50	0.02	7830.00	65.67
<b>Element Total</b>				<b>150.95</b>
<b>South Internal Wall</b>				
Gypsum board (x2)	1.15	0.25	640.00	182.80
Air (20°C)	1.00	1.12	1.23	1.38
Steel	0.50	0.04	7830.00	141.80
<b>Element Total</b>				<b>325.97</b>
<b>Hallway</b>				
Gypsum board (x2)	1.15	0.24	640.00	178.30
Air (20°C)	1.00	1.10	1.23	1.34
Steel	0.50	0.03	7830.00	117.59
<b>Element Total</b>				<b>297.23</b>
<b>Exterior Wall</b>				
Concrete	0.90	1.33	2400.00	2864.27
<b>Element Total</b>				<b>2864.27</b>
<b>Spandrel Panel</b>				
Steel	0.50	0.004	7830.00	14.61
Fiberglass Insulation	0.80	0.04	112.00	4.01
Steel	0.50	0.004	7830.00	14.61
<b>Element Total</b>				<b>33.22</b>

The differential equations describing the heat flow in the test cell are shown in Table 4. These equations were found using the RC network.

*Table 4: Building Element Differential Equations*

Temperature Node	Differential Equation
Floor Surface	$c_{p\_floor} \frac{dT_{floor}}{dt} = (T_{ambient} - T_{floor})U_{in}A + I_{sw}\alpha A_{floor}$
Ceiling Surface	$c_{p\_ceiling} \frac{dT_{ceiling}}{dt} = (T_{amb} - T_{ceiling})U_{in}A_{ceiling}$
Hallway Ambient	$c_{p\_hallway} \frac{dT_{hallway}}{dt} = (T_{amb} - T_{ambhallway})U_{wall}A_{wall}$
Eastern Wall (Interior Side) Surface	$c_{p\_eastwall} \frac{dT_{eastwall}}{dt} = (T_{out\_eastwall} - T_{in\_eastwall})U_{eastwall}A + (T_{amb} - T_{in\_east})U_{in}A$
Eastern Wall (Exterior Side) Surface	$c_{p\_out\_eastwall} \frac{dT_{out\_eastwall}}{dt} = (T_{in\_eastwall} - T_{out\_eastwall})U_{extwall}A_{extwall} + (T_{out} - T_{out\_eastwall})U_{out}A_{extwall} + \alpha I_{sw} + F_a \varepsilon \sigma (T_{sky}^4 - T_{out}^4) - F_a \varepsilon \sigma (T_{out\_eastwall}^4 - T_{sky}^4) - h_c (T_{out\_eastwall} - T_{air})$
Test Cell Ambient	$c_{p\_air} \frac{dT_{amb}}{dt} = (T_{ambhall} - T_{amb})U_{wall}A_{wall} + (T_{ceil} - T_{amb})U_{in}A_{ceiling} + (T_{floor} - T_{amb})U_{in}A_{floor} + (T_{extwall} - T_{amb})U_{in}A_{extwall} + (T_{out} - T_{amb})U_{window}A_{window} + (T_{out} - T_{amb})U_{spandrel}A_{spandrel} + Q_{sens} + Q_{lat}$

#### 4.1 Calculation of Internal Heat Loads

The heat gains within the test cell come from the occupants, interior lighting, heater, conditioned ventilation air, and the plug load.

#### 4.1.1 Occupancy

The occupancy heat load is calculated using only the sensible heat contribution of the occupancy heat load (9). The occupant's activity within the cell are defined as 'seated, very light work' within the ASHRAE Handbook. This activity level has a sensible heat load of 75W [51]. The heat load is therefore found by multiplying this value by the *Arduino* occupancy count  $A_o$ .

$$Q_{occ} = A_o * 75 \quad (9)$$

#### 4.1.2 Interior Lighting

The interior lighting is calculated using the lighting status data from the *Arduino* (1-ON, 0-OFF) and multiplying it by the heat load from the florescent bulbs (10). The amount of heat energy gained when the lights are on is the product of the 4 fluorescent bulbs, the input energy from each of the 32 watts tubes, efficiency of the light fixture (0.85) [52], and the percentage of the heat energy that is convective (33% with a lens) rather than radiative (67% with a lens) [51]. As previously stated, radiative heat load from lighting is not considered in this research therefore, the interior lighting equation calculates the convective heat load only.

$$Q_{light} = Arduino * 4 * 0.85 * 32 * (1 - rad) \quad (10)$$

#### 4.1.3 Ventilation

The enthalpy equation used to calculate the ventilation heat load is shown in (11) with inputs of incoming air temperature (in kelvin) and the air heat capacity. The temperature of the incoming air for the left ventilation duct fluctuates from 20°C-30°C and the right duct fluctuates from 8°C to 30°C. The heat capacity fluctuation due to the temperature difference in the left duct is  $\pm 0.0005$  J/kg K and the right duct is  $\pm 0.001$  J/kg K. Since both the left and right ducts demonstrate temperatures primarily around 25 °C, the heat capacity value used is 1.0063J/kg K, which is the heat capacity of air at 25°C [53].

$$h = c_{pa} * T \quad (11)$$

The density of the air is calculated using (12) with the temperature of the incoming ventilation air (in kelvin), the atmospheric pressure  $P_{da}$ , 101,325Pa, and the specific gas constant for dry

air ( $R_d = 287.05\text{J/kgK}$ ) . This equation only calculated the density of the dry component of the air as latent load is not considered [54].

$$\rho = \frac{P_{da}}{R_d * T} \quad (12)$$

The heat energy being added to the test cell can therefore be calculated by multiplying the enthalpy of the air  $h$  (kJ/kg) by the density of the air  $p$  (kg/m<sup>3</sup>) and by the volumetric flow rate  $v$  (m<sup>3</sup>/s), found from the *WindSensor Rev P*(13).

$$Q_{vent} = h * p * v \quad (13)$$

As previously discussed in Section 4, it is assumed that the airflow rate of the air exfiltrating to the hallway is equal to the total ventilation input airflow rate from both ducts. The heat loss from the room is therefore also calculated using the enthalpy, density values (found from the ambient room temperature), and volumetric flow rate.

#### 4.1.4 Heater

The heater within the test cell is a hot water heater that adds sensible heat into the room through convective heat transfer. The initial convective heat transfer coefficient equation used for the heater is for turbulent natural heat transfer (14), used for conditions when the temperature difference is greater than 10°C [55]. This was later altered to the natural convection heat transfer coefficient (15), as discussed in Section 5.2. The  $L$  term in this equation is four times the area, divided by the perimeter [55].

$$h_{c\_turbulent} = 1.52 * (T_{amb} - T_{heater})^{0.33} \quad (14)$$

$$h_{c\_natural} = 1.32(\Delta T/L)^{0.25} \quad (15)$$

$$Q_{heater} = h_c * (T_{amb} - T_{heater}) \quad (16)$$

#### 4.1.5 Thermal Storage

The heat storage in the test cell is modeled for the ceiling, floor, and exterior wall along with the ambient air. The ceiling, floor, and exterior wall are the only elements considered due to

their high heat storage capacity compared to the other elements in the space, as shown in Table 3.

The heat capacity,  $C$  (J/K) values used within the white box model was found using the specific heat capacity  $c_p$  (kJ/kgK), density  $\rho$  (kg/m<sup>3</sup>), and volume  $v$  (m<sup>3</sup>) of each of the modeled building elements [55].

$$C = c_p * \rho * v * 1000 \quad (17)$$

The heat capacity of the air within the test cell was also calculated. The density of the air was determined using the temperature and relative humidity data collected from the *Omnisense* sensors from November through February in the equation (18) shown below [54].

$$\rho = \frac{P_{da}}{R_d T} + \frac{P_{wv}}{R_v T} \quad (18)$$

The specific heat capacity of air used within this calculation is 1.01kJ/kgK. The results demonstrated the heat capacity of the cell averaging 35,116.58 J/K  $\pm$  0.5%.

#### 4.1.6 Calculation of External Heat Loads

The only radiative heat load included in the model is the short-wave solar entering through the window. The solar radiation lands on the northern wall of the cell, as well as the floor. As the simplifications of the model assume negligible heat storage properties for the internal walls, the radiation heat load is calculated using only the floor heat storage capacity and the area of the floor which receives the radiation.

The short and long wave values were found using the calculation process described in [50], (see Appendix A). The solar radiation data used within the calculations were measured at the weather station installed on the roof of the building. The direct solar radiation values  $I_{SW}$  are used to calculate the short-wave solar radiation heat gain within the test cell. It is assumed that one third of the floor, an area of 2.78 m<sup>2</sup>, is impacted by the incoming radiation. The solar heat gain coefficient (SHGC) value used for the window is 0.7 for double pane, uncoated window type [51], the absorption,  $\alpha$ , of the concrete floor is 0.6 [51].

$$Q_{sol} = I_{SW} * SHGC * A_{floor} * \alpha \quad (19)$$

During the heating season, the conductive heat losses from the test cell are primarily through the exterior façade with the conductive heat gains coming from the interior hallway. As previously stated, due to the assumptions of this model these are the only two elements within the cell under consideration for conductive heat transfer.

The east-facing wall experiences the largest conduction heat loss as it is the exterior facing wall and features low insulative components such as window and spandrel panel units. The window and spandrel panel are represented in the model as one equivalent resistance to simulate conductive heat transfer. The concrete portion of the wall however, is modeled as a 3R2C system incorporating both conduction and heat storage. The exterior surface temperature of the concrete wall is therefore needed for the conduction calculations. The test cell does not have sensors installed on the exterior façade so the exterior surface temperature is found using back calculation of the wall's energy balance. The energy balance for the exterior wall during the heating season is shown below in (22) [55]. The heat gains in this equation include the absorbed short-wave radiation while the heat losses in this equation include the emitted long wave radiation and the convective and conductive heat losses. The convective coefficient used in this equation is forced convection under conditions of airflow between 1 m/s to 5 m/s [55]; it is assumed the east façade being sheltered by surrounding buildings falls within this range. The equation (20) shown below, takes input of the wind velocity, which for our study is the wind speed taken from the weather station on the roof of the building. The term  $I_{sw}$  represents the short-wave radiation, while  $T_{sky}$ ,  $T_{air}$ ,  $T_{ext\ surface}$ ,  $T_{interior}$  represent the sky, exterior ambient, exterior surface, and interior surface temperatures respectively. The temperature of the sky is found using the simplified relationship shown in (21) below [55]. The  $F_a$  term is the view factor (0.5 for vertical wall components),  $\varepsilon$  is the emissivity value for the concrete (0.93 [51]),  $\sigma$  is Stephan-Boltzman's constant ( $5.67 \times 10^{-8}$ ),  $\alpha$  is the absorptivity of concrete (0.6 [51]), and  $U$  is the conduction heat transfer coefficient.

$$h_c = 5.9 + 3.6V \quad (20)$$

$$T_{sky} = 1.2 * T_{air} - 14 \quad (21)$$

$$\alpha I_{sw} + \alpha I_{Lw} - F_a \varepsilon \sigma (T_{ext\ surface}^4 - T_{sky}^4) - h_c (T_{ext\ surface} - T_{air}) - U (T_{interior} - T_{exterior}) = 0 \quad (22)$$

The U-values used for the window, spandrel panel, exterior wall, interior wall and door are shown in Table 5 with full calculations in Appendix D U-value Calculations. The conductance and conductivity values used to calculate the overall U-value is found from Building Science for A Cold Climate [56]. The door and window U-values were both determined from the ASHRAE Handbook: Fundamentals [51]. The ASHRAE door and window type definitions are shown in Table 5. The spandrel panel, interior wall, and window u-values include the air film resistivity as these elements are represented as one equivalent resistance in the RC network. The exterior wall, floor, and ceiling u-values do not include air film resistivity because the air films are modeled in the RC network for these elements.

*Table 5: U-value for Elements of the Test Cell*

<b>Test Cell Element</b>	<b>Construction</b>	<b>U-value</b>
Exterior Wall	28" concrete	4.8
Floor/Ceiling	13.75" concrete	3.78
Windows	Double pane, aluminum frame	3.18
Spandrel Panel	1.75" spandrel panel filled with fiberglass insulation	0.82
Interior Walls	Steel studded wall 16" OC	1.95
Door	Foam-insulated steel slab with metal edge in steel frame	2.10

The conduction calculation (23) is completed using the element's U-value, exposed surface area, and temperature gradient [55]. The hallway heat exchange calculations are conducted using the door position data, so the conductive heat exchange through the door is only included when the data indicates that the door is closed. The exterior wall's temperature gradient is the difference between the exterior temperature and the test cell's ambient temperature. The interior wall's temperature gradient is the difference in the hallway and test cell ambient temperatures.

$$Q_{cond} = UA\Delta T \quad (23)$$

## 4.2 White Box Model Implementation in Matlab

The RC Network white box model was created in the simulation program *Simulink*, a plugin within *Matlab*. *Simulink* is a block diagram environment used for model-based design. Dynamic systems can be created using the block library and solved using the range of solver apps. *Simulink* and *Matlab* are integrated programs that allow for data to be transferred between them.

The white box model was created by constructing each of the differential equations from Table 4, using the program's mathematical blocks. An example of the sub-system circuit for the temperature of the floor is shown in Figure 16.

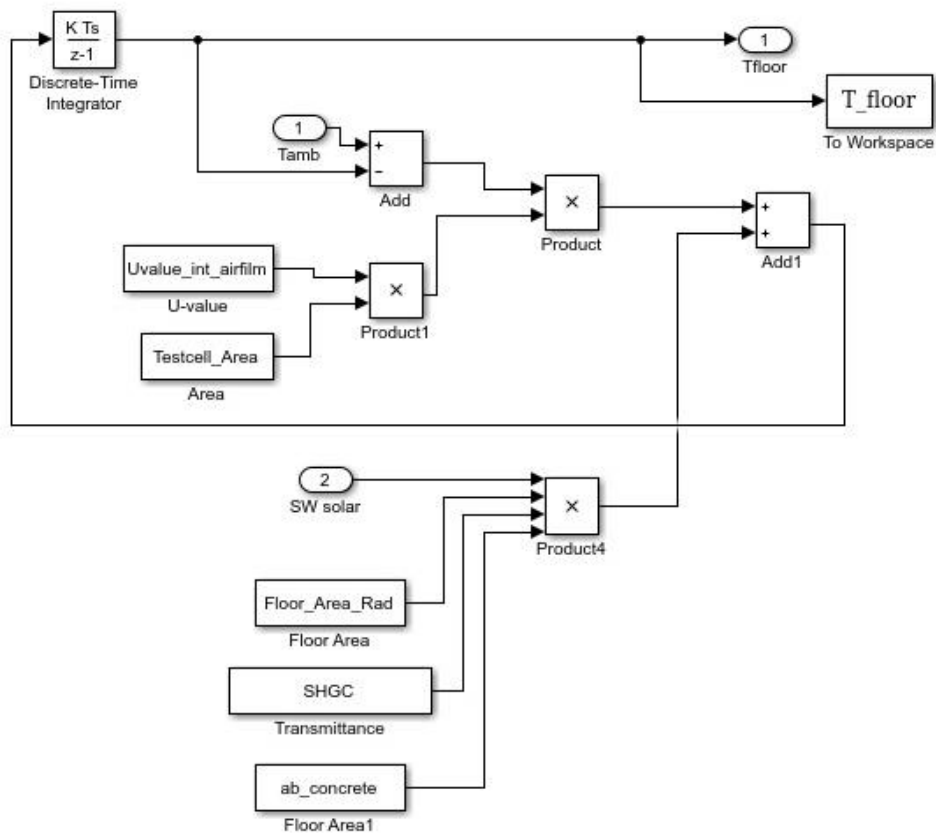


Figure 16 Simulink Implementation of Differential Temperature Equations

To organise the model, each differential equation is created within their own sub-system's block as shown in Figure 17. The sub-systems are then linked together to replicate the RC Network. For example, in Figure 16 the input node 1,  $T_{amb}$  is linked to the output node from

the  $T_{amb}$  differential sub-circuit and the output node  $T_{floor}$  is sent to the ambient temperature subsystem.

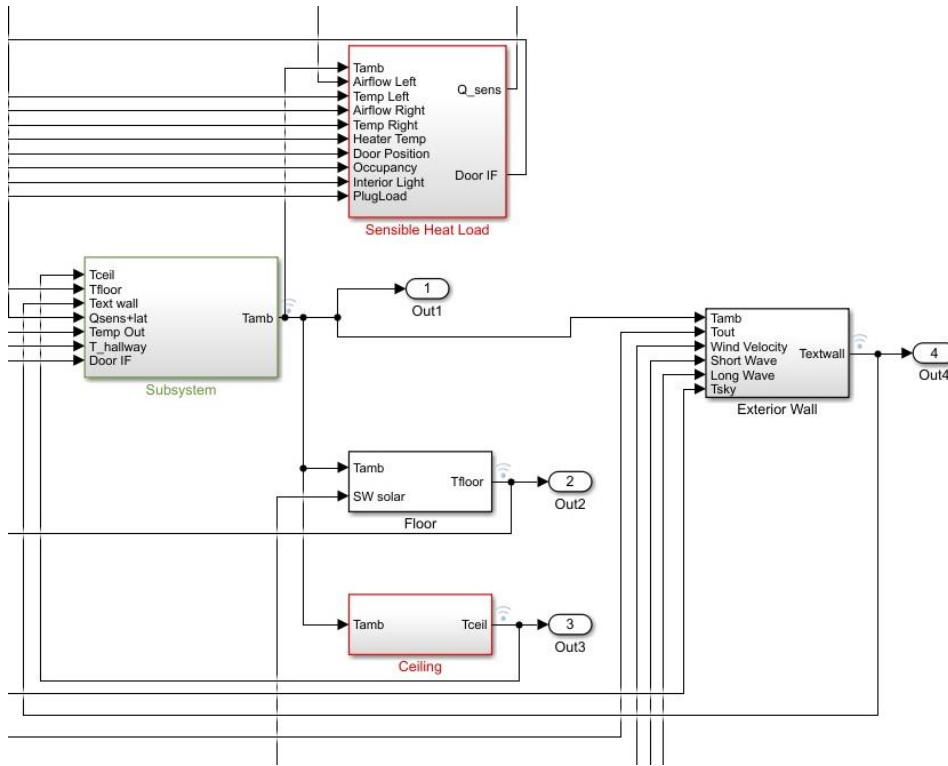


Figure 17 Grey Box Model Subsystem Structure

The material properties and scientific values used within the model are input as variables instead of their actual values to utilize the workspace parameter storage option in *Simulink*. All of the variable values are stored in this space to facilitate quick changes of values, if necessary, without having to find their location in the model.

## 5 Grey Box Model Creation

The grey box model was created by expanding the Simulink white box model to include the input data collected from the test cell. The first step to running the grey box model was configuring the input data in *Matlab* before being uploaded to *Simulink*. The excel files with the sensor measurements were uploaded into *Matlab* using the excel table upload function, *xlsread*. The data values requiring calibration, namely the ventilation airflow temperature and airflow rate, were then calibrated within the code. In order for *Simulink* to be able to read the *Matlab* data, the data must be configured as double arrays with the first row being the time stamp and the second row the respective data value. The arrays are then saved as version 7.3 .mat files. The *Matlab* code is shown in Appendix E Matlab Code .

In *Simulink*, the .mat files were loaded into the model using .mat source blocks. Simulink reads data from the .mat files and outputs the data as signals. The source blocks are then directly connected to rate transition blocks to transfer the data points into one congruent time step. This step is needed because the data collected from the sensors and data loggers have different measurement time increments. In this research, the *Arduino* data was collected per second and averaged into 1-minute sets, the thermocouple surface measurements were collected at 1-minute intervals, the ambient data along with weather station data at 5-minute intervals, and the solar data at 15-minute intervals. The grey box models were simulated at 1-minute time steps, the rate transition blocks determined the output value of the data source blocks based on the time step defined in their data arrays. From the rate transition blocks the signals were sent to their respective locations within the model.

To see the signals being transferred between the blocks in the model, sink blocks can be installed anywhere by connecting the input of the sink block to the signal line. Throughout the troubleshooting of the model this feature became useful to check the calculations in the model. The sink blocks send the data to *Matlab* in the form of data arrays. The predicted temperature results from the simulation are collected using this method where sink blocks are installed at each subsystem output and the results are found in the *Matlab* workspace.

The simulation is set up by first configuring the simulation period and the settings for the simulation time steps. The time step has the options of being fixed or variable steps as well as

having a minimum and maximum size. This model is configured as a fixed step solver with a step size of 1 minute, simulating for 5 hours. Before the simulation is run, the initial temperatures of the ambient air, ceiling slab, floor slab, and exterior wall are input into the integrator blocks situated within each of the subsystems.

### **5.1 First Generation, First Iteration Grey box Model (G1v1)**

The first generation, first iteration grey box model is the white box RC network with inputs of the test cell BAS points. This model uses the estimated resistance and capacitance values to represent the building elements. To test the model under a variety of conditions eleven simulation days spanning November to February were chosen based on time of day, occupancy, and exterior conditions. These simulation days are used for the remainder of this study to evaluate the performance of future model iterations and compare model performances. Images of the first-generation model are shown in Appendix F Simulink Images.

### **5.2 First Generation, Second Iteration Grey box Model (G1v2)**

Following the G1v1 simulations, some shortcomings of the model were observed, notably the performance discrepancies due to the addition of the heater and occupancy related heat loads. To address the first observation, the second iteration model was created with representation of the convective heat transfer from the heater using a natural convection coefficient instead of the turbulent convection coefficient previously used. This model is an alteration of the first iteration model where every element besides the heater convective heat transfer calculation is the same as before. Note that convective heat transfer was added to the ceiling element in the model to correct the initial model's shortcomings, however, this did not improve the model and resulted in more inconsistencies. The convective element was therefore not included in the G1v2 model.

### **5.3 First Generation, Third Iteration Grey box Model (G1v3)**

To address the second observation, poor prediction results for occupied simulations, the G1v3 model was created. The G1v3 model optimizes the internal mass heat capacity value to improve the performance of the model during daytime occupied conditions when it is subjected to additional heat loads. It is common for grey box models to use a representative internal heat capacity value that includes both the heat capacity of the air along with miscellaneous building

elements such as furniture, as discussed in Section 2.6. The internal heat capacity value of the test cell was found using *Simulink*'s parameter estimation tool.

To set up the parameter estimation tool, the output signal, initial input parameters, and the parameter being estimated are defined. For this research the output signal is the measured ambient temperature, the initial input parameter is the ambient temperature at the beginning of the simulation, and the parameter for estimation is the internal heat capacity. The parameter optimisation tool settings were set to use a nonlinear least squares method and a trust-region-reflective algorithm with a tolerance of 0.001. The parameter estimation was run on every simulation day for the G1v3 model. The optimal heat capacity value was determined by then running each of the internal heat capacity values on all of the other simulation days to determine the value that best represents the test cell. The steps taken to determine the optimal heat capacity value are described in Table 6.

*Table 6 Internal Heat Capacity Optimisation using G1v3 Model*

Date	Internal Heat Capacity from Parameter Estimation	Comments
November 29 <sup>th</sup> , 2017	457.9 kJ/K	This date was chosen first for analysis because it is the median heat capacity value.
January 6 <sup>th</sup> , 2018	1,834.2 kJ/K	This value was analyzed second, as it is the next highest value
January 8 <sup>th</sup> , 2018	252.7 kJ/K	Due to the less accurate results of the higher heat capacity value, this value was chosen as it is the next lowest value below 457.9 kJ/K
February 7 <sup>th</sup> , 2018	239.0 kJ/K,	The lower heat capacity value, 252.7 kJ/K, demonstrated better results than the initial 457.9 kJ/K. Sequentially lower values were tested until a minimum error was found
January 2 <sup>nd</sup> , 2018	219.1 kJ/K	
November 17 <sup>th</sup> , 2018	112.7 kJ/K.	

Using the optimized internal heat capacity value, the prediction performance of the grey box model improved. However, the G1v3 model still incorporates knowledge of the exterior wall resistivity values and uses the initial temperatures of the ceiling, floor, and exterior wall slabs to set up the simulation. In order to develop the model to the point where only building automation system (BAS) points are used within the simulation, the relationship between the slab temperatures and the energy loads of the cell was found using linear regression. These regression models will replace the building elements physical representation in the model.

#### 5.4 Second Generation (G2) Model

Because the objective of this thesis is to model the thermal dynamics of a space based on inference from building automation system data rather than known characteristics, it was necessary to eliminate the resistivity and capacitance values for the building elements in this model. To replace these, a stepwise linear regression model was created, correlating the relationships between the surface temperatures of the ceiling, floor, exterior wall, window, spandrel, and interior wall elements as well as the BAS points. The subtractive approach was conducted within R-studio, using the dataset of BAS points collected between November 16<sup>th</sup>, 2017 and February 29<sup>th</sup>, 2018. The data points were cleaned to eliminate any noise that would skew the results. The data cleaning criteria was occupancy between 0 and 4; lighting between 0 and 1; short and long wave radiation above 0W; the right and left ventilation airflow between 0 and 1m<sup>3</sup>/s; right and left ventilation temperature between 0 and 50 °C; and all the surface temperature measurements - heater, ceiling, floor, ambient, spandrel, interior wall, and window above 5 °K. The most important cleaning criteria within this set was the surface temperature measurements of at least 5 °K. When the thermocouple logger malfunctioned, it would record the surface temperature as -3 °K. This problem occurred on multiple occasions, in short spurts, for the heater thermocouple throughout the data collection period. The cleaning criteria assured that these heater measurements were not included within the regression analysis.

The cleaned data was split into training data (80% of cleaned data set) and testing data (20% of cleaned data set). The training data set was used within the subtractive regression analysis to determine the model that best balances simplicity and accuracy, as described in Section 2.7. The input variables to the regression analysis were: the ambient test cell and hallway temperature, the heater surface temperature, the occupancy count, the light position, the left

and right ventilation airflow rate, the left and right ventilation air temperature, the plug load, the short and longwave solar radiation, the exterior temperature, and wind speed. The regression analysis was conducted for a general model as well as a split occupied and unoccupied condition model.

The regression analysis for the general model used the complete data set. The general linear regression models for all of the building elements were added to the G1 grey box model replacing their physical representation circuits. This eliminated all of the surface temperature node differential equations, leaving only the ambient temperature equation within the model.

For the split linear regression model, the data sets were found using the filter application within excel to divide the overall dataset into occupied times and unoccupied times. To compare the performance of the split regression model and the general regression model, the grey box model with all of the surface temperature general regression models, was altered to replace one element at a time with the split regression model. The surface temperature prediction results of the element represented with the split model is compared to the results of that element when represented with the complete regression model. This was repeated for each building element where, in each grey box iteration only the building element under investigation is represented with the split regression model.

The performance of the regression models was analyzed by the adjusted  $R^2$  value and the root mean squared error (RMSE). The closer the adjusted  $R^2$  value is to one, the greater performance of the model when it was tested against the unseen testing data. The RMSE results is an additional assessment of the strength of the fit, by calculating how far off the model is from the actual conditions. The significance of the variables within the model was analyzed based on their p-value and t-value. The p-value tells us the significance of the variable, and tells us the probability of seeing this result in a random collection of data [57]. For example, a p-value of 0.05 means there is a 5% chance that the results would occur again in a collected of random data, so there is a 95% probability that this variable has an effect on the model. The t-value correlates the p-value except it is a measurement of the difference between the population mean and a hypothesized value, measured in units of standard deviation [57]. The null hypothesis for the regression analysis is that all variables have no significance in the regression model. If the p-value is less than 0.01, there is a 90% probability that rejecting the null hypothesis is correct,

less than 0.05 a 95% probability, and 0.001 a 99% probability. Similarly, in terms of the t-values, the greater the magnitude of the t-value, the greater the evidence against the null hypothesis. Rejecting the null hypothesis means the variable is significant in the regression model.

These regression models were then used within the *Simulink* grey box model to replace the differential equations of the building elements. Images of the model can be seen in Appendix F Simulink Images.

### 5.5 Third Generation (G3) Model

The analysis from the G2 model demonstrated the window, spandrel panel, and exterior wall as having the largest WAPE values compared to all of the other building elements. To improve the performance, neural networks were created for each of these elements within Matlab using the Neural Net Fitting App. Within the app the inputs, output, and neural network settings are defined. For this model the inputs to the neural network are the same as the inputs to the linear regression analysis: the ambient test cell and hallway temperature, the heater surface temperature, the occupancy count, the light position, the left and right ventilation airflow rate, the left and right ventilation air temperature, the plug load, the short and longwave solar radiation, the exterior temperature, and wind speed. The output of the neural network is the surface temperature measurement. The app was set to split the data into 70% training, 15% validation and 15% testing. The hidden layer size for each neural network was determined using an optimisation process. The number of hidden layers within each neural net was continually increased until a minimum RMSE value was found. The minimum RMSE criteria was the lowest observed RMSE value where the two consecutive larger hidden layer models have greater RMSE. Once the hidden layer size was determined, the neural network was fit using a Levenberg-Marquardt algorithm. Following the results in *Matlab*, the *getsim* function was used to create a *Simulink* block of the neural network. The neural network blocks for the window, spandrel panel, and exterior wall were created in this manner. To evaluate the performance of the neural networks compared to the linear regression models, the neural network of each element was implemented one at a time into the G2 linear regression grey box model. Three G3 models were created, each one having one of the three elements - the window, spandrel, and exterior wall - being represented with their neural network. The models were simulated on

the eleven days; the overall prediction performance of the window, spandrel panel, and exterior wall surface temperatures using the neural networks were compared to using linear regression models.

## 5.6 Final Model

The Final model for this research is the G2 model. The G3 model did not demonstrate improvement in predicting the surface temperatures of the window, spandrel panel, or exterior wall therefore the elements were reverted back to linear regression models. The Final Model for this research is the G2 model with all elements represented with linear regression equations.

## 5.7 Sensitivity Analysis

Following the creation of the Final model, a sensitivity analysis was conducted. This analysis investigates the sensitivity of the model and the ability of the Final model to be implemented within a different environment. The model being used within a new environment will require the internal mass heat capacity value to be optimized and the regression models re-trained.

To investigate the ability to determine the internal heat capacity parameter using the Final model, the parameter estimation tool within *Simulink* was once again used. The results from the parameter estimation using the Final model are compared to the results found previously using the G1v3 model, to see if the Final model results are within range of the optimal value determined from the G1v3 model.

In addition to determining the internal mass heat capacity value, the linear regression models needed to be trained from data collected from the new building. An investigation into the amount of data needed to accurately predict the ambient temperature was conducted. This analysis trained the grey box models using varied sizes of data sets, spanning 1 week's worth of data to 1 month's worth of data. This will determine the length of time that surface temperature data will need to be collected in order to create accurate linear regression models. The testing periods used in this analysis are shown Table 7.

*Table 7 Regression Model Training Period Analysis using the Final Model*

Dataset Duration	Dates Included
1 week	December 1 <sup>st</sup> 2017-December 7 <sup>th</sup> 2017
	February 16 <sup>th</sup> 2018 – February 22 <sup>nd</sup> 2018
2 weeks	December 1 <sup>st</sup> 2017 – December 14 <sup>th</sup> 2017
	February 16 <sup>th</sup> 2018 – February 29 <sup>th</sup> 2018
1 month	December 1 <sup>st</sup> 2017 – December 31 <sup>st</sup> 2017

All of the regression equations for these models were found using the same process as described in Section 2.7 and using the same regression model structures, with all building elements except the ceiling slab using the split model. The simulations created for these time periods were also tested for their ability to determine the optimal internal heat capacity values. The heat capacity values are then compared to the results from the G1v3 model and the Final model to see if results within the same range can be determined.

Finally, a sensitivity analysis was also conducted to investigate the ability of the model to perform outside the training season. A simulation day of April 9<sup>th</sup>, 2018 was selected to evaluate the performance of the final model in predicting building element surface temperature and ambient temperature. This simulation is for occupied, daytime conditions.

## 5.8 Error Analysis

As noted in Section 3.5, the plug load data used in this study was not the actual collected data. Due to malfunctions in equipment and user error, large data gaps in the data collection prevented the use of the actual data. An observed data trend between the plug load value and occupancy count determined the plug load values used within this study. To analyze the implications of this simplification on the results of this research, three simulation days were selected when the equipment was working properly. Simulation results when using the actual plug load data were compared to results when using the calculated values to evaluate the impact of the approximated plug load data.

Point measurements of the surface temperatures, ventilation ducts air temperature and flow rate, and ambient temperature were used within this study. An investigation was conducted to analyze the error associated with this simplification. An analysis of true variations in surface

temperature was conducted by taking multiple temperature readings across the window and floor area. The data points were inspected to observe the true deviations in temperature occurring across the element's surface. The point measurement errors associated with the ventilation sensors and ambient sensors were not investigated. This is due to the ventilation sensors being calibrated using a balometer, which mitigated the point temperature and airflow measurement error (see Section 6.11.2). The ambient temperature point measurement was unfortunately not analyzed due to time constraints and is an unknown error factor within this research.

Another sensor error that occurred within this research, discussed in Section 3.5, is the test cell being installed without relative humidity sensors for the ventilation air. This study therefore did not consider any latent heat loads from the incoming ventilation air, instead using the assumption of dry air for calculating the enthalpy. Relative humidity sensors have since been installed within the ventilation ducts. The simulation day of April 9<sup>th</sup> 2018, was used to conduct a comparison in ambient prediction results when calculating the proper enthalpy of the incoming ventilation air verses when using the dry air assumption.

## 6 Grey Box Model Results

The grey box model was tested using multiple simulations, of three-hour periods, for selected days between the middle of November and the end of February. The simulation periods were chosen strategically to represent the full range of domain inputs, namely variation in time of day, day of the week, level of use, and outdoor conditions. These are summarized in Table 8 below. The simulations were run in series starting with the simplest conditions- at night without occupants, moving to the most complex conditions- during the day with variable indoor and outdoor conditions.

*Table 8 Summary of Simulation Periods used for Model Testing*

<b>Period</b>	<b>Tout</b>	<b>Wind Speed</b>	<b>Total Global Solar Radiation</b>	<b>Occupied?</b>	<b>Time of day</b>
November 17, 2017 (0:05 – 3:05)	0.93°C	0.5 to 1.5 m/s	0	No	Night
November 29, 2017 (0:05 – 3:05)	4.7°C	0.5 to 1.5 m/s	0	No	Night
January 6, 2018 (0:05 – 3:05)	-19.19°C	0.5 to 1.5 m/s	0	No	Night
December 31, 2017 (9:35-12:35)	-16.04°C	0.5 to 1.5 m/s	400W/m <sup>2</sup>	No	Daytime
January 13, 2018 (9:35-12:35)	-13.04°C	0 m/s	400W/m <sup>2</sup>	No	Daytime
January 2, 2018 (9:05-12:05)	-10.02°C	2-4 m/s	50W/m <sup>2</sup>	No	Daytime
February 12, 2018 (13:50 – 16:50)	-2.51°C	0.5-2 m/s	120W/m <sup>2</sup>	Yes	Daytime
January 8, 2018 (10:05 – 13:05)	0.5°C	1-2.5 m/s	50W/m <sup>2</sup>	Yes	Daytime
February 7, 2018 (16:05-19:05)	-3.57°C	0.5-1.5 m/s	50W/m <sup>2</sup>	Yes	Daytime
December 8, 2017 (14:20 – 17:20)	1.04°C	2.5–3.5 m/s	50W/m <sup>2</sup>	Yes	Daytime
December 5, 2017 (11:35-14:35)	10.93°C	2-4 m/s	50W/m <sup>2</sup>	Yes	Daytime

## 6.1 G1 Model

The G1 model has all of the building elements represented with differential equations (shown in Table 4), using estimated resistivity and capacitance values. The inputs to the model are the initial indoor ambient temperature, ceiling and floor surface temperatures, as well as, the exterior wall interior and exterior surface temperatures. The model was simulated under three conditions nighttime (unoccupied) simulations, daytime unoccupied simulations, and daytime occupied simulations. The accuracy of the simulated temperature was examined at Prediction Windows of 15, 30, 45 60, 120, and 180 minutes. Note that the true weather, HVAC data, and occupancy data were fed to each model, as the prediction of these elements is beyond the scope of this thesis. Error bars are not displayed on the surface temperature results from Generation 1 simulations as the graphs were zoomed in to allow to see the temperature variations in the results; the error bars resulted in too much overlap and had the upper or lower limit falling outside the graph area. When analyzing the results keep in mind, surface temperature sensors are accurate to  $\pm 0.5^{\circ}\text{C}$ . The error bars are displayed for the ambient temperature results, with the ambient temperature measurement accurate to within  $\pm 0.4^{\circ}\text{C}$ .

### 6.1.1 Nighttime Simulation

The first three simulation periods were selected during the simplest condition: at night between 12 am and 5 am when the ventilation is off and there are no occupants. The first two occurred in November before the heater of the test cell was turned on. The third such simulation occurred during February and included this heat load.

The prediction error (equation (8)) from November 17<sup>th</sup> are summarized in Table 9. The G1 model predicted the surface temperatures to within 0.6% accuracy. The graph of predicted versus actual temperature, Figure 18, demonstrates the ceiling and exterior wall having temperature deviations that increased to  $0.1^{\circ}\text{C}$  for the 180-minute forecast, while the floor slab has no temperature deviations. It is observed at the 30-minute Prediction Window that the exterior wall temperature deviation jumps from  $0.1^{\circ}\text{C}$  to 0. A review of the raw data indicated the thermocouple measurement decreased by  $0.1^{\circ}\text{C}$  at the 30-minute time step and then returned to its original value at the 45-minute time step. The thermocouples have an accuracy of  $\pm 0.5^{\circ}\text{C}$  therefore the jump seen in the temperature is likely only a measurement fluctuation.

Ambient temperature (Figure 18) also demonstrates good prediction results, with the largest deviation of 0.2°C occurring in the last hour of the Prediction Window.

*Table 9 Prediction Error for Temperatures of Simulated Elements as a Function of Prediction Window Duration for November 17, 2017 ( $T_{out} = 0.93^{\circ}\text{C}$ , wind speed = 0.5 to 1.5 m/s)*

Prediction Error						
	15 minutes	30 minutes	45 minutes	60 minutes	120 minutes	180 minutes
Ambient	-0.125%	0.182%	0.070%	-0.033%	-0.357%	-1.003%
Exterior Wall	-0.443%	-0.024%	-0.468%	-0.481%	-0.531%	-0.583%
Ceiling	-0.421%	-0.421%	-0.421%	-0.421%	-0.423%	-0.425%
Floor	0.000%	-0.001%	-0.001%	-0.002%	-0.003%	-0.005%

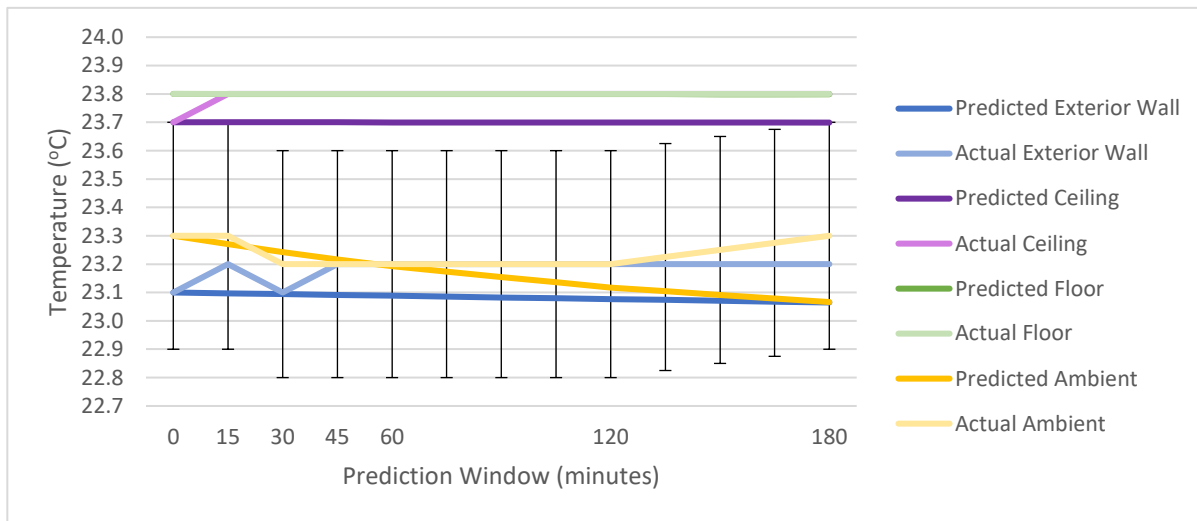


*Figure 18 November 17, 2017 Actual vs Predicted Temperatures for each Prediction Window*

The results from the November 29<sup>th</sup> simulation are summarized in Table 10, with surface temperature predictions within 0.5% accuracy for the 180-minute Prediction Window. Similar to the previous model, it can be seen that the exterior prediction error jumps by 0.1°C (Figure 19) at the 15-minute and 45-minute prediction time; more than likely due to noise of the surface temperature measurement. The ambient temperature is predicted within 1.5%, as shown in Figure 19, and deviates at the 60-minute Prediction Window by 0.2°C and at the 180-minute Prediction Window by 0.3°C. Both of these deviations are within the accuracy of the measurement device.

*Table 10 Prediction Error for Temperatures of Simulated Elements as a Function of Prediction Window Duration for November 29, 2017 ( $T_{out} = 4.7^{\circ}\text{C}$ , wind speed = 0.5 to 1.5 m/s)*

Prediction Error						
	15 minutes	30 minutes	45 minutes	60 minutes	120 minutes	180 minutes
Ambient	-0.007%	-0.020%	0.423%	0.866%	0.445%	1.407%
Exterior Wall	-0.449%	-0.011%	-0.460%	-0.021%	-0.513%	-0.547%
Ceiling	0.000%	0.000%	-0.001%	-0.001%	-0.002%	-0.003%
Floor	0.000%	-0.001%	-0.001%	0.432%	0.430%	0.429%

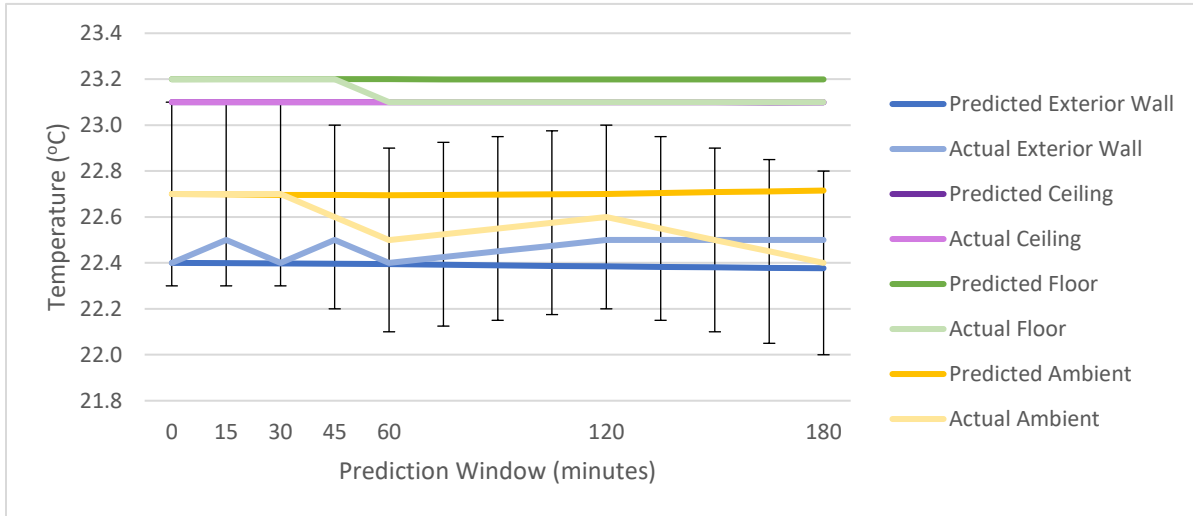


*Figure 19 November 29, 2017 Actual vs Predicted Temperatures for each Prediction Window*

The results for January 6<sup>th</sup> are summarized in Table 11, demonstrating surface temperature predictions to within 0.6% for the 180-minute Prediction Window. As shown in Figure 21, the floor and ceiling elements show good prediction results with prediction error close to 0% for the entire simulation, while the exterior wall demonstrated similar results to the other night simulations with 0.1°C deviations. The ambient temperature demonstrated good prediction performance for the first hour of the simulation and then gradually increased in prediction error to 1.5%, 0.5°C off, at the 180-minute Prediction Window.

*Table 11 Prediction Error for Temperatures of Simulated Elements as a Function of Prediction Window Duration for January 6, 2018 ( $T_{out}=-19.19^{\circ}\text{C}$ , wind speed ranging from 0.5 to 1.5 m/s)*

<b>Prediction Error</b>						
	15 minutes	30 minutes	45 minutes	60 minutes	120 minutes	180 minutes
Ambient	-0.008%	-0.016%	-0.024%	-0.516%	-1.044%	-1.564%
Exterior Wall	0.479%	-0.545%	-0.570%	0.404%	0.305%	-0.297%
Ceiling	0.000%	-0.001%	-0.002%	-0.003%	-0.006%	-0.008%
Floor	-0.001%	-0.002%	-0.003%	-0.004%	-0.008%	-0.013%

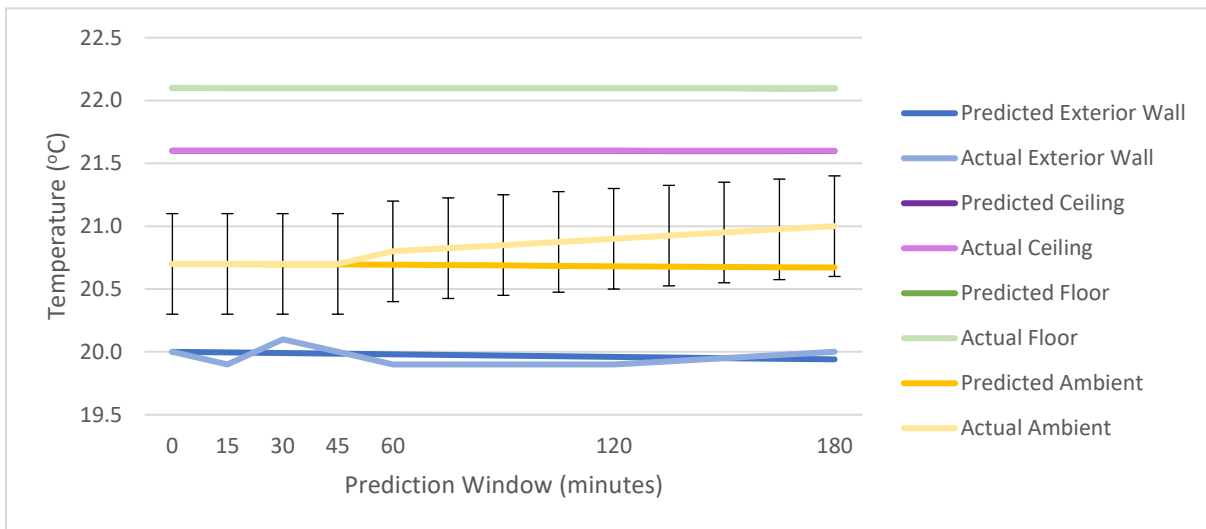


*Figure 20 January 6<sup>th</sup>, 2018 Actual vs Predicted Temperatures for each Prediction Window*

### 6.1.2 Daytime Unoccupied Simulations

Following the nighttime simulations of the test cell, the next grouping of simulations examined the daytime conditions without occupants. When compared to the nighttime simulations, these simulations have additional solar and ventilation system heat loads. The simulation times within this group were chosen based on exterior conditions - the first two simulations occur at times of high solar radiation and the last simulation during a period of high wind speeds.

The results from the December 31<sup>st</sup> simulation, shown in Table 12, indicate good prediction accuracy for the floor and ceiling slabs. As shown in Figure 21, these elements are predicted to within 0.1°C of the actual measurements which, is lower than the accuracy rating of the measurement device. This model is observed to have worse prediction accuracy for the exterior

wall than the previous nighttime simulations. The exterior wall had a prediction error of up to 2.5% at the 120-minute Prediction Window onward. This is due to the actual temperature increasing while the predicted temperature remains steady, as shown in this same figure. Despite the larger prediction error for the exterior wall, the ambient temperature still demonstrates good prediction performance with prediction error within 1%, 0.3°C off, at the 180-minute Prediction Window period.

*Table 12 Prediction Error for Temperatures of Simulated Elements as a Function of Prediction Window Duration for December 31, 2017 ( $T_{out}=-16.04^{\circ}\text{C}$ , wind speed ranging from 0.5 to 1.5m/s)*

Prediction Error						
	15 minutes	30 minutes	45 minutes	60 minutes	120 minutes	180 minutes
Ambient	-0.020%	-0.021%	-0.014%	-0.006%	0.959%	0.982%
Exterior Wall	-0.021%	-0.043%	-0.065%	-0.575%	-2.095%	-2.182%
Ceiling	0.000%	0.000%	-0.001%	-0.001%	-0.461%	-0.462%
Floor	0.457%	0.013%	0.469%	0.023%	-0.414%	-0.416%

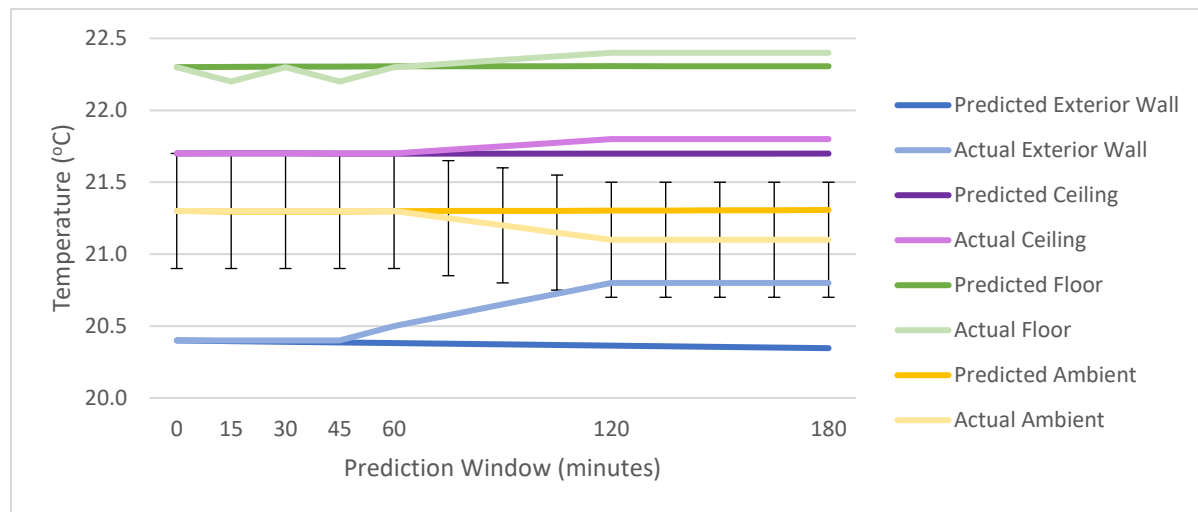


*Figure 21 December 31<sup>st</sup>, 2017 Actual vs Predicted Temperatures for each Prediction Window*

The January 13<sup>th</sup> simulation, summarized in Table 13, predicted the surface temperature of all building elements to within 1% accuracy. The exterior wall demonstrated 0.5% jumps in prediction error, once again due to measurement fluctuations. The ambient temperature demonstrates fluctuations in the middle of the simulation, shown in Figure 22, where the prediction results are off by 0.3°C and 0.4°C before settling to within 0.1°C at the 120-minute

Prediction Window onward. This is observed to be due to jumps in the actual ambient temperature measurements. As the ambient temperature measurement device is only accurate to within 0.4°C, these jumps, similar to the surface temperature deviations, are likely caused by measurement fluctuations.

*Table 13 Prediction Error for Temperatures of Simulated Elements as a Function of Prediction Window Duration for January 13, 2018 ( $T_{out}=-13.04^{\circ}\text{C}$ , wind speed ranging from 0 m/s, and solar radiation 400W/m<sup>2</sup>).*

Prediction Error						
	15 minutes	30 minutes	45 minutes	60 minutes	120 minutes	180 minutes
Ambient	-1.018%	-0.714%	0.046%	-1.377%	-0.396%	-0.208%
Exterior Wall	-0.487%	-0.506%	-0.056%	-0.075%	-0.621%	-0.229%
Ceiling	0.000%	0.000%	0.000%	-0.001%	-0.002%	-0.440%
Floor	0.010%	0.018%	0.025%	0.031%	0.045%	0.045%

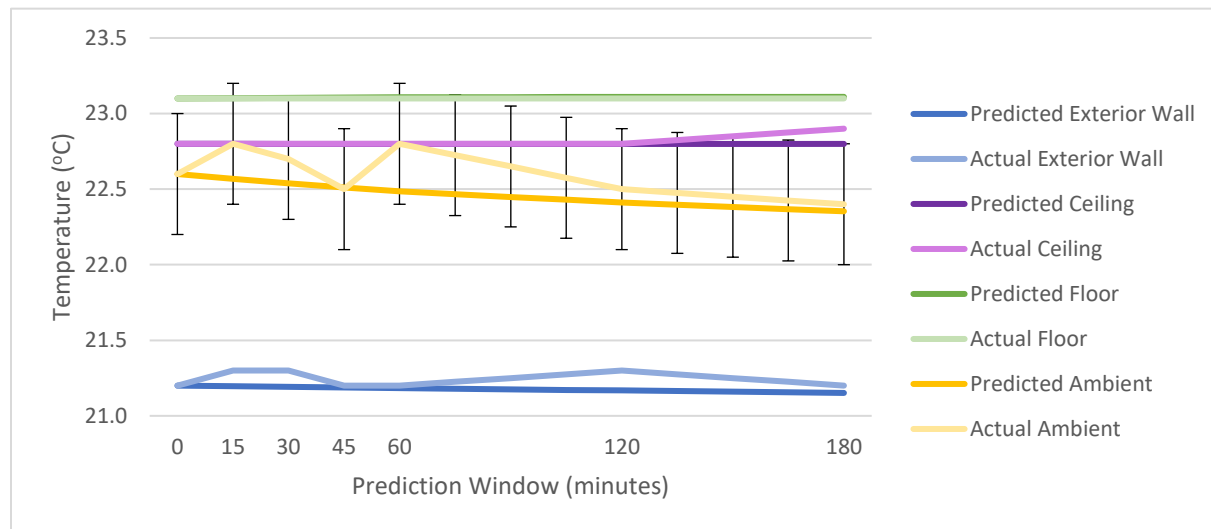


*Figure 22 January 13<sup>th</sup>, 2018 Actual vs Predicted Temperatures for each Prediction Window*

The January 2<sup>nd</sup> simulation results are summarized in Table 14, with surface temperature prediction errors less than 0.5%, and ambient temperature prediction error less than 1% (Figure 23). The fluctuations seen in the exterior wall temperature, similar to previous simulations, are believed to be measurement fluctuations. The ambient temperature prediction for this simulation demonstrates similar behaviour to previous models, with accuracy of within 0.1°C until the last two hours of the simulation when the predicted temperature deviated by 0.3°C.

*Table 14 Prediction Error for Temperatures of Simulated Elements as a Function of Prediction Window Duration for January 2, 2018 ( $T_{out}=-10.02^{\circ}\text{C}$ , wind speed ranging from 2-4 m/s, and solar radiation  $50\text{W}/\text{m}^2$ ).*

Prediction Error						
	15 minutes	30 minutes	45 minutes	60 minutes	120 minutes	180 minutes
Ambient	0.059%	0.115%	0.172%	0.230%	0.930%	1.138%
Exterior Wall	0.475%	-0.038%	-0.054%	0.419%	0.345%	0.272%
Ceiling	0.000%	0.000%	-0.001%	-0.001%	-0.002%	-0.003%
Floor	0.000%	0.000%	-0.001%	-0.002%	-0.004%	-0.006%

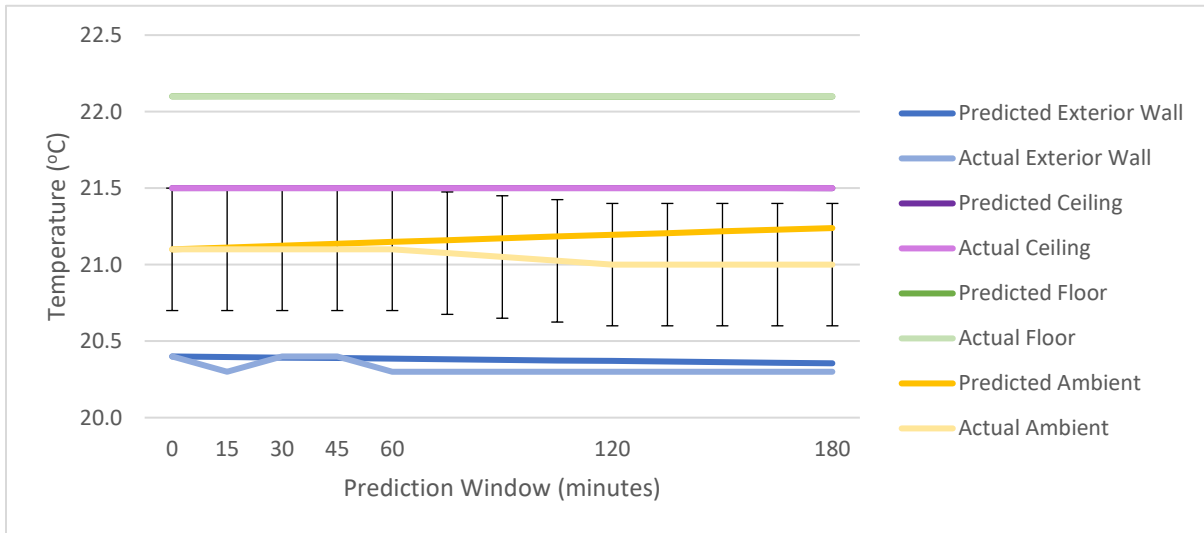


*Figure 23 January 2<sup>nd</sup>, 2018 Actual vs Predicted Temperatures for each Prediction Window*

### 6.1.3 Daytime Occupied Simulations

The final set of simulations were during occupied test cell conditions, with occupancy varying between 1-3 people. These simulations have additional heat loads due to the heat generated by the occupants, desktop computer plug load, and interior lighting. The last few simulations within this group were chosen specifically during windier periods to analyze the impact of the wind speed on the accuracy of the model.

The simulation from February 12<sup>th</sup>, summarized in Table 15, demonstrated worse prediction results compared to the previous unoccupied periods. The ceiling and floor elements are accurate to within 1.5%, while the exterior wall demonstrated prediction results to within 3% accuracy, deviating by up to  $0.6^{\circ}\text{C}$  (Figure 24) at the 120-minute Prediction Window. The ambient temperature also demonstrated slightly higher prediction error with the ambient

temperature accuracy off by 1.5%, 0.3°C, at the 180-minute Prediction Window. The actual temperatures of all three surfaces in Figure 24 are observed to increase at the 30-minute Prediction Window. Inspecting the data for this simulation there is no indication of an occurrence that would result in the temperature increase between the start of the simulation and the 30-minute period. Since the data does not demonstrate any increase in heat load, the predicted temperature stays stagnant and the actual temperature increases. This could be due to convective heat transfer, which is not modeled within the RC network, or a heat load that is missed within the grey box model. One observation made when looking at the data for this simulation is the occupancy count increases to 3 people at the 30-minute Prediction Window and stays at 3 people until the 90<sup>th</sup> minute when it reduces to 0. This is hypothesized to be the reason why the predicted ambient temperature starts increasing and deviating away from the actual ambient temperature at the 30-minute Prediction Window. The predicted temperature does not decrease at the 90-minute Prediction Window, when the occupants leave, because the interior lighting stays on for the remainder of the simulation.

*Table 15 Prediction Error for Temperatures of Simulated Elements as a Function of Prediction Window Duration for February 12, 2018 ( $T_{out}=-2.51^{\circ}C$ , wind speed ranging from 0.5-2 m/s, and solar radiation 120W/m<sup>2</sup>)*

<b>Prediction Error</b>						
	15 minutes	30 minutes	45 minutes	60 minutes	120 minutes	180 minutes
Ambient	0.065%	-0.074%	0.423%	0.417%	1.025%	1.527%
Exterior Wall	-1.376%	-2.279%	-0.954%	-1.863%	-2.795%	-1.072%
Ceiling	-0.426%	-1.268%	-0.428%	-1.269%	-1.271%	-1.273%
Floor	-0.437%	-0.870%	-0.001%	-1.300%	-1.301%	1.331%

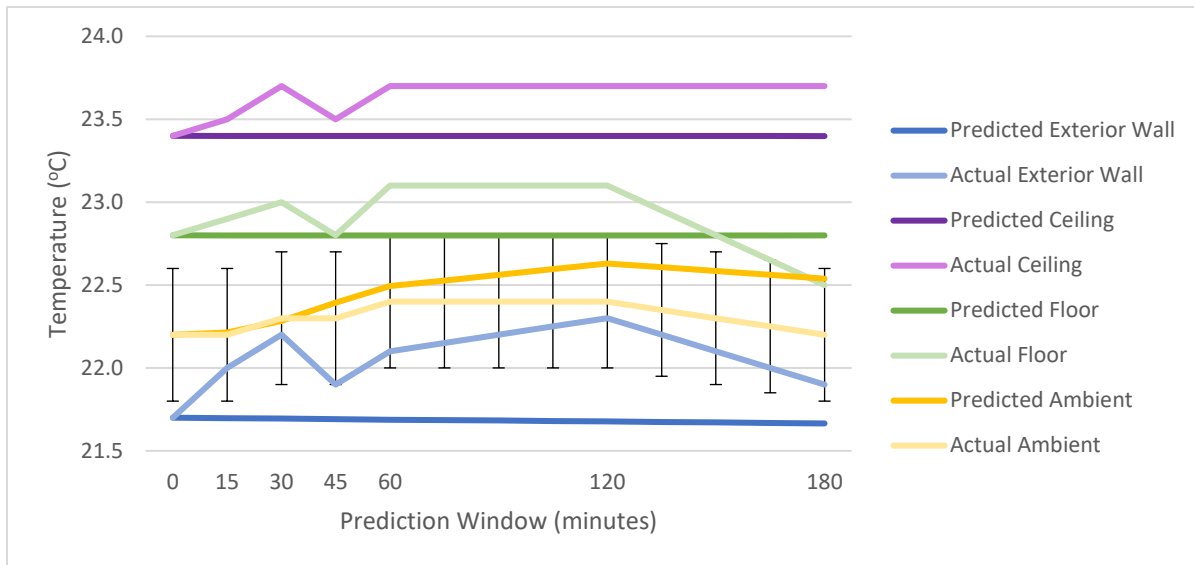
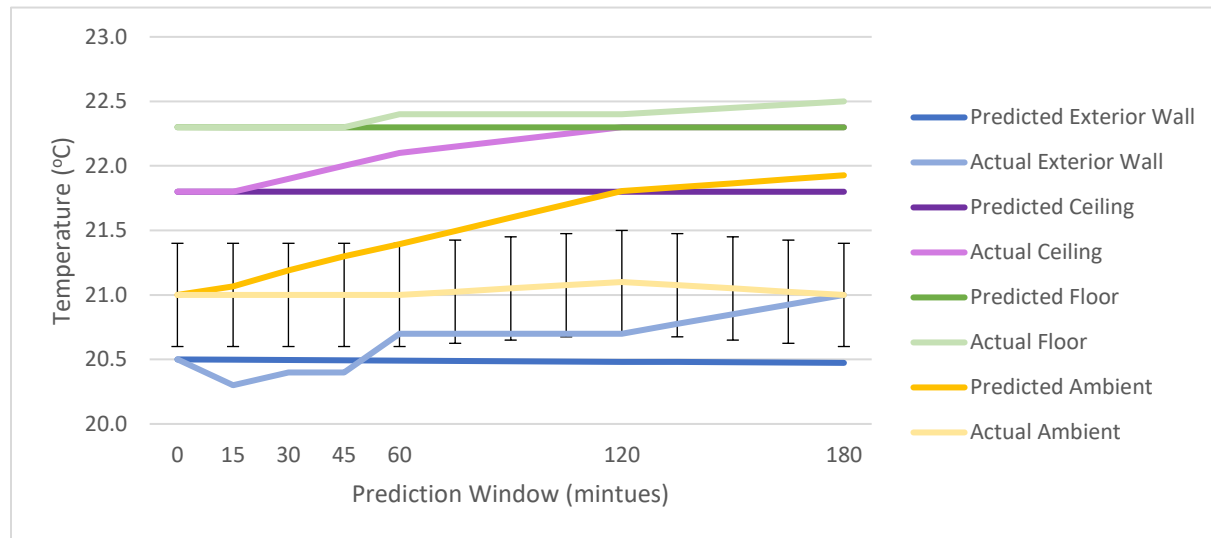


Figure 24 February 12<sup>th</sup>, 2018 Actual vs Predicted Temperatures for each Prediction Window

The results shown in Table 16 for the January 8<sup>th</sup> simulation indicates the model underpredicting the surface temperatures of all building elements. Figure 25 demonstrates how the predicted ceiling and exterior wall element temperatures deviate from the actual temperatures by 0.5°C at the 180-minute Prediction Window. The large surface temperature prediction error of the ceiling and exterior wall may be the cause of temperature stratification within the test cell; both thermocouples are located higher in the room than the location of the ambient sensor and may be experiencing warmer ambient conditions. The data for this simulation demonstrates an increase in occupancy count from 0 to 1 person within the first 15 minutes, an increase to 2 people at 70 minutes, and then a drop-in occupancy at the 130<sup>th</sup> minute to zero. This data roughly matches the predicted ambient temperature profile seen in Figure 25 with a mildly increasing temperature slope until the 15<sup>th</sup> minute, a steeper slope until the 120<sup>th</sup> minute, and then a milder slope again for the last 180 minutes. The increase in occupant related heat loads within the test cell is also thought to be the reason that the actual ceiling and exterior wall temperatures start increasing.

*Table 16 Prediction Error for Temperatures of Simulated Elements as a Function of Prediction Window Duration for January 8, 2018 ( $T_{out}=0.5^{\circ}\text{C}$ , wind speed ranging from 1-2.5 m/s, and solar radiation  $50\text{W}/\text{m}^2$ )*

Prediction Error						
	15 minutes	30 minutes	45 minutes	60 minutes	120 minutes	180 minutes
Ambient	0.319%	0.900%	1.430%	1.871%	3.338%	4.416%
Exterior Wall	0.974%	0.467%	0.455%	-1.012%	-1.055%	-2.508%
Ceiling	0.000%	-0.458%	-0.910%	-1.359%	-2.244%	-2.244%
Floor	-0.001%	-0.001%	-0.002%	-0.450%	-0.451%	-0.895%



*Figure 25 January 8<sup>th</sup>, 2018 Actual vs Predicted Temperatures for each Prediction Window*

The February 7<sup>th</sup> simulation had the worst results of all the simulation days, as shown in Table 17. The ambient temperature prediction is off by close to 9% at the 180-minute Prediction Window, as illustrated in Figure 26. The surface temperature prediction results however, demonstrate similar prediction error range as those seen during the other occupied simulations, with all elements having prediction error within 1.5% at the 180-minute Prediction Window. The thermocouple surface temperature data in Figure 26 demonstrates an increase in the exterior wall temperature at the 45-minute Prediction Window, with a jump back down at the 60-minute Prediction Window. Similar to the previous simulation, this observed behaviour may be connected to the occupant count, which reduces from 2 people at 45 minutes to 0 people at 60 minutes. It is noted that an increase in occupancy also indicates larger heat loads within the test cell due to the use of the desktop computer. The predicted ambient temperature increases steadily throughout the simulation. Akin to previous simulations, this is believed to be due to

the occupancy count and the fact that the lights within the test cell continue to be on in the test cell after the occupants leave.

*Table 17 Prediction Error for Temperatures of Simulated Elements as a Function of Prediction Window Duration for February 7, 2018 ( $T_{out}=-3.57^{\circ}\text{C}$ , wind speed ranging from 0.5-1.5 m/s, and solar radiation  $50\text{W}/\text{m}^2$ )*

Prediction Error						
	15 minutes	30 minutes	45 minutes	60 minutes	120 minutes	180 minutes
Ambient	1.706%	3.394%	3.801%	4.603%	6.534%	8.558%
Exterior Wall	-0.925%	-1.835%	-2.727%	-0.987%	-1.509%	-1.586%
Ceiling	-0.465%	-0.467%	-0.927%	-0.929%	-1.388%	-1.842%
Floor	-0.002%	-0.477%	-0.479%	-0.949%	-0.952%	-1.419%

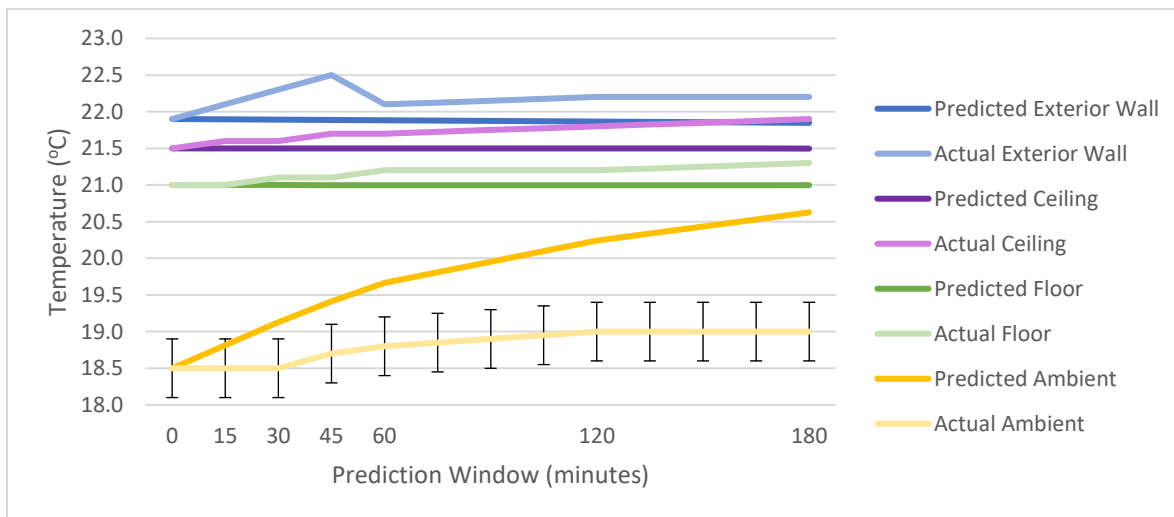


*Figure 26 February 7<sup>th</sup>, 2018 Actual vs Predicted Temperatures for each Prediction Window*

The December 8<sup>th</sup> prediction results in Table 18 are more accurate than the previous results from the February 7<sup>th</sup> simulation. The ambient temperature has a prediction error that increases steadily until it reaches 2.5%, 0.5°C off (Figure 27), at the 180-minute Prediction Window. The surface temperature elements demonstrate varied prediction results. The ceiling temperature remains within 1% error, the floor within 1.5%, and the exterior wall within 2%. This model did not demonstrate worse prediction results compared to other occupied simulations due to the higher wind speeds, as initially expected. The exterior wall performance does not demonstrate the same correlation to occupancy that was seen for other simulations. This simulation indicates the exterior wall temperatures are opposite to the occupancy data - the temperature is lowest at

the 60-minute period when there is the highest occupancy count. The ambient data in this model, similar to previous occupancy simulations, demonstrates correlation to occupant related heat loads. Figure 27 demonstrates the predicted ambient temperature continually increasing throughout the model, most likely due to the occupancy count continually increasing until the 120<sup>th</sup> minute, and the interior lighting remaining on for the entire simulation.

*Table 18 Prediction Error for Temperatures of Simulated Elements as a Function of Prediction Window Duration for December 8, 2017 ( $T_{out}=1.04^{\circ}C$ , wind speed ranging from 2.5-3.5m/s, and solar radiation 50W/m<sup>2</sup>)*

Prediction Error						
	15 minutes	30 minutes	45 minutes	60 minutes	120 minutes	180 minutes
Ambient	-0.152%	0.590%	1.322%	1.218%	1.499%	2.643%
Exterior Wall	1.903%	0.450%	-0.499%	1.871%	-0.550%	-0.123%
Ceiling	0.444%	0.000%	-0.878%	-0.001%	-0.441%	-0.878%
Floor	0.881%	0.438%	-0.001%	0.437%	-0.437%	-0.437%

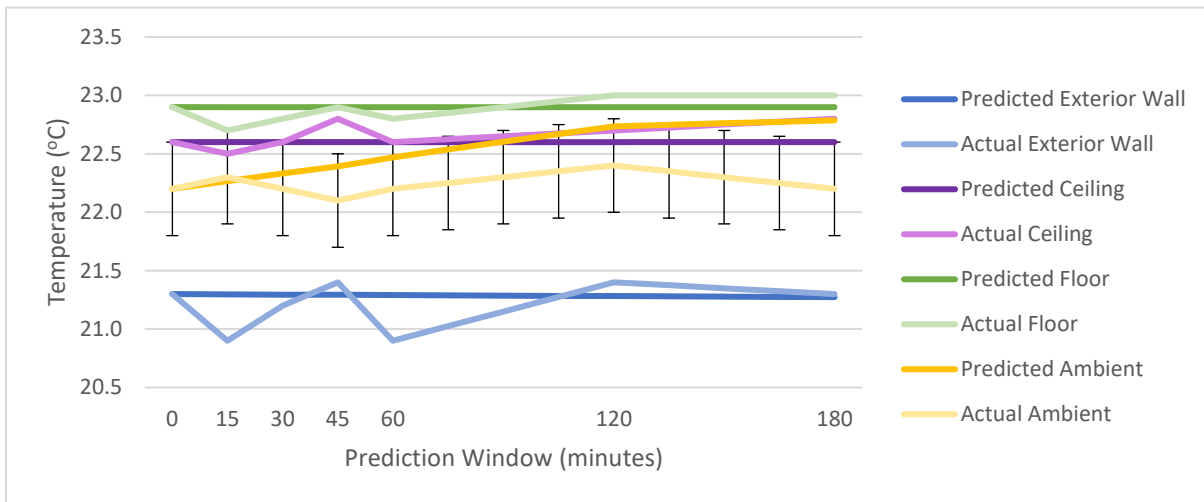


*Figure 27 December 8<sup>th</sup>, 2017 Actual vs Predicted Temperatures for each Prediction Window*

The December 5<sup>th</sup> model demonstrates good ambient prediction results, as shown in Table 19, with prediction error of less than 1.5% for the 180-minute Prediction Window. The ceiling and floor surface temperatures have good performance with errors of less than 0.5% for the entire prediction period. The exterior wall has a jump in error at the 30-minute Prediction Window, as shown in Figure 28, where the actual temperature decreases by 0.4°C. The predicted ambient temperature, as illustrated in Figure 28, is not observed to increase as steeply as seen in previous

simulations, believed to be due to the occupants only being present for the first 35 minutes of the simulation.

*Table 19 Prediction Error for Temperatures of Simulated Elements as a Function of Prediction Window Duration for December 5, 2017 ( $T_{out}=10.93^{\circ}C$ , wind speed ranging from 2-4m/s, and solar radiation  $50W/m^2$ )*

Prediction Error						
	15 minutes	30 minutes	45 minutes	60 minutes	120 minutes	180 minutes
Ambient	0.1605%	0.3163%	0.4335%	0.3807%	1.4049%	0.8821%
Exterior Wall	-0.0053%	1.7910%	0.8763%	-0.0217%	-0.0438%	-0.0659%
Ceiling	-0.0004%	0.4233%	0.4229%	-0.0008%	-0.4218%	-0.0030%
Floor	-0.4274%	0.0000%	0.0000%	0.0000%	0.0004%	-0.4269%

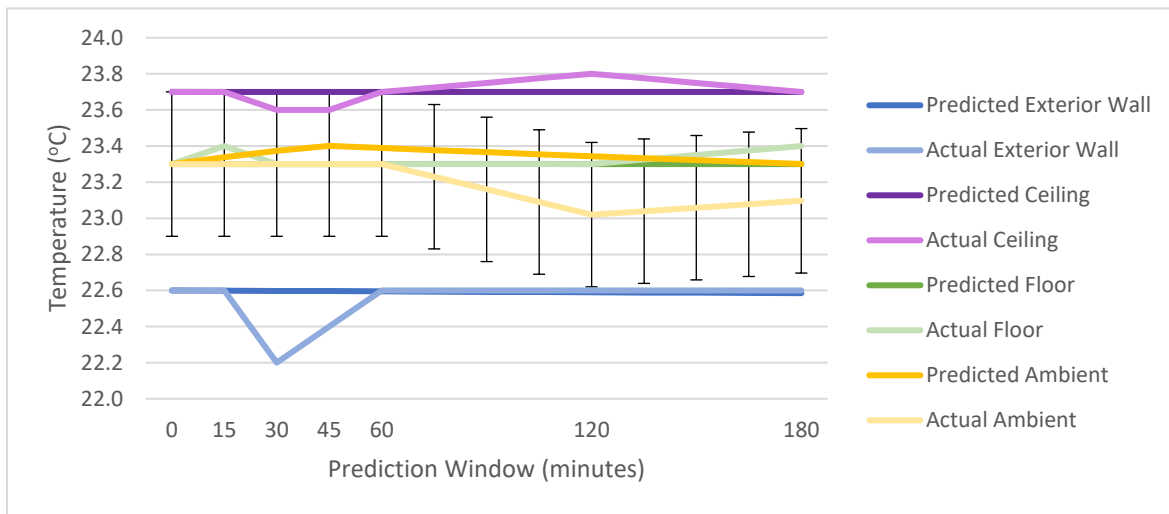


*Figure 28 December 5<sup>th</sup>, 2017 Actual vs Predicted Temperatures for each Prediction Window*

#### 6.1.4 Summary of G1v1 model Performance

The G1v1 grey box model demonstrates the ability to predict the ambient temperature of the room 3 hours in advance to within 10% accuracy. The most obvious observation from the G1v1 simulations is the extreme discrepancy in results between the unoccupied models and the occupied models. The nighttime simulation period, the simplest test cell conditions, demonstrated prediction ability to within 2% error for the 3-hour prediction period. The daytime unoccupied conditions demonstrated similar results, with the model predicting the ambient temperature at the 3-hour mark within 2% error. The last simulation period during

occupied daytime conditions demonstrated more varied results with the ambient temperature predicted in the range of 0.9%-9% accuracy at the 3-hour Prediction Window.

The results from the daytime occupied conditions were analyzed more thoroughly to identify the discrepancy in results. The results demonstrated that the best ambient temperature prediction occurred for the February 12<sup>th</sup> simulation, which, is the only simulation day within the occupied simulation group that does not have the heat load from the heater. A strong correlation between the predicted ambient temperature and the occupancy and interior lighting conditions was also observed in the occupied models. To address both of these discrepancies, two new iterations of the G1 grey box model were created to improve the model performance.

## 6.2 G1v2 model I: Heater Convective Heat Load

The G1v2 model was altered to calculate the heater heat flux using a natural heat convection coefficient. The model was simulated on the three worst simulation days: February 7<sup>th</sup> (Table 20), January 8<sup>th</sup> (), and December 8<sup>th</sup> ().

*Table 20 Prediction Error for G1v2 Model on February 7<sup>th</sup>, 2018 using Turbulent and Natural Convection when Representing the Heater Unit*

<b>February 7, 2018 (4:00 PM)</b>						
<b>Prediction Error</b>						
	15 minutes	30 minutes	45 minutes	60 minutes	120 minutes	180 minutes
Ambient – turbulent conv.	1.7065%	3.3935%	3.8011%	4.6032%	6.5337%	8.5584%
Ambient – natural conv.	1.6355%	3.2538%	3.6014%	4.3497%	6.1205%	8.0382%

*Table 21 Prediction Error for G1v2 Model on January 8<sup>th</sup>, 2018 using Turbulent and Natural Convection when Representing the Heater Unit*

<b>January 8, 2018 (10:00 AM)</b>						
<b>Prediction Error</b>						
	15 minutes	30 minutes	45 minutes	60 minutes	120 minutes	180 minutes
Ambient – turbulent conv	0.3186%	0.8995%	1.4295%	1.8714%	3.3384%	4.4157%
Ambient – natural conv.	0.2686%	0.8014%	1.2883%	1.6910%	3.0383%	4.0368%

*Table 22 Prediction Error for G1v2 Model on December 8<sup>th</sup>, 2017 using Turbulent and Natural Convection when Representing the Heater Unit*

<b>December 8, 2017(2:40 PM)</b>						
<b>Prediction Error</b>						
	15 minutes	30 minutes	45 minutes	60 minutes	120 minutes	180 minutes
Ambient – turbulent conv	-0.1525%	0.5901%	1.3222%	1.2176%	1.4991%	2.6432%
Ambient – natural conv.	-0.1905%	0.5153%	1.2127%	1.0775%	1.2640%	2.3412%

As evidenced by the errors in these tables, Figure 29-Figure 31 illustrate improved prediction performance for the simulation days using the natural convective heat coefficient compared to the simulations using turbulent convection coefficient. All three simulation days of February 7<sup>th</sup>, January 8<sup>th</sup>, and December 8<sup>th</sup>, demonstrate lower prediction error after altering the convection coefficient in the heater energy load calculation.

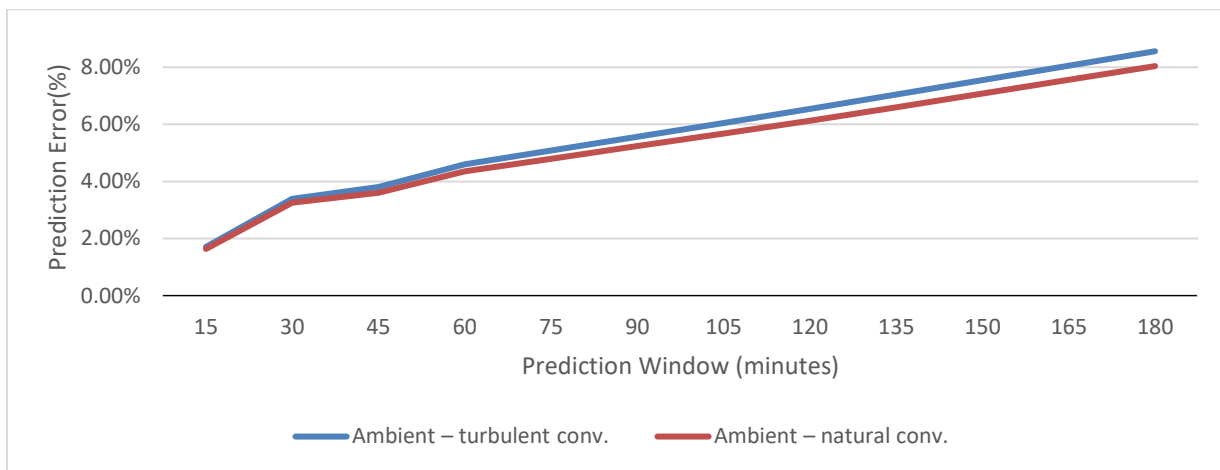


*Figure 29 Ambient Temperature Prediction Error for February 7th, 2018 when using Turbulent and Natural Convection to Represent the Heater Unit*

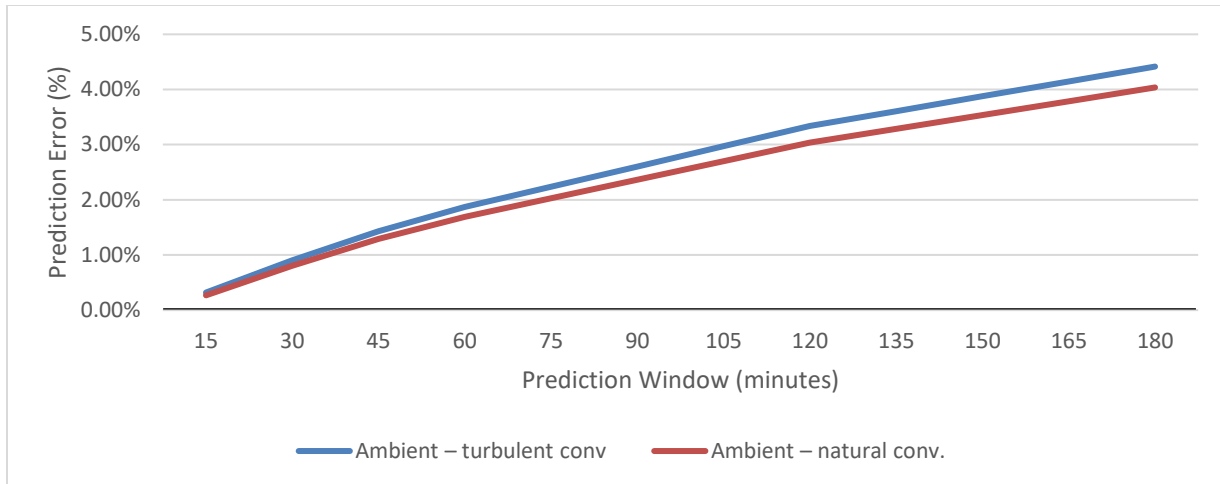


*Figure 30 Ambient Temperature Prediction Error for January 8th, 2018 when using Turbulent and Natural Convection to Represent the Heater Unit*

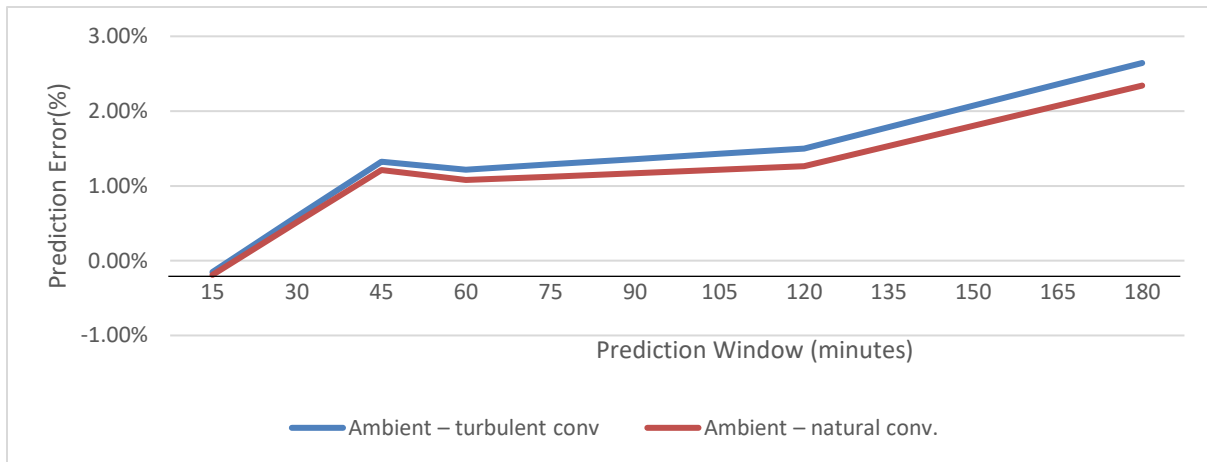


*Figure 31 Ambient Temperature Prediction Error for December 8th, 2017 when using Turbulent and Natural Convection to Represent the Heater Unit*

These figures show the natural convection coefficient better represents the heat transfer mechanism occurring between the heater and ambient air within the test cell. The natural convection coefficient is therefore used to calculate the heater's energy load for the remainder of the models moving forward in this study. It is believed that this alteration in the model does not make the model less representative of the true conditions of the cell. The initial reasoning behind the use of the turbulent equation was the temperature difference of 10 degrees between the hot water pipe and the ambient air; the fact that the natural convection coefficient produced more accurate results indicates that, although the hot water pipe has a 10-degree difference, enough heat is lost when transferring from the pipe to the metal cover that the metal cover in

contact with the ambient air is not at a 10-degree difference. It is acknowledged that the convective heat exchange model from the heater to the room is a simplified model which, using natural convective coefficient or turbulent convective coefficient, does not truly represent the actual heat exchange of the system.

### 6.3 G1v3 Model: Cp Parameter Optimization

The second alteration to the G1v1 models was optimization of the internal heat capacity value to improve the model prediction results under occupied conditions. Parameter estimation of the internal heat capacity value was conducted using the *Simulink* parameter estimation toolbox. The internal heat capacity results for each simulation day are shown in Table 23.

*Table 23 Internal Mass Heat Capacity found using the Parameter Estimation Tool*

<b>Date</b>	<b>Internal Heat Capacity (kJ/K)</b>
November 17 <sup>th</sup> , 2017	112.7
November 29 <sup>th</sup> , 2017	457.9
January 6 <sup>th</sup> , 2018	1,834.2
December 31 <sup>st</sup> , 2017	395.0
January 13 <sup>th</sup> , 2018	105.4
January 2 <sup>nd</sup> , 2018	219.1
February 12 <sup>th</sup> , 2018	777.6
January 8 <sup>th</sup> , 2018	252.7
February 7 <sup>th</sup> , 2018	239.0
December 8 <sup>th</sup> , 2017	93.9
December 5 <sup>th</sup> , 2017	38.4

As noted in this table, there was a significant range in internal heat capacity values, which is troublesome. The results do not demonstrate any correlation to the conditions of the test cell as all three conditions, nighttime unoccupied, daytime unoccupied, and daytime occupied, result in both high and low internal heat capacity values. These values are highly erroneous and demonstrate error in the parameter estimation method used or potentially in the grey box model itself. Because of the high white box model accuracy, the parameter estimation is suspect, highlighting a need for further investigation to determine the source and impact of this error in future research. For the sake of completing the thermal dynamic models of the mass elements, an approximate value was desired and thus each of the values found in parameter estimation was tested for all sample days to find an acceptable representative value for this thesis.

To determine the best fit internal heat capacity value, the grey box model was simulated with seven of the heat capacity values, chosen strategically as discussed in Section 5.3. The grey box model was run for every simulation day, with each of the internal heat capacity values, to determine the value that most accurately predicts the ambient temperature for all simulation conditions. The overall RMSE, MAE, and WAPE values from this analysis are presented in

Table 24. The order of the results in

Table 24 is based on the analysis order, described in Section 5.3. It is noted that the WAPE results are presented with a larger number of significant digits in order to identify the best performing model.

*Table 24 Internal heat capacity performance*

	<b>RMSE</b>	<b>MAE</b>	<b>WAPE</b>
Final Model	0.384	0.234	0.0521%
07-Feb	0.116	0.084	0.0178%
08-Jan	0.116	0.084	0.0179%
29-Nov	0.126	0.089	0.0189%
06-Jan	0.143	0.093	0.0202%
02-Jan	0.116	0.083	0.0176%
17-Nov	0.140	0.099	0.0213%

The analysis indicates that the grey box model using the internal heat capacity value of 219.1 kJ/K, found on January 2<sup>nd</sup>, most accurately predicted the ambient temperature for the eleven simulation days. Therefore, this value is the internal heat capacity that is carried forward for the remainder of this research. It is noted that the value used in this research is not the true optimal heat capacity value but the best performing value out of the simulation days analyzed. It can be hypothesized from the results that the optimal heat capacity value falls within the range of 112kJ/K - 250kJ/K, as values outside this range had worse prediction results than the final internal heat capacity value. It is observed that this range is similar to the internal heat capacity value used in the work by Reynders *et al.* [21]., who used the assumption that the true internal heat capacity of the modeling space is five times the heat capacity of the air. To determine the true internal heat capacity value for the test cell, an optimization would need to be conducted with continuous data from the test cell, rather than eleven three-hour periods, which is outside the scope of our research.

The performance comparison of the G1v2 model using the initial internal heat capacity value of 35.1 kJ/K (found from calculations in Section 4.1.5) against the G1v3 model using the new internal heat capacity value of 219.1 kJ/K are shown below. The results from the unoccupied nighttime simulations, shown in Figure 32-Figure 34 demonstrate little or no improvement in ambient prediction performance compared to the original heat capacity value. This result was expected as the nighttime simulations are not subjected to large heat loads. Therefore, these models do not need the larger heat capacity value to achieve accurate ambient temperature predictions. Overall, the unoccupied nighttime simulations for the G1v3 model demonstrate prediction error below 1.5% at the 3-hour Prediction Window.

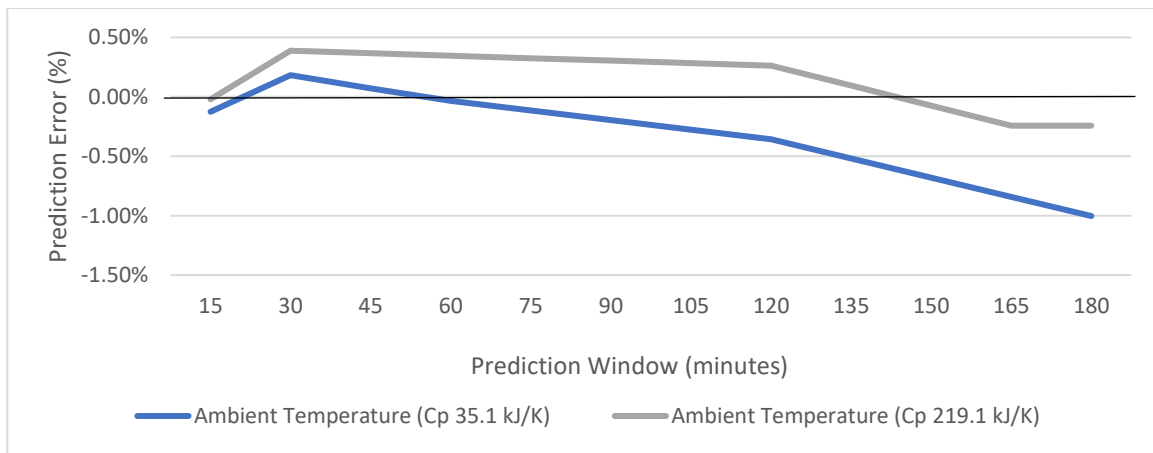


*Figure 32 Ambient Temperature Prediction for November 17th, 2017 comparing the use of the Initial and Optimized Internal Heat Capacity Values*

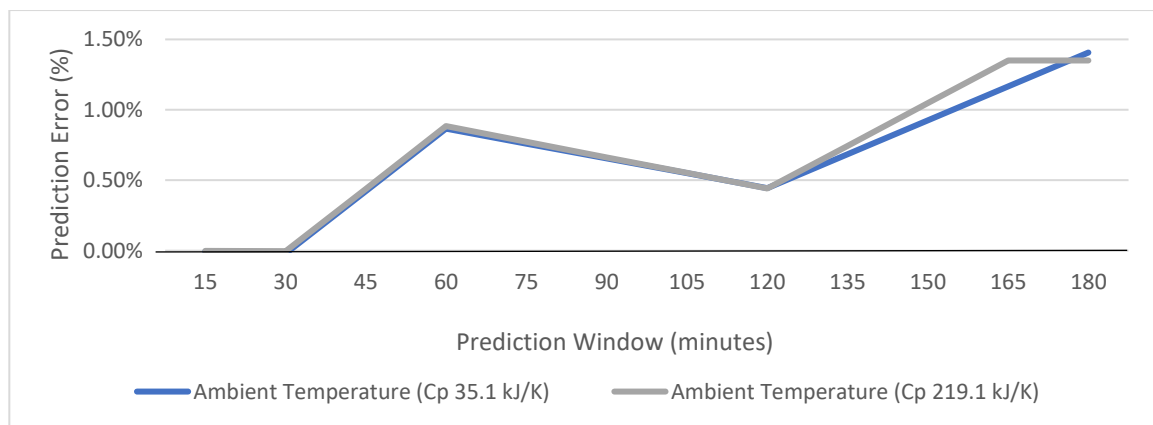


*Figure 33 Ambient Temperature Prediction for November 29th, 2017 comparing the use of the Initial and Optimized Internal Heat Capacity Values*

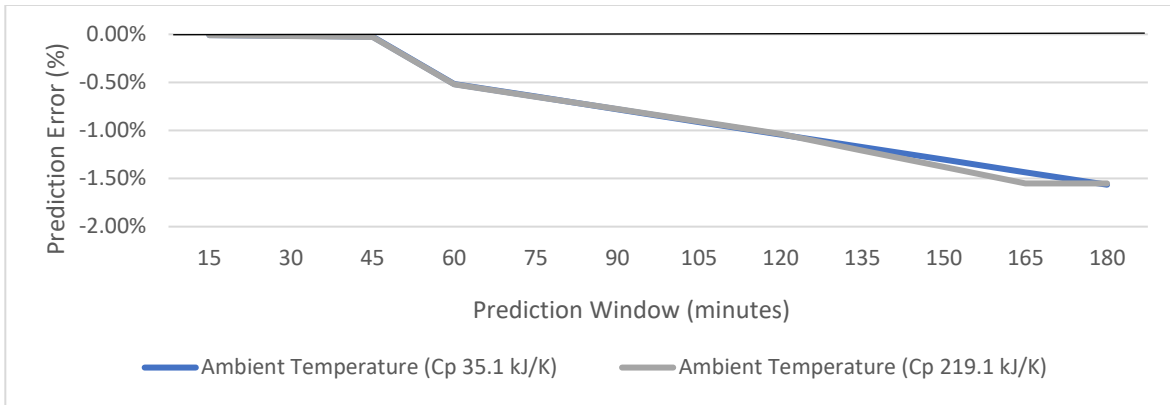


*Figure 34 Ambient Temperature Prediction for January 6th, 2018 comparing the use of the Initial and Optimized Internal Heat Capacity Values*

The unoccupied daytime simulation results, shown in Figure 35 - Figure 37, illustrate mixed performances. Compared to the G1v2 model, the G1v3 model demonstrates the December 31<sup>st</sup> simulation (Figure 35) with little improvement in prediction accuracy, the January 13<sup>th</sup> simulation (Figure 36) with lower prediction accuracy for the first 120 minutes, and the January 2<sup>nd</sup> simulation (Figure 37) with better prediction results. The larger deviation in model performance due to the internal heat capacity value demonstrates the stronger influence of this value on the daytime simulations compared to the nighttime simulations.

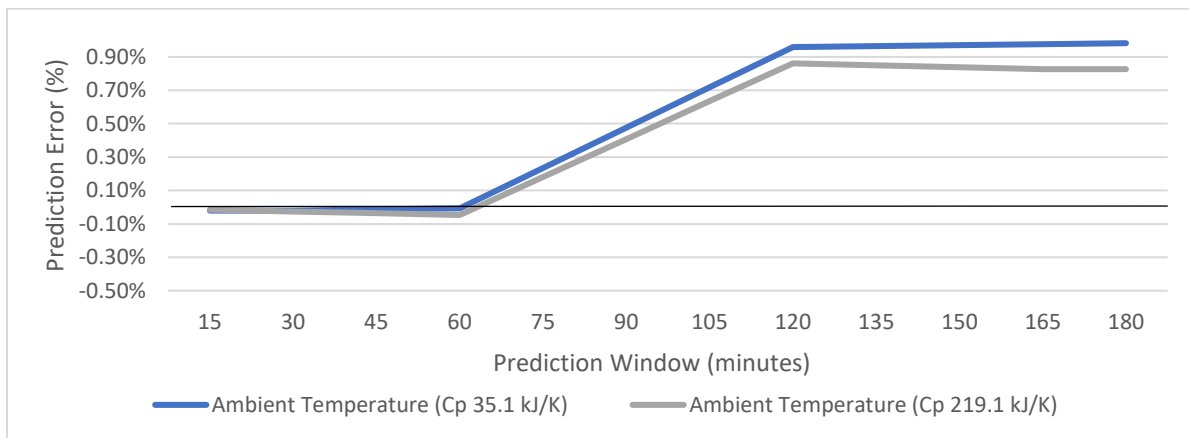


*Figure 35 Ambient Temperature Prediction for December 31st, 2017 comparing the use of the Initial and Optimized Internal Heat Capacity Values*

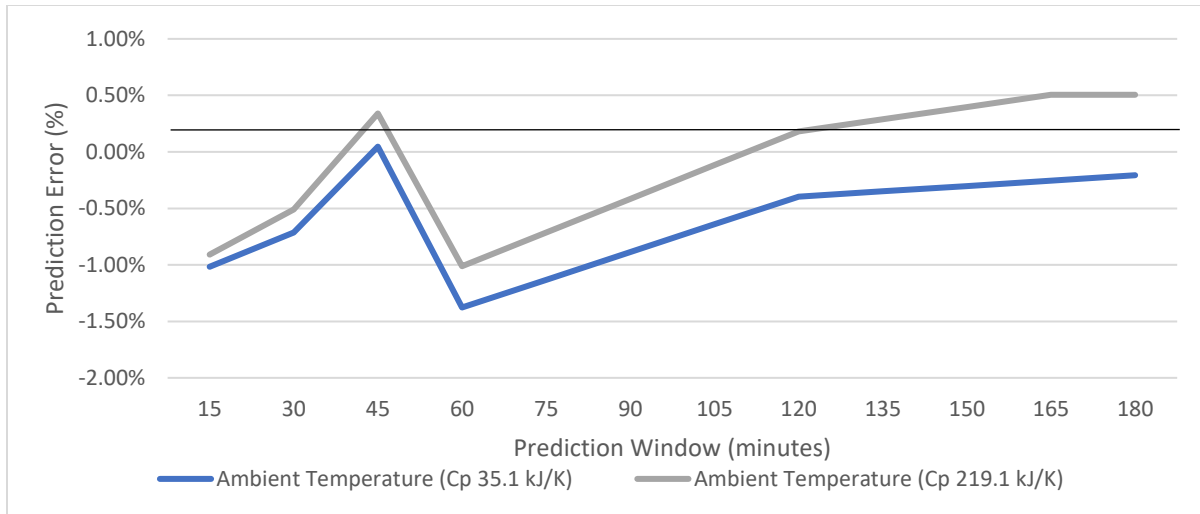


*Figure 36 Ambient Temperature Prediction for January 13<sup>th</sup>, 2018 comparing the use of the Initial and Optimized Internal Heat Capacity Values*

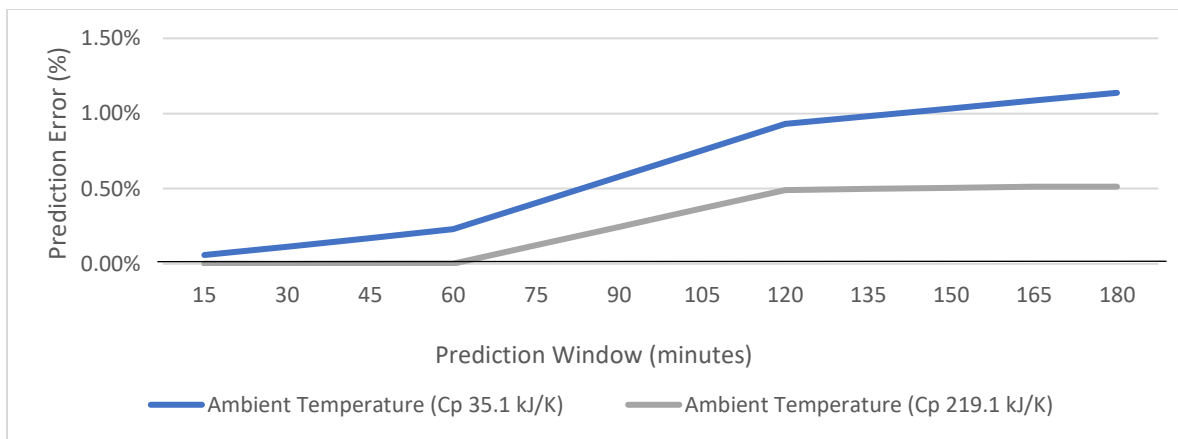


*Figure 37 Ambient Temperature Prediction for January 2<sup>nd</sup>, 2018 comparing the use of the Initial and Optimized Internal Heat Capacity Values*

The results from the occupied simulations, shown in Figure 38-Figure 42, demonstrate significant improvement in ambient temperature prediction ability with the larger internal heat capacity. The February 12<sup>th</sup> (Figure 38) and December 5<sup>th</sup> (Figure 42) simulation improvements were the smallest of the occupied models however, they still demonstrated better results with the new internal heat capacity. The other simulation days demonstrated greater improvement: January 8<sup>th</sup> (Figure 39) illustrates prediction error reduction at the 180-minute Prediction Window from 4% to 1%, February 7<sup>th</sup> (Figure 40) from 8% to 0.5%, and December 8<sup>th</sup> (Figure 41) from 2.5% to 0.6%. The significant model improvements for the occupied models was expected due to larger heat loads present under these conditions.

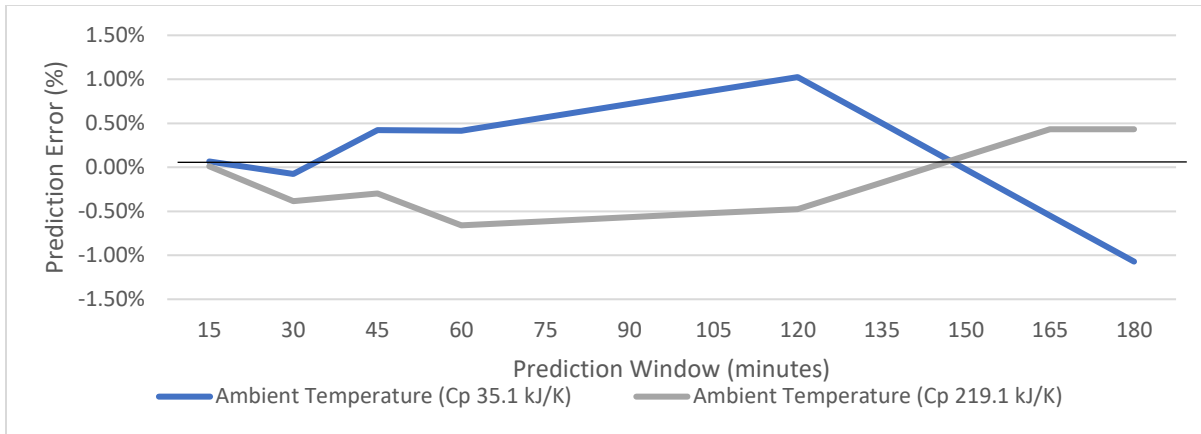


Figure 38 Ambient Temperature Prediction for February 12<sup>th</sup>, 2018 comparing the use of the Initial and Optimized Internal Heat Capacity Values

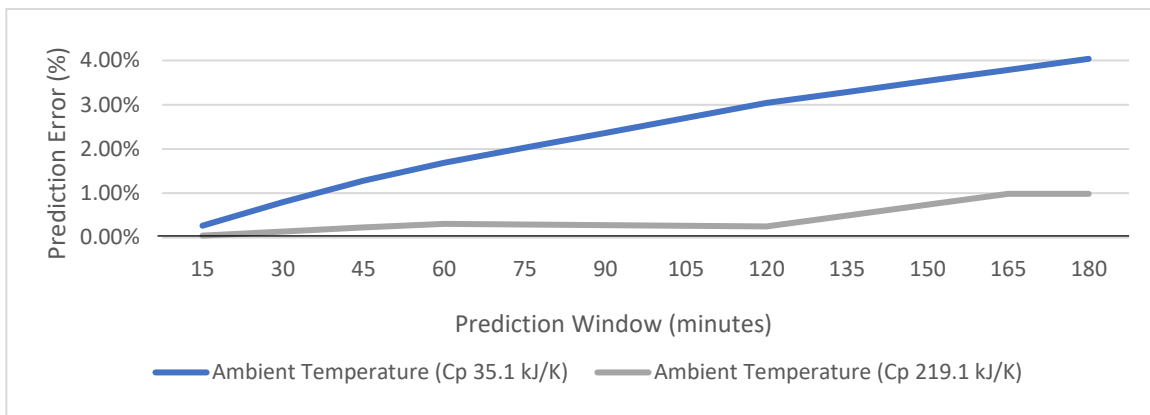


Figure 39 Ambient Temperature Prediction for January 8<sup>th</sup>, 2018 comparing the use of the Initial and Optimized Internal Heat Capacity Values

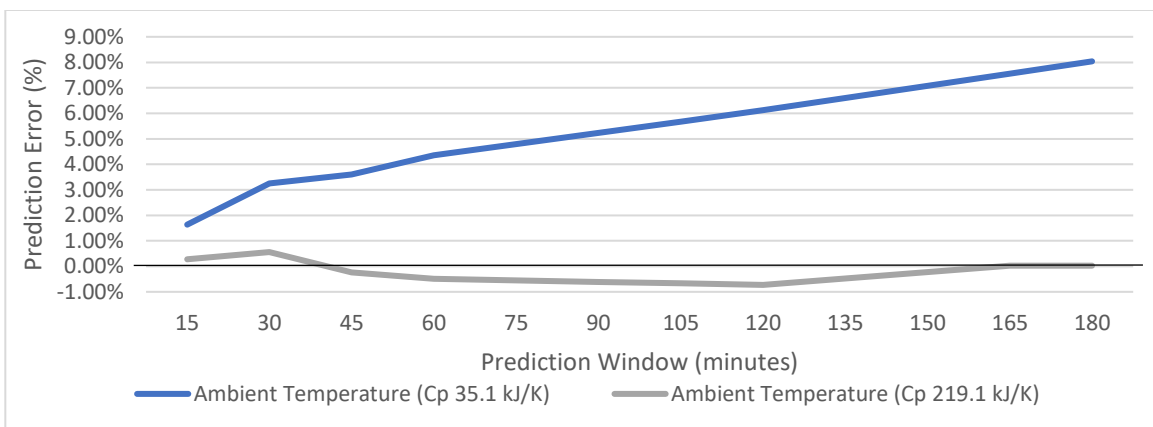


Figure 40 Ambient Temperature Prediction for February 7<sup>th</sup>, 2018 comparing the use of the Initial and Optimized Internal Heat Capacity Values

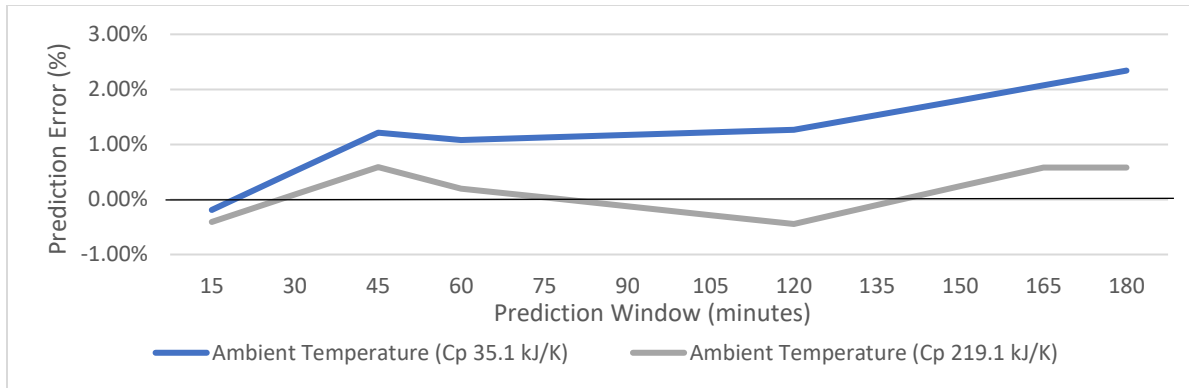


Figure 41 Ambient Temperature Prediction for December 8<sup>th</sup>, 2017 comparing the use of the Initial and Optimized Internal Heat Capacity Values

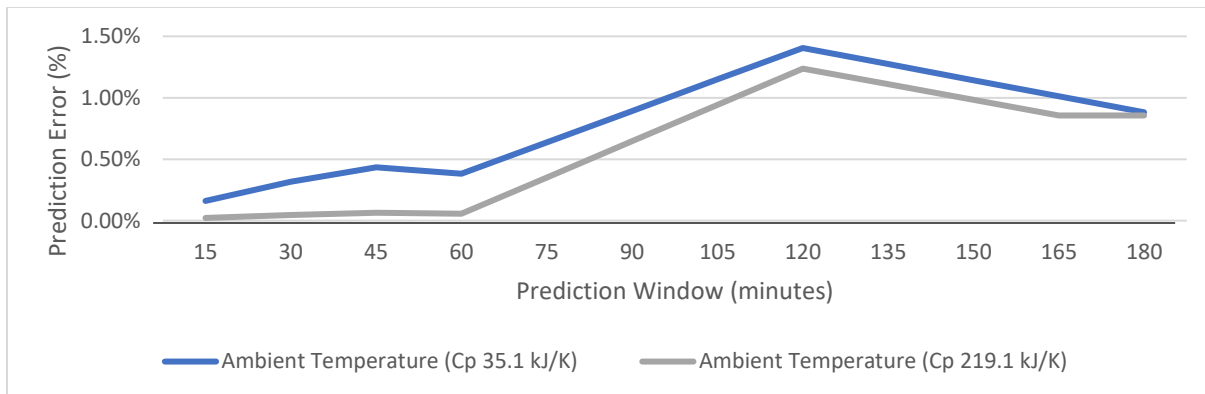


Figure 42 Ambient Temperature Prediction for December 5<sup>th</sup>, 2017 comparing the use of the Initial and Optimized Internal Heat Capacity Values

#### 6.4 Summary of G1 model

The G1 model was altered from its initial state based on observations from the G1v1 model results. The first observation was lower ambient temperature prediction error for models that occurred at times when the heater of the test cell was off. To adjust the model the convective heat transfer calculation was changed from a turbulent convective heat transfer coefficient to a natural convective heat transfer coefficient. The performance of the three worst prediction days with the natural convection model demonstrated improved performance over the previous model. The natural convection heat transfer model is therefore carried forward for the remainder of the research.

The second observation from the G1v1 model results, was the large discrepancy between the occupied model results and the unoccupied model results. The model demonstrated that it was

not able to predict the ambient temperature of the test cell with the same degree of accuracy when subjected to the additional plug load, occupancy, and interior lighting heat loads. Therefore, the parameter estimation tool within Simulink was used to solve for the optimal internal mass heat capacity value. From this analysis, the internal mass heat capacity value of 219k J/K was found to best represent the test cell, as it had the most accurate ambient temperature predictions overall for the simulation days. With the new internal heat capacity value, the occupied simulations predict the ambient temperature to within 1.5% accuracy at the 180-minute Prediction Window.

### 6.5 G2 model: Regression Analysis

The results from the regression analysis, shown in Table 25, demonstrate all of the elements except the ceiling performing better when using the split occupancy linear regression model when compared to the general linear regression model. This was an unexpected finding as the ceiling is one of the elements thought to be most affected by the heating loads and one that would derive the greatest benefit from a split occupancy model. The second observation from the regression analysis are the exterior wall, spandrel panel, and window unit having the largest WAPE values. This result is due to the fact that all three of these elements face the exterior and are influenced by both the interior and exterior conditions.

*Table 25 Results of the general regression model and the split regression model for each building element with RMSE, MAE and WAPE performance measurements.*

<b>Complete Regression Model</b>						
	<b>Exterior Wall</b>	<b>Ceiling</b>	<b>Floor</b>	<b>Spandrel</b>	<b>Window</b>	<b>Interior Wall</b>
RMSE	1.395	0.580	0.535	1.014	1.219	0.709
MAE	0.821	0.390	0.398	0.760	0.873	0.463
MAPE	0.173%	0.076%	0.077%	0.217%	0.293%	0.090%
<b>Split Regression Model</b>						
RMSE	1.382	0.586	0.458	1.007	1.137	0.654
MAE	0.791	0.390	0.323	0.706	0.718	0.420
MAPE	0.167%	0.075%	0.063%	0.202%	0.257%	0.081%

The regression models used in the composition of the G2 model are outlined below. This section outlines the regression equations used for each building element. The regression models are analyzed based on their adjusted  $R^2$  values and RMSE. The Student t-test p-value and t-value is used to analyze the significance of the variables within the models. As described in

Section 5.2, the smaller p-value and larger t-value, the larger the influence of the variable on the ambient temperature. A summary of the p-value confidence intervals for rejecting the null hypothesis is shown in Table 26.

*Table 26 Summary of p-value confidence intervals*

<b>p-value</b>	<b>&lt;0.05</b>	<b>&lt;0.01</b>	<b>&lt;0.001</b>
Confidence of null hypothesis rejection	95%	90%	99%

### 6.5.1 Exterior Wall

The final split occupied (24) and unoccupied (25) regression models determined for the exterior wall are shown below.

$$\begin{aligned}
 T_{ExtWall\_Split\_Occ} & \quad (24) \\
 & = -4.041 + 0.779T_{amb} + 0.293T_{hall} - 0.014T_{heater} + 0.106Occ \\
 & \quad - 0.268Light + 97.860V_{left} - 0.072T_{left} + 5.044V_{right} \\
 & \quad + 0.017T_{right} + 0.001Q_{SWRad} + 0.002Q_{LWRad} - 0.005T_{out} \\
 & \quad + 0.124v_{wind}
 \end{aligned}$$

$$\begin{aligned}
 T_{ExtWall\_Split\_Unocc} & \quad (25) \\
 & = -78.930 + 0.701T_{amb} + 0.611T_{hall} - 0.011T_{heater} \\
 & \quad + 0.128Light + 26.19V_{left} - 0.071T_{left} - 43.550V_{right} \\
 & \quad + 0.036T_{right} - 0.049W_{pl} - 0.0004Q_{SWRad} + 0.002Q_{LWRad} \\
 & \quad + 0.010T_{out} - 0.051v_{wind}
 \end{aligned}$$

The results for the exterior wall regression models are summarized in Table 27. The adjusted  $R^2$  value for both models demonstrates good performance with values close to 1. The unoccupied model indicates a better fit compared to the occupied model with a larger adjusted  $R^2$  value however, it also shows a larger RMSE. The exterior wall results demonstrate that in the four months of training data there is a larger set of data for unoccupied conditions than occupied conditions, as seen in the difference in the degrees of freedom for both models. This

is partially due to Christmas vacation occurring within this modeling period, resulting in larger unoccupied periods.

*Table 27 Performance of the Exterior Wall Occupied Regression Model*

	<b>Adjusted R<sup>2</sup></b>	<b>RMSE</b>	<b>Degree of Freedom</b>
Occupied	0.7736	0.4643	7010
Unoccupied	0.8289	0.4801	86849

The occupied exterior regression model resulted in most variables having p-values within the 99% confidence interval, with exception of the right ventilation duct airflow rate that resulted in a p-value within the 90% confidence interval. To determine the degree of influence of these variables on the regression model, the t-values in Table 28 were analyzed. The results demonstrate that the exterior wall surface temperature, during occupied conditions, is most heavily influenced by the ambient test cell and hallway temperatures, the heater temperature, the left ventilation airflow rate, and the wind speed. It is unexpected to see the exterior wall influenced by the hallway ambient temperature and the left ventilation airflow rate, especially since the left vent is not the primary supply duct to the room. It is hypothesised that the consistency in their data influences the exterior wall because the exterior wall also maintains a relatively consistent temperature due to its large thermal mass. The plug load data was eliminated from the regression model during the subtractive process; this data may be insignificant because it is not the true plug load data.

*Table 28 Student t-test P-values and t-values for Occupied Exterior Wall Regression Model*

	<b><i>T<sub>amb</sub></i></b>	<b><i>T<sub>Hall</sub></i></b>	<b><i>T<sub>Heater</sub></i></b>	<b><i>Occ</i></b>	<b><i>Light</i></b>	<b><i>V<sub>left</sub></i></b>	<b><i>T<sub>left</sub></i></b>	<b><i>V<sub>right</sub></i></b>	<b><i>T<sub>right</sub></i></b>
P-value	<2e-16	<2e-16	<2E-16	<2E-16	9.07E-11	<2e-16	<2e-16	0.083	<2E-16
t-value	83.089	15.695	-26.11	12.22	-6.49	15.79	-16.90	1.73	13.16

<b><i>Q<sub>SWRad</sub></i></b>	<b><i>Q<sub>LWRad</sub></i></b>	<b><i>T<sub>out</sub></i></b>	<b><i>v<sub>wind</sub></i></b>
3.92E-15	<2e-16	6.77E-05	<2E-16
7.88	10.17	-3.99	15.80

The results for the unoccupied conditions in Table 29 demonstrate all of the variables in the equation having p-values within the 99% confidence interval. The t-value results indicate the exterior wall, during unoccupied conditions, is most significantly influenced by the ambient test cell, and hallway temperatures, the temperature of the air supply from the right, and left

vent as well as the heater surface temperature. Similar to the occupied model, the influence of the ambient hallway temperature, with such far proximity to the exterior wall, is thought to be due to the consistency of the hallway temperature, as well as, its similarity in value to the ambient temperature of the test cell. The supply airflow temperatures, along with the heater temperature, are expected for the unoccupied condition because they are the only heat loads conditioning the space during this time. It is noted that no data was eliminated in this linear regression model.

*Table 29 Student t-test P-values and t-values for Unoccupied Exterior Wall Regression Model*

	$T_{amb}$	$T_{Hall}$	$T_{Heater}$	$Light$	$V_{left}$	$T_{left}$	$V_{right}$	$T_{right}$	$W_{pl}$
P-value	<2e-16	<2e-16	<2E-16	<2E-16	<2e-16	<2e-16	<2e-16	<2E-16	<2E-16
t-value	238.94	129.17	-61.27	17.39	14.42	-75.06	-43.17	84.98	-27.97

$Q_{SWRad}$	$Q_{LWRad}$	$T_{out}$	$v_{wind}$
<2e-16	<2e-16	<2e-16	<2E-16
-11.22	36.10	30.94	-21.38

### 6.5.2 Ceiling

The general ceiling linear regression equation (26) found from the subtractive linear regression fitting is presented below.

$$\begin{aligned}
 T_{Ceil_{All}} = & -11.31 + 0.4159T_{amb} + 0.5274T_{hall} + 0.004486T_{heater} + 0.12790cc \quad (26) \\
 & + 0.2188Light - 4.705V_{left} + 0.07443T_{left} + 0.001568T_{right} \\
 & - 0.005181W_{pl} - 0.000633Q_{SWRad} + 0.0009701Q_{LWRad} \\
 & + 0.01525T_{out} - 0.01742v_{wind}
 \end{aligned}$$

The ceiling regression model results in Table 30 show the model fit well to the unseen testing data, with high adjusted  $R^2$  value and low RMSE. This is a better prediction performance than seen previously with the exterior wall.

Table 30 Performance of the General Ceiling Regression Model

Adjusted R <sup>2</sup>	RMSE	Degree of Freedom
0.9334	0.2633	93873

The ceiling regression model has all independent variables resulting in p-values within the 99% confidence interval, as shown in Table 31. The t-values indicate the variables with the largest influence include the ambient test cell and hallway temperature, the left ventilation duct air supply temperature, and the exterior temperature. Similar to the exterior wall, the left ventilation duct air supply temperature and the hallway temperature are thought to be influential on the ceiling temperature because of their consistent value. The exterior temperature is an unexpected result as the test cell has a high ceiling, with the measurement sensor far from the exterior facade. This model is also observed to have omitted the right ventilation supply duct airflow rate through the subtractive regression fitting process. This is another unforeseen result as the right ventilation duct is the primary air supply duct for the test cell and is situated higher in the test cell, in closer proximity to the ceiling.

Table 31 Student t-test P-values and t-values for Ceiling General Regression Model

	$T_{amb}$	$T_{Hall}$	$T_{Heater}$	$Occ$	$Light$	$V_{left}$	$T_{left}$	$T_{right}$	$W_{pl}$
P-value	<2e-16	<2e-16	<2e-16	<2e-16	<2e-16	<2e-16	<2e-16	<2e-16	<2e-16
t-value	275.49	213.97	53.18	26.88	55.72	-12.1	160.87	10.11	-19.87

$Q_{SWRad}$	$Q_{LWRad}$	$T_{out}$	$v_{wind}$
<2e-16	<2e-16	<2e-16	<2e-16
-33.94	30.84	94.13	-14.12

### 6.5.3 Floor

The occupied (27) and unoccupied linear (28) regression models for the floor slab, found from the subtractive regression analysis, are presented below.

$$\begin{aligned}
 T_{Floor\_Split\_Occ} = & 8.153 + 0.431T_{amb} + 0.612T_{hall} + 0.015T_{heater} + 0.111Occ \quad (27) \\
 & - 0.031Light + 225.7V_{left} - 0.165T_{left} - 66.3V_{right} \\
 & + 0.051T_{right} + 0.001W_{pl} + 0.004Q_{LWRad} + 0.015T_{out} \\
 & + 0.092v_{wind}
 \end{aligned}$$

$$\begin{aligned}
T_{Floor\_Split\_Unocc} & \quad (28) \\
& = -18.950 + 0.542T_{amb} + 0.529T_{hall} + 0.015T_{heater} \\
& + 0.067Light + 64.2V_{left} - 0.050T_{left} - 39.530V_{right} \\
& + 0.042T_{right} - 0.122W_{pl} - 0.001Q_{SWRad} + 0.0003Q_{LWRad} \\
& + 0.003T_{out} + 0.023v_{wind}
\end{aligned}$$

The results for the floor regression model presented in

Table 24, show the occupied and the unoccupied models having poor fit when compared to the unseen testing data. The occupied model only fits the testing data 68% of the time. The unoccupied model demonstrates slightly better results with the model fitting the test data 79% of the time. It is hypothesized that these results are worse than the other models due to the fact that the floor is also influenced by the heating loads of the space below the test cell which is not monitored in this study. The lower fit of the occupied model compared to the unoccupied model may also stem from the lower amount of training data.

*Table 32 Performance of the Occupied and Unoccupied Floor Regression Models*

	<b>Adjusted R<sup>2</sup></b>	<b>RMSE</b>	<b>Degree of Freedom</b>
Occupied	0.6787	0.4644	7010
Unoccupied	0.7859	0.4805	86849

The floor slab occupied regression model resulted in the majority of the variables having p-values within the 99% confidence interval, with the exception of the plug load, as shown in Table 33. Through inspection of the t-values, the largest influences on the floor temperature are the ambient test cell and hallway temperature, the left and right ventilation duct supply air temperature, the supply air flow rate from the left duct, and temperature of the heater. The ventilation duct values are unexpected influences for the floor due to the duct openings being high on the test cell wall, closer to the ceiling. Similar to previous models, it is believed that the relation to the left duct airflow temperature and hallway temperature are due to the consistency in their values, similar to the steady floor temperature. The occupied floor regression model omits short wave solar radiation data, as it was eliminated during the subtractive regression model fitting process. The short-wave radiation entering the test cell does hit and influence a portion of the floor within the cell however, the thermocouple installed on

the floor slab is not in the sunlight and therefore indicates no relationship to the short-wave radiation.

*Table 33 Student t-test P-values and t-values for Occupied Floor Regression Model*

	$T_{amb}$	$T_{Hall}$	$T_{Heater}$	<b>Occ</b>	<b>Light</b>	$V_{left}$	$T_{left}$	$V_{right}$	$T_{right}$
P-value	<2e-16	<2e-16	<2E-16	<2E-16	0.472	<2e-16	<2e-16	<2E-16	<2E-16
t-value	46.134	33.277	27.998	12.513	-0.719	36.265	-38.829	-22.753	38.124

$W_{pl}$	$Q_{LWRad}$	$T_{out}$	$v_{wind}$
0.581	<2E-16	<2E-16	<2E-16
0.552	24.181	11.288	11.763

All variables within the floor slab unoccupied model have p-values within the 99% confidence interval, as shown in Table 34. The unoccupied model is most heavily influenced by the ambient temperature of the test cell and hallway, the temperature of the air supply from the right ventilation duct, and the heater temperature. Similar to the occupied condition, the significance of the air supply temperature for the right duct was unanticipated due to the proximity of the duct opening to the floor, as well as, the fact that there is no connection between the HVAC system in the test cell to the HVAC system of the space below the test cell. The hallway temperature, similar to the occupied condition, is believed to influence the floor slab because of its consistency and similarity in value to the ambient test cell temperature. The heater temperature is thought to impact the temperature of the floor because this system is also installed within the space below the test cell and uses the same hot water loop.

*Table 34 Student t-test P-values and t-values for Unoccupied Floor Regression Model*

	$T_{amb}$	$T_{Hall}$	$T_{Heater}$	<b>Light</b>	$V_{left}$	$T_{left}$	$V_{right}$	$T_{right}$
P-value	<2e-16	<2e-16	<2E-16	<2E-16	<2e-16	<2e-16	<2E-16	<2E-16
t-value	184.547	111.813	84.024	9.171	35.312	-52.505	-39.151	98.768

$W_{pl}$	$Q_{SWRad}$	$Q_{LWRad}$	$T_{out}$	$v_{wind}$
<2E-16	<2e-16	3.73E-05	<2E-16	<2E-16
-70.236	-14.954	4.124	9.707	9.73

#### 6.5.4 Spandrel

The spandrel panel occupied (29) and unoccupied (30) regression models found from the subtractive regression analysis are displayed below.

$$\begin{aligned}
 T_{Spandrel\_Split\_Occ} & \quad (29) \\
 & = -5.817 + 0.096T_{amb} + 0.732T_{hall} - 0.004T_{heater} + 0.228Occ \\
 & \quad - 0.317Light + 0.037T_{left} - 5.261V_{right} + 0.010T_{right} \\
 & \quad - 0.001Q_{SWRad} + 0.005Q_{LWRad} + 0.150T_{out} - 0.152v_{wind}
 \end{aligned}$$

$$\begin{aligned}
 T_{Spanrel\_Split\_Unocc} & \quad (30) \\
 & = -2.210 + 0.287T_{amb} + 0.477T_{hall} + 0.014T_{heater} \\
 & \quad + 0.331Light + 25.150V_{left} + 0.093T_{left} + 3.062V_{right} \\
 & \quad - 0.083W_{pl} - 0.001Q_{SWRad} + 0.004Q_{LWRad} + 0.144T_{out} \\
 & \quad - 0.077v_{wind}
 \end{aligned}$$

The regression models demonstrate good performance, as presented in Table 35, with adjusted  $R^2$  values close to 1. The unoccupied conditions demonstrate the better performance with the larger adjusted  $R^2$  value and lower RMSE. As previously stated, this may be due to the larger amount of training data.

*Table 35 Performance of the Occupied and Unoccupied Spandrel Regression Models*

	<b>Adjusted R2</b>	<b>RMSE</b>	<b>Degree of Freedom</b>
Occupied	0.7907	0.5817	7011
Unoccupied	0.9337	0.4479	86849

The occupied spandrel regression model results are shown in Table 36, it had almost all p-values within the 99% confidence interval, except for the right ventilation duct flow rate that resulted in a p-value outside all confidence intervals. The occupied model is most heavily influenced by the exterior temperature, the long wave radiation, the temperature of the hallway, occupancy count, and the exterior wind speed. The exterior temperature, wind speed, and long wave radiation variables were expected to be significant for this model as the spandrel faces the exterior. The ambient hallway temperature is believed to influence the spandrel temperature more heavily than the ambient temperature of the room due to the hallway temperature usually being slightly warmer than the test cell. The hallway ambient temperature could be more

representative of the conditions in the corner of the test cell near the spandrel panel. The occupancy count was not a foreseen influence for the spandrel temperature. The occupied model omits the left duct airflow measurement as well as the plug load due to its elimination in subtractive regression fitting process.

*Table 36 Significance of the Variables within the Occupied Spandrel Regression Model*

	$T_{amb}$	$T_{Hall}$	$T_{Heater}$	$Occ$	$Light$	$V_{left}$	$T_{left}$	$V_{right}$	$T_{right}$
P-value	<2e-16	<2e-16	6.33E-01	<2E-16	4.66E-10	<2e-16	0.115	6.97E-10	<2e-16
t-value	8.434	32.615	-6.191	21.059	-6.239	8.987	-1.578	6.175	8.434

$Q_{SWRad}$	$Q_{LWRad}$	$T_{out}$	$v_{wind}$
2.87E-10	<2e-16	<2e-16	<2E-16
-6.315	23.764	88.354	-15.544

The unoccupied spandrel regression model, with results shown in Table 37, has all variable p-values within the 99% confidence interval. The major influencers within this model are the exterior temperature, the ambient test cell and hallway temperature, the left vent air supply temperature, and the heater temperature. The exterior wall and ambient test cell temperatures are expected values for this model as these are the two ambient temperatures surrounding the spandrel panel. The heater temperature is believed to be due to the proximity of the heater to the panel. The hallway and left vent air supply temperatures were unexpected values for this model due to the spandrel panel's lower thermal mass and more varied temperature measurements. Previously, these input variables were believed to be influential because of their steady measurements matching the steady surface temperature measurements of the more thermally massive floor, ceiling, and exterior wall elements. As these variables are only indicated to be significant for the unoccupied model, the spandrel may have steadier temperature when the cell is unoccupied, with fewer heat loads. This model omits the airflow temperature from the right duct. As stated in the occupied model, the ducts are too far away to have significant influence in the regression model.

Table 37 Student t-test P-values and t-values for Unoccupied Spandrel Regression Model

	$T_{amb}$	$T_{Hall}$	$T_{Heater}$	$Light$	$V_{left}$	$T_{left}$	$V_{right}$	$T_{amb}$	$W_{pl}$
P-value	<2E-16	<2E-16	<2E-16	<2E-16	<2E-16	<2E-16	7.59E-06	<2E-16	<2E-16
t-value	105.22	108.18	83.83	48.48	18.09	121.06	4.48	105.22	-51.79

$Q_{SWRad}$	$Q_{LWRad}$	$T_{out}$	$v_{wind}$
<2E-16	<2E-16	<2E-16	<2E-16
-41.208	72.404	498.377	-34.669

### 6.5.5 Window

The occupied (31) and unoccupied (32) regression models found from the subtractive regression analysis are presented below.

$$\begin{aligned}
 T_{Window\_Split\_Occ} & \quad (31) \\
 & = -92.3 - 0.132T_{amb} + 1.161T_{hall} - 0.014T_{heater} + 0.246Occ \\
 & \quad - 0.746Light - 88.670V_{left} + 0.060T_{left} + 0.006T_{right} \\
 & \quad + 0.001Q_{SWRad} + 0.006Q_{LWRad} + 0.241T_{out} - 0.278v_{wind}
 \end{aligned}$$

$$\begin{aligned}
 T_{Window\_Split\_Unocc} & \quad (32) \\
 & = 2.0 + 0.103T_{amb} + 0.526T_{hall} + 0.017T_{heater} + 0.276Light \\
 & \quad + 105.200V_{left} + 0.118T_{left} + 29.480V_{right} - 0.029T_{right} \\
 & \quad - 0.035W_{pl} - 0.001Q_{SWRad} + 0.008Q_{LWRad} + 0.244T_{out} \\
 & \quad - 0.193v_{wind}
 \end{aligned}$$

The window regression model results demonstrate good prediction performance with adjusted  $R^2$  values close to 1, as shown in Table 38. The RMSE values for these models, however, are the largest of all the regression models. This is most likely due to the low thermal inertia and resistivity properties of the window, resulting in surface temperatures that vary more than the other building elements.

*Table 38 Performance of the Occupied and Unoccupied Window Regression Models*

	<b>Adjusted R<sup>2</sup></b>	<b>RMSE</b>	<b>Degree of Freedom</b>
Occupied	0.7758	0.8616	7011
Unoccupied	0.9153	0.735	86849

The window regression model, under occupied conditions, demonstrates all p-values within the 99% confidence interval, as shown in Table 39. The largest influences on the window temperature, determined from the t-values, are the exterior temperature, the hallway temperature, the wind speed and the long wave solar radiation. It is noted that the influence of the exterior temperature however, is significantly greater than all other variables within this model. The exterior conditions such as the exterior temperature and wind speed were expected to have significant influences on the window temperature due to the unit facing the exterior. The hallway temperature is hypothesized to have a larger influence than the test cell’s ambient temperature for similar reasons to the spandrel panel. The test cell ambient measurements are taken at a location far from the window; the heater below the window is likely creating a warmer ambient temperature than what is recorded by the test cell ambient measurement device. As the ambient temperature in the hallway is usually slightly warmer than the test cell, it has a closer resemblance to the ambient air close to the window pane. The occupied model eliminated the plug load as well as the right duct air flow measurements during the subtractive regression analysis. As previously stated, the air duct measurement has no influence on the window because it is too far away, and the plug load data is eliminated as it is not the true value.

*Table 39 Student t-test P-values and t-values for Occupied Window Model*

	<b><i>T<sub>amb</sub></i></b>	<b><i>T<sub>Hall</sub></i></b>	<b><i>T<sub>Heater</sub></i></b>	<b><i>Occ</i></b>	<b><i>Light</i></b>	<b><i>V<sub>left</sub></i></b>	<b><i>T<sub>left</sub></i></b>	<b><i>T<sub>right</sub></i></b>
P-value	3.45E-14	<2e-16	<2E-16	<2E-16	<2E-16	<2e-16	2.69E-16	0.000291
t-value	-7.596	34.04	-14.576	15.275	-9.778	-8.438	8.207	3.625

<b><i>Q<sub>SWRad</sub></i></b>	<b><i>Q<sub>LWRad</sub></i></b>	<b><i>T<sub>out</sub></i></b>	<b><i>v<sub>wind</sub></i></b>
3.33E-09	<2e-16	<2e-16	<2E-16
5.922	17.217	94.744	-19.178

The unoccupied window regression model, with results shown in Table 40, demonstrates all variables with p-values within the 99% confidence interval. The largest influences on the window surface temperature are the exterior temperature, the longwave solar radiation, the

heater temperature, the hallway temperature, and the speed of the wind. The exterior conditions similar to the occupied model is expected to be the most significant influencers of this model due to the low thermal mass of the window and its placement on the exterior wall of the building. It is noted, similar to the previous model, the exterior temperature has significantly higher degree of influence in comparison to all other variables. One of the only differences in this model in comparison to the occupied condition is the influence of the heater temperature. This is hypothesized to be due to the lower amount of heating loads during unoccupied conditions, which makes the heater load more significant.

*Table 40 Student t-test P-values and t-values for Unoccupied Window Model*

	$T_{amb}$	$T_{Hall}$	$T_{Heater}$	$Light$	$V_{left}$	$T_{left}$	$V_{right}$	$T_{right}$	$W_{pl}$
P-value	<2E-16	<2e-16	<2E-16	<2E-16	<2e-16	<2E-16	<2E-16	<2E-16	<2E-16
t-value	22.922	72.72	62.895	24.554	37.83	81.192	19.086	-45.285	-13.004

$Q_{SWRad}$	$Q_{LWRad}$	$T_{out}$	$v_{wind}$
<2E-16	<2e-16	<2e-16	<2E-16
-21.999	84.406	499.845	-53.163

### 6.5.6 Interior Wall

The interior wall occupied (33) and unoccupied (34) regression models found from the subtractive linear regression analysis are presented below.

$$\begin{aligned}
 T_{IntWall\_Split\_Occ} & \quad (33) \\
 & = 74.86 + 0.062T_{amb} + 0.599T_{hall} - 0.006T_{heater} + 0.226Occ \\
 & - 0.482Light - 36.710v_{left} + 0.065T_{left} - 34.48V_{right} \\
 & + 0.012T_{right} - 0.002Q_{SWRad} + 0.003Q_{LWRad} + 0.027T_{out} \\
 & - 0.093v_{wind}
 \end{aligned}$$

$$\begin{aligned}
 T_{IntWall\_Split\_Unocc} & \quad (34) \\
 & = 13.80 + 0.269T_{amb} + 0.586T_{hall} + 0.010T_{heater} + 0.180Light \\
 & - 9.986v_{left} + 0.079T_{left} - 14.38V_{right} + 0.009T_{right} - 0.075W_{pl} \\
 & - 0.001Q_{SWRad} + 0.001Q_{LWRad} + 0.013T_{out} - 0.022v_{wind}
 \end{aligned}$$

The results from the interior wall regression models, shown in Table 41, demonstrate contradicting results where the unoccupied model shows good performance while the occupied model does not. The unoccupied model has an adjusted  $R^2$  result close to 0.9, and low RMSE. The occupied model however, has poor adjusted  $R^2$  value, closer to 0.5, and large RMSE. These results are believed to be due to model not considering the airflow within the test cell which, has significant effects on this surface temperature due to its low thermal mass and its proximity to the ventilation output.

*Table 41 Performance of the Occupied and Unoccupied Interior Wall Regression Models*

	<b>Adjusted <math>R^2</math></b>	<b>RMSE</b>	<b>Degree of Freedom</b>
Occupied	0.5323	0.549	7010
Unoccupied	0.877	0.3303	86849

The results from the occupied interior wall, presented in Table 42, demonstrate all variables with p-values within the 99% confidence interval. The t-values indicate that the variables with the largest influence on the model are the hallway temperature, the occupancy, the outdoor temperature, and the long wave radiation. The influence of the exterior temperature along with the long wave radiation, were unexpected results in this model due to the distance between the monitored interior wall and the exterior wall. The plug load was eliminated during the subtractive process, as seen in the other models, due to the values used within this research not being the true measurements.

*Table 42 Student t-test P-values and t-values for Occupied Interior Wall Model*

	$T_{amb}$	$T_{Hall}$	$T_{Heater}$	<b>Occ</b>	<b>Light</b>	$V_{left}$	$T_{left}$	$V_{right}$
P-value	2.75E-08	<2e-16	<2e-16	<2e-16	<2e-16	5.34E-07	<2e-16	7.59E-06
t-value	5.563	27.202	-9.503	22.139	-9.90	-5.018	12.942	-10.029

$T_{right}$	$Q_{SWRad}$	$Q_{LWRad}$	$T_{out}$	$v_{wind}$
3.30E-14	<2e-16	<2e-16	<2e-16	<2E-16
7.602	-11.963	16.14	16.716	-10.058

The results from the unoccupied model, shown in Table 43, have all the variables with p-value within the 99% confidence interval. The t-values demonstrate the ambient test cell and hallway temperature, left vent air supply temperature, temperature of the heater, and outdoor

temperature as the variables with the most significance on the regression model. Unlike the occupied model, the ambient test cell temperature is one of the most significant variables along with the hallway temperature, as was expected for the interior wall. The outdoor temperature's impact on the interior wall temperature again is an unforeseen variable in this model, as the interior wall is far within the modeling space away from the exterior wall.

*Table 43 Student t-test P-values and t-values for Unoccupied Interior Wall Model*

	$T_{amb}$	$T_{Hall}$	$T_{Heater}$	$Light$	$V_{left}$	$T_{left}$	$V_{right}$	$T_{right}$	$W_{pl}$
P-value	2.75E-08	<2e-16	<2e-16	<2e-16	1.36E-15	<2e-16	<2e-16	<2e-16	<2e-16
t-value	133.22	180.18	79.83	35.59	-7.99	120.54	-20.71	32.66	-63.04

$Q_{SWRad}$	$Q_{LWRad}$	$T_{out}$	$v_{wind}$
<2e-16	<2e-16	<2e-16	<2E-16
-30.03	23.60	60.84	-13.42

### 6.5.7 Summary of G2 model

The second-generation model replaces all RC network building element branches with linear regression models. Two linear regression models, a general model and a split occupied-unoccupied model, were created using subtractive regression analysis. The models were compared for better surface temperature prediction ability. The results from the simulations demonstrate the split regression model having better surface temperature prediction accuracy for all elements except for the ceiling slab. The final G2 model is therefore a grey box model with split regression models representing the exterior wall, window, spandrel, floor, and interior wall, and a general model for the ceiling. The results from this analysis also demonstrated the window, spandrel panel, and exterior wall having significantly worse WAPE values compared to the other building elements.

Overall, the significant variable analysis within each building elements regression model indicated the plug load data, lighting, and right ventilation air supply and temperature are not significant variables. These variables were either eliminated from the regression equation through the subtractive regression fitting process or were present within the regression models

with minimal influence. The right ventilation data is the most unexpected result from this analysis as it is the main conditioning vent to the test cell.

## 6.6 G3 Model: Neural Network Analysis

To improve the surface temperature prediction performance of the exterior wall, window, and spandrel panel, neural networks were created for each element. The neural nets were trained using the same cleaned data set used to train the linear regression models.

The results from the hidden layer optimisation are presented in Table 44. The findings demonstrate the window unit having a much smaller optimal hidden layer size than the other two models and had much higher RMSE. This is most likely due to the low thermal mass of the window making the temperature harder to predict.

*Table 44 Hidden Layer Optimisation for each Neural Network*

	<b>Exterior Wall</b>	<b>Spandrel</b>	<b>Window</b>
Hidden Layer Size	30	27	19
RMSE	0.2354	0.2427	0.4240

Three new grey box models were created that replaced the split linear regression model of the window, spandrel panel, and exterior wall with their neural net models. The new grey box models were simulated for all eleven simulation days to compare the surface temperature prediction results of the neural networks to the split linear regression models. The results shown in Table 45, demonstrate that none of the neural network models performed better than the split linear regression models. Therefore, none of the neural networks were incorporated into the grey box model.

Table 45 Comparison of the Split Regression Models and the Neural Network Models for the Exterior Wall, Spandrel Panel and Window

<b>Split Regression Model</b>			
	Exterior Wall	Spandrel	Window
RMSE	1.382	1.007	1.240
MAE	0.791	0.706	0.777
WAPE	0.167%	0.202%	0.257%
<b>Neural Network Model</b>			
	Exterior Wall	Spandrel	Window
RMSE	1.748	1.151	3.212
MAE	1.036	0.771	1.653
WAPE	0.219%	0.222%	0.570%

## 6.7 Final Model

Based on the results from the model variations presented, the final model for this research is the G2 model incorporating split linear regression models to represent the building elements. This model incorporates the RC network representations of the ambient temperature and sensible heat loads, with the linear regression equations for each of the building elements, see *Simulink* model images in Appendix D. The only input parameter for this grey box model is the initial ambient test cell temperature. All the result graphs below display the error associated with the measurement devices, 0.4°C for ambient temperature measurements [49], and 0.5°C for the calibrated thermocouple measurements [48].

The results from the November 17<sup>th</sup> simulation are summarized in Table 46, this simulation demonstrated prediction accuracy within 3% for all the building element surface temperatures (Figure 43) and within 0.5% for the ambient temperature (Figure 44). Observations from this model include underprediction of all of building element temperatures except for the interior wall. The exterior wall demonstrated the worst prediction results, varying around 3% while the other building elements vary within the 1.5% error range. The window unit demonstrates the largest variance in error varying between 2.3% underprediction and 1.2% overprediction. Overall, the results of the simulation were good with the ambient temperature predicted to within 0.1°C.

Table 46 Prediction Error for Temperatures of Simulated Elements as a Function of Prediction Window Duration for November 17, 2017 ( $T_{out}=0.93^{\circ}\text{C}$ , wind speed ranging from 0.5 to 1.5 m/s)

Prediction Window							
	0 minutes	15 minutes	30 minutes	45 minutes	60 minutes	120 minutes	180 minutes
Exterior Wall	-2.85%	-2.91%	-2.60%	-2.96%	-2.85%	-2.81%	-2.56%
Ceiling	-0.26%	-0.54%	-0.33%	-0.36%	-0.22%	0.00%	0.20%
Floor	-1.59%	-1.36%	-1.12%	-1.11%	-1.26%	-1.00%	-0.80%
Spandrel	-0.72%	-0.59%	-0.93%	-0.95%	-0.51%	-0.64%	0.00%
Window	-0.13%	-0.47%	-2.29%	-1.68%	0.03%	-0.17%	1.20%
Interior Wall	0.12%	-0.13%	0.09%	0.06%	0.23%	0.05%	0.27%
Ambient	0.00%	-0.02%	0.40%	0.39%	0.38%	0.35%	-0.08%

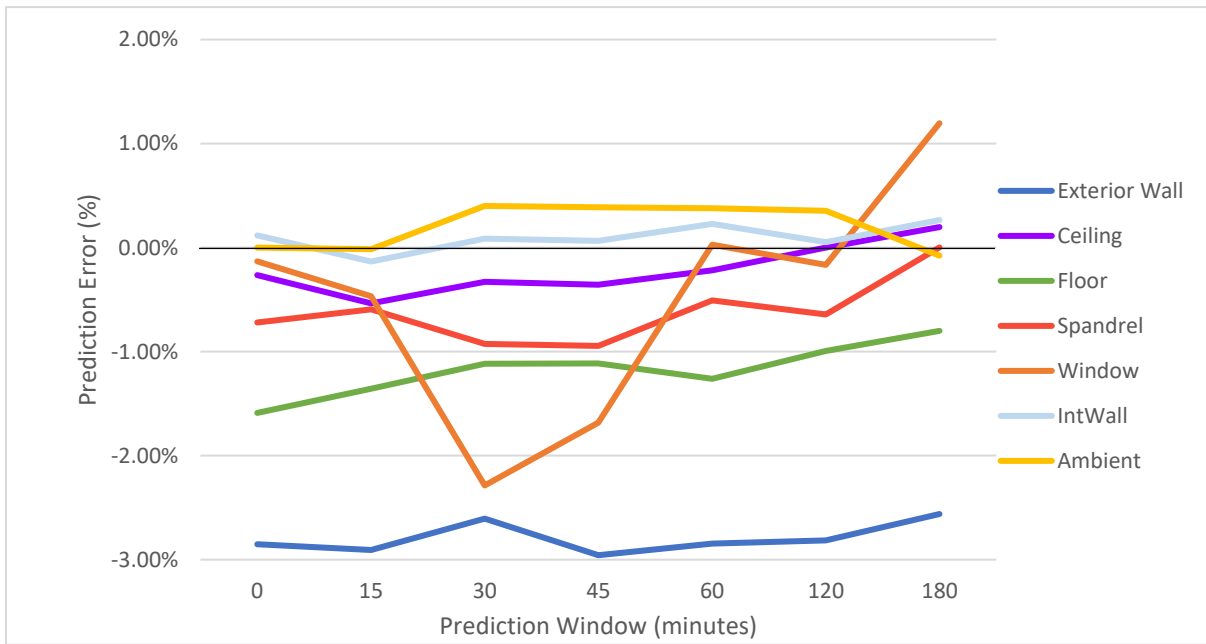
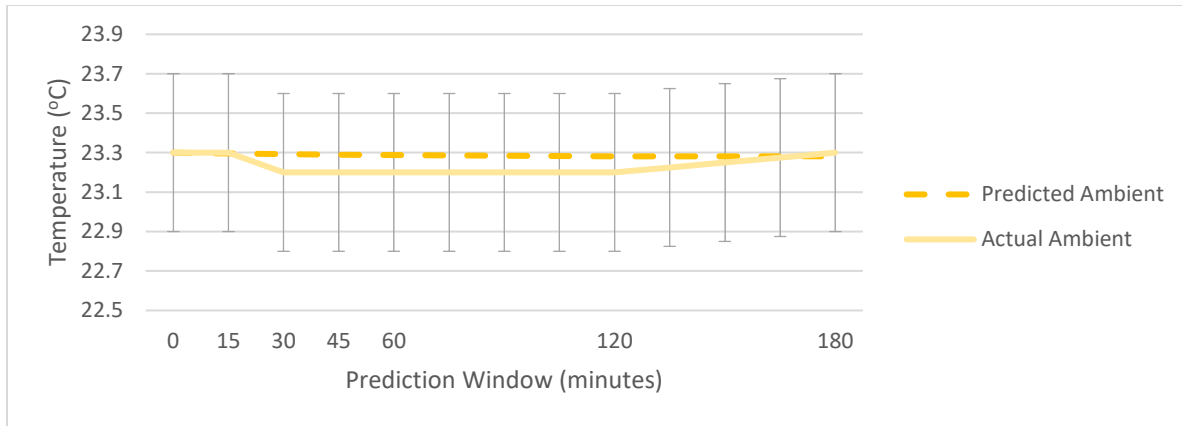


Figure 43 November 17, 2017 Prediction Error for all Building Elements along with Ambient Temperature



*Figure 44 November 17<sup>th</sup>, 2017 Predicted vs Actual Ambient Temperature*

The results from the November 29<sup>th</sup> simulation, presented in Table 47, demonstrate poor surface temperature predictions for the spandrel panel and window unit. The simulation begins with the spandrel temperature underpredicting by 4% (Figure 45) and the window underpredicting by close to 11% (Figure 45). Both results, however, improve throughout the simulation until the 180-minute Prediction Window when the spandrel is below 1% error and the window below 2%. The linear regression results for the spandrel and window models demonstrate two of the significant variables influencing their temperature prediction is the exterior temperature and the wind speed. The underprediction results from this model are surprising as this model has a warmer exterior temperature than the previous simulation on November 17<sup>th</sup>. The wind speeds for this model however, are higher than the speeds for November 17<sup>th</sup>, and could be the reason why both of these elements have worse prediction results. The higher wind speeds increase the amount of convective heat loss on the exterior of the window, this convective heat loss decreases throughout the simulation as the wind speeds decrease. It is observed in Figure 45, that all of the elements have an upward slope near the end of the simulation. This is believed to be caused by the ambient temperature prediction, which influences all of the surface temperature linear regression models. Within Figure 47, the actual temperature decreases throughout the simulation, while the predicted ambient temperature stays relatively constant. This results in a temperature difference of 0.3°C by the end of the simulation. This deviation could be a measurement fluctuation in the ambient temperature sensor, as is it has a measurement accuracy of +/- 0.4°C. The over prediction of the ambient temperature at the 180-minute Prediction Window could be the cause of the over predictions seen in the building elements.

Table 47 Prediction Error for Temperatures of Simulated Elements as a Function of Prediction Window Duration for November 29, 2017 ( $T_{out}=0.93^{\circ}C$ , wind speed ranging from 0.5 to 1.5 m/s)

Prediction Window							
	0 minutes	15 minutes	30 minutes	45 minutes	60 minutes	120 minutes	180 minutes
Exterior Wall	0.80%	0.59%	0.80%	0.44%	1.26%	1.77%	2.30%
Ceiling	-0.59%	-0.71%	-0.52%	-0.51%	-0.25%	0.57%	1.02%
Floor	0.27%	0.58%	0.25%	0.38%	1.11%	2.00%	2.14%
Spandrel	-3.90%	-3.64%	-3.91%	-3.54%	-2.84%	-1.34%	0.84%
Window	-10.60%	-10.48%	-10.18%	-9.17%	-8.91%	-5.88%	-1.91%
Interior Wall	0.66%	0.38%	0.30%	0.32%	0.63%	1.16%	1.62%
Ambient	0.00%	0.00%	-0.01%	0.43%	0.88%	0.48%	1.48%

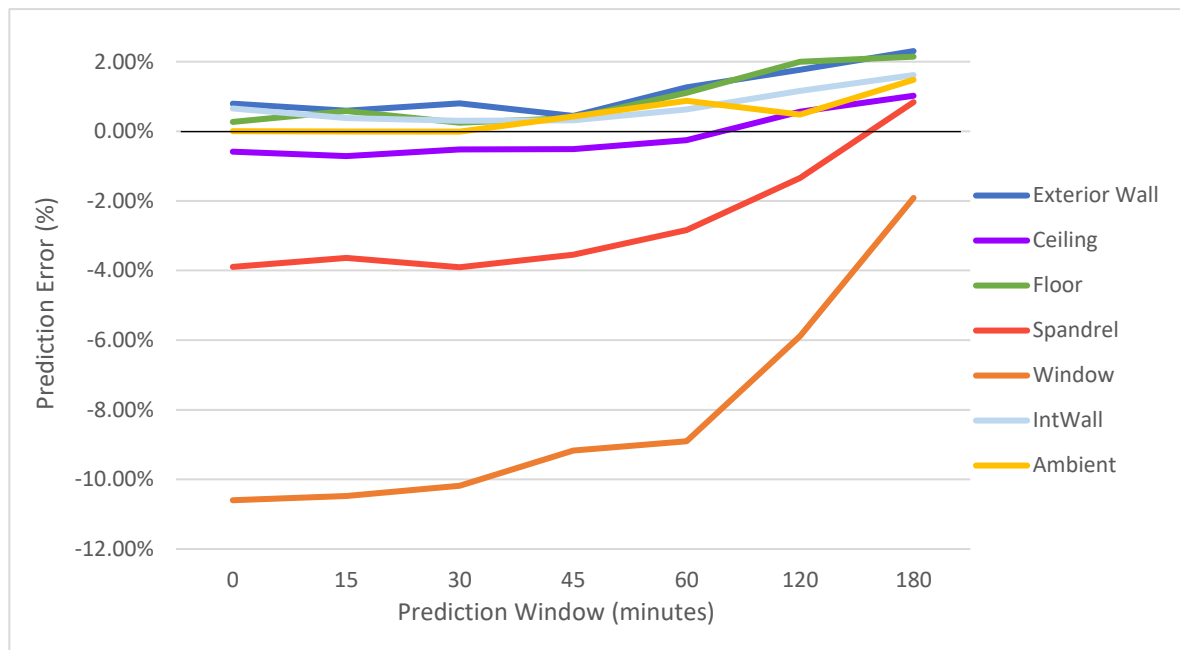


Figure 45 November 29, 2017 Prediction Error for all Building Elements along with Ambient Temperature

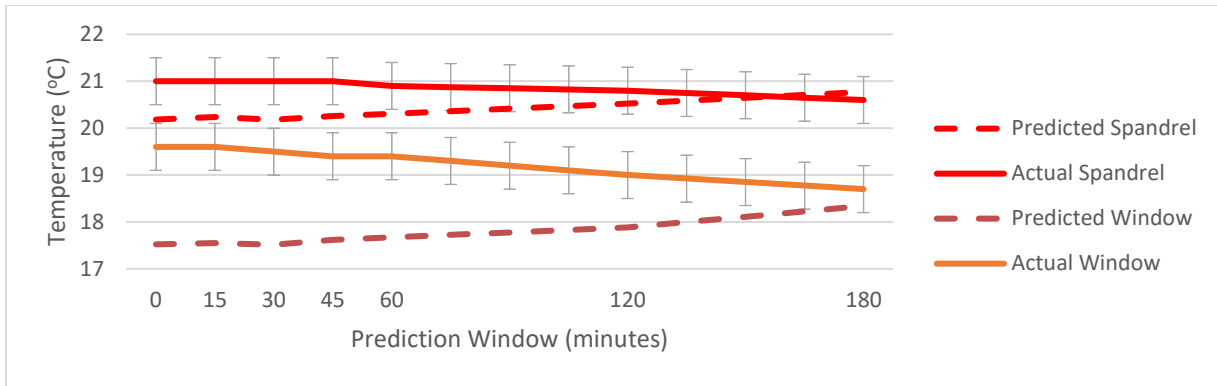


Figure 46 November 29th, 2017 Predicted vs Actual Surface Temperature of the Window and Spandrel Panel

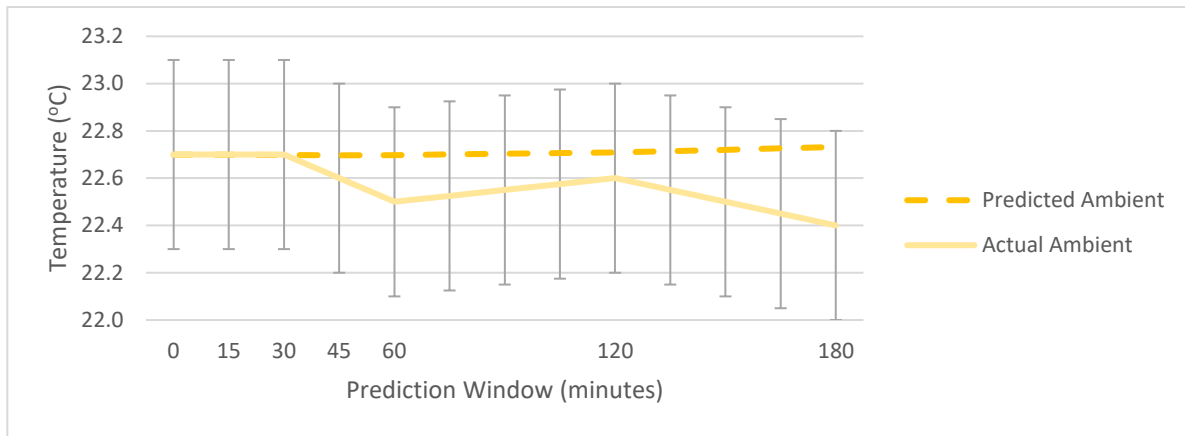


Figure 47 November 29th, 2017 Predicted vs Actual Ambient Temperature

The January 6<sup>th</sup> simulation, illustrated in Table 48 and Figure 48, demonstrated prediction results with all of the building elements predicted to within 6 %, and ambient temperature predicted to within 1.5%. This simulation demonstrates the window, spandrel panel, and exterior wall having the worst prediction results. The window and spandrel underpredictions, shown in Figure 49, may be due to the extreme cold temperatures of this simulation. The variations seen in the prediction error is believed to be caused by the varying wind speed for this simulation. The ambient temperature results, shown in Figure 50, demonstrate predicted accuracy to within 0.3°C, despite the prediction errors of the façade elements.

Table 48 Prediction Error for Temperatures of Simulated Elements as a Function of Prediction Window Duration for January 6, 2018 ( $T_{out}=-19.19^{\circ}\text{C}$ , wind speed ranging from 0.5 to 1.5 m/s)

Prediction Window							
	0 minutes	15 minutes	30 minutes	45 minutes	60 minutes	120 minutes	180 minutes
Exterior Wall	3.02%	0.48%	-0.60%	-0.91%	0.20%	0.22%	0.35%
Ceiling	-2.00%	-1.94%	-1.95%	-2.08%	-2.05%	-2.07%	-1.60%
Floor	-1.86%	-1.86%	-1.89%	-1.73%	-1.82%	-1.76%	-1.34%
Spandrel	-3.42%	-3.13%	-2.58%	-3.41%	-2.67%	-1.64%	-0.15%
Window	-5.63%	-3.92%	-1.50%	-4.26%	-3.59%	0.38%	1.48%
Interior Wall	-1.44%	-1.36%	-1.38%	-1.53%	-1.50%	-1.05%	-0.53%
Ambient	0.00%	0.01%	0.01%	0.02%	-0.45%	-0.91%	-1.35%

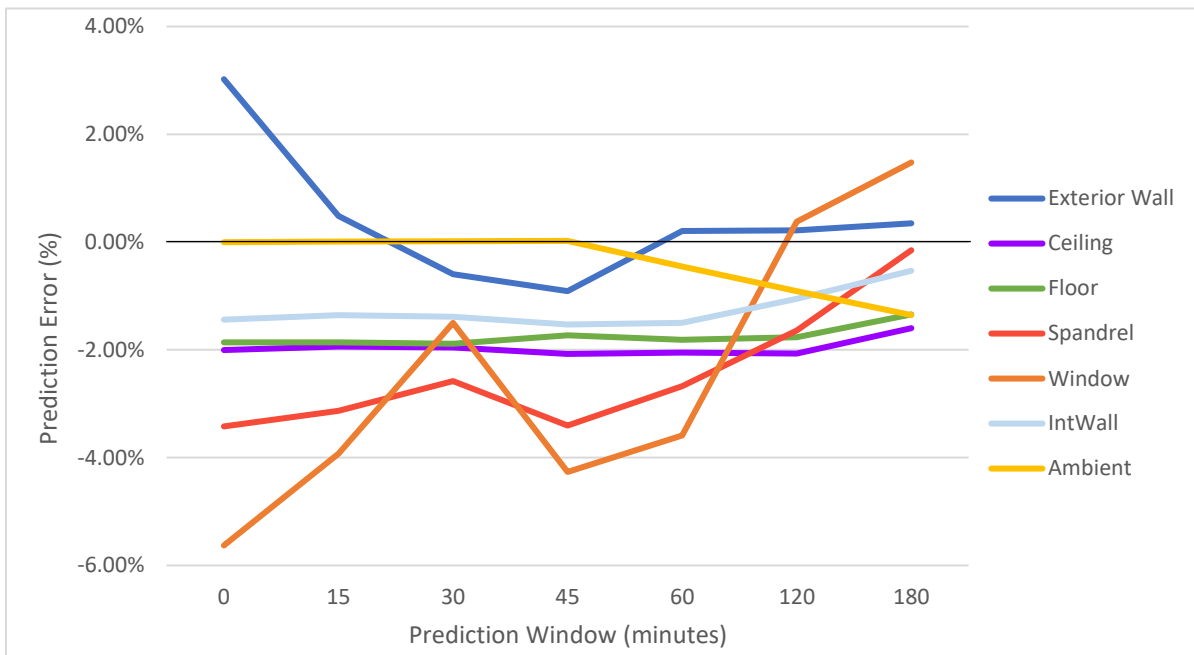


Figure 48 January 6<sup>th</sup>, 2018 Prediction Error for all Building Elements along with Ambient Temperature

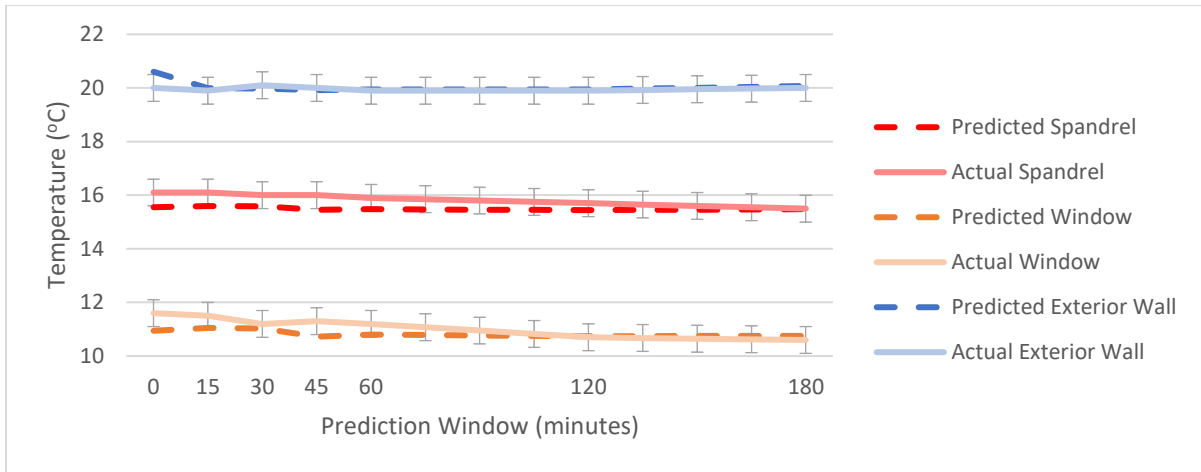


Figure 49 January 6th, 2018 Predicted vs Actual Surface Temperature of the Window and Spandrel Panel

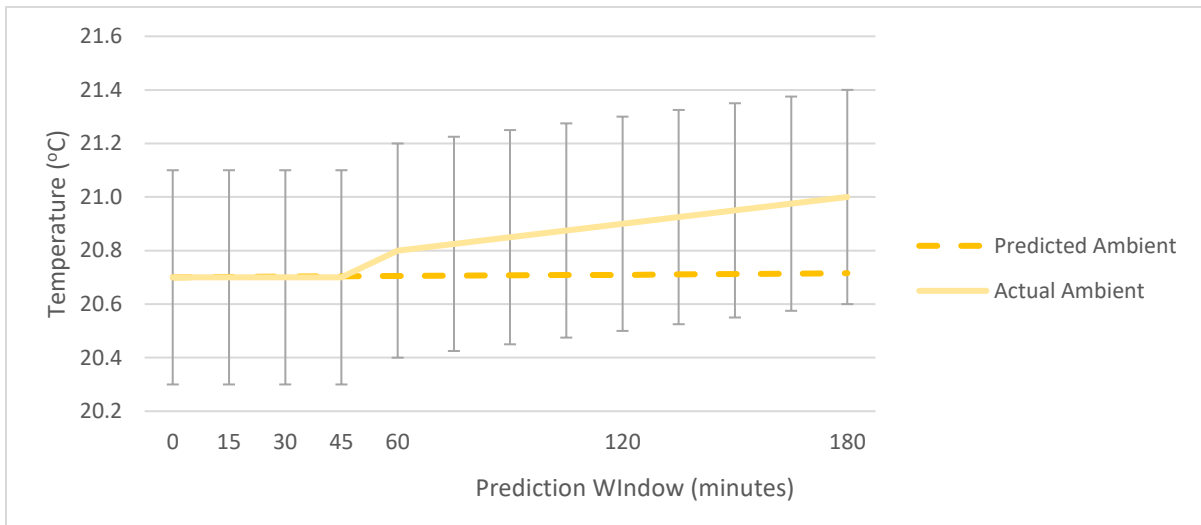


Figure 50 January 6<sup>th</sup>, 2018 Predicted vs Actual Ambient Temperature

The December 31<sup>st</sup> simulation demonstrates mixed prediction results, as illustrated in Table 49 and Figure 51. The predicted surface temperature of the window is off by as much as 9%, with the spandrel panel off by up to 4%. Comparatively, the other building elements had good prediction results, to within 2% accuracy. The 1°C deviation in predicted window temperature and 0.6°C deviation in spandrel temperature at the 30-minute Prediction Window can be seen in Figure 52 to be caused by the predicted temperatures increasing when the actual temperatures remain steady. This is believed to be due to the large longwave radiation values in this simulation, which is a significant input variable in both window and spandrel panel regression

models. Despite these larger prediction errors, the ambient temperature is still predicted to within 0.3°C of the actual temperature, as shown in Figure 53.

*Table 49 Prediction Error for Temperatures of Simulated Elements as a Function of Prediction Window Duration for December 31, 2017 ( $T_{out}=-16.04^{\circ}\text{C}$ , wind speed ranging from 0.5 to 1.5 m/s, and solar radiation  $400\text{W}/\text{m}^2$ )*

Prediction Window							
	0 minutes	15 minutes	30 minutes	45 minutes	60 minutes	120 minutes	180 minutes
Exterior Wall	1.31%	1.483%	1.863%	1.772%	1.587%	0.442%	0.393%
Ceiling	-0.55%	-0.479%	-0.102%	-0.158%	-0.098%	-0.084%	0.057%
Floor	0.00%	0.424%	0.184%	0.759%	0.379%	0.424%	0.271%
Spandrel	1.06%	1.213%	3.578%	1.737%	1.979%	-0.034%	0.487%
Window	2.92%	3.868%	8.687%	0.900%	-2.471%	-2.216%	-2.311%
Interior Wall	-0.19%	-0.048%	0.362%	0.312%	-0.078%	0.455%	0.118%
Ambient	0.00%	0.004%	0.013%	0.024%	0.036%	1.044%	1.117%

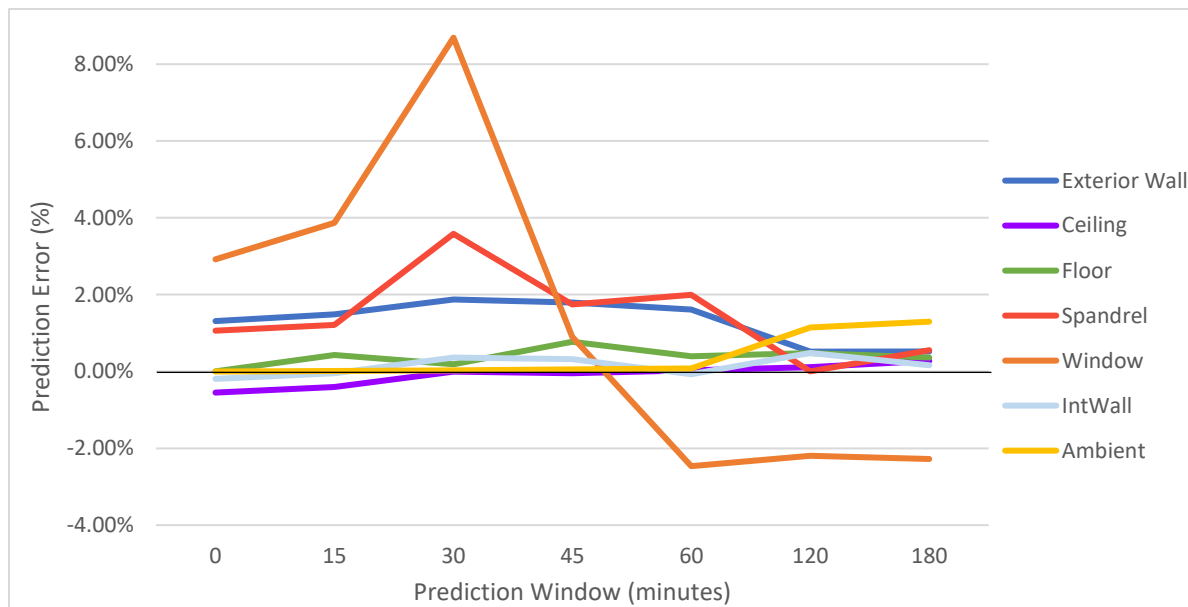


*Figure 51 December 31<sup>st</sup>, 2017 Prediction Error for all Building Elements along with Ambient Temperature*

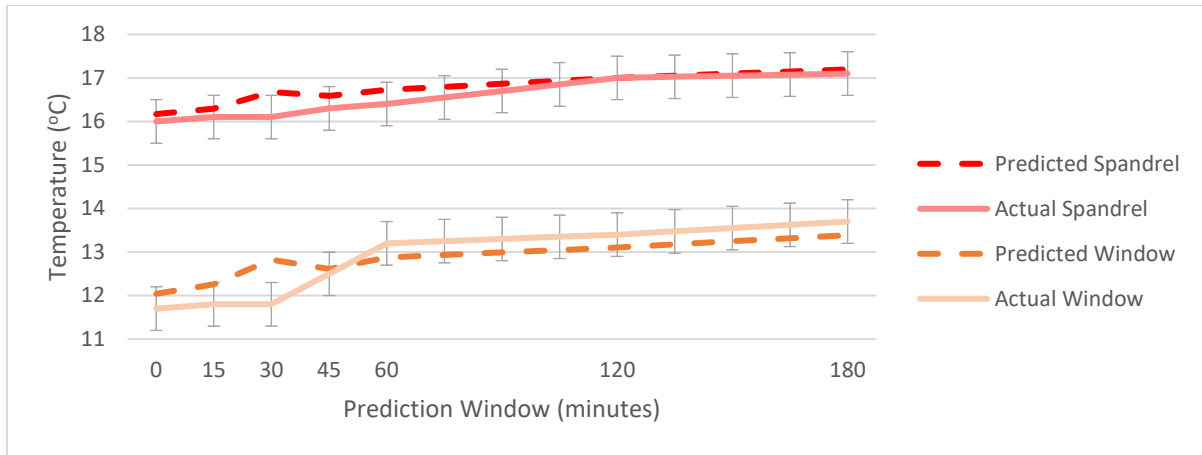


Figure 52 December 31<sup>st</sup>, 2017 Predicted vs Actual Surface Temperature for the Window and Spandrel Panel

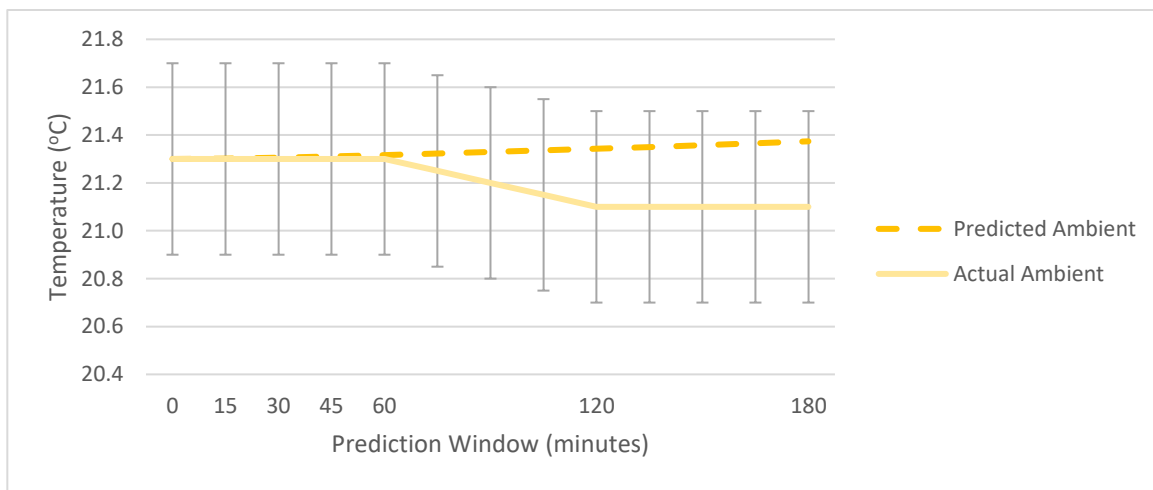


Figure 53 December 31<sup>st</sup>, 2017 Predicted vs Actual Ambient Temperature

The simulation for January 13<sup>th</sup> demonstrates prediction accuracy to within 2% for all of the building elements except the window, as illustrated in Table 50 and Figure 54. The window prediction error increases to close to 10% at the 60-minute prediction time. The window data, shown in Figure 55, demonstrates a jump in the measured temperature around the 60<sup>th</sup> minute. None of the data collected from the test cell indicate major changes around the 60<sup>th</sup> minute which, is why the predicted temperature does not increase with the actual data. This jump must be caused by a heat source not modeled within this grey box model. The predicted window temperature however can be observed to gradually increase throughout the simulation, believed to be caused by the gradual increase in exterior temperature and increase in long wave radiation. Similar to previous simulations, despite the prediction error for the window, the ambient

temperature is predicted to within 0.2°C (Figure 56). It is noted that this simulation demonstrates greater variance in the actual ambient temperature measurements compared to other simulation days which could be caused by the higher right duct ventilation rate increasing the degree of air mixing within the test cell.

*Table 50 Prediction Error for Temperatures of Simulated Elements as a Function of Prediction Window Duration for January 13, 2018 ( $T_{out}=-13.04^{\circ}C$ , wind speed ranging from 0 m/s, and solar radiation 400W/m<sup>2</sup>)*

Prediction Window							
	0 minutes	15 minutes	30 minutes	45 minutes	60 minutes	120 minutes	180 minutes
Exterior Wall	2.04%	1.70%	1.41%	1.91%	2.02%	1.71%	2.11%
Ceiling	-0.65%	-0.62%	-0.65%	-0.65%	-0.50%	-0.10%	-0.53%
Floor	0.17%	0.16%	0.01%	-0.06%	0.00%	0.22%	0.22%
Spandrel	-2.26%	-1.42%	-1.21%	-1.64%	-2.39%	-2.46%	-1.65%
Window	-5.40%	-2.90%	-3.87%	-8.77%	-9.68%	-4.75%	-4.12%
Interior Wall	-0.61%	-0.60%	-0.63%	-0.64%	-0.93%	-0.50%	-0.92%
Ambient	0.00%	-0.89%	-0.47%	0.39%	-0.94%	0.35%	0.78%

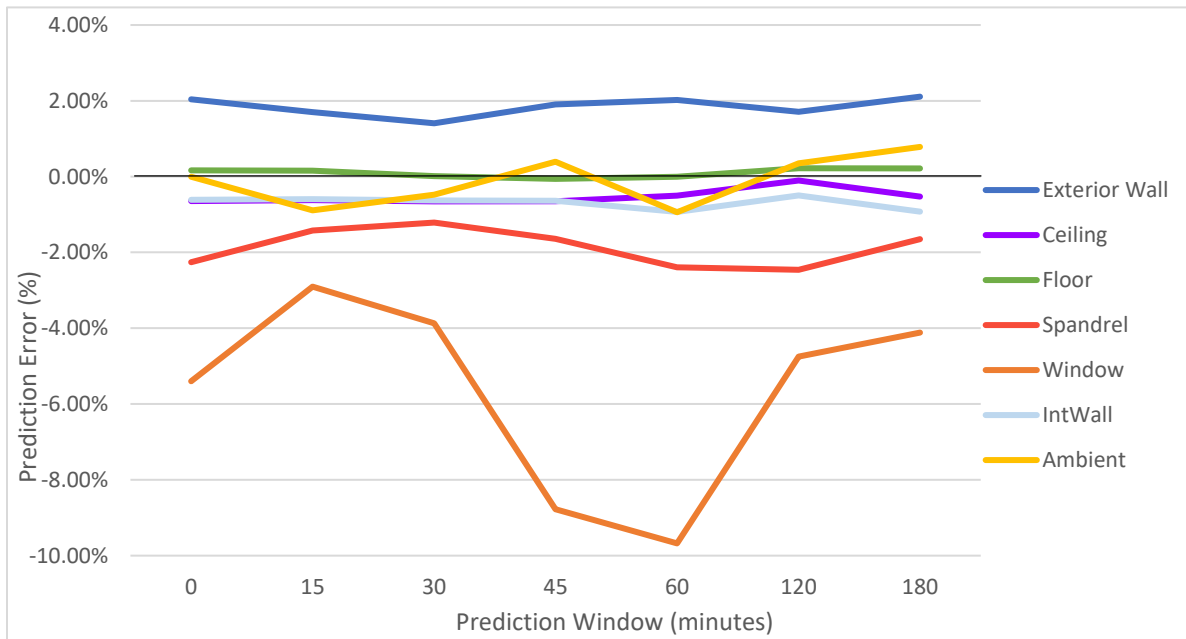


*Figure 54 January 13<sup>th</sup>, 2018 Prediction Error for all Building Elements along with Ambient Temperature*

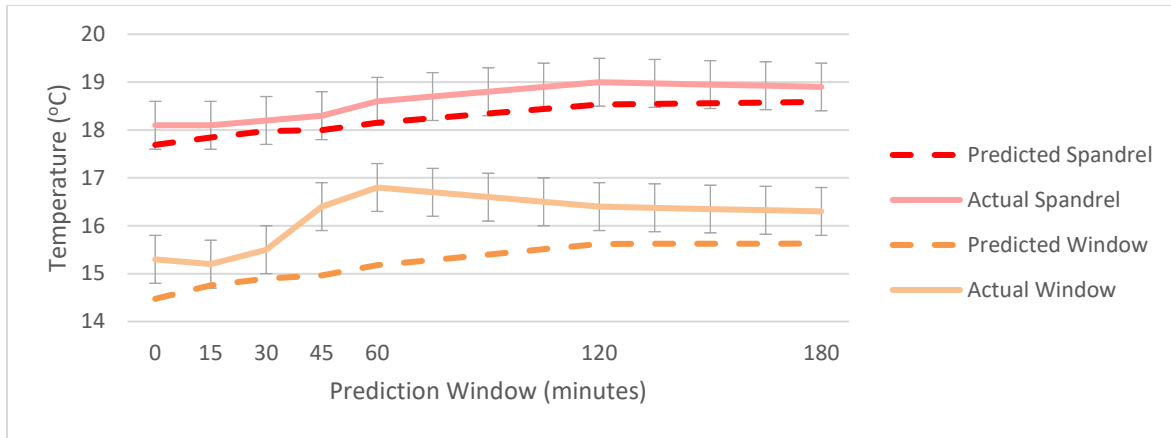


*Figure 55 January 13th, 2018 Predicted vs Actual Surface Temperature for the Window and Spandrel Panel*

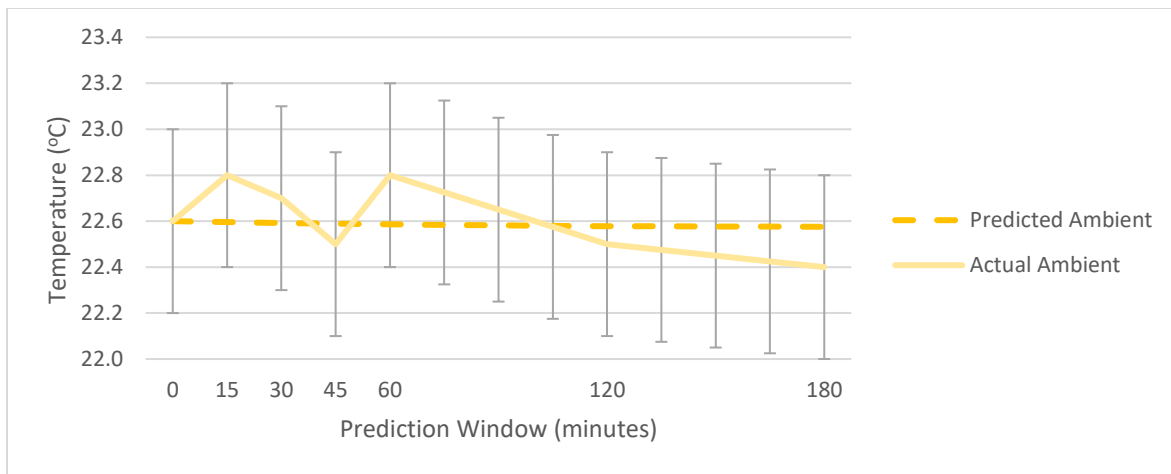


*Figure 56 January 13th, 2018 Predicted vs Actual Ambient Temperature*

The results from the January 2<sup>nd</sup> simulation, summarized in Table 51 and Figure 57, demonstrate over prediction, between 2% to 14%, for all building elements. The prediction error of the interior elements is observed to remain constant throughout the simulation with the ceiling error staying around 2%, the interior wall around 3.5%, and the floor around 5%. The exterior wall demonstrated relatively constant prediction error of around 3% with a slight increase in the last hour. Similar to previous simulations, the window and spandrel panel had the least accurate temperature predictions. The prediction error for the window starts at 8% and increases to 13%, with similar results for the spandrel panel starting at 6% and ending close to 9%. The spandrel panel and window temperatures are observed to be off by 1.5°C and 1.7°C respectively (Figure 58). It is unexpected to see these temperatures overpredicted, as the colder

exterior temperature and higher wind speeds dictating the linear regression models would be thought to produce underpredicted temperature results. The gradual increase in predicted temperature for both elements is believed to be due to the increase in exterior temperature throughout this simulation, and increasing long wave radiation value. Similar to previous simulations, the observed upwards trend of the building elements at the end of the simulation is believed to be due to the ambient temperature prediction results (Figure 59). The ambient temperature demonstrated prediction accuracy to within 1.5%, with the temperature being overpredicted by 0.3°C at the 180-minute Prediction Window.

*Table 51 Prediction Error for Temperatures of Simulated Elements as a Function of Prediction Window Duration for January 2, 2018 ( $T_{out}=-10.02^{\circ}\text{C}$ , wind speed ranging from 2-4 m/s, and solar radiation  $50\text{W}/\text{m}^2$ )*

Prediction Window							
	0 minutes	15 minutes	30 minutes	45 minutes	60 minutes	120 minutes	180 minutes
Exterior Wall	1.00%	2.97%	2.55%	2.77%	3.32%	3.76%	4.45%
Ceiling	1.18%	1.29%	1.41%	1.49%	1.57%	2.04%	2.52%
Floor	0.80%	4.51%	4.52%	4.66%	4.77%	4.76%	4.89%
Spandrel	2.61%	5.73%	6.13%	6.66%	6.97%	8.22%	8.98%
Window	7.81%	7.58%	7.64%	8.74%	10.03%	10.91%	12.97%
Interior Wall	1.12%	3.32%	3.44%	3.53%	3.59%	3.50%	3.96%
Ambient	0.00%	0.08%	0.16%	0.25%	0.33%	1.16%	1.52%

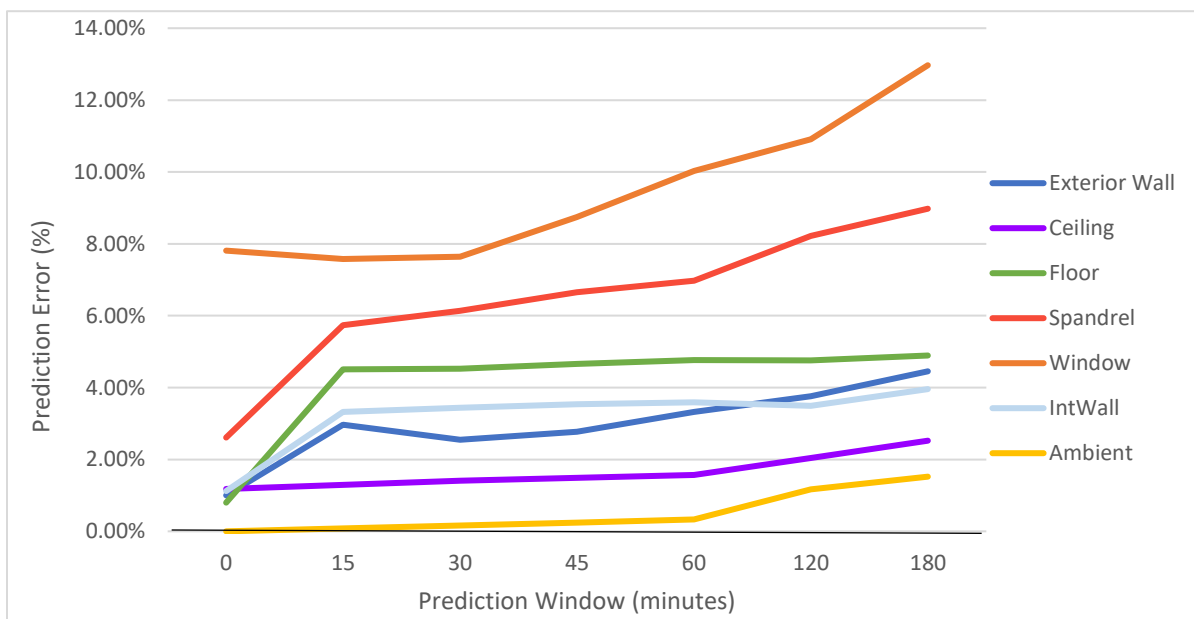


Figure 57 January 2<sup>nd</sup>, 2018 Prediction Error for all Building Elements along with Ambient Temperature

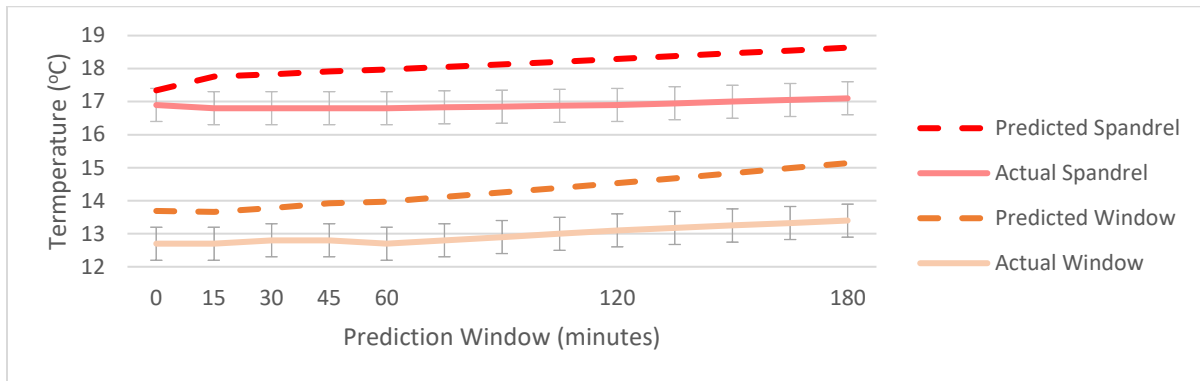


Figure 58 January 2<sup>nd</sup>, 2018 Predicted vs Actual Surface Temperature of the Window and Spandrel Panel

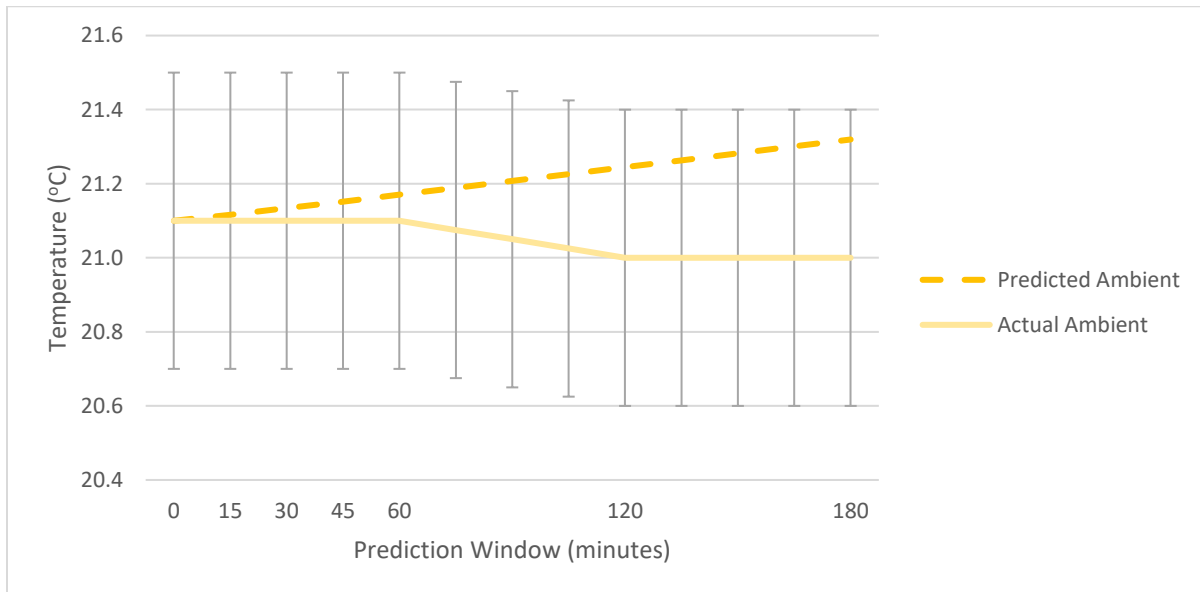


Figure 59 January 2<sup>nd</sup>, 2018 Predicted vs Actual Ambient Temperature

The February 12<sup>th</sup> simulation predicted all the building elements except the window to within 4% accuracy as illustrated in Table 52 and Figure 60. The window has very sporadic results, jumping from 7% underprediction to 7% overprediction. These results are caused by the variance in actual window temperature measurements, as shown in Figure 61. The predicted window temperature appears to closely follow the exterior temperature data, especially near the end of the simulation when the exterior temperature decreases rapidly. The other building elements are observed to peak in the middle of the simulation. This pattern is believed to be

caused by the occupancy count increasing to 3 people at the 30-minute prediction time and decreasing back to zero occupants at the 90-minute time. The ambient temperature prediction for the room indicates close precision until the 90<sup>th</sup> minute when the actual ambient temperature decreases and the predicted ambient continues to increase (Figure 62). This is believed to be due to the lighting that continues to be on in the room after the occupants leave. Despite these discrepancies, the ambient temperature is predicted to within 0.3°C.

*Table 52 Prediction Error for Temperatures of Simulated Elements as a Function of Prediction Window Duration for February 12, 2018 ( $T_{out}=-2.51^{\circ}\text{C}$ , wind speed ranging from 0.5-2 m/s, and solar radiation  $120\text{W}/\text{m}^2$ )*

Prediction Window							
	0 minutes	15 minutes	30 minutes	45 minutes	60 minutes	120 minutes	180 minutes
Exterior Wall	-0.08%	-1.52%	-0.01%	0.95%	0.33%	-2.63%	-3.71%
Ceiling	0.05%	0.50%	1.83%	1.83%	1.76%	0.26%	-1.61%
Floor	-0.02%	-1.07%	2.68%	2.18%	1.92%	-0.79%	-1.35%
Spandrel	0.05%	0.14%	2.26%	3.78%	2.56%	1.41%	-1.73%
Window	-0.52%	1.28%	7.32%	-0.68%	0.15%	5.10%	-0.18%
Interior Wall	-0.13%	-1.31%	0.11%	-1.64%	-1.30%	-4.09%	-4.06%
Ambient	0.00%	0.05%	-0.26%	-0.06%	-0.32%	0.16%	1.22%

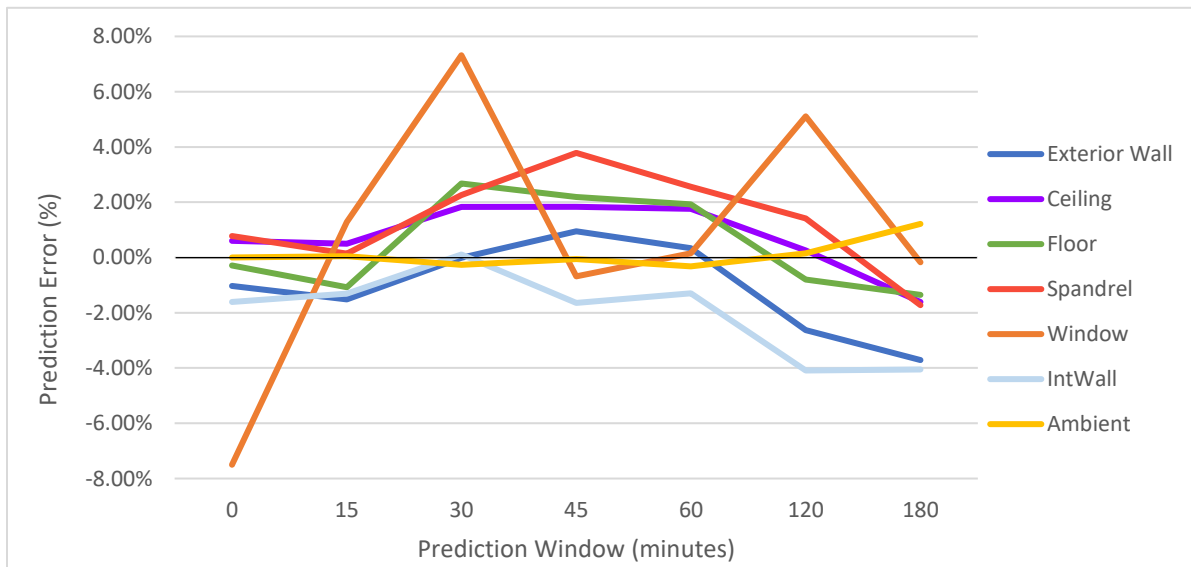


*Figure 60 February 12<sup>th</sup>, 2018 Prediction Error for all Building Elements along with Ambient Temperature*

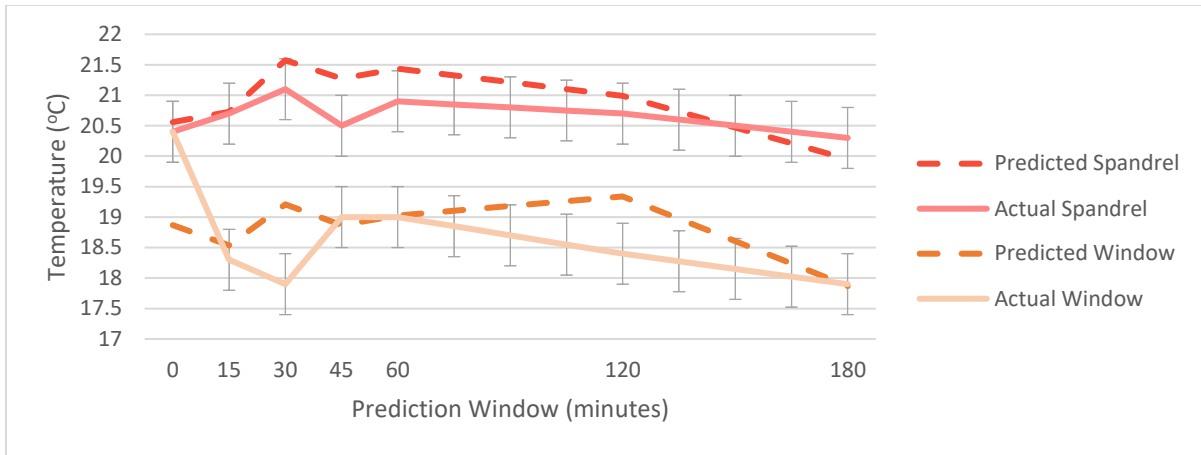


Figure 61 February 12th, 2018 Predicted vs Actual Surface Temperature for the Window and Spandrel Panel.

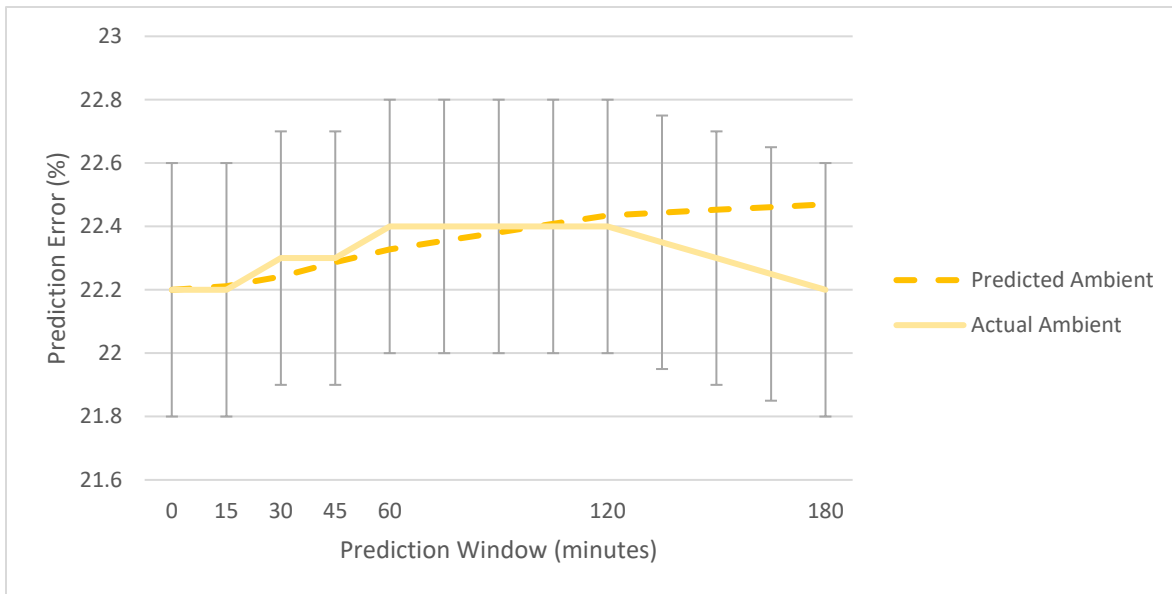


Figure 62 February 12<sup>th</sup>, 2018 Predicted vs Actual Ambient Temperature

The January 8<sup>th</sup> simulation demonstrates unique prediction results with the window, spandrel panel, and interior wall following the same prediction error pattern as shown in Table 53 and Figure 63. These elements display high prediction errors at the beginning of the simulation, settle in the middle, before slightly increasing again near the end. All three of these elements demonstrate a sharp increase in predicted error at the 15-minute Prediction Window, as shown in Figure 64. This is believed to be due to an increase in long wave radiation at this time, which has significant influence on all three regression models, along with a change in occupancy status. At the 15-minute mark the simulation transitions from the unoccupied regression models

to the occupied regression models due to occupants entering the test cell. The predicted ambient temperature steadily increases throughout this simulation due to the presence of the occupants as well as the interior lighting being on for the entire simulation. Overall, the ambient temperature is predicted to within 1.7% accuracy, with deviation of 0.35°C at the 180-minute Prediction Window, as illustrated in Figure 65.

*Table 53 Prediction Error for Temperatures of Simulated Elements as a Function of Prediction Window Duration for January 8, 2018 ( $T_{out}=0.5^{\circ}C$ , wind speed ranging from 1-2.5 m/s, and solar radiation 50W/m<sup>2</sup>)*

Prediction Window							
	0 minutes	15 minutes	30 minutes	45 minutes	60 minutes	120 minutes	180 minutes
Exterior Wall	-1.10%	-0.94%	-0.78%	-0.87%	-2.60%	-0.85%	-2.40%
Ceiling	0.64%	2.29%	1.72%	1.25%	0.68%	0.60%	0.94%
Floor	-0.98%	-0.23%	0.14%	-0.24%	-0.36%	0.80%	0.14%
Spandrel	0.43%	4.95%	2.47%	0.97%	-0.14%	-0.82%	1.61%
Window	0.06%	5.98%	2.53%	0.77%	-0.72%	-0.55%	1.36%
Interior Wall	-0.92%	2.07%	1.09%	0.38%	-0.54%	-1.09%	0.52%
Ambient	0.00%	0.09%	0.25%	0.40%	0.54%	0.76%	1.65%

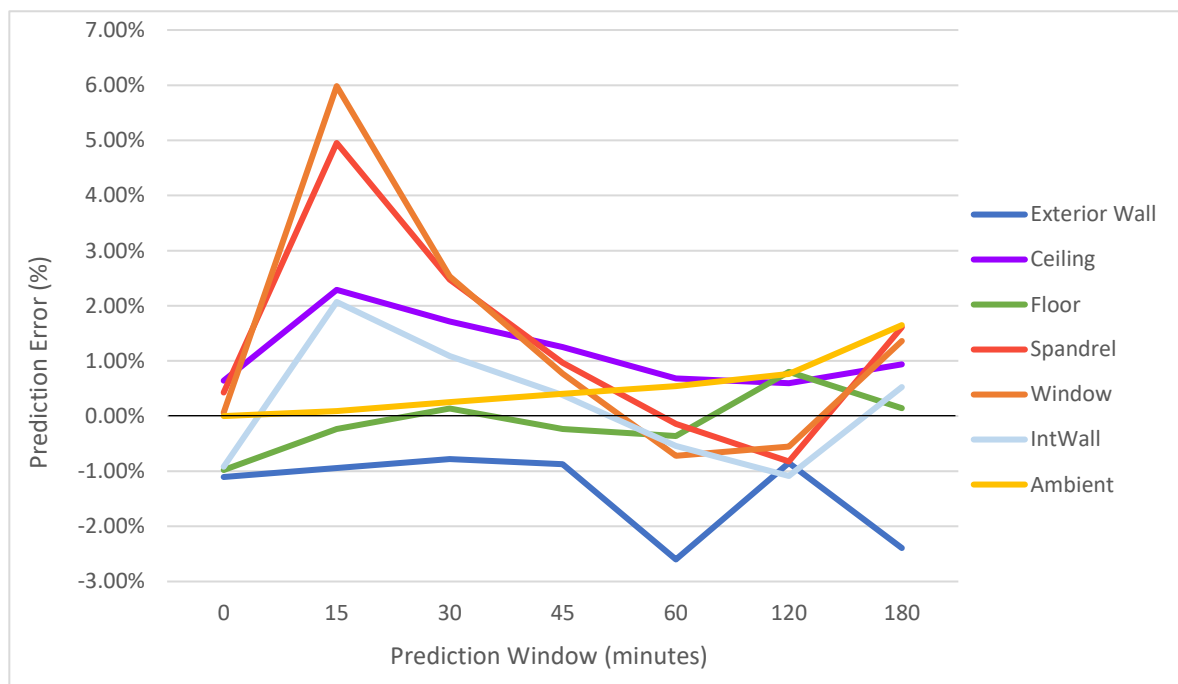


*Figure 63 January 8<sup>th</sup>, 2018 Prediction Error for all Building Elements along with Ambient Temperature*

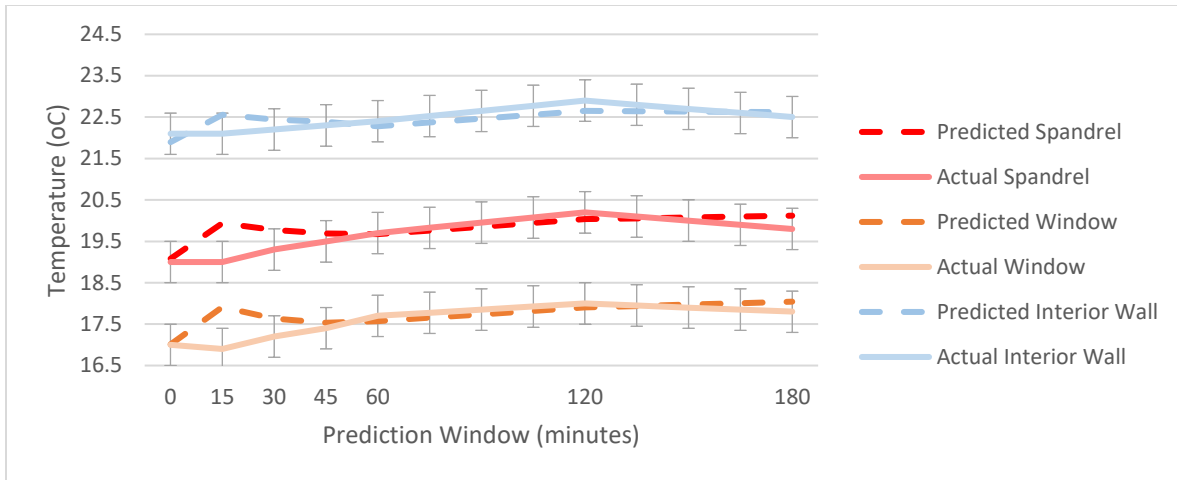


Figure 64 January 8th, 2018 Predicted vs Actual Surface Temperature for the Window, Spandrel Panel, and Interior Wall

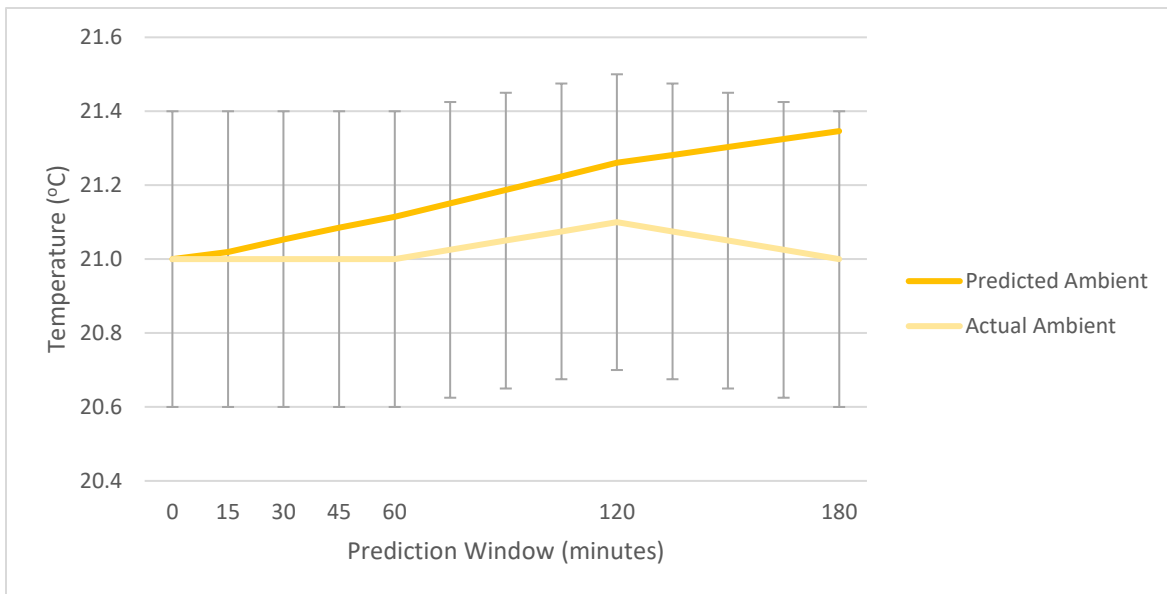


Figure 65 January 8th, 2018 Predicted vs Actual Ambient Temperature

The results from the February 7<sup>th</sup> simulation, summarized in Table 54 and Figure 66, demonstrate very strange results with the exterior wall having a very high prediction error. The model predicts the exterior temperature around 18°C, which is a much lower value than other simulations and much lower than the actual value as shown in Figure 67. There is believed to be caused by a data value within this dataset that is slightly off, resulting in a large prediction error. Inspection of the data does not indicate any data point that is obviously wrong however, a value that is slightly different from previous simulations can produce the error when

propagated within the linear regression equation. All of the other building elements within this model demonstrate prediction accuracy to within 7%. The ambient temperature has very good prediction results, as shown in Figure 68, despite the high error in the exterior wall temperature; the predicted ambient temperature is within 0.2°C of the actual temperature.

*Table 54 Prediction Error for Temperatures of Simulated Elements as a Function of Prediction Window Duration for February 7, 2018 ( $T_{out}=-3.57^{\circ}C$ , wind speed ranging from 0.5-1.5m/s, and solar radiation 50W/m<sup>2</sup>)*

Prediction Window							
	0 minutes	15 minutes	30 minutes	45 minutes	60 minutes	120 minutes	180 minutes
Exterior Wall	-17.34%	-18.32%	-18.81%	-19.20%	-17.75%	-17.07%	-15.78%
Ceiling	-3.06%	-3.47%	-3.07%	-3.55%	-3.49%	-4.34%	-4.12%
Floor	0.10%	-0.66%	-0.89%	-1.00%	-1.14%	-2.70%	-2.06%
Spandrel	-3.75%	-5.56%	-4.41%	-5.45%	-6.54%	-6.36%	-4.85%
Window	-5.73%	-6.62%	-2.60%	-5.97%	-6.42%	-6.25%	-3.88%
Interior Wall	-0.66%	-2.51%	-2.75%	-4.01%	-5.81%	-8.82%	-8.25%
Ambient	0.00%	0.34%	0.70%	-0.03%	-0.23%	-0.40%	0.42%

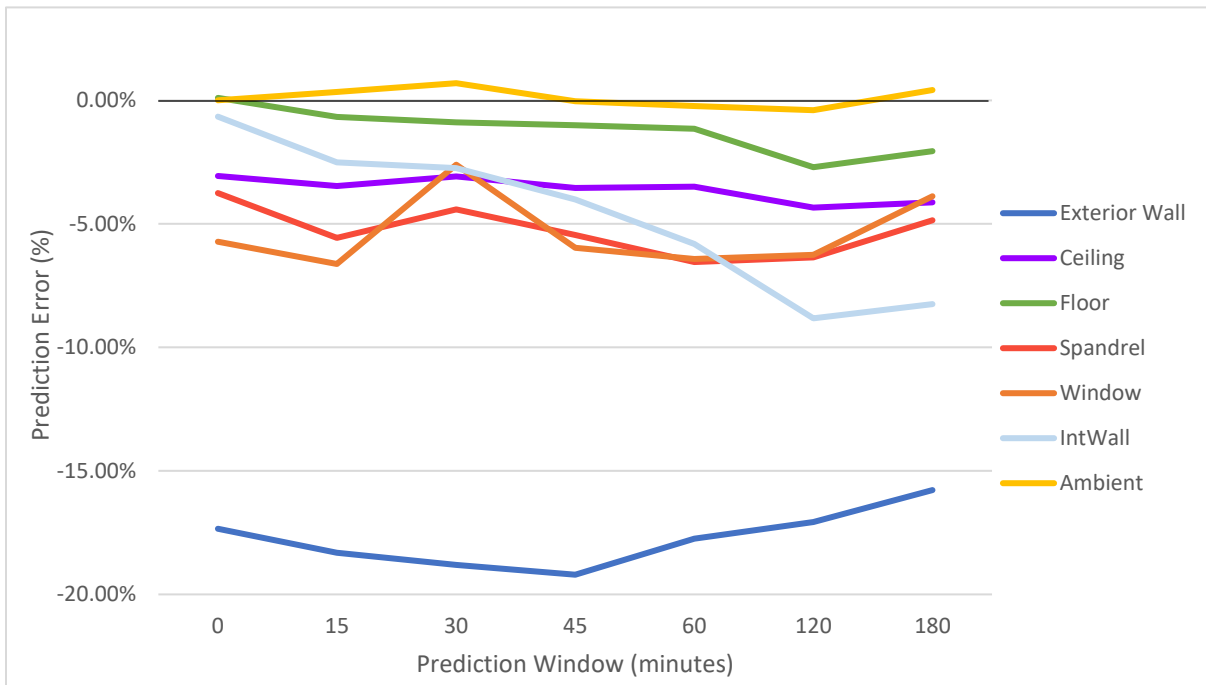


*Figure 66 February 7<sup>th</sup>, 2018 Prediction Error for all Building Elements along with Ambient Temperature*

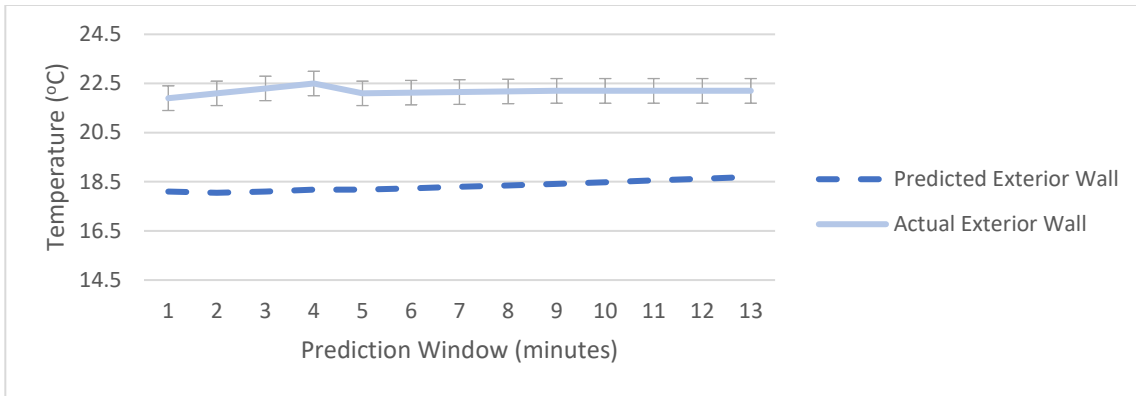


Figure 67 February 7th, 2018 Predicted vs Actual Surface Temperature of the Exterior Wall

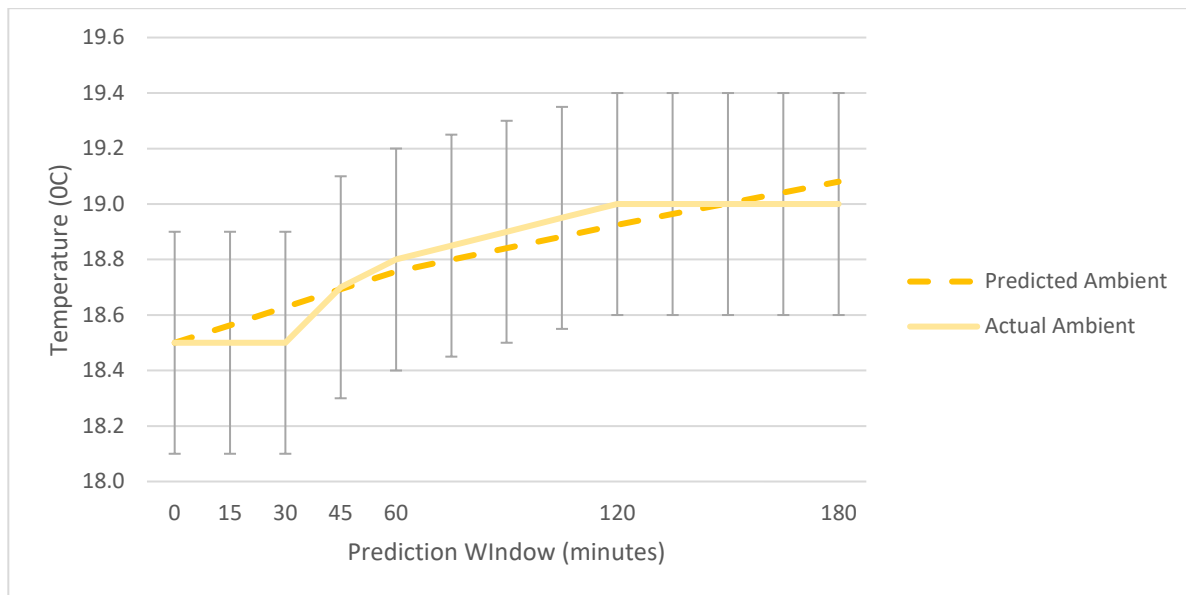


Figure 68 February 7<sup>th</sup>, 2018 Predicted vs Actual Ambient Temperature

The simulation results for December 8<sup>th</sup>, illustrated in Table 55 and Figure 69, are similar to those in the January 8<sup>th</sup> simulation, with the window, spandrel, and interior wall elements mimicking the same prediction error pattern. All three elements display an increase in predicted temperature at the 45-minute Prediction Window as shown in Figure 70. This simulation does not indicate a long wave radiation increase, as shown in the January 8<sup>th</sup> simulation. The increase in predicted temperature could be a combination of lower wind speeds occurring at that time along with an increase in the left vent airflow rate. These two values are significant variables in the building element regression models and could therefore be influencing the results. The ambient temperature results demonstrate the temperature being predicted to within 0.2°C for the entire simulation (Figure 71). The variability of the actual ambient temperature in this

model, similar to previous simulations, can be connected to higher ventilation airflow rates at this time.

*Table 55 Prediction Error for Temperatures of Simulated Elements as a Function of Prediction Window Duration for December 8, 2017 ( $T_{out}=1.04^{\circ}\text{C}$ , wind speed ranging from 2.5-3.5m/s, and solar radiation 50W/m<sup>2</sup>)*

Prediction Window							
	0 minutes	15 minutes	30 minutes	45 minutes	60 minutes	120 minutes	180 minutes
Exterior Wall	1.54%	3.66%	2.52%	0.05%	2.77%	0.90%	1.86%
Ceiling	1.37%	1.37%	1.91%	1.44%	1.06%	1.64%	0.84%
Floor	1.12%	2.62%	2.61%	-0.25%	-0.82%	-0.11%	1.37%
Spandrel	1.34%	-0.36%	0.25%	4.63%	0.35%	0.63%	1.08%
Window	2.61%	0.14%	0.18%	8.05%	1.97%	1.59%	1.72%
Interior Wall	-0.52%	-0.75%	-0.73%	2.56%	-0.60%	-1.23%	-1.89%
Ambient	0.00%	-0.39%	0.14%	0.68%	0.31%	-0.23%	0.85%

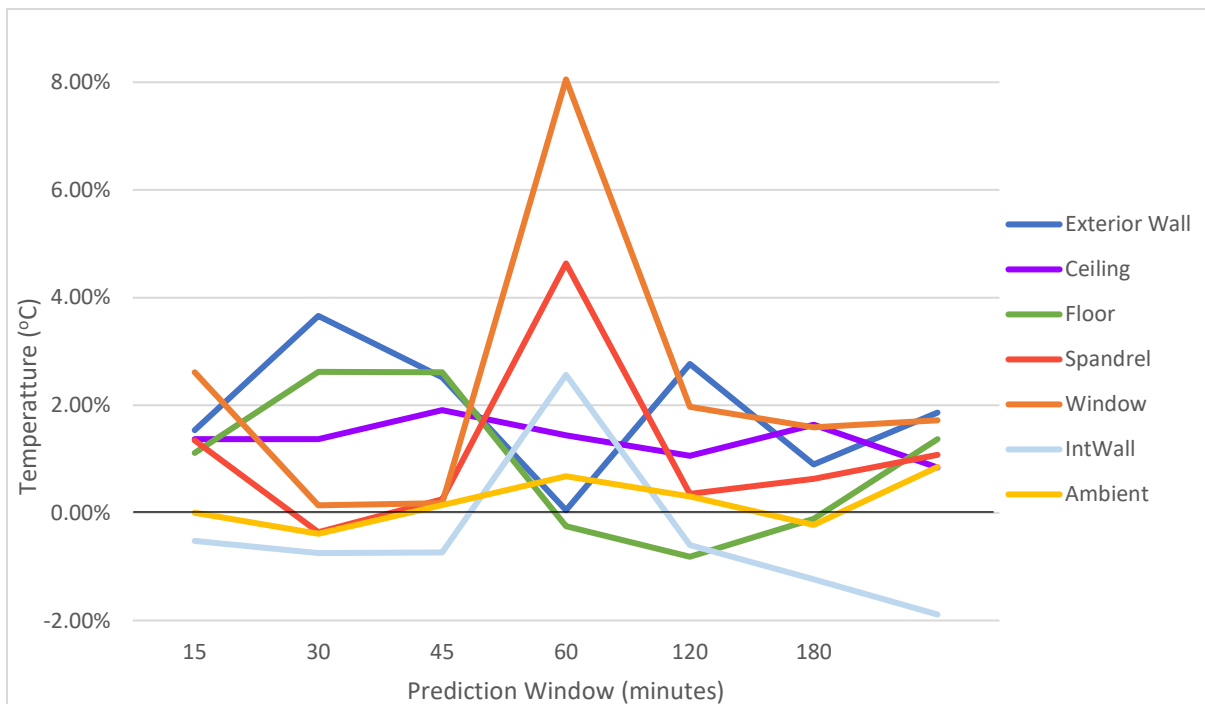


*Figure 69 December 8<sup>th</sup>, 2017 Prediction Error for all Building Elements along with Ambient Temperature*

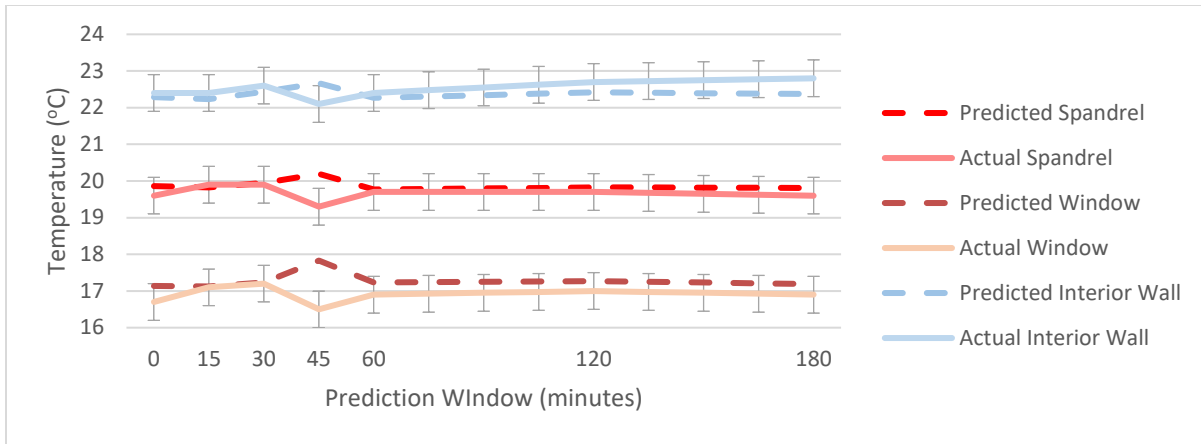


Figure 70 December 8th, 2017 Predicted vs Actual Surface Temperature for the Window, Spandrel Panel, and Interior Wall

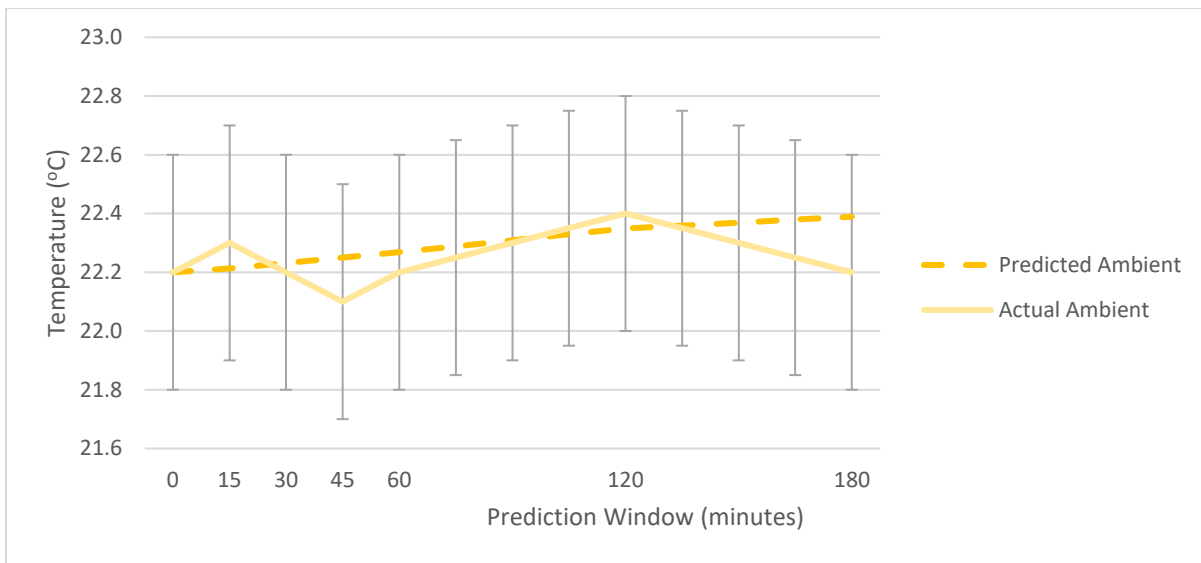


Figure 71 December 8th, 2017 Predicted vs Actual Ambient Temperature

The simulation for December 5<sup>th</sup> demonstrated all of the building element surface temperatures being underpredicted, as shown in Table 56 and Figure 72. The window and spandrel results demonstrate much lower predicted temperatures until the 45-minute Prediction Window, when both temperatures have a significant increase (Figure 73). This jump is caused by the simulation changing from the occupied regression models to the unoccupied regression models, as the occupancy drops to 0 at the 45-minute Prediction Window. All of the other building elements have a relatively constant prediction error within 7%. The ambient temperature for this simulation displays prediction results within 0.1°C of the actual temperature for the entire simulation, as illustrated in Figure 74.

Table 56 Prediction Error for Temperatures of Simulated Elements as a Function of Prediction Window Duration for December 5, 2017 ( $T_{out}=10.93^{\circ}\text{C}$ , wind speed ranging from 2-4m/s, and solar radiation  $50\text{W}/\text{m}^2$ )

Prediction Window							
	0 minutes	15 minutes	30 minutes	45 minutes	60 minutes	120 minutes	180 minutes
Exterior Wall	-4.25%	-4.46%	-2.71%	-8.37%	-8.68%	-9.44%	-10.26%
Ceiling	-6.41%	-6.50%	-6.87%	-6.16%	-6.02%	-6.90%	-6.87%
Floor	-5.31%	-6.04%	-5.39%	-5.12%	-4.41%	-5.07%	-5.62%
Spandrel	-9.20%	-8.83%	-6.38%	-2.16%	-3.33%	-5.48%	-6.98%
Window	-15.33%	-16.30%	-15.49%	-3.26%	-4.77%	-7.04%	-8.21%
Interior Wall	-6.80%	-7.15%	-5.38%	-4.72%	-5.35%	-6.57%	-7.34%
Ambient	0.00%	-0.10%	-0.22%	-0.33%	-0.43%	0.33%	-0.46%

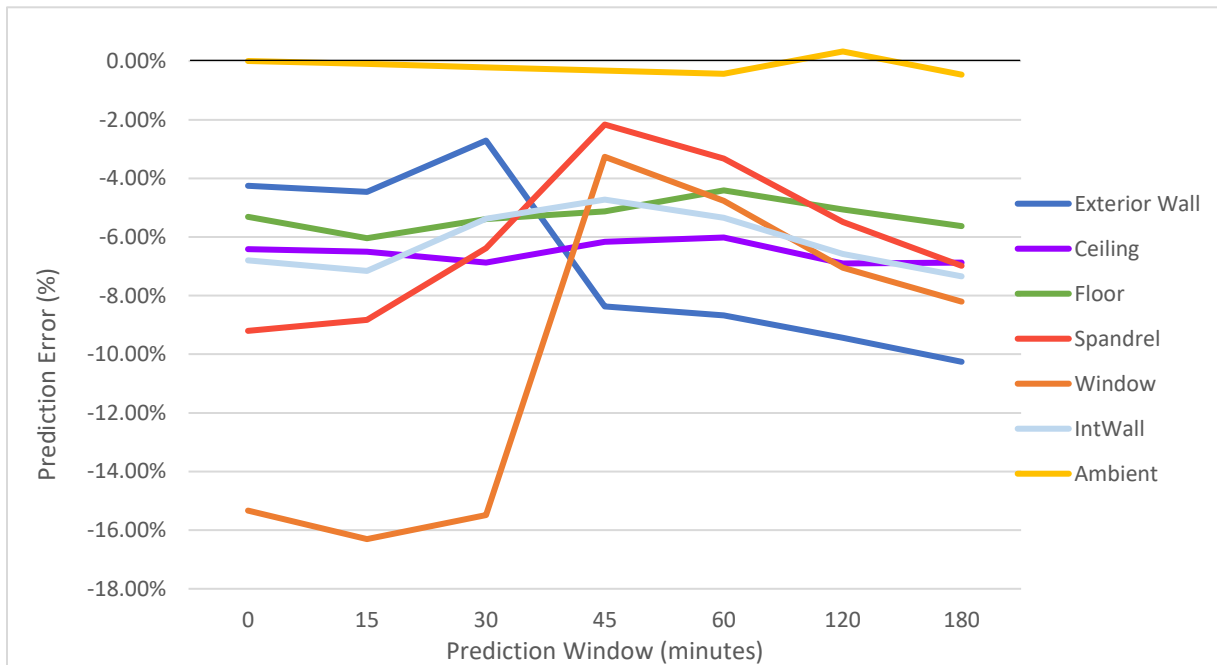


Figure 72 December 5<sup>th</sup>, 2017 Prediction Error for all Building Elements along with Ambient Temperature

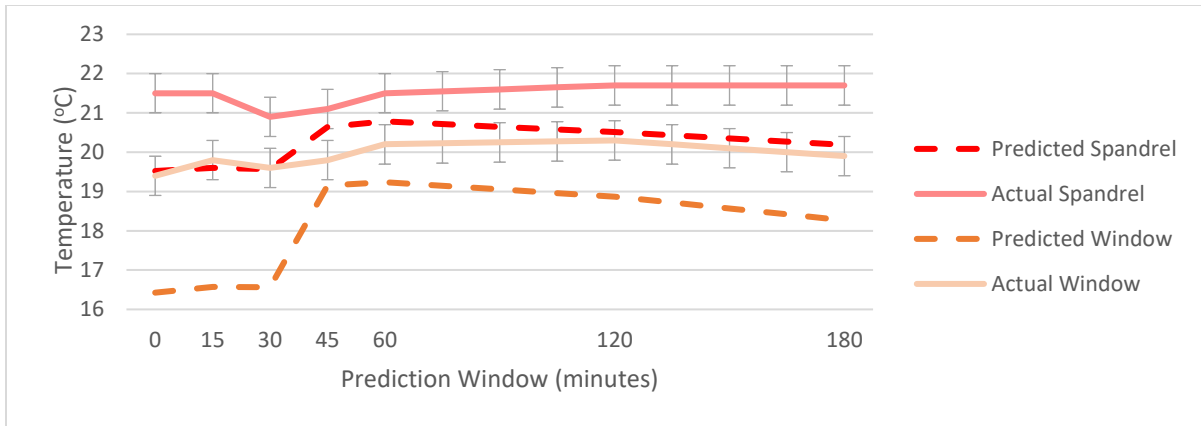


Figure 73 December 5th, 2017 Predicted vs Actual Surface Temperature for the Window and Spandrel Panel

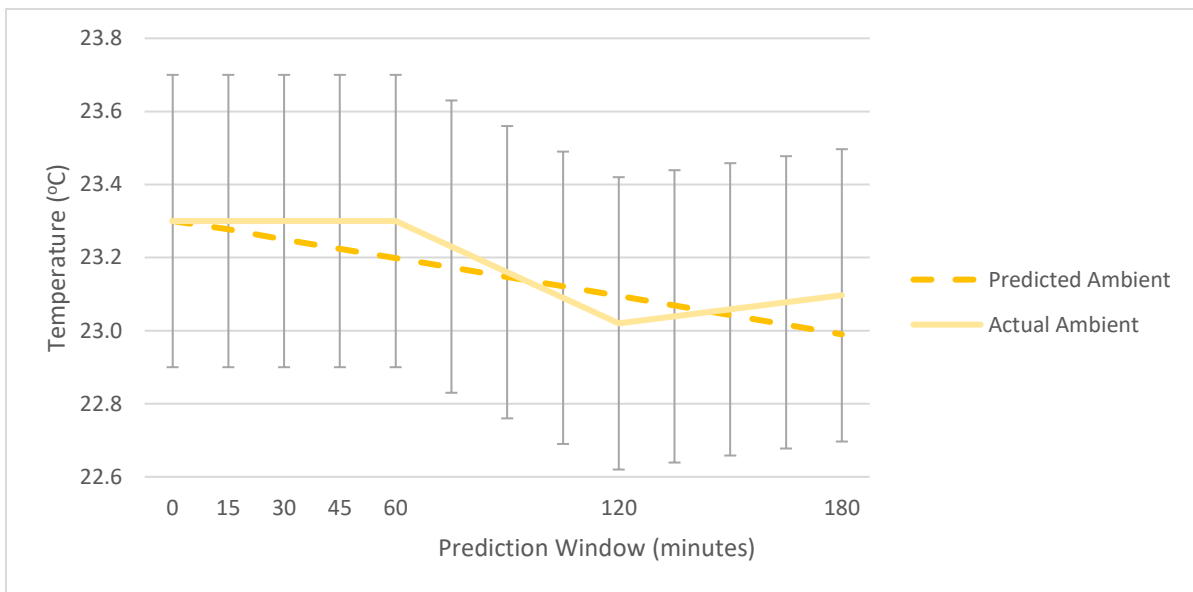


Figure 74 December 5<sup>th</sup>, 2017 Predicted vs Actual Ambient Temperature

## 6.8 Summary of Final Model Results

The final model demonstrated surface temperature prediction results for the building elements can be off by as much as 20% from the true value. For the large majority of the models the interior elements, ceiling, floor, and interior wall, had prediction errors within +/- 7%. The exterior wall can be included within this group with the exception of the February 7<sup>th</sup> simulation, which had abnormal prediction results. Overall, the window and spandrel panel had the worst prediction results, due to their lower thermal mass, with prediction errors of up to 16%. Many of the occupied simulations demonstrated the window and spandrel having jumps

in the prediction results caused by the model switching between occupied and unoccupied regression models. These elements were impacted the most due to their low thermal mass and resistivity properties. It can be observed in the regression model analysis that these models, as well as the interior wall, had higher RMSE and lower adjusted  $R^2$  values compared to the other building elements.

The ambient temperature was predicted for all simulation days within 1.5% of the actual value despite the large surface temperature prediction errors for the building elements. These results are all within the measurement error of the ambient temperature sensor of the test cell. It is believed that the accuracy of the predicted ambient temperature is mostly due to the optimized internal mass heat capacity value. One observation from these results is a strong influence from the interior lighting heat load on the predicted ambient temperature which, led to overprediction of the ambient temperature in multiple occupied simulations.

## 6.9 Overall Summary of Results

The ambient temperature prediction results at the 180-minute Prediction Window for the G1v1, G1v3, and Final Model (G2) are compared in Figure 75. As the neural network analysis demonstrated none of the neural networks performing better than the linear regression models, no grey box G3 model came to fruition. The results from this comparison demonstrate all three models having best and worst prediction performances. The G1v1 model is observed in Figure 75 to have the most extreme prediction errors for simulation days of February 7<sup>th</sup>, January 8<sup>th</sup>, and December 8<sup>th</sup>. The larger errors occur for the G1v1 occupied models due to the use of the original internal heat capacity value in this model.

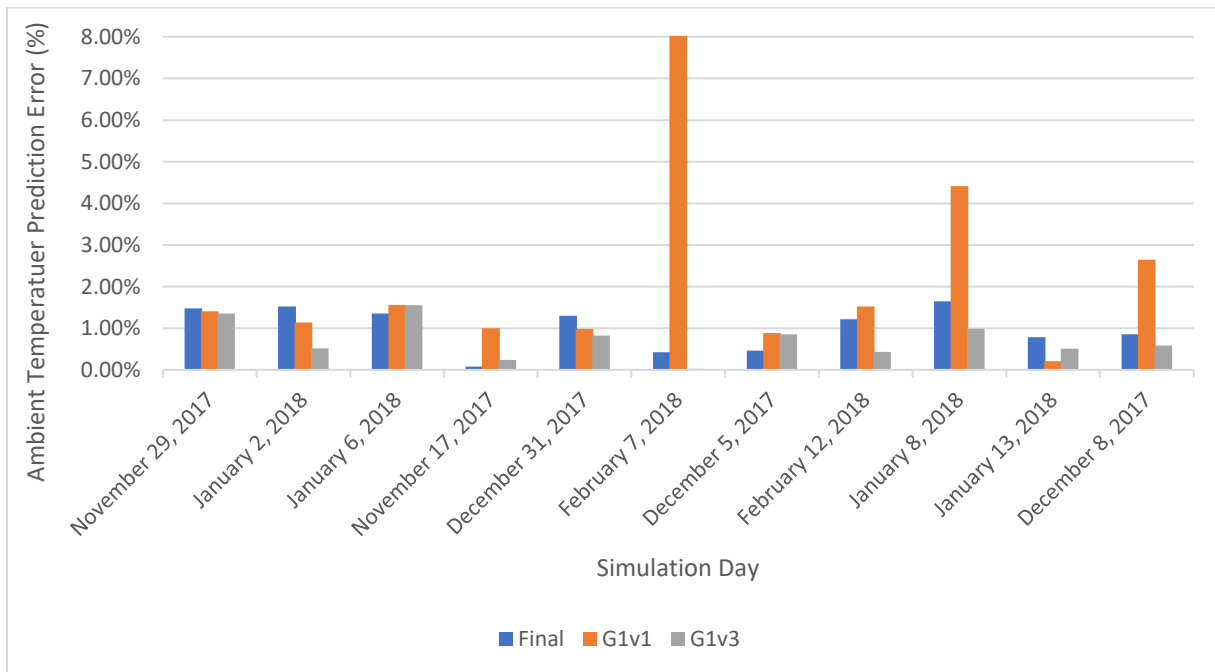


*Figure 75 Comparison of Ambient Temperature Prediction Performance for the G1v1, G1v3, and Final Model at the Three-Hour Prediction Window.*

To analyze the performance of each grey box model iteration in more detail, the full simulation period results for the eleven simulation days are compared. The nighttime occupied simulations are shown in Figure 76- Figure 78 .

The November 17<sup>th</sup> simulation, shown in Figure 76, demonstrates the G1v1 model having decreasing prediction error. This is due to the model predicting a continual decrease in the ambient temperature, when in actuality the ambient temperature remains relatively constant.

The G1v3 and Final Model predicted a steadier ambient temperature, due to their higher internal heat capacity, resulting in better prediction results.

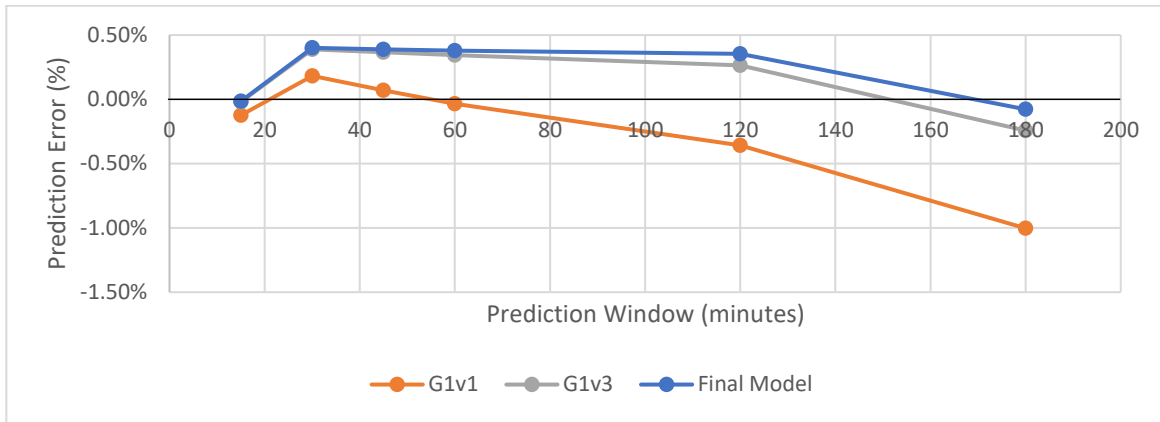


*Figure 76 Comparison of the G1v1, G1v3, and the Final Model Performance for the Simulation day of November 17th, 2017*

All three models demonstrated almost identical results for the November 29<sup>th</sup> simulation, as shown in Figure 77. The major jumps in the prediction error is due to fluctuations in the actual ambient temperature measurements.

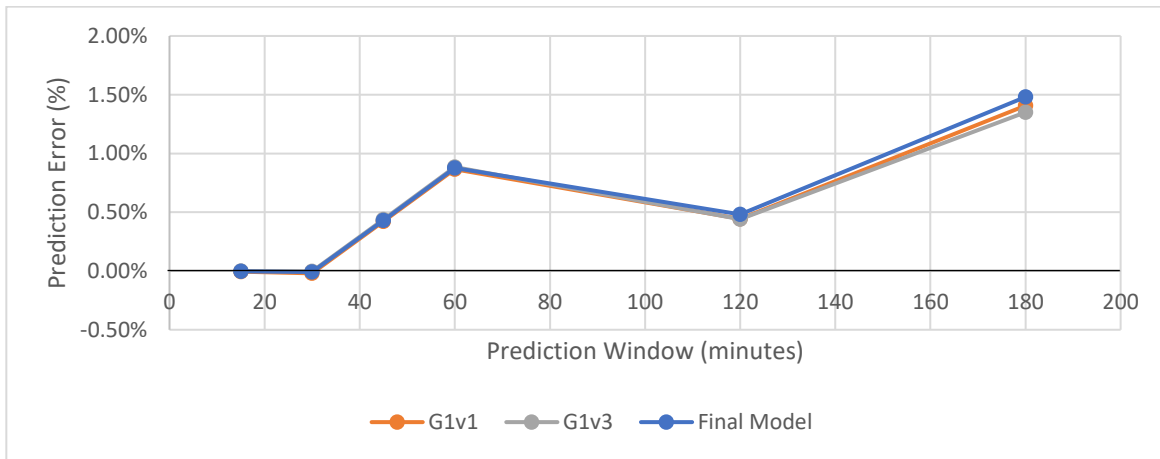


*Figure 77 Comparison of the G1v1, G1v3, and the Final Model Performance for the Simulation day of November 29th, 2017*

The January 6<sup>th</sup> simulation day, illustrated in Figure 78, resulted in the Final model having the lowest prediction error. As the only difference between the Final model and the G1v3 model is the use of multiple linear regression models for the building elements, these regression models are the cause of the differing prediction performance. The decrease in prediction error is caused

by the actual ambient measurement increasing throughout the simulation, either due to measurement fluctuation or a heating load not monitored by the test cell.

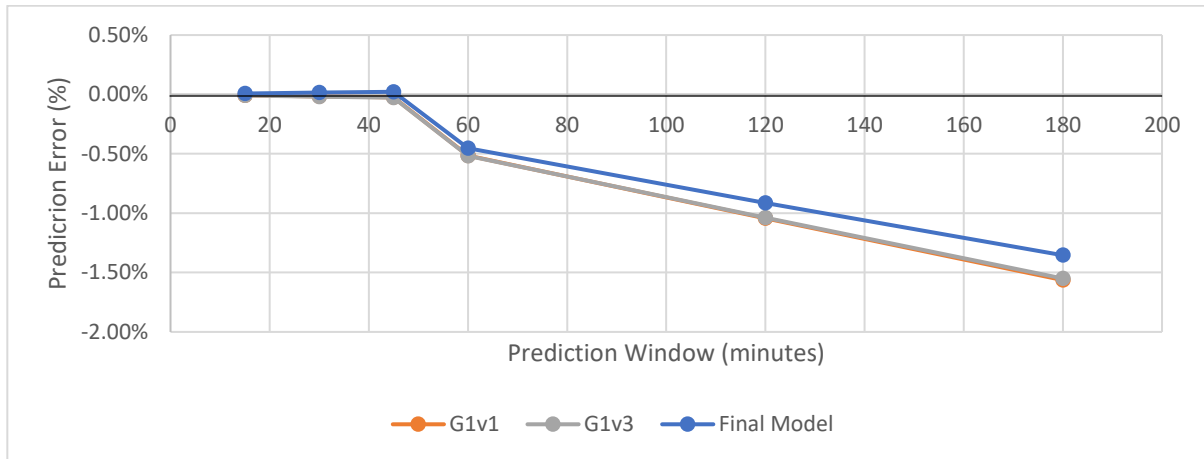


*Figure 78 Comparison of the G1v1, G1v3, and the Final Model Performance for the Simulation day of January 6<sup>th</sup>, 2018*

The results for the daytime unoccupied models demonstrated greater variance between the three grey box model performances in comparison to the nighttime unoccupied simulations as shown in Figure 79-Figure 81. All three simulation days December 31<sup>st</sup> (Figure 79), January 13<sup>th</sup> (Figure 80), and January 2<sup>nd</sup> (Figure 81) resulted in the Final Model having the greatest prediction error with the G1v3 model having the lowest prediction error. The Final Model having lower accuracy than the G1v1 model is an unexpected result as it was hypothesized it would perform better with the larger internal heat capacity.

The December 31<sup>st</sup> simulation shows both the G1v3 and G1v1 models performing better than the Final Model, as shown in Figure 79. This is caused by the prediction performance of the surface temperature regression models. The overall shape of the prediction error is caused by the actual ambient temperature gradually decreasing near the end of the simulation. As previously stated, due to measurement device fluctuations or due to the influence of a heat load not monitored in the test cell.

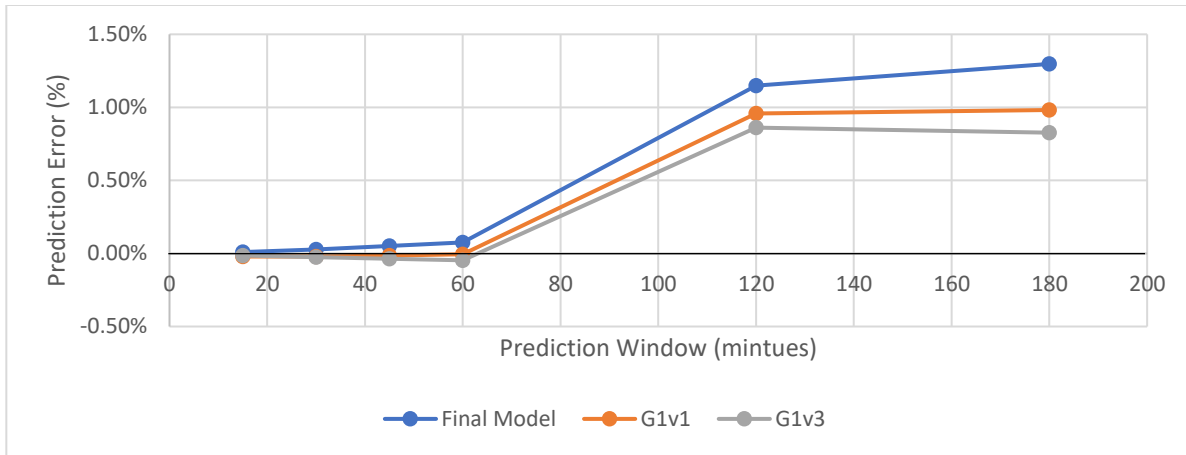


*Figure 79 Comparison of the G1v1, G1v3, and the Final Model Performance for the Simulation day of December 31, 2017*

The January 13<sup>th</sup> simulation demonstrated the Final Model and the G1v3 model having more similar results compared to the December 31<sup>st</sup> simulation, as shown in Figure 80. The prediction error shape is caused by the actual ambient temperature fluctuating throughout the simulation. The actual temperature increases at 15-minute Prediction Window, creating the under prediction, then decreases at the 45-minute Prediction Window, creating the overprediction, and finally increasing again at the 60-minute Prediction Window.

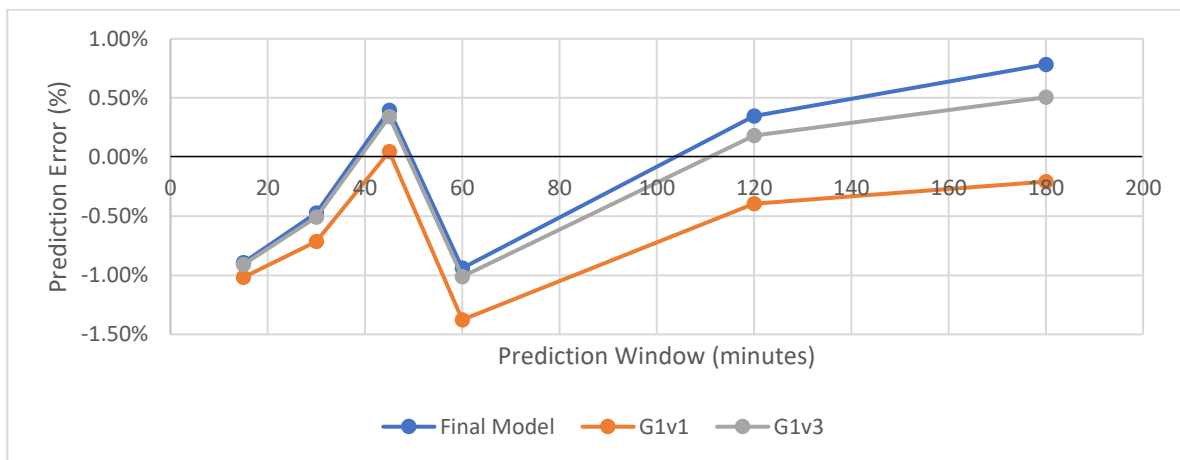


*Figure 80 Comparison of the G1v1, G1v3, and the Final Model Performance for the Simulation day of January 13, 2018*

The results from the January 2<sup>nd</sup> simulation, shown in Figure 81, illustrates the G1v3 model performing most accurately while the Final model performs least accurately. The discrepancy in results is caused by the surface temperature prediction results for the regression models in

the Final Model. The overall prediction error shape for this simulation is caused by a gradual decrease in the actual ambient temperature throughout the simulation while the simulations predict the ambient to stay at a relatively constant temperature; creating a gradually increasing over prediction.

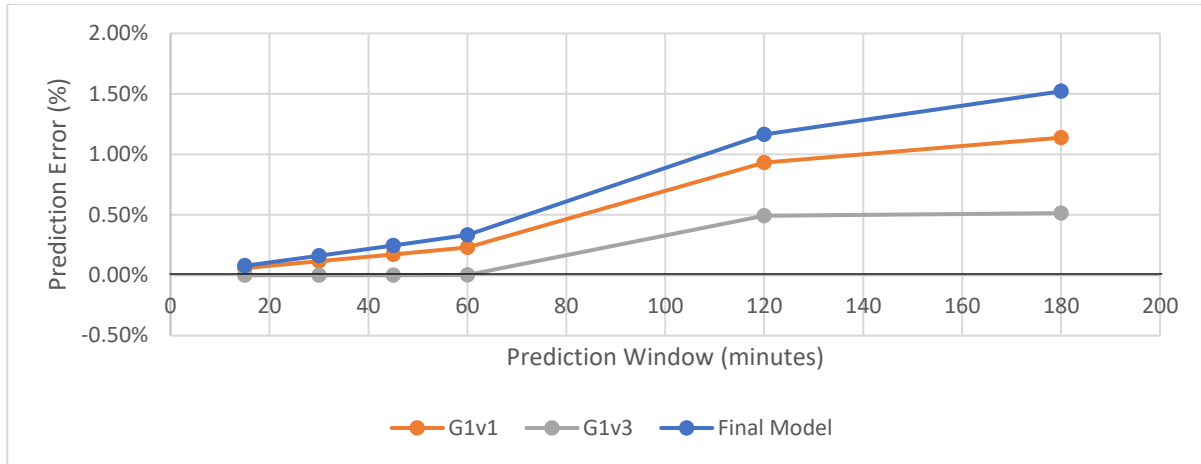


*Figure 81 Comparison of the G1v1, G1v3, and the Final Model Performance for the Simulation day of January 2, 2018*

The daytime occupied simulations, shown in Figure 82-Figure 86, show the G1v1 model consistently having the largest prediction error. These simulations indicate most visibly, of all the simulation groups, the improved prediction performance with the larger interior heat capacity. For the majority of the simulations, the G1v3 model has the lowest prediction error with the exception of the December 5<sup>th</sup> (Figure 86) simulation day when the Final Model has the lowest prediction error. For the February 12<sup>th</sup> simulation (Figure 82), the Final Model is observed to have a prediction performance in the middle of the G1v1 and the G1v3 model prediction results, while the January 8<sup>th</sup> (Figure 83), February 7<sup>th</sup>(Figure 84), and December 8<sup>th</sup> (Figure 84) models demonstrate the Final Model having comparable results to the G1v3 model.

The simulation for February 12<sup>th</sup> demonstrates the Final model performing best for the majority of the simulation until the 180-minute Prediction Window, as shown in Figure 83 . The shape of the prediction results is caused by the actual ambient temperature behavior which, increases at the beginning of the simulation and decreases at the end. This causes all the models to overpredict the ambient temperature at the end of the simulation.

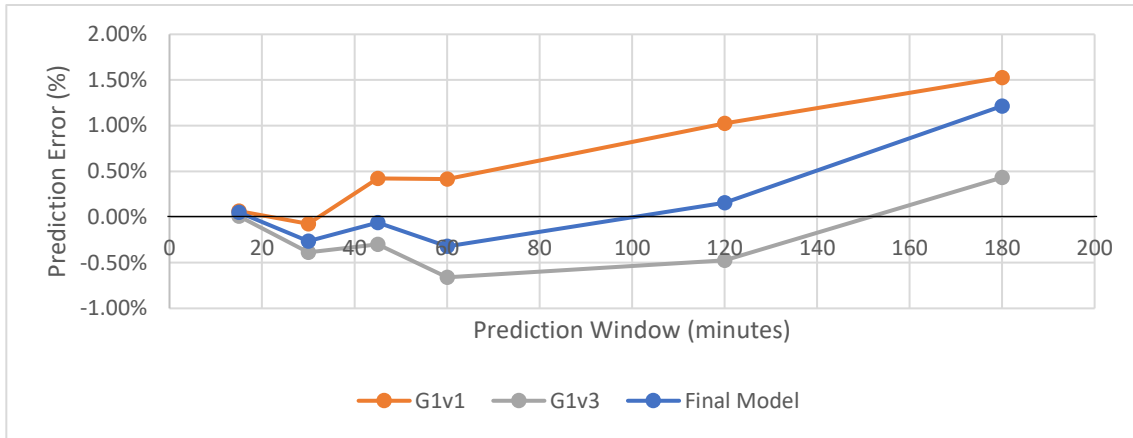


*Figure 82 Comparison of the G1v1, G1v3, and the Final Model Performance for the Simulation day of February 12, 2018*

The simulation results for January 8<sup>th</sup>, illustrated in Figure 83, demonstrates the Final model and the G1v3 model having similar prediction error results. The G1v1 model performs significantly worse, with prediction error of almost 5%. The actual ambient temperature does not deviate very much during this simulation, the Final model and the G1v3 model closely replicate this while the G1v1 model increases in temperature throughout the simulation.

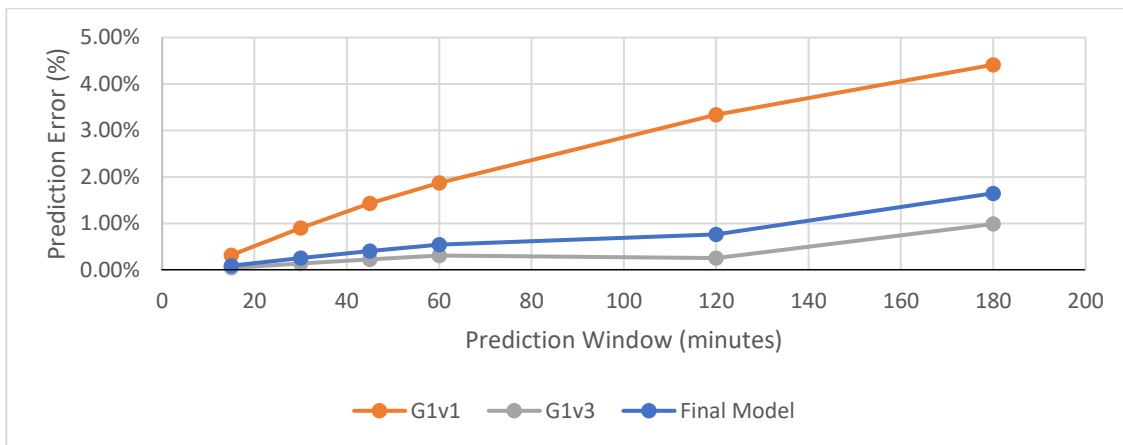


*Figure 83 Comparison of the G1v1, G1v3, and the Final Model Performance for the Simulation day of January 8, 2018*

The February 7<sup>th</sup> simulation closely resembles the previous January 8<sup>th</sup> simulation, as shown in Figure 84. The G1v1 model is observed to have significantly higher prediction error compared to the Final Model and the G1v3 model. This is due to the G1v1 model having lower internal heat capacity value. For this simulation period the actual ambient temperature does not have significant variance, only a slight increase in temperature at the 45-minute Prediction Window

which, can be seen in the prediction error of the three models. The more accurate prediction results for the Final Model and the G1v3 model, similar to other simulations, is due to their higher internal heat capacity values that slows the thermal dynamics appropriately.

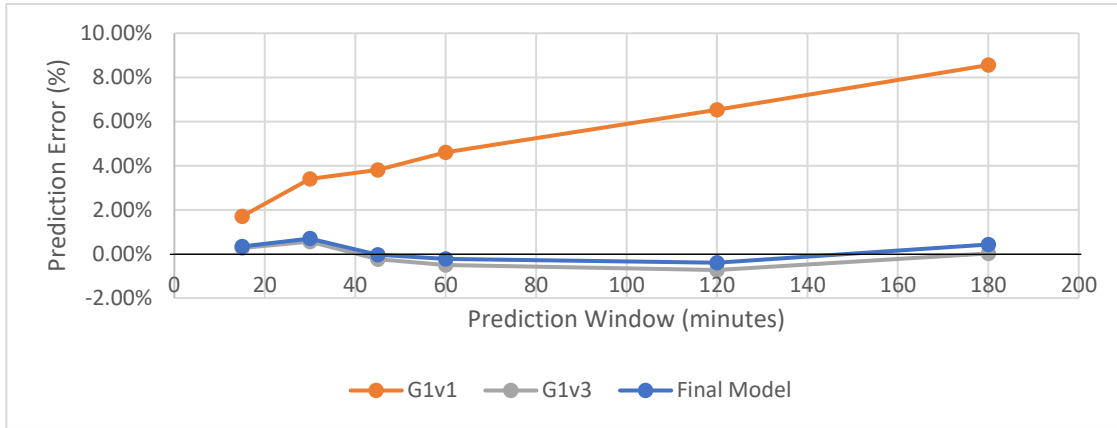


Figure 84 Comparison of the G1v1, G1v3, and the Final Model Performance for the Simulation day of February 7, 2018

The December 8<sup>th</sup> simulation, illustrated in Figure 85, demonstrates similar results to the previous models, with significantly worse prediction performance for the G1v1 model compared to the Final and G1v3 models. The jumps in prediction errors are caused by fluctuations in the actual ambient temperature measurements for this simulation day.

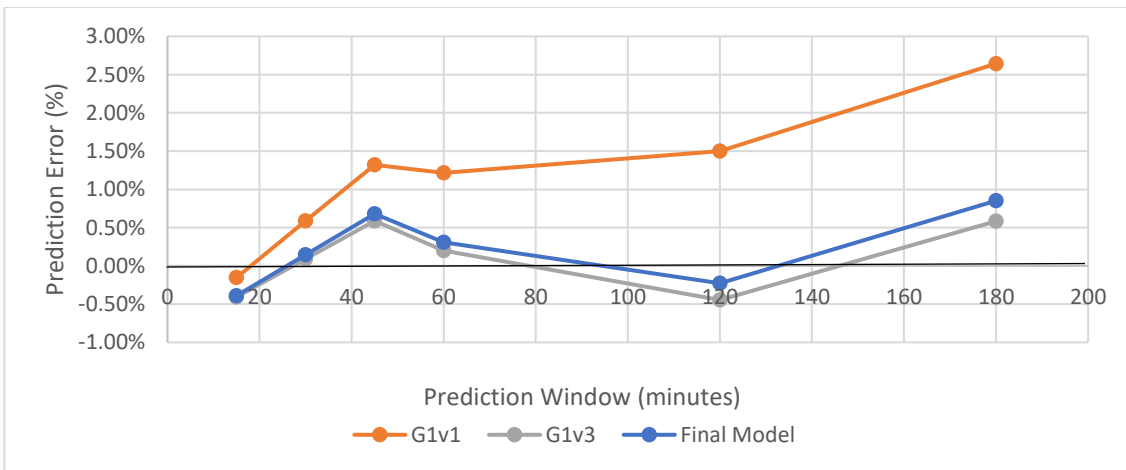
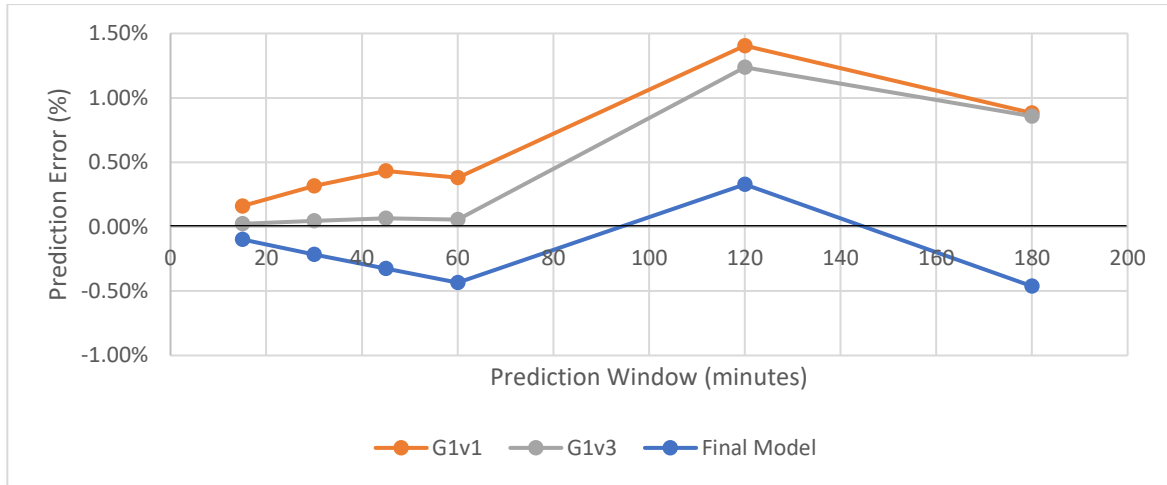


Figure 85 Comparison of the G1v1, G1v3, and the Final Model Performance for the Simulation day of December 8, 2017

The December 5<sup>th</sup> simulation, illustrated in Figure 86, demonstrates much different results compared to the other occupied simulations. This is due to the higher accuracy in the building

element regression models for this particular day. The prediction error results, where the G1 models over predicts at the end of the simulation while the Final model is able to accurately represent the decrease in temperature, may be due to the Final model's ability to change the regression models based on occupancy which, changes throughout this simulation.



*Figure 86 Comparison of the G1v1, G1v3, and the Final Model Performance for the Simulation day of December 5, 2017*

### 6.9.1 Findings from Model Comparison

Overall, the Final Model does not demonstrate the most accurate prediction results of the three model iterations, however it shows similar results to the G1v3 model. This is substantial as the G1v3 model represents the building elements with their RC network physical representations. The Final Model performing to the same level of accuracy as this model indicates that the accuracy of a grey box model can be maintained without the building construction specifications.

## 6.10 Sensitivity Analysis

The goal of this research is to create a grey box thermal dynamic model that expands the range of buildings capable of implementing MPC HVAC systems with grey box thermal dynamic models. The model created in this study was made specifically for the test cell using a process of calculated steps. A sensitivity analysis was conducted to determine the ability of the model to be implemented within a different building for use in MPC HVAC systems. The sensitivity analysis conducted includes: investigating the ability to determine the internal heat capacity using the final model, analyzing the time period required for training the linear regression models to achieve the same level of accuracy, and testing the model outside the training season.

### *6.10.1 Heat Capacity with Final Model*

The results from the parameter estimation analysis using the Final Model are compared to the results from the G1 model in Table 57. The results from the parameter estimation using the Final Model were observed to be for the most part lower than the results from the G1 model. As discussed in Section 6.3, it is hypothesized that the true internal heat capacity value of the test cell is somewhere between 112kJ/K-250kJ/K. The results from the Final Model parameter estimation demonstrated four values within this hypothesized range, as highlighted in Table 57. As previously stated, the use of a constant data stream in an optimization algorithm instead of the three-hour blocks used within this analysis would produce the true optimal internal heat capacity value. It is also noted the large variance in internal heat capacity values found on the different simulation days; these are poor results, caused by error in the model or in the parameter estimation method used.

*Table 57 Heat Capacity Values found for the Final Grey Box Model in Comparison to those found previously in the G1 Model.*

<b>Simulation Day</b>	<b>G1v3 Cp (kJ/kg)</b>	<b>Final Cp (KJ/kg)</b>
November 17th	112.66	41.50
November 29th	457.90	122.06
January 6th	1 834.20	223.53
December 31st	39.50	114.13
January 13th	105.43	98.91
January 2nd	219.07	116.26
February 12th	77.76	159.93
January 8th	252.67	532.35
February 7th	239.03	263.18
December 8th	93.91	102.12
December 5th	38.42	307.06

### **6.10.2 Training Period**

Grey box models were created using one week, two weeks’, and one months’ worth of training data. Linear regression equations were created for each model using the same split/general structures previously determined. The results from the linear regression analysis demonstrated increased improvement in performance for the thermally lightweight elements: the window, spandrel panel, and interior wall, with increasingly large amounts of training data points. The thermally massive elements, however, did not demonstrate any correlation between performance and the amount of training data points. The window and spandrel panel regression models demonstrated the exterior temperature being the most significant variable. All other building elements demonstrated inconsistencies in the significant variables. It was observed that the February models, compared to the December models and models determined previously in this study, were more highly influenced by the ventilation data points. This may be due to the ventilation loads gradually transitioning to cooling rather than heating near the end of the month. As the ventilation system is the only source of cooling in the test cell, this is the dominant source of conditioning during cooling season.

The results of the grey box model when using different lengths of training data sets are shown in Table 58. The results from this analysis demonstrate training with two weeks of data gives the same, or unexpectedly, better results than the final model. The models with one week of training data resulted in worse RMSE, 0.8°C higher, compared to the model using two weeks

of data. Surprisingly, the one-month data also had worse prediction results than the two-week data. This may be caused by the large number of unoccupied periods in the month of December from holidays, skewing the model. Overall, these results demonstrate that the model can be trained well using a collection period of two weeks.

*Table 58 Performance of the Final Model when Trained with 1 week, 2 weeks, and 4 weeks of data*

	<b>Final Model 4 months</b>	<b>December 1 week</b>	<b>February 1 week</b>	<b>December 2 weeks</b>	<b>February 2 weeks</b>	<b>December 1 month</b>
RMSE	0.1280	0.1792	0.2034	0.1274	0.1265	0.1365
MAE	0.0931	0.1356	0.1381	0.0932	0.0911	0.1005
MAPE	0.429%	0.631%	0.650%	0.432%	0.418%	0.465%

The ability to determine the internal mass heat capacity value was also tested with these shorter training models, as shown in Table 59. The results demonstrate all training models found at least two values within the hypothesized internal heat capacity value range, 112kJ/K-250kJ/K, determined in Section 6.3. As previously stated in the other parameter estimation sections of this paper, using a constant string of data within an optimization function would find the true internal heat capacity value of the test cell, and the variance in results indicate something amiss in this procedure. It can be derived from this analysis that the two weeks of data required to train the grey box model is plenty of data to find the optimal internal heat capacity value as two values within the hypothesized range were found here with only 33 hours of data (11 simulations, 3 hours in length).

*Table 59 Internal heat capacity values found from the parameter estimation tool for the 1 week, 2 week and one-month models*

	<b>Final Model 4 months (kJ/K)</b>	<b>December 1 week (kJ/K)</b>	<b>February 1 week (kJ/K)</b>	<b>December 2 weeks (kJ/K)</b>	<b>February 2 weeks (kJ/K)</b>	<b>December 1 month (kJ/K)</b>
17-Nov	41.50	178.41	148.37	163.75	138.92	118.71
29-Nov	122.06	83.83	373.71	176.90	100.50	1,115.89
06-Jan	223.53	911.66	686.33	256.83	911.66	301.57
31-Dec	114.13	268.81	92.53	209.37	63.99	110.16
13-Jan	98.91	233.37	583.57	110.16	492.20	201.38
02-Jan	116.26	1,210.21	222.40	1,189.19	70.32	1,132.61
12-Feb	159.93	206.28	576.08	133.89	519.35	205.95
08-Jan	532.35	1,324.22	1,099.06	806.19	1,855.86	865.65
07-Feb	263.18	463.30	602.22	397.13	553.92	368.03
08-Dec	102.12	913.42	1,069.80	10.54	1,172.93	384.85
05-Dec	307.06	167.78	976.46	138.02	145.58	72.77

### 6.10.3 Seasonal Sensitivity

To test the Final Model’s generalisation ability, the model was simulated for a period outside the training season. This research was conducted for the winter season therefore, the sensitivity analysis was conducted during the spring, on April 9<sup>th</sup> 2018, during daytime occupied conditions. The exterior and interior conditions on April 9<sup>th</sup> are outlined in Table 60.

*Table 60 April 9th, 2018 Simulation Conditions*

<b>Period</b>	<b>Average T<sub>out</sub></b>	<b>Wind Speed</b>	<b>Solar Radiation</b>	<b>Occupied?</b>	<b>Time of day</b>
April 09, 2018 (11:05 – 14:05)	5.27°C	1.5 to 4 m/s	600 W/m <sup>2</sup>	Yes	Daytime

The results from the April 9<sup>th</sup> simulation, illustrated in Table 61 and Figure 87, demonstrate the surface temperatures being predicted within 15% accuracy and the ambient temperature within 2.5% accuracy. The surface temperature prediction results are similar to those seen during occupied conditions for the winter season simulations, where the building element errors were as severe as 16% prediction error. The window and spandrel panel demonstrate the worst prediction results, with prediction errors above 10% for the first part of the simulation, decreasing to close to zero at the 180-minute Prediction Window (Figure 87). The measurement data, seen in Figure 88, demonstrates much higher actual surface temperatures at the beginning

of the simulation than the predicted temperatures. The improvement in prediction error at the end of the simulation is believed to be due to the simulation switching to occupied regression models when occupants enter the room at the 60-minute Prediction Window. The ambient temperature demonstrated slightly worse results than the winter simulations, reaching a prediction error above 2%. It is observed that the actual temperature in the test cell falls by 0.6°C between the 15<sup>th</sup> and 30<sup>th</sup> minute of the simulation. This observation is believed to be due to a decrease in ventilation air temperature, from 25°C to 13°C, at the 12<sup>th</sup> minute of the simulation lasting until the 30<sup>th</sup> minute.

*Table 61 Prediction Error for Temperatures of Simulated Elements as a Function of Prediction Window Duration for April 4<sup>th</sup>, 2017 (T<sub>out</sub>=5.27°C, wind speed ranging from 1.5 to 4 m/s, and solar radiation 600W/m<sup>2</sup>)*

	Prediction Window					
	15 minutes	30 minutes	45 minutes	60 minutes	120 minutes	180 minutes
Exterior Wall	0.46%	1.6021%	0.5750%	3.8637%	1.5889%	1.1353%
Ceiling	-1.61%	-0.3015%	-0.5784%	0.3112%	0.1752%	0.5684%
Floor	-4.45%	-2.1996%	-1.9989%	2.3925%	5.1910%	-3.0342%
Spandrel	-9.25%	-8.5132%	-11.6437%	-8.1855%	-7.8534%	-3.2688%
Window	-12.71%	-8.6073%	-9.9394%	-11.3825%	-7.1207%	-0.7601%
Interior Wall	-0.78%	1.9392%	2.2646%	6.3892%	4.9017%	-0.0036%
Ambient	-0.05%	2.4927%	1.1105%	1.0611%	-0.5236%	0.5925%

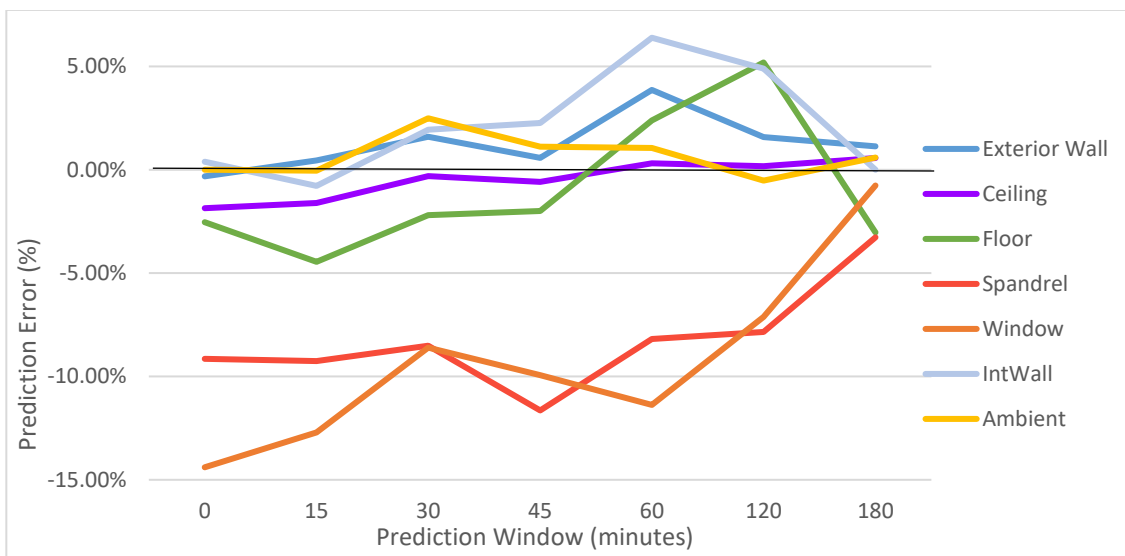


*Figure 87 April 4<sup>th</sup>, 2017 Prediction Error for all Building Elements along with Ambient Temperature*

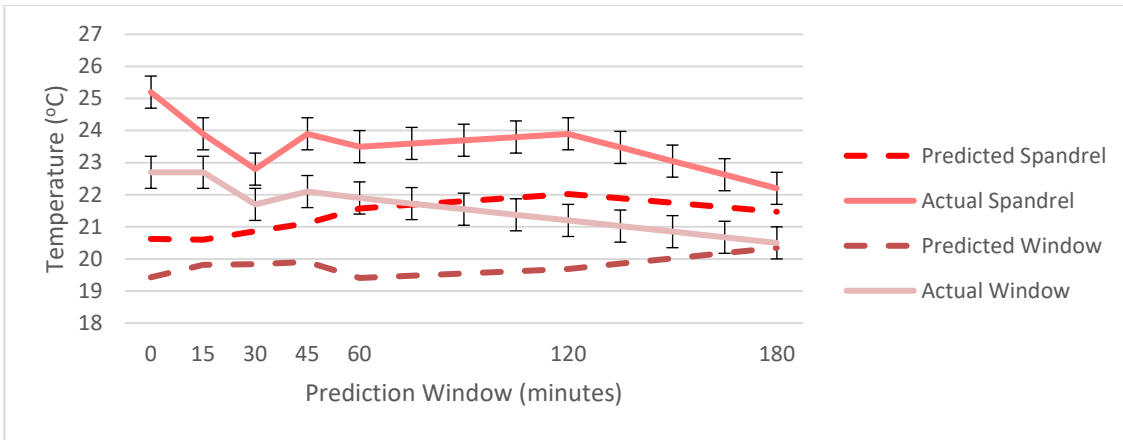


Figure 88 April 4<sup>th</sup>, 2017 Predicted vs Actual Surface Temperature for the Window and Spandrel Panel

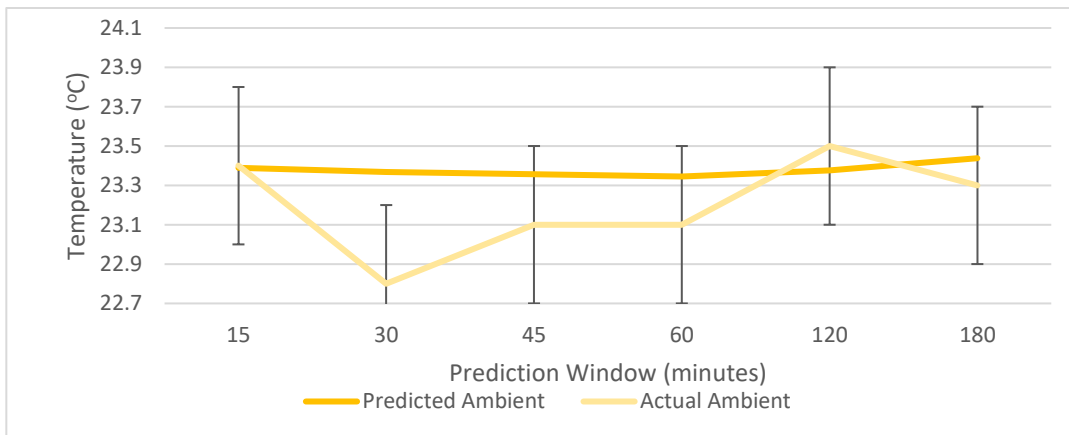


Figure 89 April 4<sup>th</sup>, 2017 Predicted vs Actual Ambient Temperature

## 6.11 Error Analysis

An error analysis was conducted on the Final Model to determine the impact of the simplifications on model accuracy. Simplifications within this study include: plug load data calculation, the single point temperature measurement for the surface temperatures, and ventilation measurements, and omission of latent heat loads.

### 6.11.1 Plug Load Error Analysis

To analyze the impact of using of calculated plug load values rather than the true plug load data, simulations were run for January 2<sup>nd</sup>, January 6<sup>th</sup>, and January 8<sup>th</sup>, using both plug load data sets as shown in Table 62. This analysis investigated the impact on the first G1v1 model and the Final Model. The results for both models indicate the January 2<sup>nd</sup> and January 8<sup>th</sup>

simulations had better prediction accuracy when using the actual plug load data, while the simulation for January 6<sup>th</sup> demonstrated worse prediction accuracy.

*Table 62 Final Model and G1v1 Model results when using true plug load data compared to calculated plug load data*

<b>First Generation Grey Box Model</b>			
	02-Jan	06-Jan	08-Jan
RMSE	0.0744	0.0963	0.3019
MAE	0.0309	0.0369	0.1434
WAPE	0.0209%	0.0254%	0.0973%
<b>First Generation Grey Box Model with Plug load</b>			
	02-Jan	06-Jan	08-Jan
RMSE	0.0367	0.1280	0.2742
MAE	0.0134	0.0530	0.1260
WAPE	0.0091%	0.0366%	0.0855%
<b>Final Model</b>			
	02-Jan	06-Jan	08-Jan
RMSE	0.0974	0.0838	0.0523
MAE	0.0409	0.0322	0.0432
WAPE	0.0277%	0.0222%	0.0293%
<b>Final Model with Plug load</b>			
	02-Jan	06-Jan	08-Jan
RMSE	0.0679	0.0852	0.0965
MAE	0.0271	0.0326	0.0423
WAPE	0.0183%	0.0224%	0.0287%

The overall performance of the four models, illustrated in Table 63, shows the G1 model and the Final Model as having better prediction results when using the true plug load data. The RMSE is observed to improve by 0.02 for both models when using the true data, indicating that the results within this study are likely lower than the results that would have been obtained if the true plug load data had been used.

*Table 63 Overall comparison results for the G1 grey box model and final grey box model*

	<b>First Generation</b>	<b>First Generation Plug</b>	<b>Final</b>	<b>Final Plug</b>
RMSE	0.3255	0.3048	0.1609	0.1456
MAE	0.2111	0.1923	0.1163	0.1019
WAPE	0.0479%	0.0437%	0.0264%	0.0232%

### *6.11.2 Point Measurement Error Analysis*

The implications of using point surface temperature measurements were investigated upon installation of the thermocouples. Before being attached with conductive paste, the thermocouples were used to gather temperature measurements across the surface of the floor and window unit. The floor represents the most thermally massive element of the cell and the window the lightest. The temperature of the floor slab was read at seven different locations across its cross section; the results show deviation in temperature readings of 0.5°C. Similarly, the temperature of the window was captured at 13 points across its cross section; the data demonstrated a maximum temperature deviation of 1.3 °C between point measurements in the sunlight and point measurements that were in the shade. As the sun only shines on the test cell for the first few hours of the day, due to the eastern orientation of the test cell, these deviations in temperature measurements only occur for a few hours of each day. It should be noted that there is an additional error associated with the window temperature measurements due to the thermocouple paste used to connect the sensor. This paste adds additional resistivity between the thermocouple and the window surface; this value is small since the paste is highly conductive however, it will have some influence of the window temperature since the window has low overall resistivity. In addition, the paste will absorb heat from solar radiation and influence the thermocouple measurement to be warmer than the actual temperature of the window surface.

To mitigate the error associated with the airflow point measurement readings, the sensor calibration was conducted using a balometer, which captures the velocity of the air from the entire duct opening (see Section 3.3). The deviation in airflow temperature for the ventilation ducts was investigated by taking temperature measurements at 10 points across the opening of the duct. The results demonstrate that the temperature deviation across the opening varied by 0.15°C.

It is noted, that one sensor that was not analyzed for point measurement error was the ambient temperature sensor. The three ambient sensors within the test cell demonstrate variations in temperature at different locations horizontally throughout the room due to their proximity to different heat loads. The implications of using the ambient temperature measurement in the middle of the room rather than the ambient temperature sensor closer to the building element

being modeled, was not investigated. The ambient temperature was also collected at different locations horizontally within the room but not at varying heights. Therefore, there is no measurement that indicates the amount of stratification that may be affecting the ceiling, floor and exterior wall sensors.

### 6.12 Latent Heat Error Analysis

A major simplification made in this study was the omission of the latent heat load in the ventilation heating load calculation. To analyze the impact of this assumption on the results of this study, the Final Model and the G1v1 Model are simulated with and without the latent heat load calculation, as shown in Table 64. For the models not considering latent heat gain, the dry air equations described in Section 4.1.3 are used. For the models considering latent heat gain, the ventilation energy is calculated with the enthalpy (35) and density (36) equations shown below. The variables in these equations include  $c_{pa} = 1.006 \text{ kJ/kgK}$  [53],  $c_{pw} = 1.84 \text{ kJ/kgK}$  [53],  $h_{we} = 2501 \text{ kJ/kg}$ ,  $x$  the humidity ratio,  $T$  the temperature (K),  $R_d = 287.05 \text{ J/kgK}$  [54],  $R_v = 461.5 \text{ J/kgK}$  [54],  $P_{da}$  the partial pressure of dry air, and  $P_{wv}$  the partial pressure of water vapor [54].

$$h = c_{pa} * T + x * (c_{pw} * T + h_{we}) \quad (35)$$

$$\rho = \frac{P_{da}}{R_d T} + \frac{P_{wv}}{R_v T} \quad (36)$$

The simulation period used for the comparison is April 4<sup>th</sup>, 2018 between 11:00 and 14:00; this period was chosen as it occurs after the temperature and relative humidity sensors for the ventilation ducts were installed. The results from this comparison, summarized in Table 64, indicate the inclusion of the latent heat load does not improve the ambient temperature prediction results of either model.

*Table 64 Final model and G1v1 model when considering and when omitting latent heat*

	<b>Final Model</b>	<b>Final Model with Latent</b>	<b>G1v1</b>	<b>G1v1 with Latent</b>
<b>RMSE</b>	0.28379	0.00462	0.29333	0.29334
<b>MAE</b>	-0.17895	0.00189	-0.17928	-0.17829
<b>WAPE</b>	-0.0337%	-0.7731%	-0.0294%	-0.0336%

## 7 Discussion

This study was conducted to determine the possibility of creating an accurate grey box thermal dynamic model without building construction specifications; and to determine if this type of model is generalizable and can predict temperatures with reasonable accuracy in new conditions. If so, there is a strong potential this type of model could be used in existing buildings to support MPC implementation. The final grey box model created within Simulink, answers the first research question by demonstrating the ability to predict the indoor ambient temperature of eleven simulation days to within 0.35°C for a 3-hour Prediction Window. These results are comparable to those found in the study conducted by Harb *et al.* [8], whose grey box model was accurate to within 0.5 °C when simulated for 8 weeks, using measurement updates every hour. The Final Model results are also supported by the findings from the comparative study conducted in Section 6.9. Figure 76 - Figure 86 demonstrate the Final Model performing to within the same level as the traditional G1v3 grey box model created within this research. This demonstrates that the Final grey box model, without the building characteristics, can achieve the same level of accuracy as typical grey box models.

One observation from the Final Model results is the large prediction errors for the building element surface temperatures, namely the window and spandrel units. These elements had prediction errors as severe as 16%, meaning that the predicted temperature was 3°C off from the actual surface temperature. A key finding from these results is the predicted indoor ambient temperature remaining with 1.7% accuracy despite the large discrepancies in the building element surface temperature predictions. The optimization of the internal heat capacity is believed to be an important factor contributing to the accuracy of the ambient temperature predictions. As shown in Figure 82-Figure 86, models using the optimized internal heat capacity value, the Final Model and the G1v3 model, had prediction errors that were up to 9% lower for the occupied simulation days compared to the G1v1 model. With the larger internal heat capacity value, the models can better predict the thermal behaviour of the space when it is subjected to larger heat loads. Overall, the Final Model despite having poor surface temperature prediction results for the low thermal mass and thermal resistance elements, demonstrates the ability to accurately predict the ambient temperature for a Prediction Window of three hours.

The second goal of this research is to identify if this type of grey box model has the generalisation ability to be implemented and perform well under new conditions. The Final Model demonstrates the ability to be implemented within new buildings, as the results in within Table 58 prove the model can be trained with two weeks of data and achieve the same degree of accuracy as a model trained with four months of data. It is noted, these performance results were tested within the same season. The linear regression equations may need to be re-trained for different seasons to improve prediction performance. This is especially true for the models for the lower thermal inertia elements that are more susceptible to heating loads. The use of a sliding window, as discussed in [7], could be useful within the Final Model to allow for periodic re-training of the linear regression models. Additional support demonstrating two weeks of training data is adequate to solve for the internal heat capacity values is shown in the study conducted by Berthou *et al.* [11], where two weeks of training data to solve for the unknown parameters within the grey box model using parameter estimation techniques. Finally, the Final Model was also analyzed for model performance outside the training season, using a simulation day in April. As shown in Figure 89, this model predicted the indoor ambient temperature to within 2.5%, a deviation of 0.5°C from the actual temperature. The April simulation demonstrated worse prediction results than the winter simulations where the ambient temperature was predicted to within 1.7%. This simulation day, April 4<sup>th</sup>, is also still within the shoulder season, and therefore only gives an indication of the generalisation of the model. To truly identify the model's ability to perform for all seasons of the year, it needs to be tested in the middle of the summer, during the cooling season.

It should be noted that the parameters used within the grey box models were actual data measurements and not predicted parameters. The results found within this thesis are therefore the optimal results for the model. The 'optimal' internal heat capacity values used within this research are also not truly the optimal values but the best performing value of the tested simulation days. These areas are outside the scope of this research and are recommended future work for this study. It is also highly suggested to further investigate parameter estimation techniques, as the findings in this model demonstrated poor estimation results, highlighting the need to refine the parameter estimation technic used. In addition, future research includes investigation of this model with changing HVAC conditioning. As the HVAC system was not able to be controlled within this study, this analysis could not be conducted. It is suggested that

future test cells, with control of the HVAC system, alter the HVAC sequences to identify the ability of the model to perform under varied conditions.

Unexpected findings from this study include the poor surface temperature prediction results of the window, spandrel panel, and exterior wall neural networks. These results may have been caused by improper training of the networks in the *Matlab* neural network fitting tool. As discussed within Section 2.4, neural networks demonstrate better thermal dynamic modeling performance than other modeling techniques due to their ability to accurately represent nonlinear systems. Therefore, it is believed this is the best modeling method for representing the low thermal mass elements of the test cell, which demonstrate the highest prediction error. It is suggested that future research investigates the use of NARX models and ANFIS models. The study by Ferracuti *et al.* [12] found NARX models to be the best performing thermal dynamic model when compared to three other modeling techniques. These models have a feedback structure which should help improve the temperature prediction performance of lightweight elements that exhibit more varied temperatures. ANFIS models include decision making ability that could work in a similar manner to the occupancy dependent model used in the linear regression analysis, which demonstrated improved performance for 5/6 building elements. An ANFIS structure with fuzzy logic decision, such as the Physical-Rule-Based ANFIS Model Structure used in [58], could be a suitable model for predicting the surface temperatures of the building elements.

Worth noting are the similarities between the Final Model and grey box models that use parameter estimation techniques. Both methods require collection of BAS points and measurements of surface temperatures for at least two weeks in order to train the models. This in turn raises the question of which model, as both require the same amount of set up and data collection, predicts the ambient temperature with greater degree of accuracy. Based on the findings in this research it is believed that the parameter estimation model would have the better prediction results. The G1v3 model is similar to a grey box model that was created using parameter estimation techniques. The G1v3 model uses estimated resistivity and capacitance values, calculated based on estimated building construction for the construction year, and an internal heat capacity value determined using parameter estimation. In Section 6.9, this model demonstrates the better performance overall when compared to the Final Model. Although this

analysis demonstrated that parameter estimation is the model type that produces more accurate results, the Final Model still has room to improve with proper internal heat capacity optimization, and the use of neural networks for the low thermal inertia elements. Therefore, the Final model with the stated changes could demonstrated to be the better model option.

To conclude, this research found the Final Model could be implemented into buildings where the construction specifications are not known, and would have the ability to accurately determine the net thermal dynamics during the heating season. This model has potential for further improvement with development of neural network models for the thermally lightweight elements, implementation of true internal heat capacity value, and seasonal testing and development. Overall, the model demonstrates promising results in the ability for MPC implementation. The refinement of this model will allow more buildings to use MPC systems with grey box thermal dynamic models to help reduce their energy use. In turn, the spread of MPC systems within building HVAC systems will help reduce the overall energy consumption of the building sector.

## 8 Conclusions

This study demonstrates the potential of creating a grey box model that can represent the thermal dynamics solely based on building automation system points. The final model eliminated all resistance and capacitance values for building element representation, replacing them with linear regression equations. The model predicted the indoor ambient temperature of the cell within 1.7% accuracy, 0.35°C, for up to three-hour Prediction Window. The analysis of the model also demonstrated a training period of 2 weeks is sufficient to create an accurate thermal dynamic model. Testing the model outside of the training period resulted in slightly higher ambient temperature prediction error than the winter simulations, with an accuracy of 2.5%. Therefore, although this research demonstrated promising results towards the model's ability to be implemented within MPC systems, there are still many areas of growth for future improvement.

The recommended future work includes:

1. Further research towards more advanced neural network models to represent low thermal inertia elements of the exterior façade, including window and spandrel panels.
2. Creation of prediction functions for the building automation system points to test true prediction ability of the system.
3. Investigating the performance of this model at a larger scale where the thermal dynamics are predicted for multiple building zones.
4. Smaller projects including testing of the model after using optimisation algorithms to find the true internal heat capacity of the test cell, as well as testing of the model for the summer season.
5. Test this model in a test cell where the HVAC operation can be changed to observe the performance of the model with new HVAC sequences.

## 9 References

- [1] B. Dawoud, E. Amer and D. Gross, "Experimental investigation of an adsorptive thermal energy storage," *International journal of energy research*, vol. 31, pp. 135-147, 2007.
- [2] O. Lucon, D. Üрге-Vorsatz, A. Z. Ahmed, H. Akbari, P. Bertoldi, L. F. Cabeza, N. Eyre, A. Gadgil, L. D. Harvey, Y. Jiang, E. Liphoto, S. Mirasgedis, S. Murakami, J. Parikh, M. V. Vilariño, P. Graham, K. Petrichenko, . J. Eom, . A. Kelemen and V. Krey, "Climate Change 2014: Mitigation of Climate Change. Contribution of Working Group III to the Fifth Assessment Report of the Intergovernmental Panel on Climate Change," in *Buildings*, Cambridge, United Kingdom and New York, USA, Cambridge University Press, 2014, pp. 671-738.
- [3] V. Harish and A. Kumar, "A review on modeling and simulation of building energy systems," *Renewable and Sustainable Energy Reviews*, pp. 1272-1292, 2016.
- [4] E. O'Dwyer, L. De Tommasi, K. Kouramas, M. Cychowski and G. Lightbody, "Modelling and disturbance estimation for model predictive control in building heating systems," *Energy and Buildings*, vol. 130, pp. 532-545, 2016.
- [5] O. Alhaj, D. Defer and I. Shahrour, "A simplified building thermal model for the optimization of energy consumption : Use of a random number generator," *Energy & Buildings*, vol. 82, pp. 322-329, 2014.
- [6] E. Carrascal, I. Garrido, A. J. Garrido and J. M. Sala, "Optimization of the heating system use in aged public buildings via Model Predictive Control," *Energies*, vol. 9, no. 4, pp. 1-21, 2016.
- [7] H. Huang, L. Chen and E. Hu, "A neural network-based multi-zone modelling approach for predictive control system design in commercial buildings," *Energy and Buildings*, vol. 97, pp. 86-97, 2015.
- [8] H. Harb, N. Boyanov, L. Hernandez, R. Streblow and D. Müller, "Development and validation of grey-box models for forecasting the thermal response of occupied buildings," *Energy and Buildings*, vol. 117, pp. 199-207, 2016.

- [9] A. Afram and F. Janabi-Sharifi, "Gray-box modeling and validation of residential HVAC system for control system design," *Applied Energy*, vol. 137, pp. 134-150, 2015.
- [10] T. L. McKinley and A. G. Alleyne, "Identification of building model parameters and loads using on-site data logs," *Third National Conference of IBPSA-USA*, pp. 9-16, 2008.
- [11] T. Berthou, P. Stabat, R. Salvazet and D. Marchio, "Development and validation of a gray box model to predict thermal behavior of occupied office buildings," *Energy and Buildings*, vol. 74, pp. 91-100, 2014.
- [12] F. Ferracuti, A. Fonti, L. Ciabattoni, S. Pizzuti, A. Arteconi, L. Helsen and G. Comodi, "Data-driven models for short-term thermal behaviour prediction in real buildings," *Applied Energy*, vol. 204, pp. 1375-1387, 2017.
- [13] M. Soudari, S. Srinivasan, S. Balasubramanian, J. Vain and U. Kotta, "Learning based personalized energy management systems for residential buildings," *Energy and Buildings*, vol. 127, pp. 953-968, 2016.
- [14] J. Ma, J. Qin, T. Salsbury and P. Xu, "Demand reduction in building energy systems based on economic model predictive control," *Chemical Engineering Science*, vol. 67, no. 1, pp. 92-100, 2012.
- [15] M. Aftab, C. Chen, C. K. Chau and T. Rahwan, "Automatic HVAC control with real-time occupancy recognition and simulation-guided model predictive control in low-cost embedded system," *Energy and Buildings*, vol. 154, pp. 141-156, 2017.
- [16] X. Xinhua and W. Shengwei, "A mixed-mode building energy model for performance evaluation and diagnosis of existing buildings," *Building Services Engineering Research & Technology*, vol. 29, no. 1, pp. 73-83, 2008.
- [17] P. Bacher and H. Madsen, "Identifying suitable models for the heat dynamics of buildings," *Energy and Buildings*, vol. 43, no. 7, pp. 1511-1522, 2011.

- [18] J. Terés-Zubiaga, C. Escudero, C. García-Gafaro and J. M. Sala, "Methodology for evaluating the energy renovation effects on the thermal performance of social housing buildings: Monitoring study and grey box model development," *Energy and Buildings*, vol. 102, pp. 390-405, 2015.
- [19] H. Huang, L. Chen and E. Hu, "A new model predictive control scheme for energy and cost savings in commercial buildings: An airport terminal building case study," *Building and Environment*, vol. 89, pp. 203-216, 2015.
- [20] J. Široký, F. Oldewurtel, J. Cigler and S. Prívvara, "Experimental analysis of model predictive control for an energy efficient building heating system," *Applied Energy*, vol. 88, no. 9, pp. 3079-3087, 2011.
- [21] G. Reynders, J. Diriken and D. Saelens, "Quality of grey-box models and identified parameters as function of the accuracy of input and observation signals," *Energy and Buildings*, vol. 82, pp. 263-274, 2014.
- [22] V. Lara, B. G. C. Molina, L. M. M. Yanes and M. A. R. B. Jose P. Monteagudo Yanes, "Offset-free model predictive control for an energy efficient tropical island hotel," *Energy and Buildings*, pp. 283-292, 2016.
- [23] B. Dong and K. P. Lam, "A real-time model predictive control for building heating and cooling systems based on the occupancy behavior pattern detection and local weather forecasting," *Building Simulation*, vol. 7, no. 1, pp. 89-106, 2014.
- [24] K. F. Woldekidan, "Indoor environmental quality (IEQ) and building energy optimization through model predictive control (MPC)," 2015.
- [25] A. Afram and F. Janabi-Sharifi, "Supervisory model predictive controller (MPC) for residential HVAC systems: Implementation and experimentation on archetype sustainable house in Toronto," *Energy and Buildings*, vol. 154, pp. 268-282, 2017.
- [26] A. Afram and F. Janabi-Sharifi, "Supervisory model predictive controller (MPC) for residential HVAC systems: Implementation and experimentation on archetype sustainable house in Toronto," *Energy and Buildings*, vol. 154, pp. 268-282, 2017.

- [27] J. Ma, J. Qin, T. Salsbury and P. Xu, "Demand reduction in building energy systems based on economic model predictive control," *Chemical Engineering Science*, vol. 67, no. 1, pp. 92-100, 2012.
- [28] X. Li and J. Wen, "Review of building energy modeling for control and operation," *Renewable and Sustainable Energy Reviews*, vol. 37, pp. 517-537, 2014.
- [29] D. Gyalistras, S. Pr, C. Sagerschnig and M. Morari, "Modeling and Identification of a Large Multi-Zone Office Building," *IEEE International Conference on Control Applications*, pp. 55-60, 2011.
- [30] H. Huang, L. Chen, M. Mohammadzaheri, E. Hu and M. Chen, "Multi-zone temperature prediction in a commercial building using artificial neural network model," in *2013 10th IEEE International Conference on Control and Automation (ICCA)*, 2013.
- [31] F. Zamora-Martínez, P. Romeu, P. Botella-Rocamora and P. Botella-Rocamora, "Towards energy efficiency: Forecasting indoor temperature via multivariate analysis," *Energies*, vol. 6, no. 9, pp. 4639-4659, 2013.
- [32] G. Mustafaraj, G. Lowry and J. Chen, "Prediction of room temperature and relative humidity by autoregressive linear and nonlinear neural network models for an open office," *Energy and Buildings*, vol. 43, no. 6, pp. 1452-1460, 2011.
- [33] G. Finch, "The Performance of Rainscreen Walls in Coastal British Columbia," University of Waterloo, 2007.
- [34] M. Siemann, J. Kim, D. Oberholzer and C. Sloop, "Performance of a Residual Building Energy Grey-Box Model Using Localized Weather Networks," ASHRAE, 2013.
- [35] J. Wen, "Review of building energy modeling for control and operation," *Renewable and Sustainable Energy Reviews*, vol. 37, pp. 517-537, 2014.
- [36] X. Li and J. Wen, "Review of building energy modeling for control and operation," *Renewable and Sustainable Energy Reviews*, vol. 37, pp. 517-537, 2014.
- [37] B. G. Vega, L. M. Castellanos and J. P. Monteagudo, "Modeling and identification of the cooling dynamics of a tropical island hotel," *Energy & Buildings*, vol. 92, pp. 19-28, 2015.

- [38] K. M. Powell, A. Sriprasad, W. J. Cole and T. F. Edgar, "Heating, cooling, and electrical load forecasting for a large-scale district energy system," *Energy*, vol. 74, pp. 877-885, 2014.
- [39] W. Suparta and K. M. Alhasa, "Adaptive Neuro-Fuzzy Interference System," in *Modeling of Tropospheric Delays Using ANFIS*, 2016, pp. 5-19.
- [40] MathWorks, "Improve Neural Network Generalization and Avoid Overfitting," MathWorks, [Online]. Available: <https://www.mathworks.com/help/nnet/ug/improve-neural-network-generalization-and-avoid-overfitting.html>. [Accessed 07 2018].
- [41] MIT, "Topic #5: 16.30/31 Feedback Control Systems," 2010. [Online]. Available: [https://ocw.mit.edu/courses/aeronautics-and-astronautics/16-30-feedback-control-systems-fall-2010/lecture-notes/MIT16\\_30F10\\_lec05.pdf](https://ocw.mit.edu/courses/aeronautics-and-astronautics/16-30-feedback-control-systems-fall-2010/lecture-notes/MIT16_30F10_lec05.pdf). [Accessed 09 2018].
- [42] T. Chai and R. Draxler, "Root mean square error (RMSE) or mean absolute error (MAE)? –," *Geoscientific Model Development*, vol. 7, pp. 1247-1250, 2014.
- [43] G. Szederkényi, R. Lakner and M. Gerzson, *Intelligent Control Systems : An Introduction with Examples*, Springer Science & Business Media, 2006.
- [44] S. J. Emmerich and A. K. Persily, "Analysis of U.S. Commercial Building Envelope Air Leakage Database to Support Sustainable Building Design," *International Journal of Ventilation*, vol. 12, no. 4, pp. 331-344, 2016.
- [45] C. S. and H. A. S., *Regression analysis by example.*, 2006.
- [46] C. J. Willmott and K. Matsuura, "Advantages of the mean absolute error (MAE) over," *CLIMATE RESEARCH*, vol. 30, p. 79–82, 2005.
- [47] C. Chase, *Demand-Driven Forecasting*, New Jersey: John Wiley & Sons, Inc., 2009.
- [48] MadgeTech, "Octtemp 8 Chanel Thermocouple Data Logger," MadgeTech, Warner, NH, 2015.
- [49] OmniSense, "OmniSense S-900-1 Wireless Sensor Product Brief," OmniSense LLC, Oxnard, CA.
- [50] G. Finch, "The Performance of Rainscreen Walls in Coastal British Columbia," Waterloo, 2007.

- [51] American Society of Heating, Refrigerating and Air-Conditioning Engineers, Inc., 2013 ASHRAE Handbook - Fundamentals (I-P Edition), American Society of Heating, Refrigerating and Air-Conditioning Engineers, Inc., 2013.
- [52] R. Kane and H. Sell, Revolution in Lamps: A Chronicle of 50 Years of Progress, The Fairmont Press, Inc., 2001.
- [53] Engineering ToolBox, "Enthalpy of Moist Air," 2004. [Online]. Available: [https://www.engineeringtoolbox.com/enthalpy-moist-air-d\\_683.html](https://www.engineeringtoolbox.com/enthalpy-moist-air-d_683.html). [Accessed 02 2018].
- [54] Engineering ToolBox, "Density of Moist Humid Air," 2004. [Online]. Available: [https://www.engineeringtoolbox.com/density-air-d\\_680.html](https://www.engineeringtoolbox.com/density-air-d_680.html). [Accessed 02 2018].
- [55] J. F. Straube and E. F. Burnett, Building Science for Building Enclosures, Westford: Building Science Press Inc., 2005.
- [56] N. B. Hutcheon and G. O. Handegord, Building science for a cold climate, Toronto: Wiley & Sons Canada, 1983.
- [57] J. O. Rawlings, D. A. Dickey and S. G. Pantula, Applied Regression Analysis : A Research Tool, Springer, 1998.
- [58] L. Huang, Z. Liao and L. Zhao, "Physical-rules-based adaptive neuro-fuzzy inferential sensor model for predicting the indoor temperature in heating systems," 2012.
- [59] A. Schirrer, M. Brandstetter, I. Leobner, S. Hauer and M. Kozek, "Nonlinear model predictive control for a heating and cooling system of a low-energy office building," *Energy and Buildings*, vol. 125, pp. 86-98, 2016.
- [60] J. Brownlee, "Autoregression Models for Time Series Forecasting with Python," Machine Learning Mastery, 02 01 2017. [Online]. Available: <https://machinelearningmastery.com/autoregression-models-time-series-forecasting-python/>. [Accessed 2018].

- [61] Owens Corning, "700 Series FIBERGLAS Insulation Product Data Sheet," 2013. [Online]. Available: <http://insulation.owenscorning.ca/assets/0/188/1af6c138-5b49-49c7-8b6b-c39ee0f4159e.pdf>. [Accessed 11 2017].
- [62] J. P. Ellenberger, Piping and Pipeline Calculations Manual - Construction, Design, Fabrication, and Examination, Elsevier, 2010.

## 10 Appendix A Solar Radiation Calculations

*Table A-1 Solar Radiation Calculation - Breaking Down the Time, Hour Angle and Sun Declination*

Hour	Date	Time	Day Number	equation of time	Local Standard Time	Apparent Standard Time	Hour Angle		Declination	
							eta	ET	LST	AST
1	Nov 16, 2017 14:50	14:50	320.62	13.81	14.50	15.02351	0.791552	45.35261	-0.34064	-19.5174
2	2017-11-16 15:05	15:05	320.63	13.81	15.05	15.57346	0.935531	53.60197	-0.34068	-19.5197
3	2017-11-16 15:20	15:20	320.64	13.81	15.20	15.72342	0.974789	55.85132	-0.34072	-19.5221
4	2017-11-16 15:35	15:35	320.65	13.80	15.35	15.87338	1.014048	58.10068	-0.34077	-19.5244
5	2017-11-16 15:50	15:50	320.66	13.80	15.50	16.02334	1.053307	60.35003	-0.34081	-19.5267
6	2017-11-16 16:05	16:05	320.67	13.80	16.05	16.57329	1.197285	68.59938	-0.34085	-19.5291
7	2017-11-16 16:20	16:20	320.68	13.79	16.20	16.72325	1.236544	70.84874	-0.34089	-19.5314
8	2017-11-16 16:35	16:35	320.69	13.79	16.35	16.87321	1.275802	73.09809	-0.34093	-19.5337

*Table A-2 Solar Radiation Calculation - Using the Time of Day Information to Calculation the Solar Altitude, Azimuth, Degree of Incidence and Zenith Angle*

Solar Altitude		Solar Azimuth		Solar Incidence		# of Daylight Hours	Sun Zenith Angle	
beta-rads	degrees	phi-rads	degrees	theta-rad	degree		thetaH-rads	degrees
0.251175	14.39128	0.764656006	43.81156	1.319621	75.60872	9.363966	1.319621	75.60872
0.174835	10.0173	0.879464215	50.38959	1.395961	79.9827	9.363611	1.395961	79.9827
0.152652	8.746333	0.909481716	52.10946	1.418144	81.25367	9.363256	1.418144	81.25367
0.129951	7.445642	0.938995406	53.80047	1.440845	82.55436	9.362902	1.440845	82.55436
0.106759	6.11684	0.9680295	55.464	1.464037	83.88316	9.362547	1.464037	83.88316
0.018014	1.032152	1.070901174	61.35812	1.552782	88.96785	9.362193	1.552782	88.96785
-0.00712	-0.40817	1.098050674	62.91367	1.57792	90.40817	9.361839	1.57792	90.40817
-0.03261	-1.86847	1.124877291	64.45072	1.603407	91.86847	9.361485	1.603407	91.86847

*Table A-3 Solar Radiation Calculations - Calculating the Clear Sky Diffuse and Total Solar Radiation*

<b>hottel clear sky radiation</b>	<b>atm trans for beam radiation</b>	<b>Outer atm normal radiation</b>	<b>Clear sky horizontal beam radiation</b>	<b>tran coeff for beam and diffuse</b>	<b>clear sky horizontal diffuse radiation</b>	<b>Total horizontal clear sky radiation</b>
<b>if&lt;pi/2</b>	<b>Taub</b>	<b>Ion</b>	<b>Icb</b>	<b>Taud</b>	<b>lcd</b>	<b>lc</b>
1	0.30651	1385.24	105.5294	0.180916	62.28778	167.8171
1	0.22735	1385.245	54.78126	0.204182	49.19921	103.9805
1	0.20425	1385.251	43.02411	0.21097	44.43905	87.46316
1	0.18224	1385.257	32.71341	0.21744	39.03252	71.74593
1	0.16315	1385.262	24.08298	0.223049	32.92389	57.00687
1	0.14148	1385.268	3.530372	0.22942	5.724816	9.255188
0	0	1385.273	0	0	0	0
0	0	1385.279	0	0	0	0

*Table A-4 Solar Radiation Calculation - Using the Measured Solar Radiation Data from the Rooftop to Determine the Direct and Diffuse Portions*

<b>Measured Radiance</b>	<b>Ratio of clear sky rad</b>	<b>Ratio of diffure sky rad</b>	<b>diffuse corrected for low sun</b>	<b>Diffuse Radiation</b>	<b>Direct(beam)Radiation</b>	<b>Direct Normal Radiation-altitude dependent</b>
<b>I</b>	<b>I/c</b>	<b>Id/I</b>	<b>IIDCorr</b>	<b>Id</b>	<b>Ib</b>	<b>Idn</b>
39.8	0.237163	0.976284	0.976284	38.85609	0.943908	3.797775
34.8	0.334678	0.966532	0.966532	33.63532	1.16468	6.69566
36.033333	0.411983	0.958802	0.365344	13.16456	22.86878	150.393
57.3	0.798652	0.638367	0.524375	30.04668	27.25332	210.3115
35.6	0.624486	0.827033	0.669701	23.84135	11.75865	110.3515
9.3666667	1.012045	0.341956	0.990043	9.273404	0.093262	5.177374
4.8	0	1	1	4.8	0	0
1.0333333	0	1	1	1.033333	0	0

Table A-565 Solar Radiation Calculation - Converting the Direct and Diffuse Solar Radiation Values to the Vertical Surface

Wall Solar Azimuth	Wall Angle of Incidence	Direct Radiation incident to surface (W/m <sup>2</sup> )	Diffuse Radiation on Surface (W/m <sup>2</sup> )	Reflected Radiation on Surface (W/m <sup>2</sup> )	Total Radiation on Vertical Surface
alpha-degree	chi	I <sub>bv</sub>	I <sub>dv</sub>	I <sub>rv</sub>	I <sub>v</sub>
133.8116	132.1107	0	19.42805	3.98	23.40805
140.3896	139.3456	0	16.81766	3.48	20.29766
142.1095	141.2613	0	6.582279	3.603333	10.18561
143.8005	143.1455	0	15.02334	5.73	20.75334
145.464	144.9928	0	11.92067	3.56	15.48067
151.3581	151.3411	0	4.636702	0.936667	5.573369
152.9137	152.9108	0	2.4	0.48	2.88
154.4507	154.3871	0	0.516667	0.103333	0.62

## 11 Appendix B Arduino Code

```
//Libraries
#include <Dhcp.h>
#include <Dns.h>
#include <Ethernet2.h>
#include <RTCLib.h>
#include <SPI.h>
#include <DS3231.h>
#include <SoftwareSerial.h>
#include <SD.h>
#include <RTCLib.h>
#include <Wire.h>
#include "DHT.h"

#define DHTPIN 24 //left duct
#define DHTPIN2 22 //right duct
#define DHTTYPE DHT22 // DHT 22 (AM2302), AM2321
#define LOG_INTERVAL 1000 // mills between entries (reduce to take
more/faster data)
#define SYNC_INTERVAL 1000 // mills between calls to flush() - to write
data to the card
uint32_t syncTime = 0; // time of last sync()
#define ECHO_TO_SERIAL 1 // echo data to serial port
#define WAIT_TO_START 0 // Wait for serial input in setup()

/* to communicate with the Bluetooth module's TXD pin */
#define BT_SERIAL_TX 6
/* to communicate with the Bluetooth module's RXD pin */
#define BT_SERIAL_RX 5
/* Initialise the software serial port */
SoftwareSerial BluetoothSerial(BT_SERIAL_TX, BT_SERIAL_RX);

//SD card file
File logfile;
RTC_DS3231 RTC;

//Define variables and ports
const int togglePin = 13;
int toggleState;
int proximity;
unsigned int Occupancy = 0;
const int ReedPin = 7;
int ReedState = 0;
int GrPin = 8;
int BlPin = 3;
int YlPin = 2;
int RdPin = 9;
float MS1;
float MS2;
float AF1;
float AF2;
int AreaDuct = 1.8;
```

```

char daysOfTheWeek[7][12] = {"Sunday", "Monday", "Tuesday", "Wednesday",
"Thursday", "Friday", "Saturday"};
//int analogPin1 = A9;      // potentiometer wiper (middle terminal)
connected to analog pin 3
int val = 0;                // variable to store the value read
int IR = 0;

const int OutPin  = A3;    // wind sensor analog pin  hooked up to Wind P
sensor "OUT" pin
const int TempPin = A4;    // temp sesnsor analog pin hooked up to Wind P
sensor "TMP" pin

const int OutPin2  = A0;    // wind sensor analog pin  hooked up to Wind P
sensor "OUT" pin
const int TempPin2 = A2;

DHT dht(DHTPIN, DHTTYPE);
DHT dht2(DHTPIN2, DHTTYPE);

const int chipSelect = 4; //SD Card

// Enter a MAC address and IP address for your controller below.
// The IP address will be dependent on your local network:
byte mac[] = {
  0xDE, 0xAD, 0xBE, 0xEF, 0xFE, 0xED
};

IPAddress ip(141,117,215,28);

// Initialize the Ethernet server library
// with the IP address and port you want to use
// (port 80 is default for HTTP):
EthernetServer server(80);

void setup() {
  /* Set the baud rate for the software serial port */
  pinMode(togglePin, INPUT);
  pinMode(ReedPin, INPUT_PULLUP);
  pinMode(GrPin, OUTPUT);
  pinMode(BlPin, OUTPUT);
  pinMode(YlPin, OUTPUT);
  pinMode(RdPin, OUTPUT);
  //pinMode(11, INPUT);
  pinMode(32, INPUT_PULLUP);
  pinMode(34, INPUT_PULLUP);
  pinMode(36, INPUT_PULLUP);
  pinMode(38, INPUT_PULLUP);
  pinMode(A3, INPUT);
  pinMode(A4, INPUT);
  pinMode(A5, INPUT);
  pinMode(A6, INPUT);
  Serial.begin(9600);
  BluetoothSerial.begin(9600); // Initialise BlueTooth

```

```

analogReference(DEFAULT);

Serial.println("DHTxx test!");
dht.begin();
dht2.begin();

delay(3000);
Serial.print("Initializing SD card...");
BluetoothSerial.print("Starting ...");
BluetoothSerial.print("Initializing SD card...");
BluetoothSerial.print("\r\n");

while (!Serial) {
    ; // wait for serial port to connect. Needed for native USB port only
}

// disable w5100 SPI while setting up SD
pinMode(53, OUTPUT);
digitalWrite(53, HIGH); // davekw7x: If it's low, the Wiznet chip
corrupts the SPI bus
digitalWrite(4, LOW);

// set up SD
if(SD.begin(4) == 0)
    Serial.println("SD failed");
else
    Serial.println("SD ok");

//Set up RTC
if (! RTC.begin()) {
    Serial.println("Couldn't find RTC");
    BluetoothSerial.print("Counldn't find RTC");
    BluetoothSerial.print("\r\n");
    while (1);
}
if (RTC.begin()) {
    Serial.println("RTC found");
    RTC.adjust(DateTime(F(__DATE__), F(__TIME__)));
}

if (RTC.lostPower()) {
    Serial.println("RTC lost power, lets set the time!");
    // following line sets the RTC to the date & time this sketch was
compiled
    // This line sets the RTC with an explicit date & time, for example to
set
    // January 21, 2014 at 3am you would call:
    RTC.adjust(DateTime(F(__DATE__), F(__TIME__)));
    // RTC.adjust(DateTime(2017, 7, 20, 5, 1, 1));
}

//Set up SD Card Logging
logfile = SD.open("Data.CSV", FILE_WRITE);  //#define LOGFILE "Data.CSV"

```

```

Serial.println("Logging to: Data");
logfile.println("Date,Time,Occupancy,Light,Door,Solar 1,HVAC Velocity
(left),HVAC Airflow (left), HVAC Temperature (left), HVAC velocity(right),
HVAC Airflow (right), HVAC Temperature(right),RH Right, Temperature Right,
HIC Right, RH Left, Temperature Left, HIC Left");
BluetoothSerial.print("Logging to: Data"); //
BluetoothSerial.println(filename);
BluetoothSerial.print("\r\n");

if (!logfile) {
  Serial.println("couldnt create file");
  BluetoothSerial.print("couldn't create SD file");
  BluetoothSerial.print("\r\n");
}

// start the Ethernet connection and the server:
Ethernet.begin(mac, ip);
server.begin();
Serial.print("server is at ");
Serial.println(Ethernet.localIP());
}

void loop() {
  delay(1000);
  int sensorVal1 = digitalRead(32);
  int sensorVal2 = digitalRead(34);
  int sensorVal3 = digitalRead(36);
  int sensorVal4 = digitalRead(38);
  int toggleState = digitalRead(togglePin);
  //ReedState = digitalRead(ReedPin);
  int proximity = digitalRead(ReedPin); // Read the state of the switch
  int windADunits = analogRead(OutPin);
  int windADunits2 = analogRead(OutPin2);
  int tempRawAD = analogRead(TempPin);
  int tempRawAD2 = analogRead(TempPin2);

//Airflow from Left Duct
float windMPH = pow((((float)windADunits - 264.0) / 85.6814), 3.36814);
Serial.println("Left Duct");
Serial.print(windMPH);
Serial.println("MPH\t");
BluetoothSerial.print("Left Duct");
BluetoothSerial.print(windMPH);
BluetoothSerial.print("MPH\t ,");
BluetoothSerial.print("\r\n");

//Convert to m/s
MS1 = (windMPH * 0.44704);
Serial.print(MS1, 2);
Serial.println(" m/s");
BluetoothSerial.print(" m/s");
BluetoothSerial.print(MS1);
BluetoothSerial.print("\r\n");

```

```

//Convert to m3/s
AF1 = (MS1) * AreaDuct;
Serial.print("AirFlow ");
Serial.print(AF1, 2);
Serial.println(" m3/s");
BluetoothSerial.print("Airflow ");
BluetoothSerial.print(AF1);
BluetoothSerial.print("m3/s");
BluetoothSerial.print("\r\n");

//Temperature of the Left Duct Ventilation Air
float tempC = (((float)tempRawAD * 5.0) / 1024.0) - 0.400) / .0195);
Serial.print(" ");
Serial.print(tempC);
Serial.println(" C");
BluetoothSerial.print(" ");
BluetoothSerial.print(tempC);
BluetoothSerial.print(" C ,");
BluetoothSerial.print("\r\n");

//Airflow from Right Duct
float windMPH2 = pow((((float)windADunits2 - 264.0) / 85.6814),
3.36814);
Serial.println("Right Duct ");
Serial.print(windMPH2);
Serial.println("MPH\t ,");
BluetoothSerial.print("Right Duct");
BluetoothSerial.print(windMPH2);
BluetoothSerial.print(" MPH\t ,");
BluetoothSerial.print("\r\n");

//Convert to m/s
MS2 = (windMPH2 * 0.44704);
Serial.print(MS2, 2);
Serial.println(" m/s");
BluetoothSerial.print(MS2);
BluetoothSerial.print(" m/s");
BluetoothSerial.print("\r\n");

//Convert to m3/s
AF2 = (MS2) * AreaDuct;
Serial.print("AirFlow ");
Serial.print(AF2, 2);
Serial.println(" m3/s");
BluetoothSerial.print(" Airflow");
BluetoothSerial.print(AF2);
BluetoothSerial.print("m3/s");
BluetoothSerial.print("\r\n");

//Temperature from the Right Duct Ventilation
float tempC2 = (((float)tempRawAD2 * 5.0) / 1024.0) - 0.4) / .0195);
Serial.print("");
Serial.print(tempC2);
Serial.println(" C");

```

```

BluetoothSerial.print("  ");
BluetoothSerial.print(tempC2);
BluetoothSerial.print(" C ,");
BluetoothSerial.print("\r\n");

//Relative Humidity from Left Duct-AM2302
float h1 = dht.readHumidity();
Serial.print("Humidity Left ");
Serial.print(h1);
Serial.println(" %");
BluetoothSerial.print("Humidity Left      ");
BluetoothSerial.print(h1);
BluetoothSerial.print("%");
BluetoothSerial.print("\r\n");

//Relative Humidity from Right Duct-AM2302
float h2 = dht2.readHumidity();
Serial.print("Humidity Right ");
Serial.print(h2);
Serial.println(" %");
BluetoothSerial.print("Humidity Right      ");
BluetoothSerial.print(h2);
BluetoothSerial.print("%");
BluetoothSerial.print("\r\n");

// Read temperature as Celsius (the default)-AM2302
float t1 = dht.readTemperature();
Serial.print("Temperature Left ");
Serial.print(t1);
Serial.println(" C");
BluetoothSerial.print("Temperature Left      ");
BluetoothSerial.print(t1);
BluetoothSerial.print("C");
BluetoothSerial.print("\r\n");

//temperature -AM2302
float t2 = dht2.readTemperature();
Serial.print("Temperature Right");
Serial.print(t2);
Serial.println(" C");
BluetoothSerial.print(" Temperature Right      ");
BluetoothSerial.print(t2);
BluetoothSerial.print("C");
BluetoothSerial.print("\r\n");

if (isnan(h1) || isnan(t1)) {
  Serial.println("Failed to read from DHT sensor!");
}
if (isnan(h2) || isnan(t2)) {
  Serial.println("Failed to read from DHT sensor!");
}

//Occupancy Count

```

```

    if (sensorVal1 == LOW && sensorVal2 == HIGH && sensorVal3 == HIGH &&
sensorVal4 == HIGH) {
        digitalWrite(8, HIGH);
        digitalWrite(9, LOW);
        digitalWrite(2, LOW);
        digitalWrite(3, LOW);
        Occupancy = 1;
    }
    if (sensorVal1 == LOW && sensorVal2 == LOW && sensorVal3 == HIGH &&
sensorVal4 == HIGH) {
        digitalWrite(8, HIGH);
        digitalWrite(3, HIGH);
        digitalWrite(2, LOW);
        digitalWrite(9, LOW);
        Occupancy = 2;
    }
    if (sensorVal1 == LOW && sensorVal2 == LOW && sensorVal3 == LOW &&
sensorVal4 == HIGH) {
        digitalWrite(8, HIGH);
        digitalWrite(3, HIGH);
        digitalWrite(2, HIGH);
        digitalWrite(9, LOW);
        Occupancy = 3;
    }

    if (sensorVal1 == LOW && sensorVal2 == LOW && sensorVal3 == LOW &&
sensorVal4 == LOW) {
        digitalWrite(8, HIGH);
        digitalWrite(3, HIGH);
        digitalWrite(2, HIGH);
        digitalWrite(9, HIGH);
        Occupancy = 4;
    }

    if (sensorVal1 == HIGH && sensorVal2 == HIGH && sensorVal3 == HIGH &&
sensorVal4 == HIGH) {
        digitalWrite(8, LOW);
        digitalWrite(3, LOW);
        digitalWrite(2, LOW);
        digitalWrite(9, LOW);
        Occupancy = 0;
    }

    Serial.print("Occupancy=");
    Serial.println(Occupancy);
    BluetoothSerial.print("Occupancy:");
    BluetoothSerial.print(Occupancy);
    BluetoothSerial.print(",");
    BluetoothSerial.print("\r\n");

//Light Switch
if (toggleState == HIGH) {
    Serial.println("Lights ON");
    BluetoothSerial.print("Lights ON ,");
}

```

```

        BluetoothSerial.print("\r\n");
    }
    else {
        Serial.println("Lights OFF");
        BluetoothSerial.print("Lights OFF");
        BluetoothSerial.print("\r\n");
    }
}

//Door Position
if (proximity == HIGH) {
    Serial.println("Door Closed");
    BluetoothSerial.print("Door Closed ,");
    BluetoothSerial.print("\r\n");
}
else {
    Serial.println("Door Open");
    BluetoothSerial.print("Door Open ,");
    BluetoothSerial.print("\r\n");
}

//PV Panel
val = analogRead(A1);    // read the input pin
float voltage = val * (5.0 / 1023.0);
Serial.print("PV1 voltage=");
Serial.println(voltage);    // debug value
BluetoothSerial.print("PV1=");
BluetoothSerial.print(voltage);
BluetoothSerial.print(",");
BluetoothSerial.print("\r\n");

DateTime now = RTC.now();
Serial.print("");
Serial.print(now.year(), DEC);
Serial.print("/");
Serial.print(now.month(), DEC);
Serial.print("/");
Serial.print(now.day(), DEC);
Serial.print(" ");
Serial.print(now.hour(), DEC);
Serial.print(":");
Serial.print(now.minute(), DEC);
Serial.print(":");
Serial.print(now.second(), DEC);
Serial.print("");
Serial.println(" ");

BluetoothSerial.print(now.year(), DEC);
BluetoothSerial.print("/");
BluetoothSerial.print(now.month(), DEC);
BluetoothSerial.print("/");
BluetoothSerial.print(now.day(), DEC);
BluetoothSerial.print(" ");
BluetoothSerial.print(now.hour(), DEC);

```

```

BluetoothSerial.print(":");
BluetoothSerial.print(now.minute(), DEC);
BluetoothSerial.print(":");
BluetoothSerial.print(now.second(), DEC);
BluetoothSerial.print(",");
BluetoothSerial.print("\r\n");

//Printing data to SD Card
now = RTC.now();
logfile.print(now.year(), DEC);
logfile.print("/");
logfile.print(now.month(), DEC);
logfile.print("/");
logfile.print(now.day(), DEC);
logfile.print(",");
logfile.print(now.hour(), DEC);
logfile.print(":");
logfile.print(now.minute(), DEC);
logfile.print(":");
logfile.print(now.second(), DEC);
logfile.print(",");
logfile.print(Occupancy);
logfile.print(",");
logfile.print(toggleState);
logfile.print(",");
logfile.print(proximity);
logfile.print(",");
logfile.print(voltage);
logfile.print(",");
logfile.print(windMPH);
logfile.print(",");
logfile.print(AF1);
logfile.print(",");
logfile.print(tempC);
logfile.print(",");
logfile.print(windMPH2);
logfile.print(",");
logfile.print(AF2);
logfile.print(",");
logfile.print(tempC2);
logfile.print(",");
logfile.print(h1);
logfile.print(",");
logfile.print(t1);
logfile.print(",");
logfile.print(hic1);
logfile.print(",");
logfile.print(h2);
logfile.print(",");
logfile.print(t2);
logfile.print(",");
logfile.print(hic2);
logfile.print(",");
logfile.println(" ");

```

```

logfile.flush();

//Ethernet logging
EthernetClient client = server.available();
if (client) {
  Serial.println("new client");
  // an http request ends with a blank line
  boolean currentLineIsBlank = true;
  while (client.connected()) {
    if (client.available()) {
      char c = client.read();
      Serial.write(c);
      // if you've gotten to the end of the line (received a newline
      // character) and the line is blank, the http request has ended,
      // so you can send a reply
      if (c == '\n' && currentLineIsBlank) {
        // send a standard http response header
        client.println("HTTP/1.1 200 OK");
        client.println("Content-Type: text/html");
        client.println("Connection: close"); // the connection will be
closed after completion of the response
        client.println("Refresh: 5"); // refresh the page automatically
every 5 sec
        client.println();
        client.println("<!DOCTYPE HTML>");
        client.println("<html>");
        client.print("Date/Time ");
        client.print(now.year(), DEC);
client.print("/");
client.print(now.month(), DEC);
client.print("/");
client.print(now.day(), DEC);
client.print("  ");
client.print(now.hour(), DEC);
client.print(":");
client.print(now.minute(), DEC);
client.print(":");
client.print(now.second(), DEC);
client.println("<br />");
client.print("Occupancy: ");
client.print(Occupancy);
  client.println("<br />");
client.print("Lighting: ");
client.print(toggleState);
  client.println("<br />");
client.print("Door Position(0-Closed, 1-Open): ");
client.print(proximity);
  client.println("<br />");
client.print("PV Voltage: ");
client.print(voltage);
  client.println("<br />");
client.print("Left WindSensor (MPH): ");

```

```

client.print(windMPH);
  client.println("<br />");
client.print("Left WindSensor (m3/s): ");
client.print(AF1);
  client.println("<br />");
client.print("Left WindSensor Temp (C): ");
client.print(tempC);
  client.println("<br />");
client.print("Right WindSensor (MPH): ");
client.print(windMPH2);
  client.println("<br />");
client.print("Right WindSensor (m3/s): ");
client.print(AF2);
  client.println("<br />");
client.print("Right WindSensor Temp (C): ");
client.print(tempC2);
  client.println("<br />");
client.print("RIght RH (%): ");
client.print(h1);
  client.println("<br />");
client.print("Right Temperature (C): ");
client.print(t1);
  client.println("<br />");
client.print("Left RH (%): ");
client.print(h2);
  client.println("<br />");
client.print("Left Temp (C): ");
client.println(t2);
client.println("</html>");
  break;
}
if (c == '\n') {
  // you're starting a new line
  currentLineIsBlank = true;
}
else if (c != '\r') {
  // you've gotten a character on the current line
  currentLineIsBlank = false;
}
}
}
delay(1);
// close the connection:
client.stop();
Serial.println("client disconnected");
}
}

```

## 12 Appendix C Calibration

*Table C-1 Right Duct Sensor Calibration Measurements*

Right Duct Calibration		
Calibration Point Temperature Sensor (°C)	Wind Sensor Rev P Arduino Reading (°C)	AM2302 Arduino Recording (°C)
24.15	27.81	24.1
8.45	11.54	7.2
8	10.79	6.8
21.5	24.81	20.3
22	25.31	21.5
22.65	26.56	22.3
23	25.56	22.7
23.7	26.06	23.8
24	26.06	23.8
24	26.56	23.8

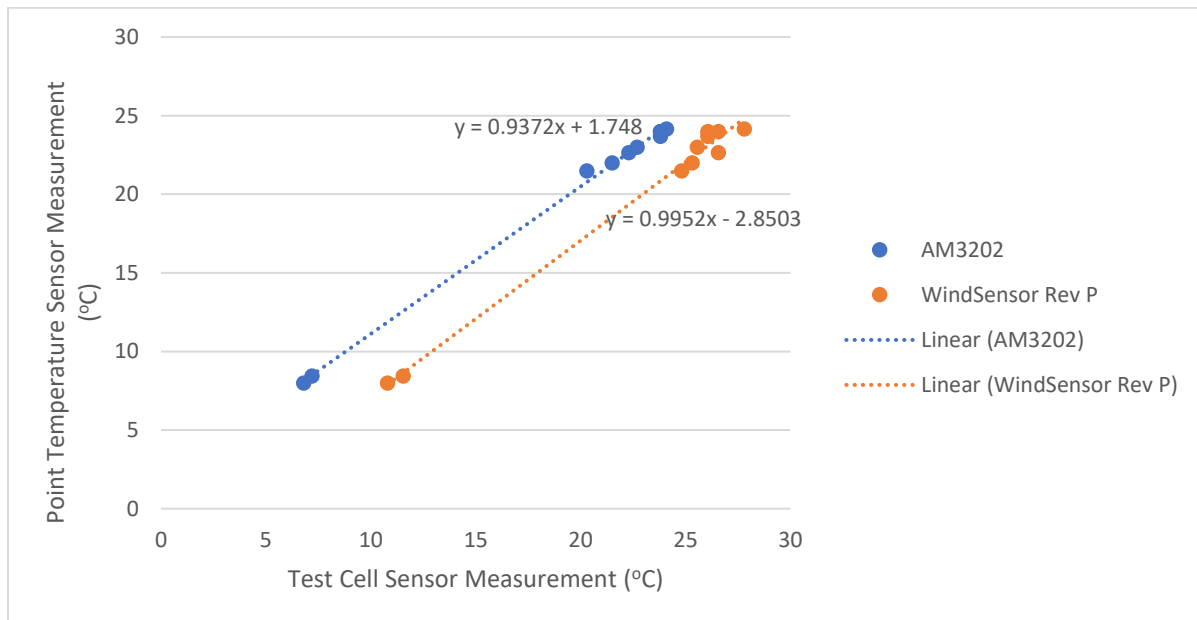


*Figure C-1 Right Ventilation Duct Sensor Calibration*

Table C-266 Right Duct WindSensor Rev P and Balometer Data for Calibration

Balometer CFM	Arduino MPH	Calculated Arduino CFM
109	12.88	115.24
112	12.65	115.07
114	13.12	115.42
119	13.36	115.60
115	13.36	115.60
112	10.22	113.23
114	9.01	112.31
114	7.51	111.18
112	7.77	111.38
114	7.77	111.38
109	7.51	111.18
122	21.58	121.82
123	18.55	119.53
118	18.34	119.36
121	18.75	119.68

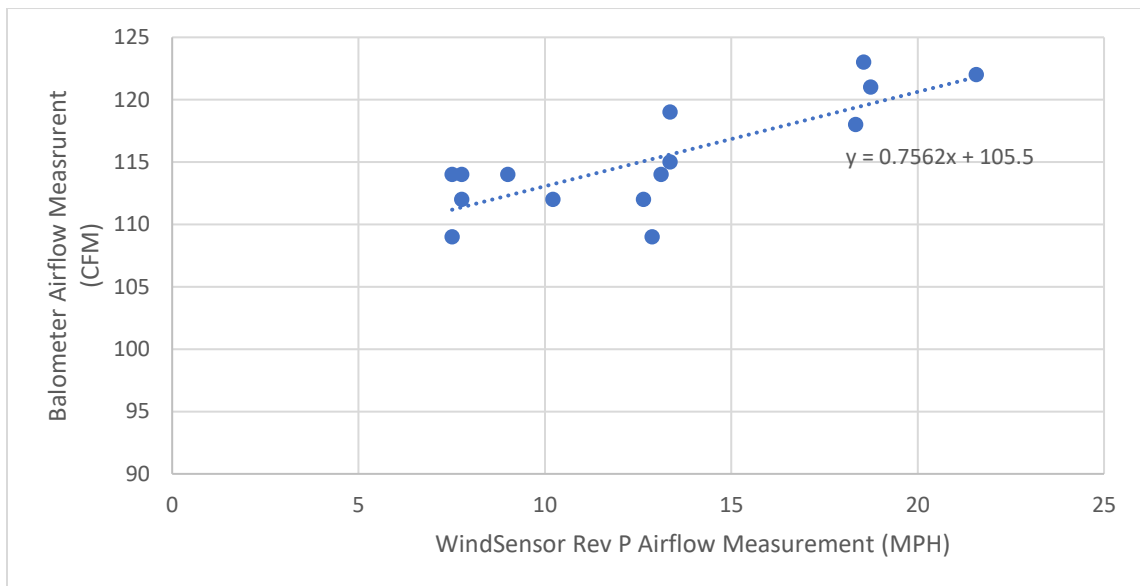


Figure C-290 Right Duct WindSensor Rev P Airflow Rate Calibration

Table C-3 Left Duct Sensor Calibration Measurements

Right Duct Calibration		
Calibration Point Temperature Sensor (°C)	Wind Sensor Rev P Arduino Reading (°C)	AM2302 Arduino Recording (°C)
21	22.4	22.06
21	22.4	22.06
21	22.3	22.81
21	22.3	22.56
21	22.3	22.81
25.5	23.2	25.31
25.5	23.3	24.81
24	23.4	25.81
24	23.5	25.56
24.38	23.6	25.81
24.3	24	26.06
24.5	24.1	26.06
23.57	25.06	22.6
23.5	24.81	22.7
23.56	25.31	22.8

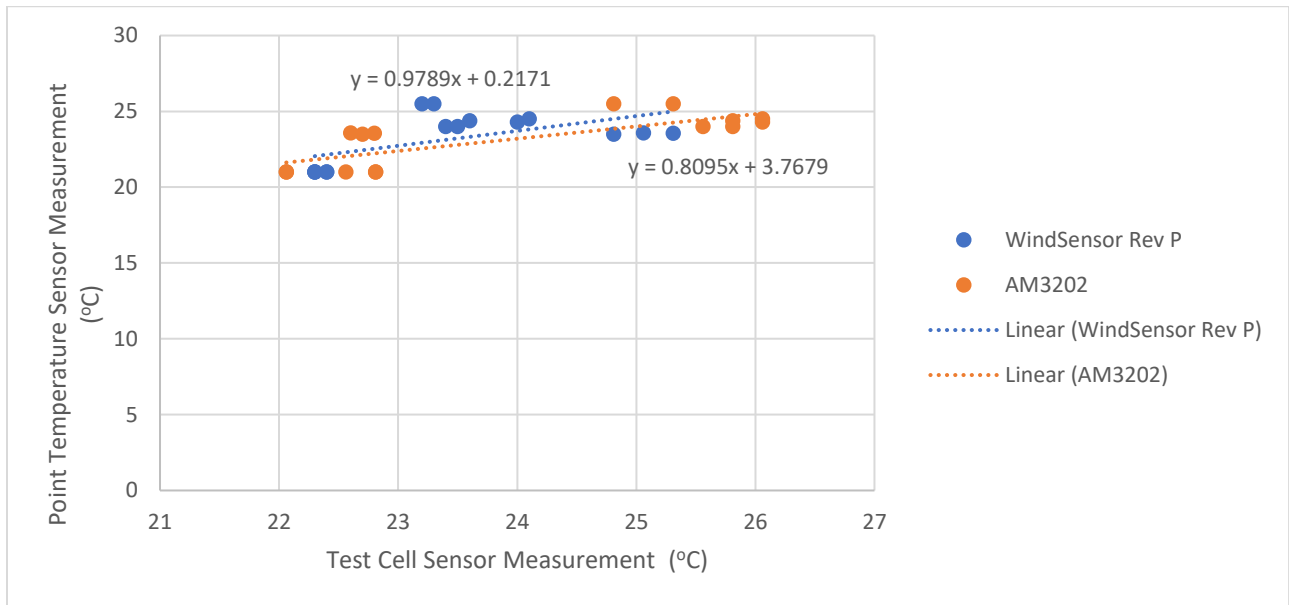


Figure C-3 Left Ventilation Duct Sensor Calibration

Table C-4 Left Duct WindSensor Rev P and Balometer Data for Calibration

Balometer CFM	Arduino MPH	Calculated Arduino CFM
68	3.67	66.64
64.6	3.86	67.09
66.8	3.57	66.41
68.8	3.67	66.64
66.4	3.67	66.64
68.8	4.62	68.87
59	0.66	59.58
66.8	1.47	61.48
62.2	1.35	61.20
61.9	1.28	61.03
59	1.39	61.29
58.2	1.47	61.48
60.2	1.39	61.29
64.6	4.62	68.87
63.5	4.4	68.36
72.9	4.62	68.87
72.9	4.62	68.87

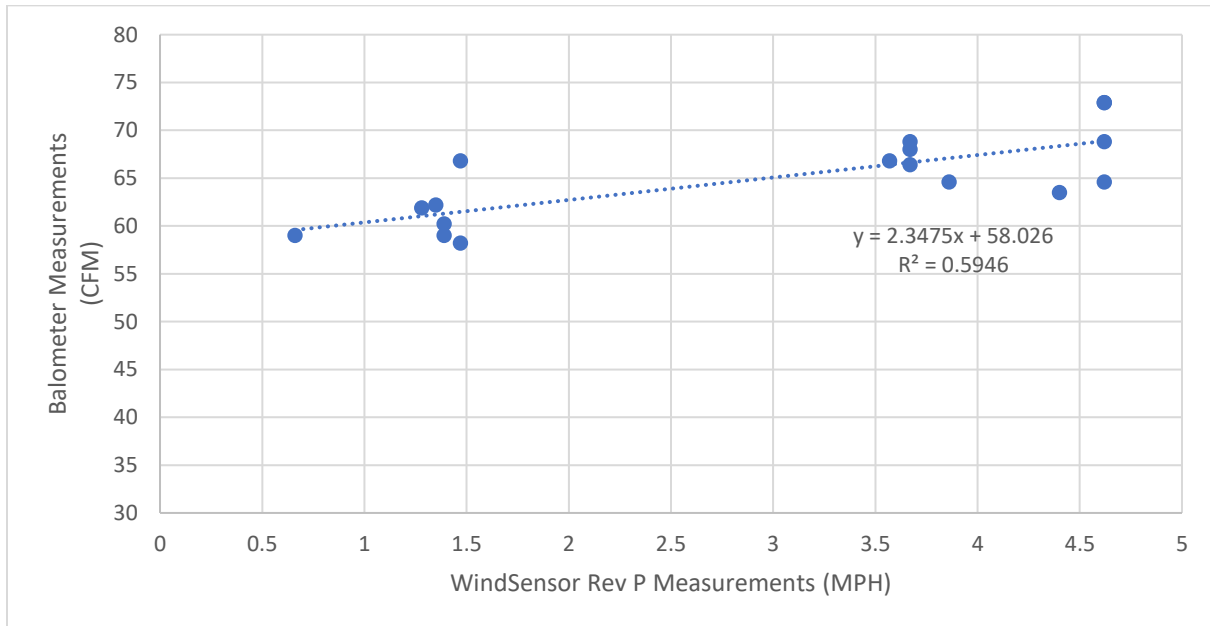


Figure C-491 Left Duct WindSensor Rev P Calibration

### 13 Appendix D U-value Calculations

*Table D-1 U-value calculation for the spandrel panel*

	Thickness (inch)	Thickness (m)	Material	Conductance (W/mK)	Conductivity (W/m <sup>2</sup> K)	Resistivity
Exterior air film					34	0.029411765
Sheet metal	0.13	0.003175	Steel, mild	45	14173.22835	7.05556E-05
Fiberglass Insulation	1.5	0.0381	Owens Curtain Wall Insulation	0.032	0.839895013	1.190625
Sheet Metal	0.13	0.003175	Steel, mild	45	14173.22835	7.05556E-05
interior air film					9.3	0.107526882

<b>Total Resistivity</b>	1.220177876
--------------------------	-------------

*Table D-2 U-value calculation for the interior walls*

	Thickness (inch)	Thickness (m)	Material	Conductance (W/mK)	Conductivity (W/m <sup>2</sup> K)	Resistivity
interior air film					8.3	0.120481928
3/8" drywall	0.375	0.009525	9.5mm plater board		16.6	0.060240964
3.5" Air cavity	3.5	0.0889	92mm, E=.82		6.425	0.15077821
0.5" Steel studs @ 16" OC			steel, mild	45	506.1867267	6.17361E-05
3/8" drywall	0.375	0.009525	9.5mm plater board		16.6	0.060240964
interior air film					8.3	0.120481928

<b>Total Resistance:</b>	0.512285729
--------------------------	-------------

*Table D-3 Interpolating Conductivity value for the Air Space from Building Science for a Cold Climate*

Temperature (°C)	Conductivity
30	6.6 [56]
10	6.1 [56]
23	6.425

*Table D-467 Exterior Wall Resistivity Calculation*

	Thickness(m)	Material	Conductance (W/mK)	Conductivity (W/m <sup>2</sup> K)	Resistivity
Concrete	0.275	Dense concrete, dry	1.32	4.8	0.208333333

*Table D-5 Ceiling/Floor Resistivity Calculation*

	Thickness (inch)	Thickness (m)	Material	Conductance (W/mK)	Conductivity (W/m <sup>2</sup> K)	Resistivity
Concrete	13.75	0.34925	Dense concrete, dry	1.32	3.779527559	0.2645833

## 14 Appendix E Matlab Code

```
clear all;
Arduino = 'Arduino_Jan2 (9AM).xlsx';
Ambient_hall = 'Hallway_Jan2 (9AM).xlsx';
Outdoor = 'Outdoor_Jan2 (9AM).xlsx';
Heater = 'Heater_Jan2 (9AM).xlsx';
Solar = 'Solar_Jan2 (9AM).xlsx';
Thermocouples = 'Thermocouples_Jan2 (9AM).xlsx';

Time1 = xlsread('Output_Jan2 (9AM).xlsx',1,'A1:A300');
Tamb_Out = xlsread('Output_Jan2 (9AM).xlsx',1,'C1:C300');
Arduino_timestamp = xlsread(Arduino,1,'A1:A61');
MPH_left= xlsread(Arduino,1,'F1:F61');
MPH_right= xlsread(Arduino,1,'I1:I61');
Temp_left= xlsread(Arduino,1,'H1:H61');
Temp_right= xlsread(Arduino,1,'K1:K61');
Door= xlsread(Arduino,1,'D1:D61');
Occupancy= xlsread(Arduino,1,'B1:B61');
InteriorLight= xlsread(Arduino,1,'C1:C61');
PlugLoad = xlsread(Arduino,1,'L1:L61');

Ambient_timestamp = xlsread(Ambient_hall,1,'A1:A61');
Ambient_Hall = xlsread(Ambient_hall,1,'B1:B61');

Out_stamp = xlsread(Outdoor,1,'A1:A61');
Outdoor_Temp= xlsread(Outdoor,1,'B1:B61');
Windv = xlsread(Outdoor,1,'C1:C61');

Heater_stamp = xlsread(Heater,1,'A1:A300');
Heater = xlsread(Heater,1,'B1:B300');
Therm_stamp = xlsread(Thermocouples,1,'A1:A100');
Floor = xlsread(Thermocouples,1,'E1:E100');
Ceiling = xlsread(Thermocouples,1,'B1:B100');
ExteriorWall = xlsread(Thermocouples, 1, 'D1:D100');

Solar_stamp = xlsread(Solar,1,'A1:A21');
SW_solar = xlsread(Solar,1,'B1:B21');
LW_solar = xlsread(Solar,1,'C1:C21');

a_size = size(MPH_left1);
x=1;
while (x<=a_size)
Cal_CFM_left (x)=(MPH_left(x)*2.3475)+58.026;
Cal_CFMH_right (x) = (MPH_right(x)*0.7562)+105.5;
Cal_Temp_right(x) = (Temp_right(x)*0.9952)-2.8503;
Cal_Temp_left(x) = (Temp_left(x)*0.9789)+0.2171;
x=x+1;
end

%Convert MPH to m3/s%
k=1;
```

```

while(k<=a_size)
    M_m3s_left(k) = Cal_CFM_left(k)*0.00047;
    M_m3s_right(k) = Cal_CFMH_right(k)*0.00047;
    k=k+1;
end
%Calculate the m/s value%
%Area of duct is 0.01943m2%
k=1;
while(k<=a_size)
    M_ms_left(k) = M_m3s_left(k)/0.01943;
    M_ms_right(k) = M_m3s_right(k)/0.01943;
    k=k+1;
end

%Calculate T-sky and hc wind
x=1;
t_size= size(Outdoor_Temp_Nov,1);
while(x<=t_size)
    T_sky(x) = (1.2*Outdoor_Temp(x))-14;
    hc_wind(x) = (3.9*Wind(x))+5.6;
    x=x+1;
end

%Combine Matrices%
C_CFM_left = [Arduino_timestamp'; M_m3s_left];
C_CFM_right = [Arduino_timestamp'; M_m3s_right];
C_Temp_left = [Arduino_timestamp'; Cal_Temp_left];
C_Temp_right = [Arduino_timestamp'; Cal_Temp_right];
C_Door_Nov = [Arduino_timestamp'; Door'];
C_Occupancy = [Arduino_timestamp'; Occupancy'];
C_InteriorLight = [Arduino_timestamp';InteriorLight'];
C_PlugLoad = [Arduino_timestamp';PlugLoad'];

C_Ambient_Hall=[Ambient_timestamp';Ambient_Hall'];

C_Outdoor_Temp = [Out_stamp'; Outdoor_Temp'];
C_Wind = [Out_stamp'; Wind_Nov'];
C_T_sky = [Out_stamp'; T_sky];
C_hc_wind = [Out_stamp'; hc_wind];

C_Heater = [Heater_stamp'; Heater'];

C_SW_solar = [Solar_stamp'; SW_solar'];
C_LW_solar = [Solar_stamp'; LW_solar'];

save('MPH_left_test.mat','C_CFM_left','-mat','-v7.3') ;
save('MPH_right_test.mat','C_CFM_right','-mat','-v7.3');
save('Temp_right_test.mat','C_Temp_right','-mat','-v7.3');
save('Temp_left_test.mat','C_Temp_left','-mat','-v7.3');
save('Door_test.mat','C_Door',' -mat','-v7.3');
save('Occupancy_test.mat','C_Occupancy','-mat','-v7.3');
save('InteriorLight_test.mat','C_InteriorLight', '-mat','-v7.3') ;
save('PlugLoad_test.mat','C_PlugLoad','-mat','-v7.3');

```

```
save('Ambient_Hall_test.mat','C_Ambient_Hall', '-mat', '-v7.3');
save('Outdoor_Temp_test.mat','C_Outdoor_Temp', '-mat', '-v7.3') ;
save('Heater_test.mat', 'C_Heater', '-mat', '-v7.3') ;
save('SW_solar_test.mat','C_SW_solar', '-mat', '-v7.3');
save('Wind_test.mat','C_Wind', '-mat', '-v7.3');
save('LW_solar_test.mat','C_LW_solar', '-mat', '-v7.3');
save('T_sky_test.mat', 'C_T_sky', '-mat', '-v7.3') ;
save('hc_wind_test.mat', 'C_hc_wind', '-mat', '-v7.3');
```

## 15 Appendix F Simulink Images

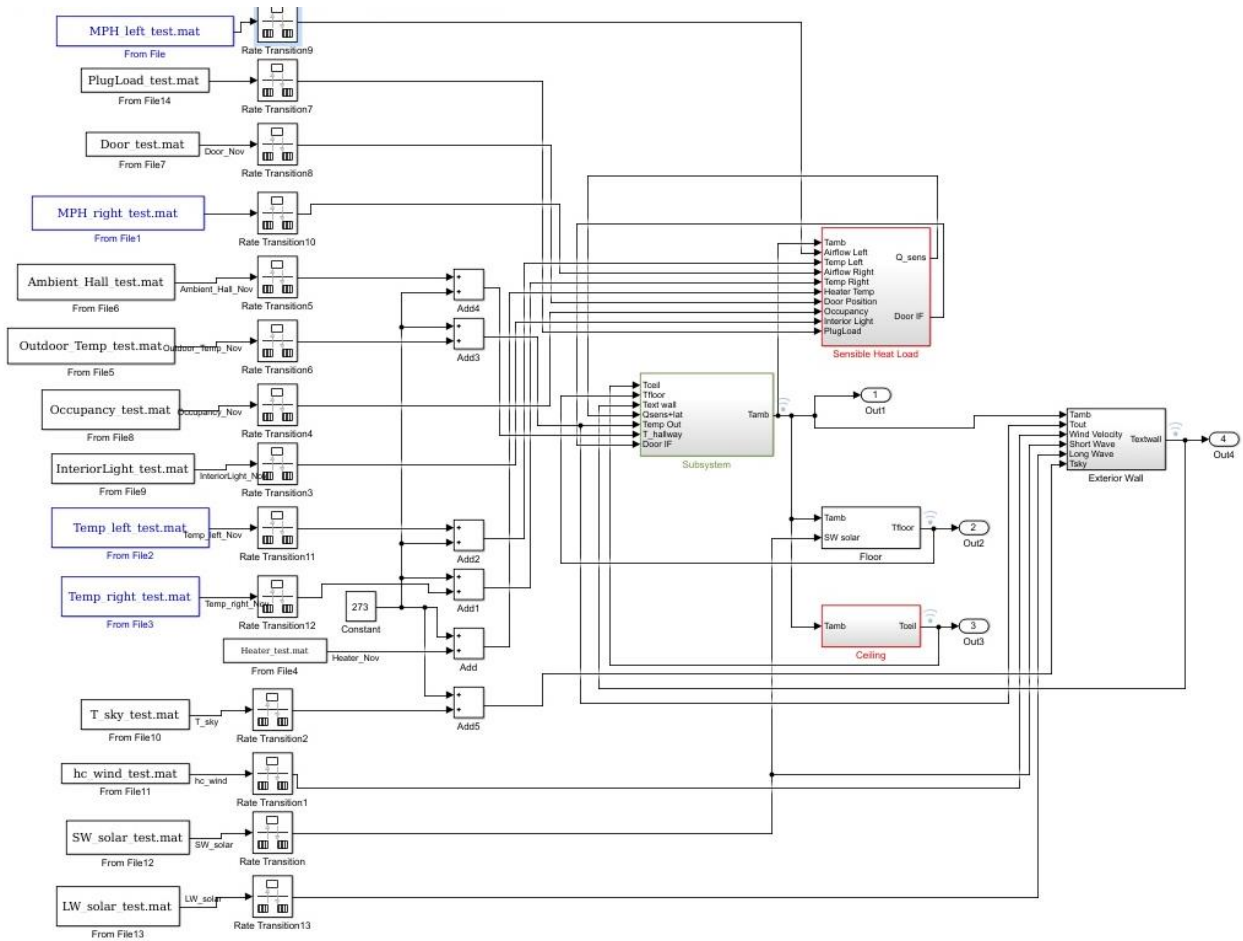


Figure F-1 Full G1v1 Model

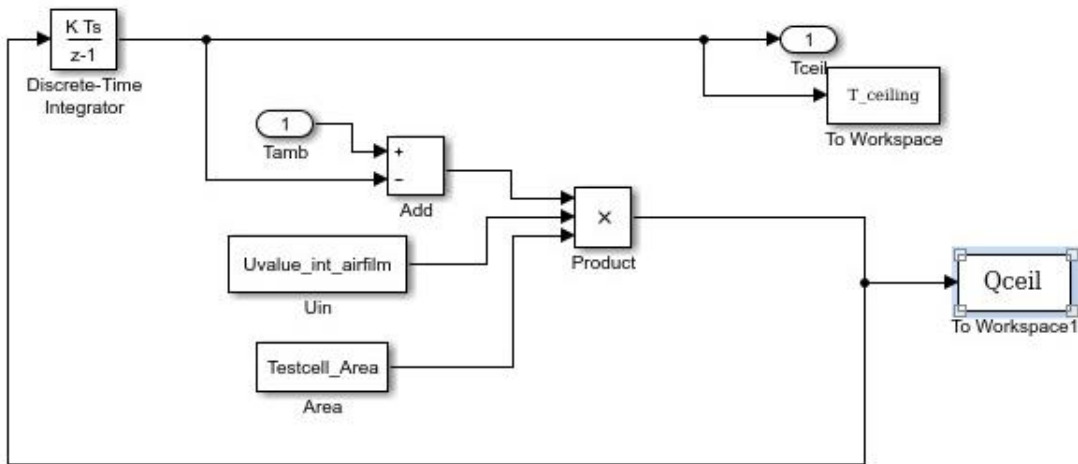


Figure F-2 G1v1 Ceiling Subsystem Differential Equation



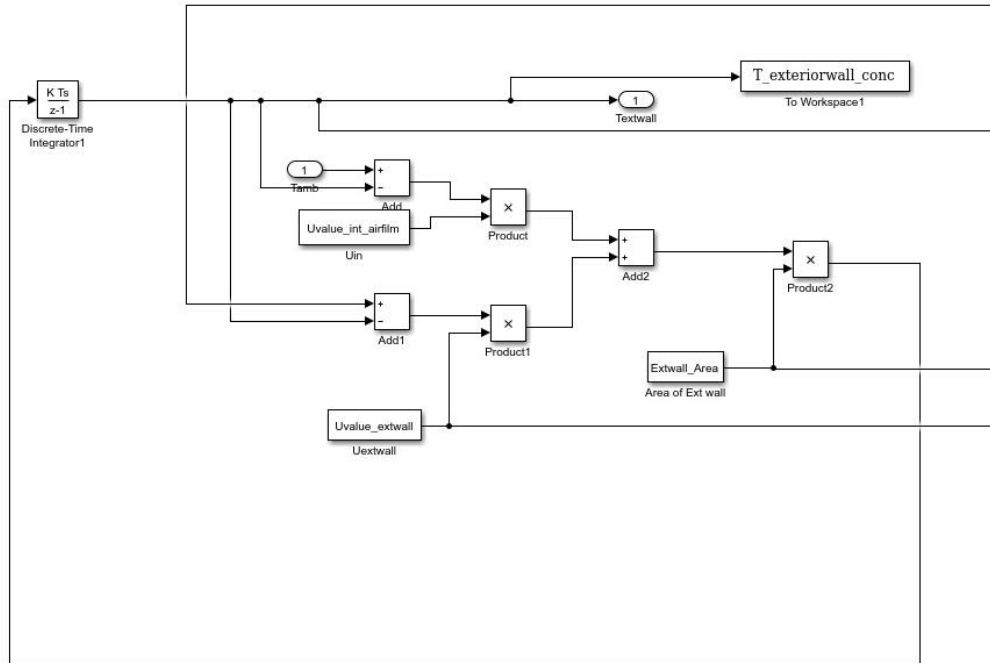


Figure F-5 Exterior Wall Subsystem - Interior node Differential Equation

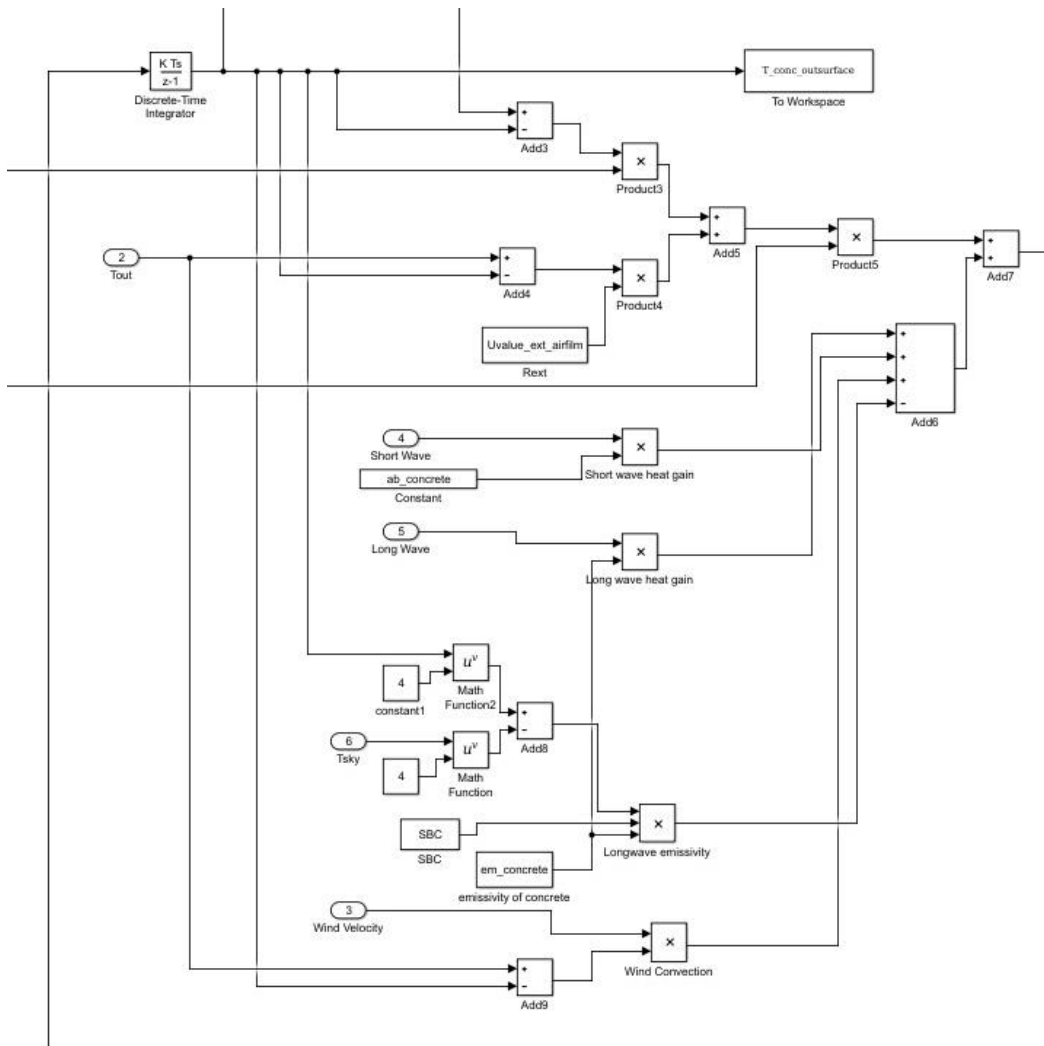


Figure F-6 Exterior Wall Subsystem - Exterior node Differential Equation

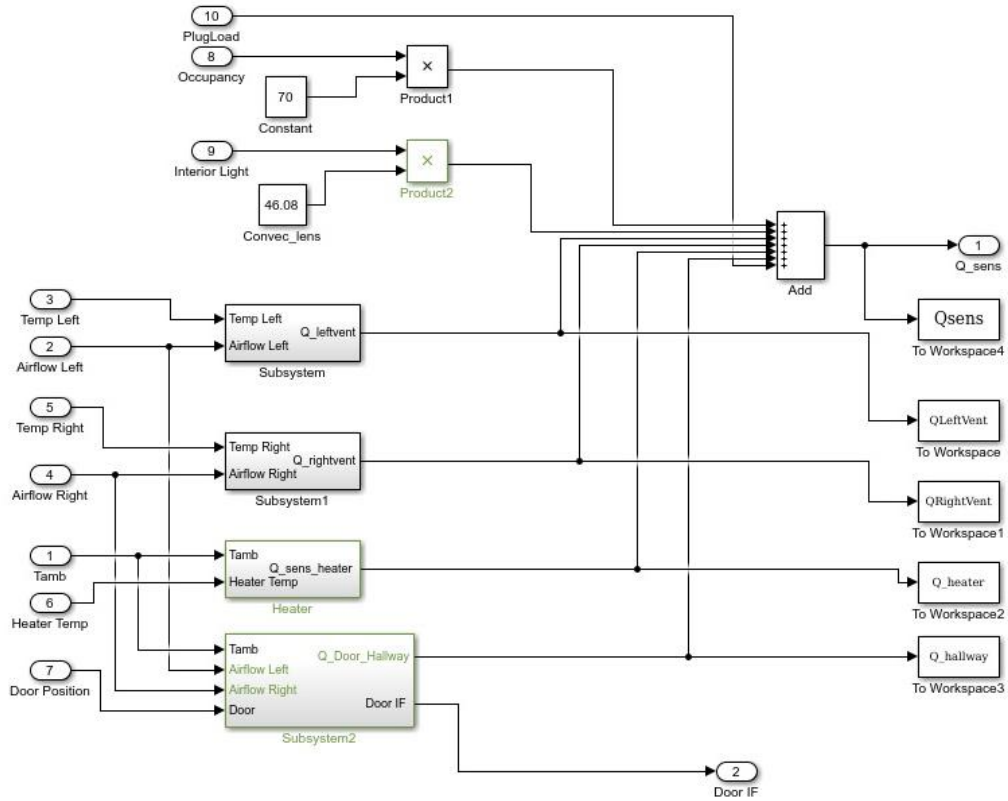


Figure F-7 G1v1 Sensible Heat Load Calculation

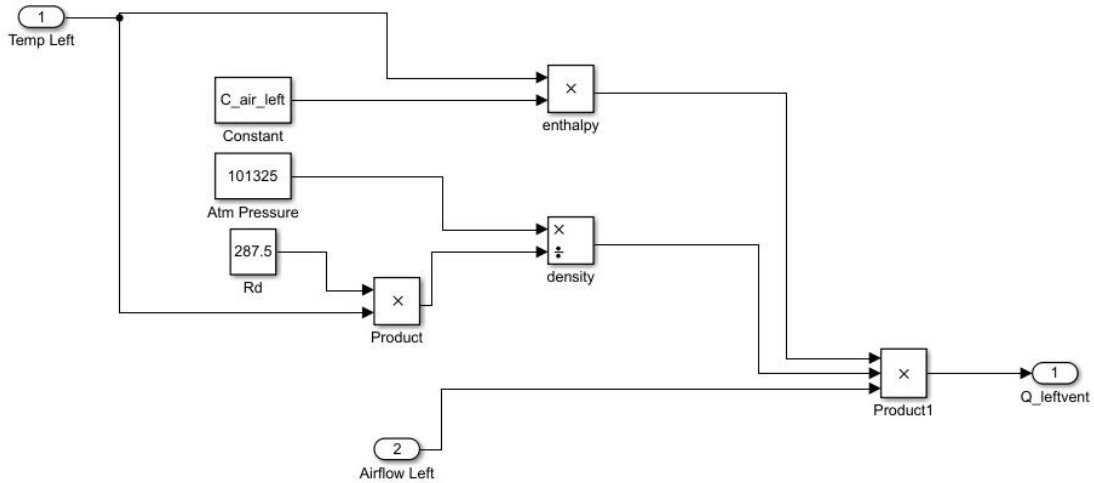


Figure F-8 Left Ventilation Subsystem - Sensible Heat Load Calculation

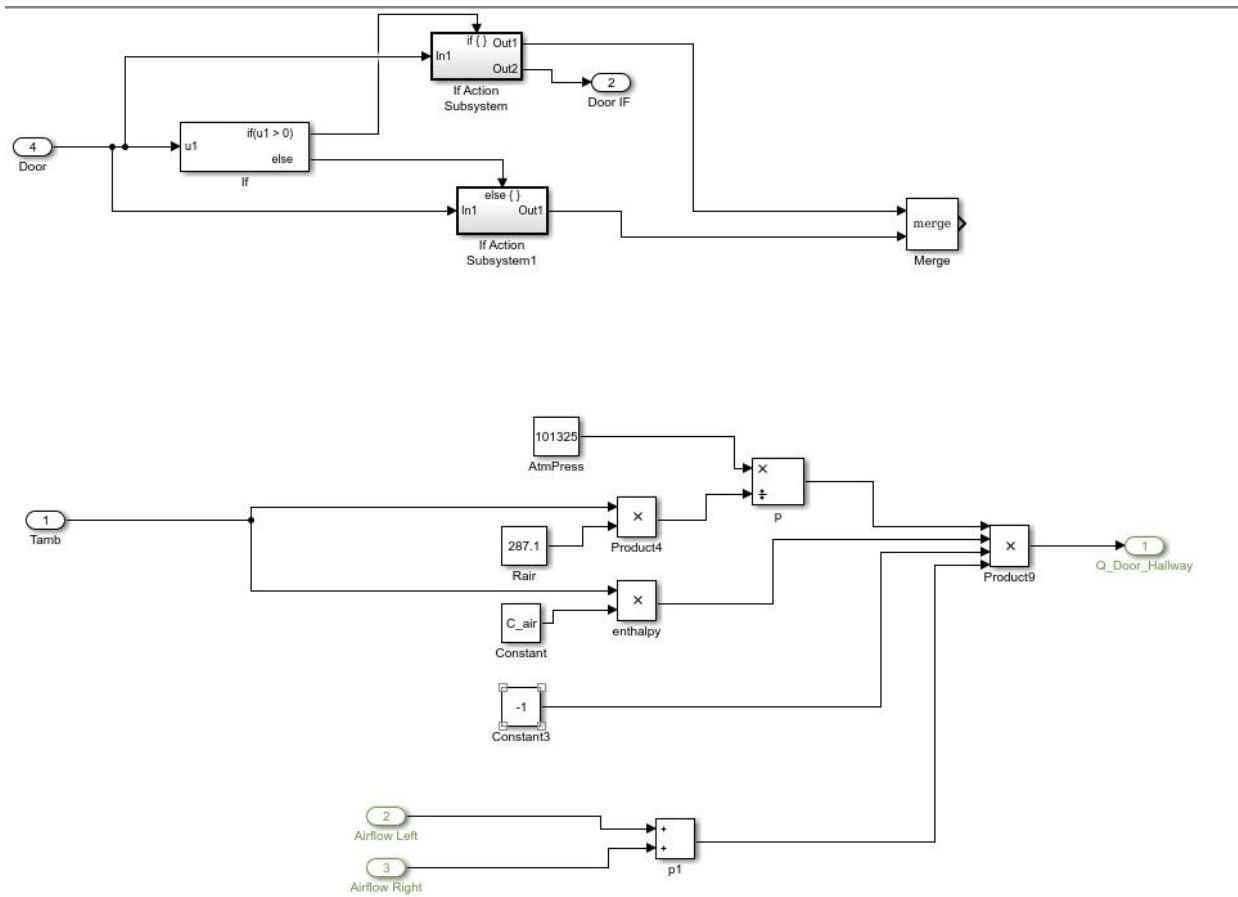


Figure F-9 Hallway Subsystem - Exfiltration Heat Loss

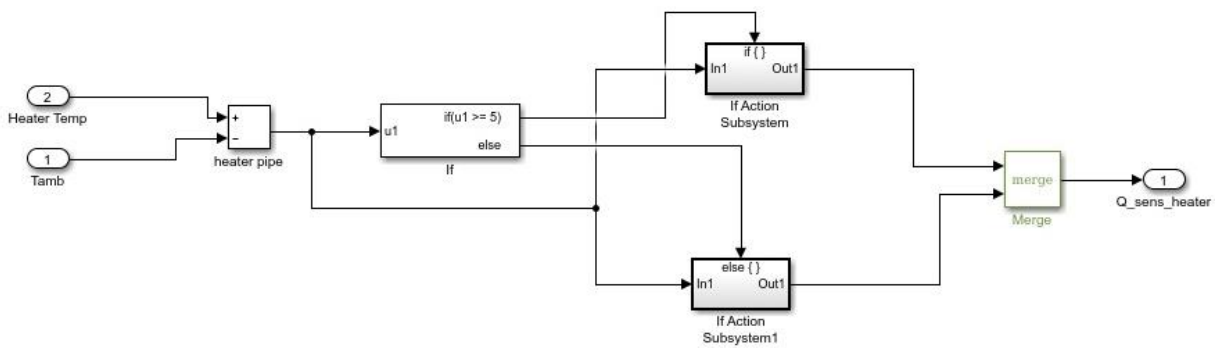


Figure F-10 Heater Subsystem - If Statement for Heater Temperature Difference from the Ambient Temperature of at least 5 degrees Kelvin

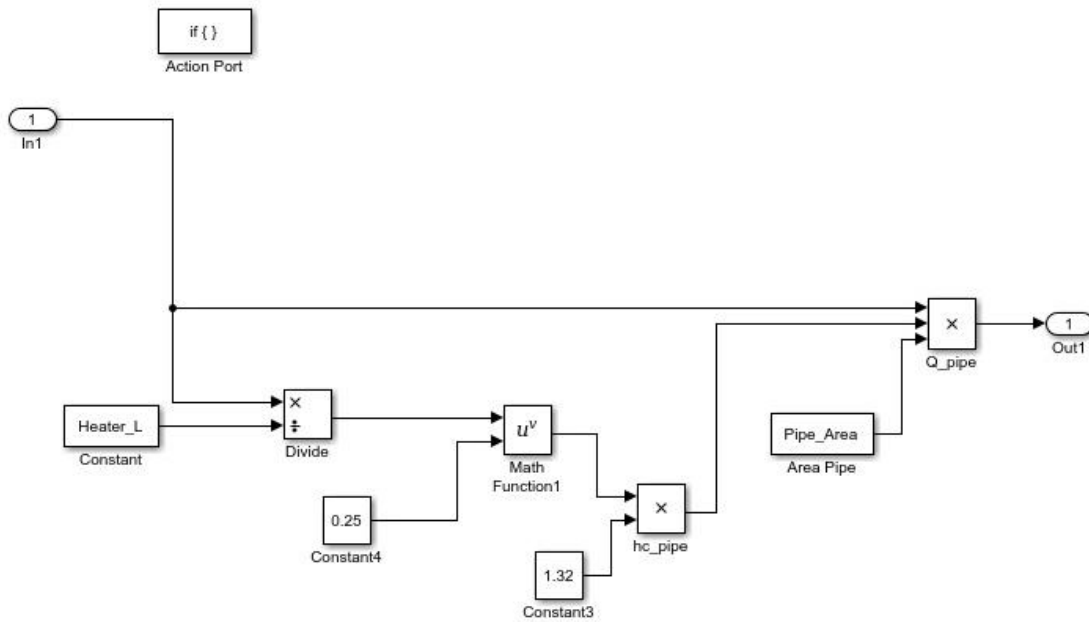


Figure F-1192 Heater If Action - Heater Heat Load Calculation when Temperature Difference is Greater Than 5 degrees Kelvin

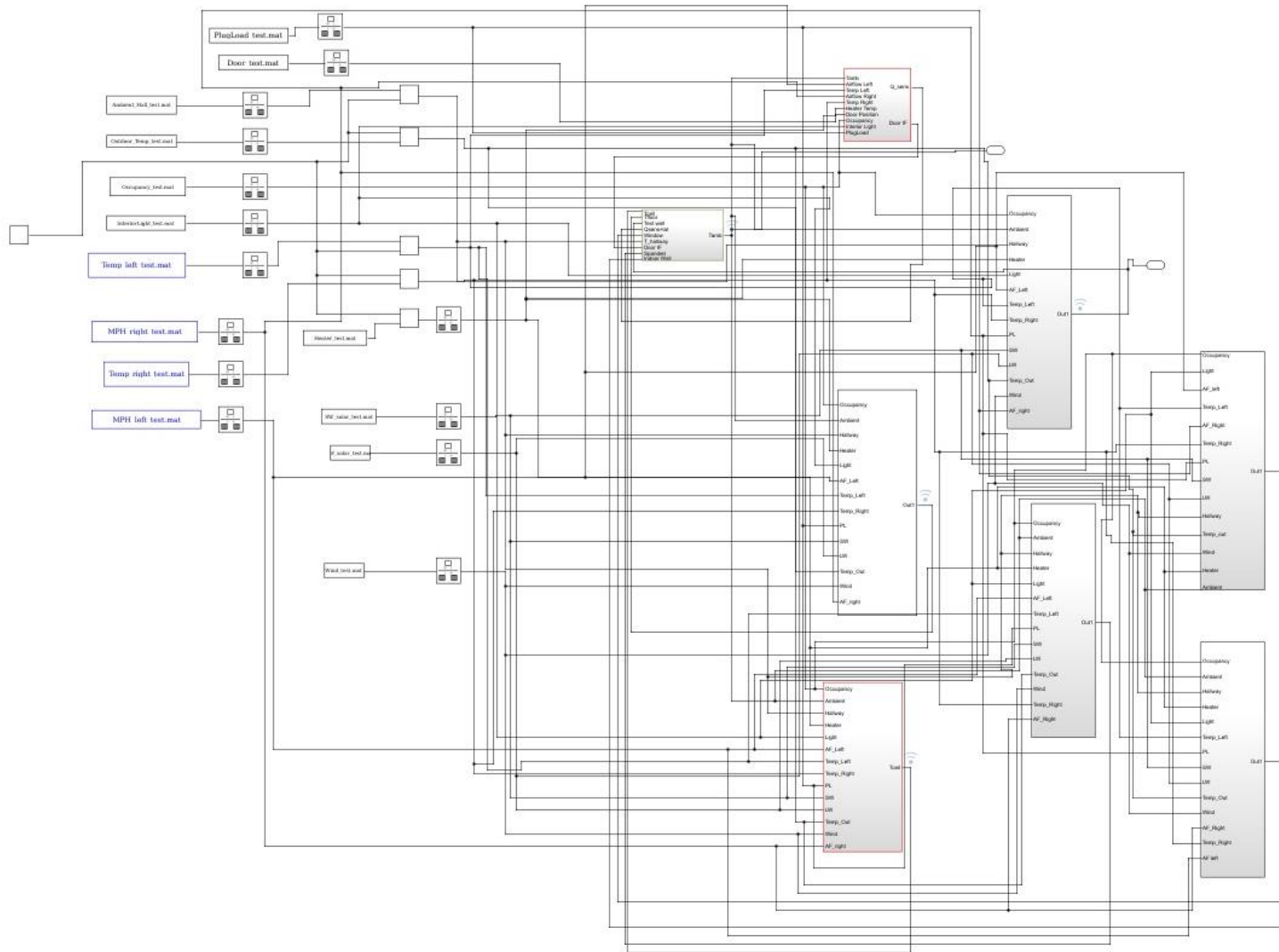


Figure F-12 Final Grey Box Model - Data Input Blocks on the Left and the Linear Regression Blocks and Heat Load Calculation Blocks on the Right

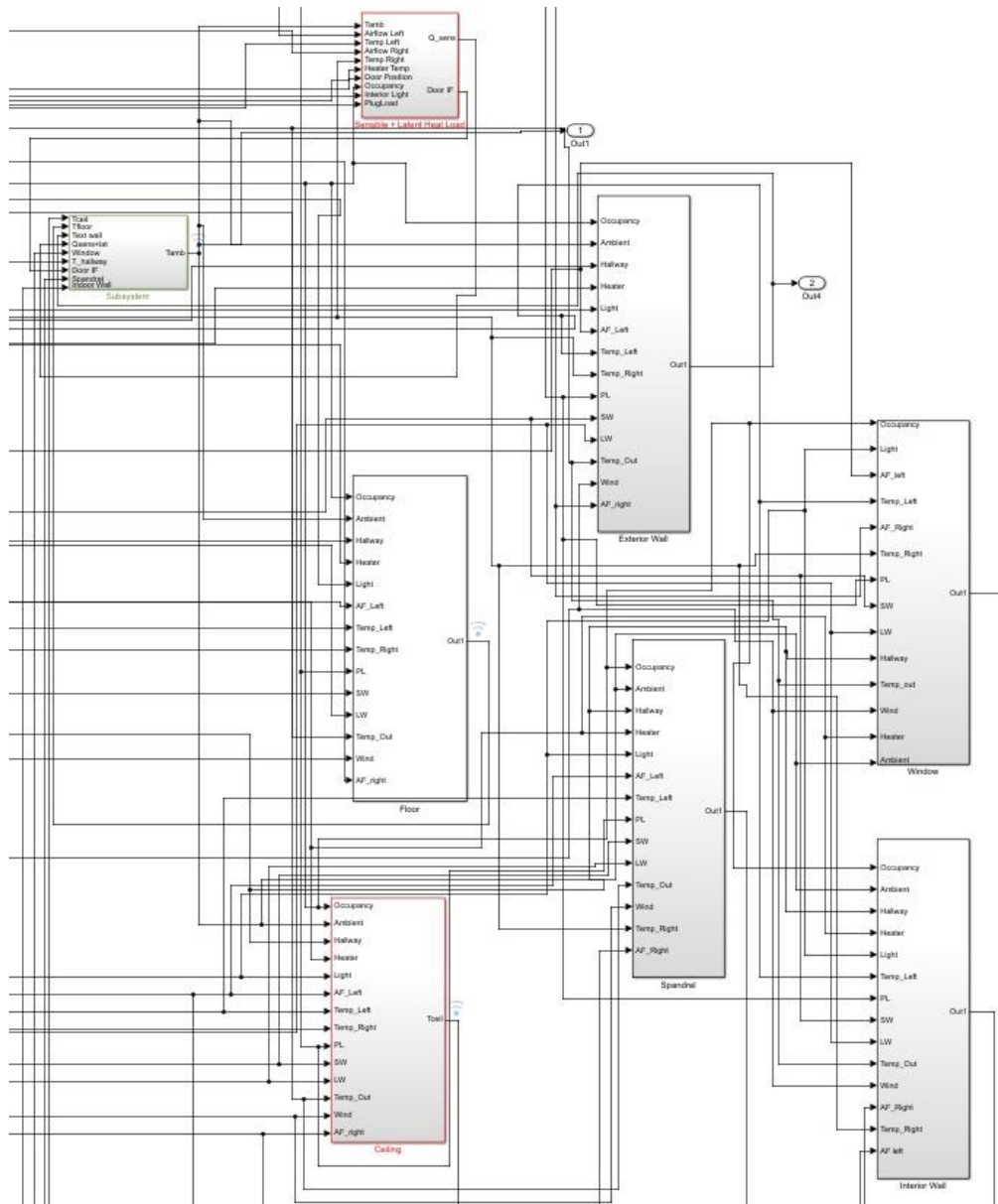


Figure F-13 Subsystem Blocks for the Final Model, Including the Ambient Temperature System (same as G1v1), Sensible Heat Load (same as G1v1), and the Regression Model Blocks

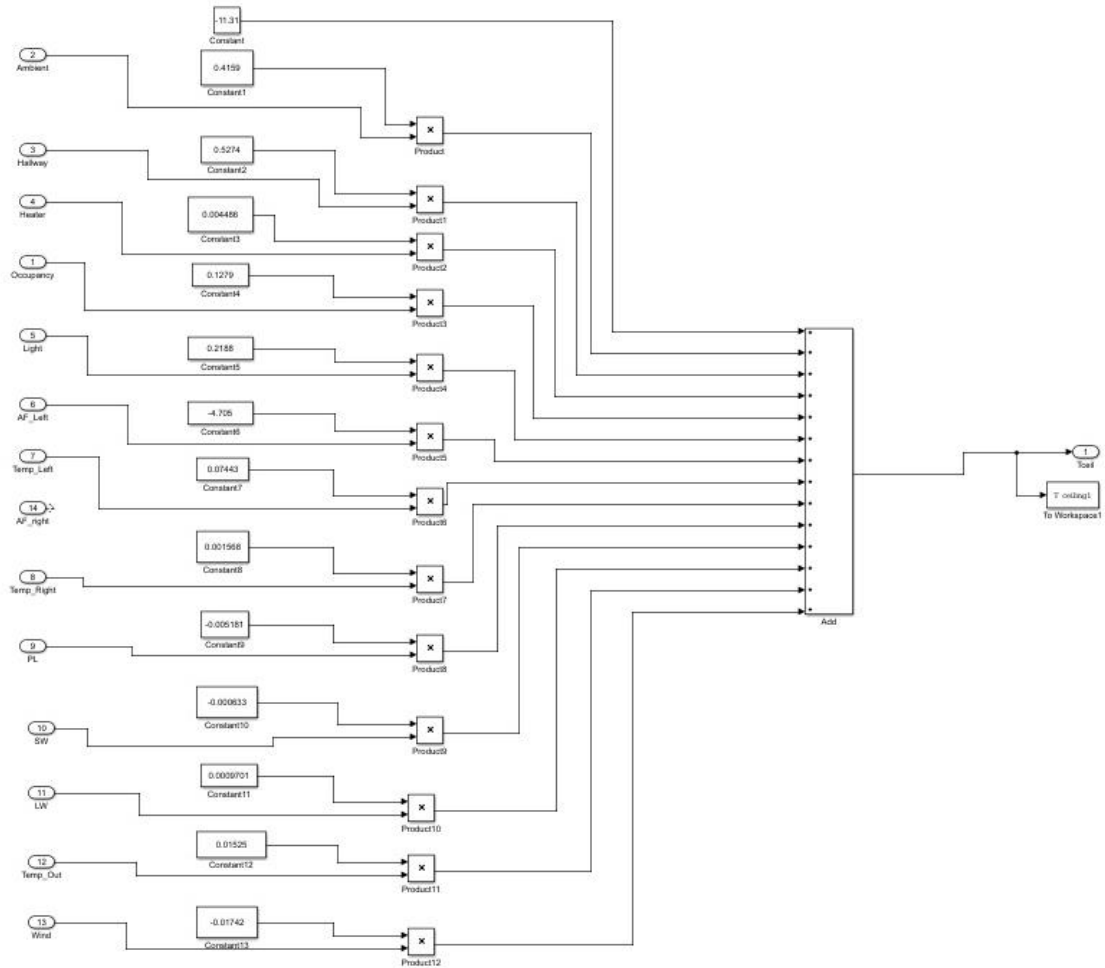


Figure F-14 Ceiling Subsystem Regression Model (not split)

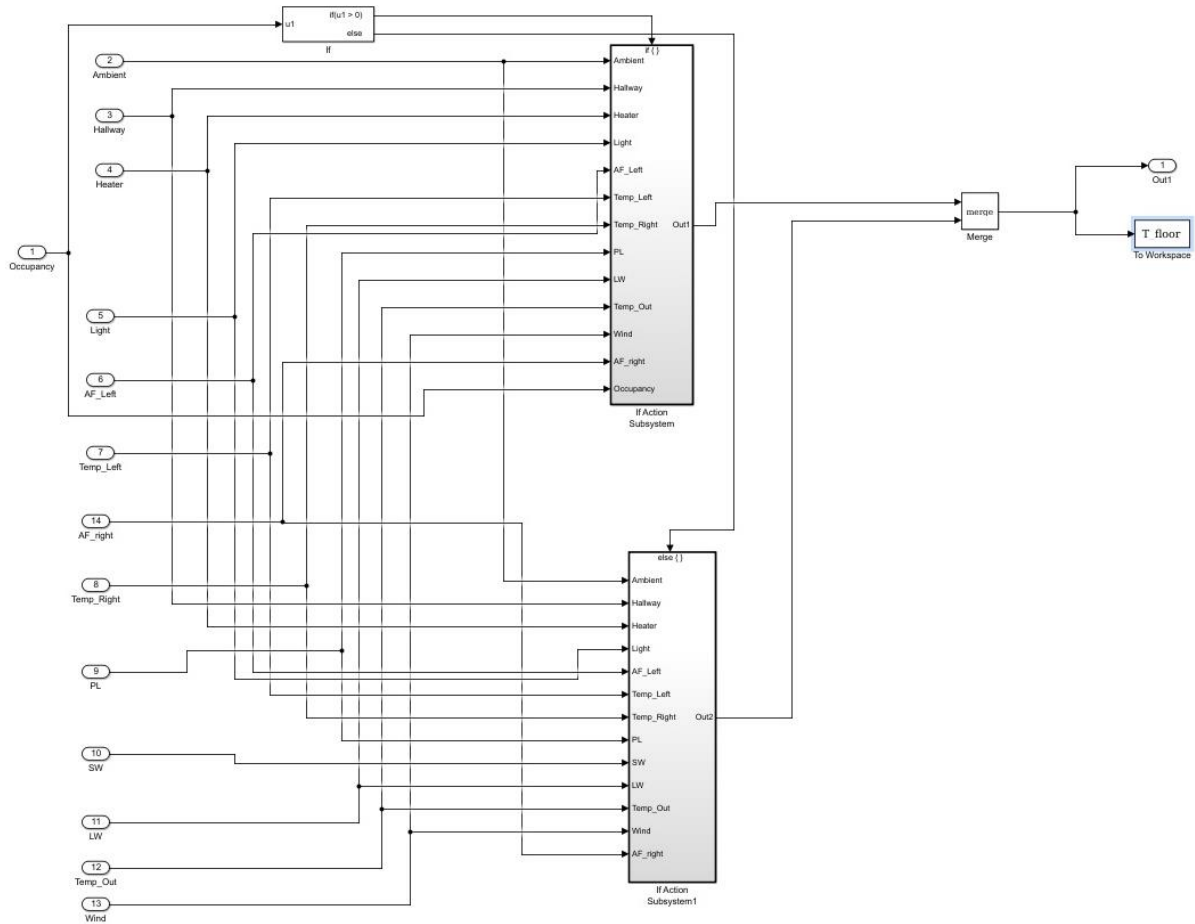


Figure F-1593 Example of Split Regression Model in all the Remaining Building Element Subsystems; Regression Models Similar to the One Seen for Ceiling Regression is in both If and Else Blocks